

HEAT TRANSFER IN TURBULENT BOUNDARY LAYERS WITH
ARBITRARY PRESSURE GRADIENTS, CONFINED FLOWS
AND VISCOUS RECIRCULATING FLOWS

by

NEIL HILTON WOOLLEY, M.Sc.

Thesis submitted for the degree of
Doctor of Philosophy
in the Victoria University of Manchester

Department of Mechanical Engineering
The University of Manchester Institute
of Science and Technology

January 1973

ProQuest Number: 11004557

All rights reserved

INFORMATION TO ALL USERS

The quality of this reproduction is dependent upon the quality of the copy submitted.

In the unlikely event that the author did not send a complete manuscript and there are missing pages, these will be noted. Also, if material had to be removed, a note will indicate the deletion.



ProQuest 11004557

Published by ProQuest LLC (2018). Copyright of the Dissertation is held by the Author.

All rights reserved.

This work is protected against unauthorized copying under Title 17, United States Code
Microform Edition © ProQuest LLC.

ProQuest LLC.
789 East Eisenhower Parkway
P.O. Box 1346
Ann Arbor, MI 48106 – 1346

THE UNIVERSITY OF
MANCHESTER
LIBRARY

10

THE UNIVERSITY OF
MANCHESTER

THE UNIVERSITY OF
MANCHESTER
LIBRARY

THE UNIVERSITY OF
MANCHESTER
LIBRARY

The University of
Manchester Institute of
Science and Technology
14 AUG 1973
LIBRARY

CONTENTS

| <u>Section</u> | <u>Content</u> | <u>Page</u> |
|----------------|---|-------------|
| (a) | Summary | (vi) |
| (b) | Acknowledgements | (viii) |
| (c) | Personal Summary | (ix) |
| (d) | List of Figures | (x) |
| (e) | Introduction | 1 |
| 1 | <u>Turbulent Boundary Layer Flows</u> | |
| 1.1 | Description of Section | 4 |
| 1.2 | Nomenclature - turbulent boundary layer flows | 5 |
| 1.3 | Literature Survey | 9 |
| 1.4 | Apparatus and Experimental Investigation | 24 |
| 1.5 | Basic Theory - External Flows | 29 |
| A. | Introduction | 29 |
| B. | Derivation of Reynolds' equations and the boundary layer approximations | 30 |
| C. | Concept of eddy diffusivity, transformations and non-dimensionalizing | 32 |
| D. | Models of turbulence | 35 |
| | (i) Prandtl mixing length hypothesis | |
| | (ii) Prandtl-Kolmogorov turbulent kinetic energy method | |
| 1.6 | Numerical Analysis - External Flows | 43 |
| A. | Summary | 43 |
| B. | Basic requirements of solution procedure | 43 |
| C. | General finite difference expressions | 44 |
| D. | Finite difference approximation to equation of motion | 45 |

| <u>Section</u> | <u>Content</u> | <u>Page</u> |
|----------------|--|-------------|
| E. | Boundary conditions and solution procedure for equation of motion | 46 |
| F. | Finite difference approximation to energy equation | 48 |
| G. | Boundary conditions and solution procedure for energy equation | 50 |
| | (i) Constant wall temperature | |
| | (ii) Constant wall heat flux | |
| H. | Finite difference approximation to the turbulent kinetic energy equation | 54 |
| I. | Boundary conditions and solution procedure for turbulent kinetic energy equation | 55 |
| J. | Models of turbulence | 58 |
| | (i) Prandtl mixing length | |
| | (ii) Prandtl-Kolmogorov hypothesis | |
| K. | Generation of initial profiles | 61 |
| | (i) Velocity | |
| | (ii) Temperature | |
| | (iii) Turbulent kinetic energy | |
| L. | Calculation of boundary layer displacement and momentum thicknesses | 67 |
| M. | Friction factor and shear stress calculation | 68 |
| N. | Calculation of free-stream velocity and true distances x and y | 69 |
| O. | Calculation of Stanton number | 71 |
| | (i) Constant wall temperature case | |
| | (ii) Constant wall heat flux case | |
| P. | Iteration of equation of motion | 72 |

| <u>Section</u> | <u>Content</u> | <u>Page</u> |
|----------------|--|-------------|
| 1.7 | Basic Theory -- Internal Flows | 75 |
| A. | Introduction | 75 |
| B. | Flow before boundary layer interference | 76 |
| C. | Flow after boundary layer interference | 77 |
| 1.8 | Numerical Analysis -- Internal Flows | 79 |
| A. | Solution of equations before boundary layer interference | 79 |
| B. | Solution of equations after boundary layer interference | 80 |
| 1.9 | Results and Discussion -- External Flow Experiments and Theory | 85 |
| A. | Constant pressure gradient parameter tests -- tests A1, A2, A3 | 85 |
| B. | Departure from two-dimensionality - test A4 | 86 |
| C. | Turbulent boundary layer laminarization -- tests A5 and A6 | 88 |
| 1.10 | Results and Discussion -- External Flow Theory | 95 |
| A. | Comparison with results of Wolfendon [37] | 95 |
| B. | Comparison with results of Schubauer and Klebanoff [21] | 101 |
| C. | Comparison with results of Klebanoff [42] | 102 |
| D. | Effect of outer layer constant changes | 103 |
| 1.11 | Results and Discussion -- Internal Flow Theory | 104 |
| 1.12 | Future Work -- Turbulent Boundary Layer Flows | 107 |
| 2 | <u>Recirculating Flows</u> | |
| 2.1 | Description of Section | 109 |

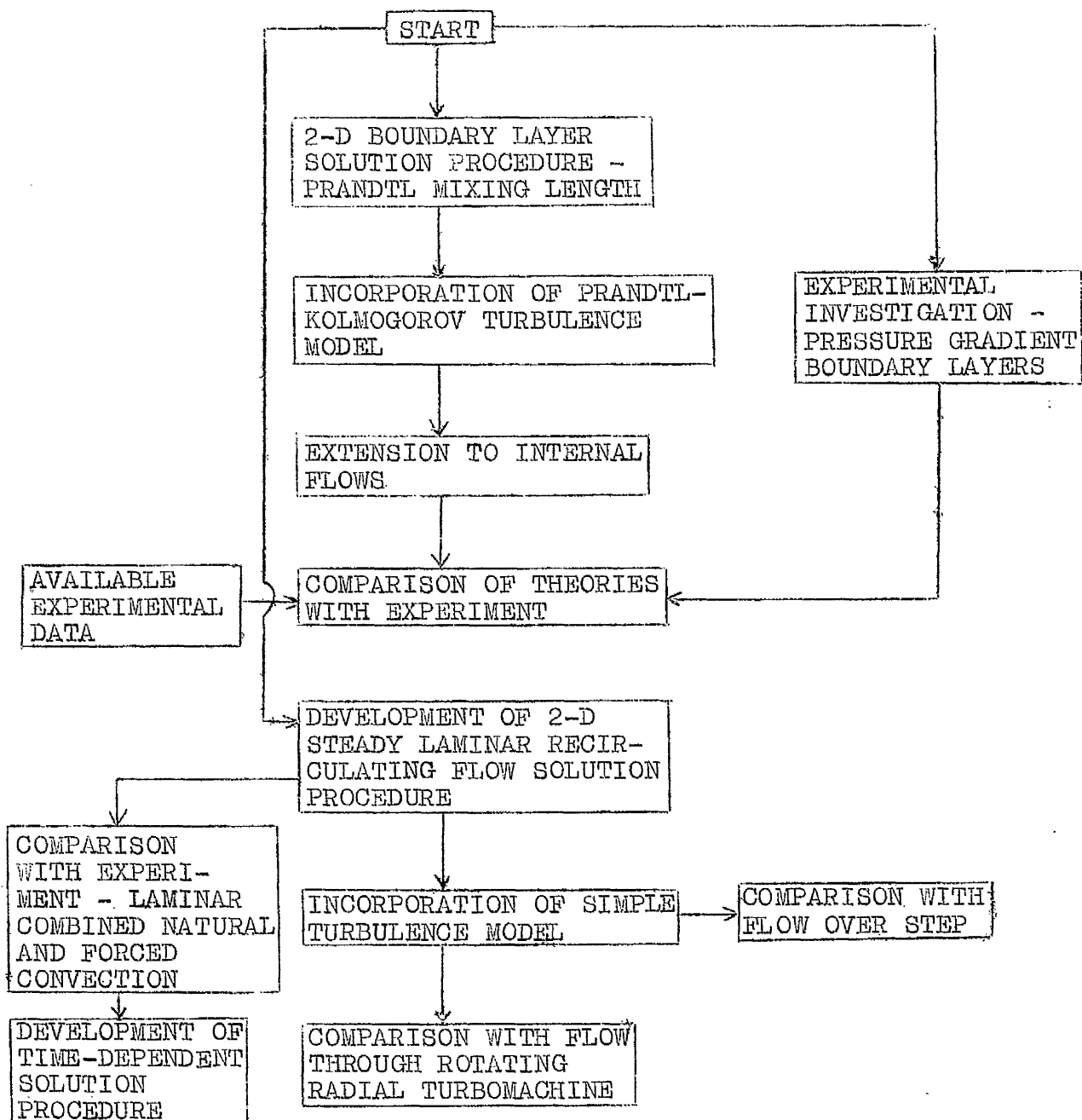
| <u>Section</u> | <u>Content</u> | <u>Page</u> |
|----------------|---|-------------|
| 2.2 | Introduction and Literature Survey | 110 |
| 2.3 | Nomenclature - Combined Natural and Forced Convection | 116 |
| 2.4 | Theory - Combined Natural and Forced Convection | 118 |
| A. | Basic equations, manipulations and non-dimensionalizing | 118 |
| B. | Boundary conditions | 120 |
| C. | General finite difference approximations | 121 |
| D. | Finite difference approximations to governing equations | 123 |
| E. | Numerical solution procedure | 128 |
| | (i) Steady state solutions | |
| | (ii) Transient solutions | |
| 2.5 | Nomenclature - Radial Turbomachine Flows | 133 |
| 2.6 | Theory - Radial Turbomachine Flows | 135 |
| A. | Viscous flow in radial turbo-machine blade passages - the problem considered | 135 |
| B. | Basic theory | 136 |
| C. | Boundary conditions | 139 |
| D. | The slip approximation | 140 |
| E. | Calculation of pressure, efficiency, torque and exit angle | 142 |
| F. | Incorporation of passage height variation and calculation of normalizing factor | 145 |
| G. | Numerical solution of equations | 146 |
| H. | Method of solution | 149 |
| I. | Calculation of hub and shroud boundary layer development | 150 |
| 2.7 | Nomenclature - Flow Over a Step | 152 |

| <u>Section</u> | <u>Content</u> | <u>Page</u> |
|----------------|---|-------------|
| 2.8 | Inclusion of Heat Transfer in Slip Approximation - Flow Over a Step | 153 |
| A. | Basic theory | 153 |
| B. | Boundary conditions | 156 |
| 2.9 | General Discussion of Theory | 158 |
| 2.10 | Results and Discussion of Theory | 163 |
| A. | Transient combined natural and forced convection | 163 |
| B. | Radial turbomachinery flows | 169 |
| C. | Flow over a step | 174 |
| 2.11 | Future Work - Recirculating Flows | 176 |
| | <hr/> Conclusions | 178 |
| | <hr/> <u>Appendices</u> | |
| 1. | References | 183 |
| 2. | Tables of results - boundary layer experiments | 189 |
| 3. | (i) Turbomachinery input data | 204 |
| | (ii) Turbomachinery output data | 205 |
| 4. | Two-dimensionality check - boundary layer experiments | 206 |
| 5. | Boundary layer and duct program | 207 |
| 6. | Transient combined natural and forced convection program | 245 |
| 7. | Turbomachinery program | 266 |
| | Diagrams | |

(a) Summary

This thesis deals with the prediction and measurement of turbulent boundary layer flows with arbitrary pressure gradients. Two models of turbulence are included - the first based on the Prandtl mixing length approach, and the second, a one-equation turbulence model based on the Prandtl-Kolmogorov hypothesis. Extensions of the prediction method to deal with internal flows are made and comparisons made with flows in the entrance region of plane rectangular ducts. The development of techniques to solve general recirculating flows is undertaken and the results of predictions are compared with experiment for three specific configurations - transient laminar combined natural and forced convection, steady flow in radial turbomachine rotors and flow over a step. For the latter two cases, a simple model to account for the effects of turbulence is included.

FLOW DIAGRAM OF DEVELOPMENT OF WORK DESCRIBED
IN THIS THESIS



(b) Acknowledgements

The author is grateful to Professor R. S. Benson for the provision of research facilities. Thanks are expressed to his supervisor, Dr. A. P. Hatton for his continuing advice, encouragement and interest through all stages of the work.

Advice on the turbomachinery aspect of the work from Mr. C. Bosman, Mr. W. G. Cartwright and Mr. M. J. Hill is gratefully acknowledged. Thanks must also be expressed to Dr. J. Byrne for numerous helpful suggestions, Mr. J. Nicholson, Mr. M. Wrigley and the staff of the computing section of the Mechanical Engineering Department for their advice throughout the course of the work, and Mr. C. Roussounelos for the use of his experimental results on reattaching boundary layers. Thanks are expressed to Mrs. J. Bruce for typing this thesis, to Mrs. S. Roe for assistance in tracing the diagrams, and to Mr. J. Davies for his practical assistance at all stages, particularly with regard to the preparation of this thesis.

Finally, thanks are due to the Science Research Council, and the University of Manchester Institute of Science and Technology for financial support.

(c) Personal Summary

The author graduated from the University of Manchester Institute of Science and Technology, Department of Mechanical Engineering in July 1968. He was awarded an S.R.C. studentship and started on a programme of research for which the degree of M.Sc. was awarded in December 1969. The research studentship was continued enabling the author to embark on the research described in this thesis. In October 1971 he took up an appointment as a temporary demonstrator in the Department of Mechanical Engineering, U.M.I.S.T. In September 1972 the author was appointed to the post of lecturer in the Department of Mechanical Engineering, Liverpool Polytechnic.

(d) List of Figures

| <u>Figure</u> | <u>Title</u> |
|---------------|--|
| 1 | Wind-tunnel working section |
| 2 | Experimental free stream velocity distributions |
| 3 | Predictions of friction factor and Stanton number for constant pressure gradient parameters |
| 4 | Predictions of shape factor and R_θ for constant pressure gradient parameters |
| 5 | Predictions and measurements of dimensionless velocity profiles - constant pressure gradient parameters |
| 6 | Predictions and measurements of dimensionless temperature profiles - constant pressure gradient parameters |
| 7 | Two-dimensionality checks on velocity boundary layers |
| 8 | Predictions and measurements of friction factor and Stanton number distributions - test A4 |
| 9 | Predictions and measurements of shape factor and R_θ distributions - test A4 |
| 10 | Friction factor and Stanton number in the laminarization region - test A5 |
| 11 | Prediction and measurements of H and R_θ distributions in the laminarization region - test A5 |
| 12 | Predictions and measurements of dimensionless velocity profiles - test A5 |
| 13 | Predictions and measurements of dimensionless temperature profiles - test A5 |
| 14 | Friction factor and Stanton number in the laminarization region - test A6 |
| 15 | Prediction and measurement of H and R_θ distributions in the laminarization region - test A6 |
| 16 | Predictions and measurements of dimensionless velocity profiles - test A6 |
| 17 | Prediction and measurement of dimensionless temperature profiles - test A6 |
| 18 | Prediction and experimental values of $(C_f \sim x)$ and $(St \sim x)$ - test A7 |
| 19 | Prediction and experimental values of $(C_f \sim x)$ and $(St \sim x)$ - test A8 |

| <u>Figure</u> | <u>Title</u> |
|---------------|--|
| 20 | Experimental and predicted values of shape factor H and Reynolds number R_θ - test A8 |
| 21 | Experimental and predicted turbulent shear stress profiles - test A8 - stations 1, 2, 3 and 4 |
| 22 | Experimental and predicted turbulent shear stress profiles - test A8 - stations 5, 7, 8 and 9 |
| 23 | Experimental and predicted turbulent shear stress profiles - test A8 - stations 10, 11, 12 and 13 |
| 24 | Theoretical and experimental profiles of turbulent kinetic energy - test A8 - stations 1, 2, 3 and 4 |
| 25 | Theoretical and experimental profiles of turbulent kinetic energy - test A8 - stations 5, 7, 8 and 9 |
| 26 | Theoretical and experimental profiles of turbulent kinetic energy - test A8 - stations 10, 11, 12 and 13 |
| 27 | Theoretical and experimental profiles of eddy diffusivity of momentum - test A8 - stations 1, 2, 3 and 4 |
| 28 | Theoretical and experimental profiles of eddy diffusivity of momentum - test A8 - stations 5, 7, 8 and 9 |
| 29 | Theoretical and experimental profiles of eddy diffusivity of momentum - test A8 - stations 10, 11, 12 and 13 |
| 30 | Predicted and experimental turbulent kinetic energy balance - test A8 - station 9 |
| 31 | Comparison of theory with results of Schubauer and Klebanoff |
| 32 | Comparison with Klebanoff's experiments |
| | (a) Defect velocity profile |
| | (b) Mean velocity profile |
| | (c) Turbulent kinetic energy and shear stress profiles |
| 33 | Comparison with Klebanoff's experiments |
| | (a) Direct viscous dissipation and production of turbulent energy near wall |
| | (b) Production and dissipation in region near wall |

FigureTitle

- 34 Comparison with Klebanoff's experiments
- (a) Production and dissipation in region away from wall
- (b) Diffusion and advection
- 35 Effect of outer layer constant variation on zero pressure gradient boundary layers
- 36 Displacement and momentum thickness and shape factor variations along the parallel wall duct
- 37 Displacement and momentum thickness and shape factor variations along the diverging duct
- 38 Wall shear stress variation along the parallel wall duct
- 39 Wall shear stress variation along the diverging duct
- 40 Friction factor variation along parallel wall duct
- 41 Friction factor variation along diverging duct
- 42 Variation of U_s/U_b along parallel and diverging ducts
- 43 Predicted shear-stress distribution in the boundary layer at various positions along the parallel wall duct
- 44 Bulk Stanton number variation along parallel wall duct
- 45 Bulk Stanton number variation along diverging duct
- 46 Coordinate system
- 47 Friction factor distribution along wall
- 48 Stanton number distribution along heated patch
- 49 Dimensionless temperature and velocity profiles at exit from heated patch
- 50 Mean Nusselt number versus Grashof number for different Reynolds numbers
- 51 Streamlines and isotherms for the three flow directions
- 52 Influence of choice of exit boundary condition temperature profiles at exit of field in downflow.

| <u>Figure</u> | <u>Title</u> |
|---------------|---|
| 53 | Influence of choice of exit boundary conditions - velocity profiles at exit of field in downflow |
| 54 | Influence of extension of boundary in y-direction on velocity profiles at the exit from the heated patch |
| 55 | Variation of mean Nusselt number with Grashof number, $Re = 120$ |
| 56 | Flow visualization photograph, $Re = 120$, $Gr = 6.2 \times 10^4$, 7.4×10^4 , and 7.6×10^4 with streamline prediction |
| 57 | Flow visualization photograph, $Re = 350$, $Gr = 21.5 \times 10^4$, 23.0×10^4 and 26.0×10^4 |
| 58 | Flow visualization photograph, $Re = 350$, $Gr = 29.6 \times 10^4$, 37.2×10^4 , 42.2×10^4 |
| 59 | Transient combined forced and natural convection in a parallel channel [(a) aiding (b) opposing] |
| 60 (a) | Coordinate and control systems |
| (b) | Predicted and measured pressure drop through rotor - case 1 |
| 61 | Experimental streaklines and predicted streamline distribution - case 1 |
| 62 | Experimental streaklines and predicted streamline distribution - case 2 |
| 63 | Experimental streaklines and predicted streamline distribution - case 3 |
| 64 | Experimental streaklines and predicted streamline distribution - case 4 |
| 65 | Prediction and measurement of radial velocity distribution - case 1 |
| 66 | Predicted and measured radial velocity and pressure drop distributions - case 2 |
| 67 | Predicted and measured radial velocity distributions - cases 3 and 4 |
| 68 | Friction factor distribution downstream of step |
| 69 | Stanton number distribution downstream of step |

(e) Introduction

The work to be described in this thesis is a continuation of a research programme on turbulent boundary layer behaviour which has been carried out in the Thermodynamics and Fluid Mechanics Division of the Department of Mechanical Engineering at U.M.I.S.T. for some years.

A wind-tunnel, having a flexible roof, had been constructed, enabling a wide variety of flow configurations to be studied. High free stream accelerations can be obtained, allowing the phenomenon of laminarization, important in turbomachinery for example, to be investigated. The primary object of the tests was to create a basis on which to build some reliance on the theoretical models postulated. The theoretical prediction method, although having reached a fairly advanced stage of development, still contained a number of features which were capable of improvement, principally the description of the turbulence and the range of applicability of the solution procedure.

Experimental results and theoretical predictions for comparison will be presented. It became clear at an early stage that the results were encouraging and it was therefore decided to extend the research into a wider range of cases and to commence further work into more difficult flow regions. Internal duct flows are important, especially in reactor technology, and extensions to the solution procedure were incorporated to deal with such situations.

Much work has been completed and a great deal of experience is available on turbulent boundary layers in

normal flow regions, but there still remain many questions unanswered in separating and recirculating flows. It was decided therefore to gain some experience in the solution of the types of equations which apply in such regions, and to relate the analysis to experimental work which was proceeding within the Department.

Because of the totally different techniques required to solve such equations, and because of the problems which were bound to be encountered in the numerical analysis alone, any complex physical assumptions were removed by initiating the analysis with laminar, rather than turbulent flow. With this restriction it was physically unreasonable to consider flow at a high Reynolds number, so, for purposes of testing the solution procedure, the important practical problem of low-speed combined natural and forced convection was chosen. Having established the numerical techniques, an extension of the solution procedure into a different coordinate system was undertaken with the analysis of the flow through the blade passages of a rotating radial turbomachine. A simple turbulence model consisting of a wall slip criterion and constant enhanced fluid viscosity was incorporated for these high Reynolds number turbomachine flows. Experimental results and potential flow theoretical solutions were available for comparison purposes.

In order to examine the validity and limitations of this simple model of turbulence, the situation of flow downstream from a backward facing step was examined. Comparisons were made with available experimental data.

Further development of the recirculating flow

solution procedure to include time-dependent flows has led to the ability to predict the onset of certain experimentally observed unsteady laminar flows in the field of combined natural and forced convection.

The thesis will therefore present work in the following areas:-

1. Boundary Layer Flows

(i) External flow situations

Prediction and measurement of mean flow and turbulence quantities in a variety of arbitrary pressure gradients.

(ii) Internal flows

Predictions and comparisons with experiment of flow and heat transfer in the entrance region of parallel walled and diverging ducts.

2. Recirculating Flows

(i) Theoretical predictions of both steady and unsteady combined natural and forced convection and their qualitative comparison with experiment.

(ii) Predictions and comparison with experiment of flow through the blade passages of a rotating radial turbomachine.

(iii) Comparison with experiment of the predicted flow and heat transfer downstream from a backward facing step.

SECTION 1

TURBULENT BOUNDARY LAYER FLOWS

1.1 Description of Section

This section is primarily concerned with those flows which have the basic boundary layer character, i.e. there is one predominant direction of flow and derivatives of velocity, temperature etc. are only of major influence normal to this streamwise direction.

Two main types of this sort of flow are considered here:-

- (i) External boundary layer flows,
- (ii) Internal flows in plane ducts.

Turbulence models based on both the Prandtl Mixing Length and the Prandtl-Kolmogorov hypotheses are investigated and results of predictions are compared with experiment for the two types of flow. The greater complexity of the analysis based on the Prandtl-Kolmogorov hypothesis has led to the ability to predict the behaviour of certain turbulence quantities with fair agreement with experiment being obtained.

Predictions will, in most cases, be compared with experiment in order to enable some reliance to be placed on the theoretical analysis.

1.2 Nomenclature - turbulent boundary layer flows

| | |
|--|---|
| a, b | Constants describing pressure gradient distribution (e.g. $p = a + b.R$) |
| a', b' | Constants describing duct geometry (e.g. $L = a' + b'.x$) |
| A | $1 + \frac{\epsilon_m}{\nu}$ |
| A _d | Duct cross-sectional area |
| A _v | Constant in Van-Driest mixing length hypothesis |
| B | $\frac{\partial}{\partial Y} \left(\frac{\epsilon_m}{\nu} \right)$ |
| B' | Constant in law of wall |
| b _i , c _i , d _i | Coefficients of tridiagonal matrix - motion equation |
| b _i ', c _i ', d _i ' | Coefficients of tridiagonal matrix - energy equation |
| b _i ", c _i ", d _i " | Coefficients of tridiagonal matrix - turbulent kinetic energy equation |
| C, D, E | Groups of variables in turbulent kinetic energy equation analysis |
| C _f | Friction factor $\left(= \frac{\tau_w}{\frac{1}{2}\rho U_s^2} \right)$ |
| C _p | Specific heat |
| C _{1→5} | Constants in turbulent kinetic energy equation analysis |
| C _{6→8} | Constants in mixing length analysis |
| d | Dimensionless turbulent kinetic energy dissipation |
| h ₁ , h ₂ | Neighbouring steps of ΔY |
| H | Shape factor $\left(= \frac{\delta^*}{\theta} \right)$ |

| | |
|------------|---|
| k | Turbulent kinetic energy $\left(= \frac{\overline{u'^2} + \overline{v'^2} + \overline{w'^2}}{2}\right)$ |
| K | Thermal conductivity |
| k' | Constant in law of wall |
| ℓ | Mixing length |
| ℓ_μ | Prandtl-Kolmogorov turbulence hypothesis length scale |
| ℓ_d | Dissipation length scale |
| L | Local duct height |
| \dot{m} | Mass flow rate through duct |
| n | Exponent in velocity power law |
| n' | Exponent in temperature power law |
| p | Pressure gradient parameter $\left(= \frac{2}{U_s} \frac{dU_s}{dR}\right)$ |
| p' | Internal flow pressure gradient $\left(= -\frac{1}{\rho} \frac{\partial \bar{p}}{\partial x}\right)$ |
| P | Pressure |
| q | Dimensionless turbulent kinetic energy $\left(= \frac{k}{U_s^2}\right)$ |
| q_t | Inner boundary value of q (i.e. at $y^+ \approx 8$) |
| q_w | Wall heat flux |
| R | Reynolds number $\left(= \int \frac{U_s dx}{\nu}\right)$ |
| R_t | Turbulence Reynolds number $\left(= \frac{k^{\frac{1}{2}} y}{\nu}\right)$ |
| R_δ | Displacement thickness Reynolds number $\left(= \frac{U_s \delta^*}{\nu}\right)$ |
| R_θ | Momentum thickness Reynolds number $\left(= \frac{U_s \theta}{\nu}\right)$ |
| St | Stanton number $\left(= \frac{q_w}{\rho C_p U_s (T_{aw} - T_{as})}\right)$ |
| S_d | Duct perimeter |
| t | Time |

| | |
|-----------------------------------|---|
| T | Dimensionless temperature |
| T _a | Dimensional temperature (°K) |
| T _a ⁺ | $\left(= \frac{T_{aw} - T_a}{q_w / \rho C_p u_\tau} \right)$ |
| u, v, w | Velocities in x, y and z directions respectively |
| U, V | Total velocity in x and y directions respectively |
| u ⁺ | $\left(= \frac{u}{\sqrt{\tau_w / \rho}} \right)$ |
| u _τ | Friction velocity $\left(= \sqrt{\tau_w / \rho} \right)$ |
| x, y, z | Independent variables |
| x _h | Distance from start of heating |
| X _{bd} , Y _{bd} | Body forces in x and y directions respectively |
| Y | Dimensionless stream function $\left(= \frac{\psi}{\nu} \right)$ |
| y ⁺ | $\left(= \frac{y \sqrt{\tau_w / \rho}}{\nu} \right)$ |
| y' | Dimensionless distance $\left(= \frac{C_b \cdot y \cdot U_s}{\nu} \right)$ |
| Z | Dimensionless velocity $\left[= \left(\frac{u}{U_s} \right)^2 \right]$ |

Greek Symbols

| | |
|------------------------------------|--|
| α | Thermal diffusivity |
| δ _i , γ _i | Coefficients in Thomas Algorithm - motion |
| δ _i ', γ _i ' | Coefficients in Thomas Algorithm - energy |
| δ _i ", γ _i " | Coefficients in Thomas Algorithm - turbulent kinetic energy |
| δ | Boundary layer thickness |
| δ _t | Thermal boundary layer thickness |
| δ _t [*] | Conduction thickness $\left[= \int_0^{\delta_t} \left(\frac{T_a - T_{as}}{T_{aw} - T_{as}} \right) dy \right]$ |

| | |
|--------------|---|
| δ^* | Displacement thickness $\left[= \int_0^\delta \left(1 - \frac{u}{U_s} \right) dy \right]$ |
| ϵ_m | Eddy diffusivity of momentum |
| ϵ_h | Eddy diffusivity of heat |
| ξ, η | Von-Mises' transformed coordinates |
| θ | Momentum thickness $\left[= \int_0^\delta \frac{u}{U_s} \left(1 - \frac{u}{U_s} \right) dy \right]$ |
| μ | Dynamic viscosity |
| ν | Kinematic viscosity |
| ρ | Density |
| σ | Prandtl Number $\left(= \frac{C_p \mu}{K} \right)$ |
| σ_k | Turbulent kinetic energy Prandtl Number |
| σ_t | Turbulent Prandtl Number $\left(= \frac{\epsilon_m}{\epsilon_h} \right)$ |
| τ | Shear stress |
| τ^+ | Dimensionless shear stress $\left(= \frac{\tau}{\tau_w} \right)$ |
| ϕ | General dependent variable |
| ψ | Stream function $\left(= \int u \, dy \right)$ |
| ω | Multiplying factor in geometric progression |

Subscripts

| | |
|-----|---|
| b | Bulk value |
| ent | At entry conditions to duct |
| i | Initial conditions |
| m | Conditions at boundary layer interference point in confined flows |
| p | Previous station |
| s | Stream or centre-line value |
| w | Wall value |
| | Overbars denote mean quantities |
| | Primes denote fluctuating quantities unless defined otherwise |

1.3 Literature Survey - Parabolic Flows

Efforts are being made by research groups in many parts of the world to produce reliable prediction methods for turbulent flows and this is apparent in the large number of articles which are appearing in the scientific journals. In this survey, attention is confined to those methods and concepts which can be directly related to the work to be presented in this thesis.

The current general availability of computer facilities has led to the emergence of calculation procedures based on the differential equations of motion and energy, rather than an integral equation approach, which could never attain the same range and generality of application. Considerable progress has been made recently in the field and many important methods have appeared when the present work was in its later stages. A survey of these methods, which are still in their relatively early stages of development, is also included as a guide to the direction which research in this field is taking.

When the Navier-Stokes equations are time-averaged, information is lost to the extent that the resulting Reynolds' equations are not closed. By manipulating the Navier-Stokes equations before time-averaging, additional equations may be derived. However the number of unknowns introduced by this process tends to increase more rapidly than the number of equations so that analytic closure becomes impossible. In order to reduce the number of unknowns to the number of describing equations, assumptions relating certain of the unknown quantities

must be introduced. It is the nature of these assumptions and the level at which they are applied which provides the major differences between the methods discussed in this survey.

The lowest closure level (1) relates the turbulent stresses to the mean velocity field and thus only involves solution of the mean momentum equation. The well-known Prandtl mixing length hypothesis, when used in a solution procedure, would generally fall into this category. The major drawback with methods based on this level of closure is that the local turbulence structure, as a consequence of the assumptions, is related strongly to the mean flow alone. Therefore situations where there is a historical turbulence effect, such as the decay of turbulence behind a grid, cannot be predicted.

The next level of closure (2) incorporates the mean turbulent kinetic energy transport equation and is the level at which much of the current research effort is being directed. Methods based on this level should give better results than level 1 for applications where the turbulence behaviour is not particularly related to the mean flow.

A higher closure level (3) uses equations based on the transport of the turbulent stresses. This level holds the most promise for the development of a general treatment for turbulent flow. One point about such methods is that the last strong link between the turbulence and the mean flow has been severed in that the turbulent diffusivity will no longer necessarily vanish when the mean velocity gradient is zero.

There are a number of other approaches which do not fit into the above three categories completely, but generally most of the currently used methods will tend to lie on one of the above levels.

Closure level 1

Usually on this level, closure of the equations is accomplished by relating the Reynolds' stress to properties of the mean velocity field. The most popular approaches using these ideas have involved the Prandtl Mixing Length hypothesis. For steady, incompressible, two-dimensional boundary layers, the governing equations are

$$\bar{u} \frac{\partial \bar{u}}{\partial x} + \bar{v} \frac{\partial \bar{u}}{\partial y} = -\frac{1}{\rho} \frac{\partial p}{\partial x} + \frac{\partial}{\partial y} (-\overline{u'v'}) \quad (1.3.1)$$

$$\frac{\partial \bar{u}}{\partial x} + \frac{\partial \bar{v}}{\partial y} = 0 \quad (1.3.2)$$

where
$$-\overline{u'v'} = \ell^2 \left| \frac{\partial \bar{u}}{\partial y} \right| \frac{\partial \bar{u}}{\partial y}, \quad (1.3.3)$$

the Prandtl Mixing Length hypothesis [1]

or
$$-\overline{u'v'} = \epsilon_m \frac{\partial \bar{u}}{\partial y}, \quad (1.3.4)$$

the Boussinesq [2] hypothesis.

Therefore the closure has come down to a specification of either the mixing length distribution or eddy diffusivity variation across the shear layer under analysis. In some cases combinations of both these techniques are used in a "zonal" treatment of the boundary layer. The mixing length distribution is generally related to the system geometry. e.g. $\ell \propto \delta$

has been used with some success in the calculation of jets, wakes and in the outer region of a turbulent boundary layer. Experiment has led to the relation

$$\ell \propto y$$

which holds for the region near a wall. In the viscous region immediately adjacent to a wall, this relation can be improved to give

$$\ell \propto y \left(1 - e^{-y^+/A^+} \right)$$

(i.e. Van Driest's [3] hypothesis).

The rapid variations which occur near to a wall can either be treated by a fine computational mesh or an overall treatment may be used. The latter technique involves the calculation of the outer limit of the near wall region which is then used as the starting point for the numerical solution procedure, instead of the wall condition.

e.g. The numerical solution at the first computation point away from the wall can be matched to the wall law

$$u^+ = \frac{1}{k}, \ln y^+ + B', \quad y^+ > 30$$

$$B' \doteq 5.0$$

assuming that the shear stress is constant in this near-wall layer.

This shear stress assumption is invalid in certain cases, e.g. highly accelerated flows, so a "Couette" flow assumption is sometimes used near the wall, with allowance made for axial pressure variation.

The resulting shear stress distribution is

$$t^+ = 1 + p^+ y^+, \quad (\text{e.g. Patankar [4]})$$

where $p^+ = (\mu/\tau_w^{3/2} \rho^{1/2}) \frac{dp}{dx}$. Such techniques often involve the solution of ordinary differential equations which often may be precomputed in parametric form.

Analysis of the heat transfer is similar to the hydrodynamic treatment. For steady, incompressible, boundary layer flow of a fluid with constant and uniform properties, neglecting viscous dissipation, the thermal energy equation is

$$\overline{u} \frac{\partial T_a}{\partial x} + \overline{v} \frac{\partial T_a}{\partial y} = \alpha \frac{\partial^2 T_a}{\partial y^2} - \frac{\partial}{\partial y} (\overline{v' T'_a})$$

$\overline{v' T'_a}$ represents the transport of internal energy by turbulent motions.

For closure it is generally assumed that

$$-\overline{v' T'_a} = \epsilon_h \frac{\partial T_a}{\partial y}$$

and that $\frac{\epsilon_m}{\epsilon_h} = \sigma_t$, a turbulent Prandtl number.

The constant value of σ_t around unity which is generally assumed is not so important for gases as, perhaps, for liquid metal heat transfer; so the assumptions relating to this term have probably not received the same attention as the turbulent motion parameters.

Patankar and Spalding [5] were among the early workers in the field with their mixing length method. They assumed a ramp distribution of mixing length near the wall with a constant value in the outer layer. The layer immediately adjacent to the wall was treated by a "Couette" flow analysis. Byrne and Hatton [6] used a method which was rather different in that a constant value

of eddy diffusivity was assumed in the outer layer, as suggested by Clauser [7]. The near wall region was treated in a similar way to Patankar and Spalding in that a ramp distribution of mixing length was used. Similar profiles of velocity were assumed in the region immediately adjacent to the wall. Mellor and Gibson [8] used a similar treatment, except in the region close to the wall where a function relating the eddy diffusivity to R_δ was supplied, based on empirical data. Cebici and Smith [21] specify the eddy diffusivity distribution based on Prandtl's Mixing Length in the core whilst using a constant eddy diffusivity, modified by an intermittancy factor, in the outer layer.

McEligot and Bankston [9] incorporate a Van Driest mixing length distribution in their calculation procedure, which also iterates to cope with any non-linearities which may become significant under certain conditions. A number of workers use a Van Driest type mixing length expression but there still remains conjecture as to the formulation of the expression. For example, McEligot and Bankston suggest, for their purposes, that

$$\ell = k'y \left(1 - e^{-y^+/A_v^+} \right)$$

where $y^+ = \frac{y}{\nu_w} \sqrt{g\tau_w/\rho_w}$ where g is constant.

A number of workers suggest that the local shear stress instead of the wall shear stress should be used when formulating y^+ , whilst, when dealing with boundary layer laminarization, Launder and Jones [10] suggest a variable A^+ , with A^+ principally dependent on the pressure

gradient. Reyhner [21] uses a form of the Van Driest expression in the inner layer and a constant value of eddy diffusivity in the outer layer. Modifications to A^+ are included in his approach.

The method of Nee and Kovaszny [11] has some different features from those mentioned up to this point. Nee and Kovaszny close their system of equations by solving a partial differential equation representing the transport of turbulent diffusivity. The effects of convection, diffusion, production and decay of turbulence are included, as well as straining due to acceleration by pressure gradients. The equation was developed based on an analogy between turbulent diffusivity and turbulent kinetic energy.

Closure level 2

This level of closure involves the use of the turbulent kinetic energy transport equation with an equation relating the turbulent stresses to the turbulent kinetic energy. Thus, to some extent, these methods should be able to handle the delayed response of turbulence structure to sudden changes in mean conditions.

The steady, two-dimensional ^{boundary} layer form of the turbulent kinetic energy equation is

$$\overline{u} \frac{\partial k}{\partial x} + \overline{v} \frac{\partial k}{\partial y} = \overline{-u'v'} \frac{\partial \overline{u}}{\partial y} - \frac{\partial}{\partial y} \left(\overline{v'k'} + \frac{\overline{v'P'}}{\rho} \right) + \nu \frac{\partial^2 k}{\partial y^2} - \nu \sum_{i,j} \left(\frac{\partial \overline{u_i'}}{\partial x_j} \right)^2.$$

| | | | | |
|-----------|-----------------|------------------------|----------------------|-------------|
| ADVECTION | PRODUC- TION | TURBULENT DIFFUSION | VISCOUS DIFFUSION | DISSIPATION |
|-----------|-----------------|------------------------|----------------------|-------------|

Closure assumptions for the turbulent diffusion and dissipation must be specified. It is generally agreed that

the dissipation term can be modelled by

$$\nu \sum_{i,j} \overline{\left(\frac{\partial u_i}{\partial x_j}\right)^2} \equiv \frac{C.k^{3/2}}{\ell_d} \quad (\text{e.g. Emmons [12]})$$

where ℓ_d is a dissipation length scale and C is constant. A popular approach for modelling the turbulent diffusion term uses the "gradient diffusion" approach

$$\left(\overline{v'k'} + \frac{\overline{v'p'}}{\rho}\right) = -N_K \cdot \epsilon_m \frac{\partial k}{\partial y} \quad (\text{e.g. Emmons [12]})$$

where N_K is either a constant or specified function. Bradshaw, Ferriss and Atwell [13] prefer to take more account of the large scale eddy motions and they use

$$\left(\frac{\overline{v'p'}}{\rho} + \overline{v'k'}\right) = G.k.Q_K$$

where G is a constant or specified function.

Q_K is a global vector velocity scale characteristic of the large eddy motions.

To close the system, the Reynolds stresses must now be related to k . One approach uses the concept of eddy viscosity with a constitutive equation relating the turbulent viscosity to the turbulent kinetic energy, i.e. $\epsilon_m = k^{\frac{1}{2}} \cdot \ell_\mu \cdot f(R_t)$, an outcome of the hypotheses of Prandtl [14] and Kolmogorov [15], where ℓ_μ is a turbulence length scale.

f describes the dependence upon the turbulence Reynolds number

$$R_t = \frac{k^{\frac{1}{2}} \ell_\mu}{\nu}$$

with $f = \text{constant}$ for $R_t \gg 1$.

To close the system, the length scales ℓ_μ and ℓ_d must be specified algebraically or by means of a differential equation.

Bradshaw et al relate the Reynolds' stresses directly to k , the turbulent kinetic energy, i.e. $\overline{u'v'} = a_1 k$, where a_1 is expected to be functions of y/δ and of shear stress profile parameters.

The use of a differential equation for length scale has received much attention recently, principally by Spalding and his coworkers.

The length scale equation of Ng and Spalding [16] has its basis in the work of Rotta [17] and may be stated as

$$\begin{aligned} \overline{u} \frac{\partial}{\partial x}(k\ell) + \overline{v} \frac{\partial}{\partial y}(k\ell) = \frac{\partial}{\partial y} \left(\frac{k^{3/2} \ell}{\sigma_1} \frac{\partial \ell}{\partial y} + \frac{k^{1/2} \ell^2}{\sigma_2} \frac{\partial k}{\partial y} \right) \\ + C_p k^{1/2} \ell^2 \left(\frac{\partial \overline{u}}{\partial y} \right)^2 - C_M' k^{3/2}, \end{aligned}$$

where σ_1 , σ_2 , C_p and C_M' are universal constants or functions of local properties for fully turbulent flows. Good predictions of a variety of boundary layer and free shear flows using the above length scale differential equation to determine ℓ have been made by Spalding et al using this technique.

A novel approach is that of Gawain and Pritchard [18], who propose that the local length scale be determined by the mean velocity field in the region of the local point.

The two-point tensor

$$\phi_{ij}(x, \xi) = \frac{u_j'(x + \xi)u_j'(x - \xi)}{u_k'u_k'}$$

is used to define the length scale

$$\ell^2 = \frac{\int \phi_{ii} \xi^2 dV}{\int \phi_{ii} dV}$$

where dV denotes a volume integration. ϕ_{ii} is assumed in terms of the mean velocity field and the integrations are performed to obtain ℓ .

Harlow and Nakayama [19] developed a transport equation for eddy viscosity from the turbulent kinetic energy equation. The turbulence length scale is obtained from a further differential equation.

Jones and Launder [20] have used a two-equation turbulence model to study a variety of boundary layer flows. They solve a differential equation with dissipation as the dependent variable, in addition to the turbulent kinetic energy equation. Their transport equation for energy dissipation is

$$\rho \frac{D\epsilon}{Dt} = \frac{\partial}{\partial y} \left(\frac{\mu_T}{\sigma_\epsilon} \frac{\partial \epsilon}{\partial y} \right) + C_1 \frac{\epsilon}{k} \mu_T \left(\frac{\partial u}{\partial y} \right)^2 - C_2 \rho \frac{\epsilon^2}{k}$$

where ϵ is the dissipation of turbulent kinetic energy, σ_ϵ , C_1 , C_2 are constants.

For low turbulence Reynolds' numbers, a modified equation is suggested

$$\rho \frac{D\epsilon}{Dt} = \frac{\partial}{\partial y} \left(\left(\mu + \frac{\mu_T}{\sigma_k} \right) \frac{\partial}{\partial y} \right) + C_1 f_1 \frac{\epsilon}{k} \mu_T \left(\frac{\partial u}{\partial y} \right)^2 - C_2 f_2 \rho \frac{\epsilon^2}{k} + 2 \cdot f_\mu \cdot \mu_T \left(\frac{\partial^2 u}{\partial y^2} \right)^2$$

where $f_1 = 1.0$

$$f_2 = 1.0 - 0.3 \exp(-R^2)$$

$$f_\mu = \exp(-2.5/(1 + R/50))$$

where $R = \frac{\rho k^2}{\mu \epsilon}$

and this form of the equation is used in the near wall region.

Bradshaw, Ferris and Atwell [13] derive a differential equation for the turbulent shear stress from

$$\bar{u} \frac{\partial k}{\partial x} + \bar{v} \frac{\partial k}{\partial y} = a k \frac{\partial \bar{u}}{\partial y} - C \frac{k^{3/2}}{l} - \frac{\partial}{\partial y} (G k Q_2)$$

$$\frac{\tau}{\rho} = - \overline{u'v'} = a k.$$

The transport velocity Q_2 is taken as $\sqrt{\frac{\tau_{\max}}{\rho}}$, τ_{\max} is the maximum value of turbulent shear stress across the boundary layer. G and l are prescribed as functions of position and a was taken as constant.

The resulting set of equations are hyperbolic and Bradshaw solved them using the method of characteristics. Using these techniques, the turbulent shear stress and turbulent kinetic energy vanish together, making the method doubtful for duct flows. However, the method works very well for external boundary layer flows. This method was one of the more successful at the Stanford conference on boundary layer predictions [21].

The method of Beckwith and Bushnell [21] is essentially the same as that of Glushko [22]. An algebraic turbulence length scale l was used with a modified form of the Prandtl [14] expression for eddy viscosity

$$\tau_t = -\rho \overline{u'v'} = \mu H(r) \alpha \cdot r \frac{\partial \bar{u}}{\partial y}$$

where $r = \frac{\sqrt{k} \cdot l}{\nu}$, a turbulent Reynolds' number. $H(r)$ was described by a three-zone relationship as a function of r .

Mellor and Herring [21] use a three-zone model relating eddy viscosity to the turbulent kinetic energy.

Much wider scope is afforded by this closure level and, for instance, the effects of free stream turbulence on the turbulence and mean flow structures become a relatively simple modification to any prediction procedure. Kearney et al [23] have predicted such effects and compared with their own experiments.

Closure level 3

The methods using this level of closure are in their infancy. In tensor notation, the equation for the transport of the turbulent stresses R_{ij} as derived from the Navier-Stokes equations is

$$\begin{aligned} \frac{\partial R_{ij}}{\partial t} + \bar{u}_k \frac{\partial R_{ij}}{\partial x_k} = & -R_{ik} \frac{\partial \bar{u}_j}{\partial x_k} - R_{jk} \frac{\partial \bar{u}_i}{\partial x_k} - \frac{\partial}{\partial x_k} (\overline{u_i' u_j' u_k'}) \\ & - \frac{1}{\rho} \left[\frac{\partial}{\partial x_j} (\overline{u_i' p'}) + \frac{\partial}{\partial x_i} (\overline{u_j' p'}) \right] \\ & + \frac{p'}{\rho} \left(\frac{\partial \bar{u}_i}{\partial x_j} + \frac{\partial \bar{u}_j}{\partial x_i} \right) + V_{ij} \end{aligned}$$

where V_{ij} is a viscous term.

$$\text{i.e.} \quad V_{ij} = \nu \frac{\partial^2 R_{ij}}{\partial x_k \partial x_k} - 2\nu \frac{\partial u_i'}{\partial x_k} \frac{\partial u_j'}{\partial x_k}.$$

For two dimensional boundary layers, this can be reduced to the following form

$$\frac{D}{Dt}(\overline{u'v'}) = \overline{-v'^2} \frac{\partial \bar{u}}{\partial y} - \frac{\partial}{\partial y} (\overline{u'v'^2}) - \frac{1}{\rho} \left(\frac{\partial}{\partial x} (\overline{p'v'}) + \frac{\partial}{\partial y} (\overline{p'u'}) \right)$$

CONVECTION PRODUCTION

DIFFUSION

$$+ \frac{1}{\rho} \left[\overline{p' \left(\frac{\partial u'}{\partial y} + \frac{\partial v'}{\partial x} \right)} \right] - 2\nu \sum_{\ell} \left(\frac{\partial u'}{\partial x_{\ell}} \frac{\partial v'}{\partial x_{\ell}} \right).$$

REDISTRIBUTION

DISSIPATION

The method of Hanjalic and Launder [24] for modelling the shear stress equation then produces the following final form

$$\frac{D}{Dt}(\overline{u'v'}) = \frac{1}{\rho} \frac{\partial}{\partial y} \left[\frac{\mu_T}{\sigma_T} \frac{\partial}{\partial y} (\overline{u'v'}) \right] + C_T \left[k \frac{\partial u}{\partial y} + \frac{k^{\frac{1}{2}}}{\ell} \overline{u'v'} \right]$$

where σ_T and C_T are constants.

Hanjalic and Launder thus solve the equation for turbulent shear stress, together with the turbulent kinetic energy equation and also a length scale equation to describe the turbulence. Using these techniques they have been able to uncouple the point of zero shear stress from the point of zero velocity gradient for flow in an asymmetric plane channel.

Daly and Harlow [25] model and solve the equations for the normal stress components, instead of turbulent kinetic energy.

A number of calculation methods do not fall into any of the groups mentioned above; for example, the

statistical method of Chung [26] who deals with chemically reacting turbulent shear flows using an analysis based on Langevins equation. Lundgren [27] uses a theory based on turbulent distribution functions and Tyldesley and Silver [28] have developed a technique whereby the detailed fluid behaviour is attributed to the motions of fluid entities of varying size, shape and velocity. Deardorff [29] uses a three-dimensional unsteady solution of the Navier-Stokes equations to give the large scale turbulence structure, whilst using a level 1 closure to describe the small scale effects.

The work on the prediction of turbulent boundary layers at U.M.I.S.T. was initiated by Hatton [30] and [31] who used an explicit solution procedure to solve the energy equation whilst assuming a universal velocity profile. Adoption of an implicit formulation scheme for the energy equation improved the numerical stability of the solution procedure and predictions were made of the flow in the entrance region of a parallel wall duct (Ref. [32]) using this technique. Incorporation of the same implicit scheme to solve the momentum equation in addition to the energy equation followed and predictions were made of simple pressure gradient boundary layer situations by Byrne and Hatton [6].

On a more general basis, a number of review articles have appeared in the literature in the last two years. Reynolds [33] gives a good survey of the recent position in boundary layer prediction procedures, whilst Bradshaw [34] presents a general discussion of the advances made since the Stanford conference and the

hopes for the future in the prediction and understanding
of turbulent flow.

1.4 Apparatus and Experimental Investigation

The experiments were performed in a low free stream turbulence ($\sim 0.06\%$), open circuit, suction wind-tunnel with an 18:1 contraction ratio. The working section of the tunnel is illustrated on fig. 1.

To obtain parallel flow, two wire mesh screens and an 0.1m length of metal honeycomb were positioned at the contraction inlet.

A "Sirocco" two-stage fan, driven by a D.C. motor with a Ward-Leonard speed control system provided the air flow. The maximum velocity at the inlet to the working section was approximately 40m per second. Higher velocities could be obtained in the working section by adjustment of the roof.

The working section was 2.4m long, 0.534m wide and 0.150m high at inlet and exit. The flexible roof was constructed from a number of 0.074m long by 0.506m wide by 0.014m thick aluminium honeycomb plates cemented to a 0.534m wide sheet of "Mylar" plastic. 0.014m sq. section soft rubber cemented to the "Mylar" was used to seal the roof with the tunnel walls. The flexible roof was adjusted by steel screwed rods which were attached to the roof and suspended from a framework above the working section. The working section had perspex sides, one of which was hinged for access. The fixed side had static pressure tapings spaced at 0.15m intervals to enable a prescribed pressure gradient to be obtained by roof adjustment. The roof had provision for suction and also for the 7.938mm diameter tube which served as an instrument holder. A self-aligning bearing maintained

the seal between roof and instrument holder. The instrument holder had a micrometer adjustment for traversing the boundary layer.

The flat plate consisted of a 2.2m long by 0.534m wide sheet of copper plated "Formica", (i.e. the 1.5mm thick "Formica" was coated with 0.075mm of copper) cemented to a 2.54cm thick plywood board. The surface was engraved into 86 strips, 25.4mm wide, radiused at their ends to give a continuous electrical path. A 0.076m thick by 0.534m wide, unheated, aluminium leading edge section preceded the flat plate. A trip-wire was positioned 25.4mm from the leading edge to encourage transition to turbulence. Static pressure tappings were provided above and below the leading edge with provision for suction from underneath.

The electrical supply to the flat plate could be applied at five points enabling cases of unheated starting lengths or discontinuous heating to be studied. Electrical heating of the flat plate was produced by a single phase transformer with a constant voltage regulator to avoid any mains voltage fluctuations. A Variac was used to control the primary supply voltage. The maximum voltage and current used in the experiments was 30 volts and 30 amps respectively.

86 copper-constantan, 36 swg thermocouples were fixed centrally to the floor of the tunnel. These thermocouples were in contact with the copper coating and the access holes were plugged with cotton wool to give good thermal insulation. The thermocouple leads were taken to three low thermal E.M.F. rotary switches.

The thermocouple readings were taken with ice as the cold junction.

For temperature traverses across the boundary layer, a 42swg Chromel-Alumel thermocouple was used with a bead diameter of 0.020mm. The two ends of the 42swg were spot welded to two larger diameter Chromel-Alumel forks. The forks and the ceramic holder were covered with an insulating coat of varnish.

Static pressures were measured by a static tube, body diameter 1.52mm, having 4 holes each 0.38mm diameter, positioned 14mm from the nose. Total pressures were measured by a flattened pitot tube, 0.254mm by 1.562mm outside dimension and 0.072mm by 1.356mm inside dimension. A "Preston" [36] tube, 0.815mm outside diameter and 0.457mm inside diameter was used for wall shear stress measurements. All pressures were obtained by an electronic transducer micromanometer. The electrical output from the manometer was displayed on a digital voltmeter.

Experimental Investigation

A settling-down period of about one hour was necessary before steady conditions were observed. In the heat transfer tests, dependent on the particular test, a period of between two and three hours was sometimes necessary to achieve steady conditions.

The required inlet velocity was set by using the first side-wall static pressure tapping as a reference value. This enabled repeatability of experiments on a day-to-day basis. The static pressures above and below the leading edge section were equalised to prevent any

disturbances being generated in the flow by the leading edge.

The roof was set to give the required pressure gradient along the plate. Because all the pressure readings were obtained relative to atmospheric pressure, it was necessary to take readings of ambient temperature and pressure before and after each traverse. The static pressure was measured by taking the mean of three readings across the boundary layer. Patel's calibration curve (ref. [35]) was used, with the "Preston" [36] tube reading, to calculate the wall shear stress. Velocity traverses were made with the flattened pitot tube. Care was taken with the near-wall readings. The position where the pitot tube just touched the wall was determined by completing an electric circuit between pitot tube and wall and then withdrawing instrument until the circuit was just broken.

The temperature traverses were made with the Chromel-Alumel thermocouple, the datum position being determined in the same way as for the pitot tube.

Plate current was maintained constant throughout a traverse. The power supplied to a strip was taken to be the product of current squared and a known resistance at that particular temperature. Heat loss through the back of the plate as a function of temperature had been obtained from the work of Woolley [37]. The plate temperature was never allowed to become greater than 20°C above ambient, both to prevent plate distortion and also to ensure that the assumptions of constant fluid properties in the analysis remained reasonable.

Further information with regard to experimental procedure and apparatus may be obtained from the work of Woolley [37] and Wolfendon [38].

1.5 External Flow - Basic Theory

A Introduction

This chapter presents the basic equations and assumptions of a two-dimensional constant property turbulent boundary layer solution procedure.

Two turbulence hypotheses were considered:

Method 1. Prandtl Mixing Length

Method 2. Prandtl-Kolmogorov.

Highly accelerated boundary layers were to form one of the areas of investigation. It was therefore felt desirable to calculate the whole of the boundary layer including the sublayer, rather than cover the near wall region by a blanket assumption, such as a universal velocity profile.

Accordingly, for method 1, a Van Driest [3] mixing length distribution was chosen, which decays exponentially as the wall is approached.

$$\text{i.e. } \epsilon_m = l^2 \left| \frac{\partial u}{\partial y} \right|$$

$$\text{where } l = C_b \cdot y \left(1 - e^{-y^+ / A_v} \right).$$

A constant eddy diffusivity was used in the outer layer given by

$$\epsilon_m = C_7 \cdot U_s \cdot \delta^*.$$

A constant value of 0.9 was assumed for the turbulent Prandtl number. Method 2 required the solution of the turbulent kinetic energy equation to enable the eddy diffusivity to be evaluated

$$\text{i.e. } \epsilon_m = C_1 \ell_\mu k^{\frac{1}{2}}.$$

An algebraic length scale distribution, as proposed by Wolfshtein [39] was used. Close to the wall ($y^+ < 8$) a Van Driest mixing length distribution was used because of the invalidity of the Emmons [12] turbulent kinetic energy equation modelling technique. A constant value of eddy diffusivity in the outer layer was again chosen, but based on an integral property of the turbulent kinetic energy rather than mean velocity (displacement thickness).

$$\text{i.e. } \epsilon_m = C_s \cdot U_s \int_0^\delta \left(\frac{k}{U_s^2} \right) dy.$$

A constant value of 0.9 was again assumed for the turbulent Prandtl number.

B Derivation of Reynolds equations and the boundary layer approximations

The Navier-Stokes equations in two dimensions for constant property flow and the energy and continuity equations form the basis of all the theory to be presented in this thesis.

The equations are

$$\frac{\partial U}{\partial t} + U \frac{\partial U}{\partial x} + V \frac{\partial U}{\partial y} = X_{bd} - \frac{1}{\rho} \frac{\partial P}{\partial x} + \nu \left(\frac{\partial^2 U}{\partial x^2} + \frac{\partial^2 U}{\partial y^2} \right) \quad (1.5.1)$$

$$\frac{\partial V}{\partial t} + U \frac{\partial V}{\partial x} + V \frac{\partial V}{\partial y} = Y_{bd} - \frac{1}{\rho} \frac{\partial P}{\partial y} + \nu \left(\frac{\partial^2 V}{\partial x^2} + \frac{\partial^2 V}{\partial y^2} \right) \quad (1.5.2)$$

$$\frac{\partial T_a}{\partial t} + U \frac{\partial T_a}{\partial x} + V \frac{\partial T_a}{\partial y} = \alpha \left(\frac{\partial^2 T_a}{\partial x^2} + \frac{\partial^2 T_a}{\partial y^2} \right) \quad (1.5.3)$$

$$\frac{\partial U}{\partial x} + \frac{\partial V}{\partial y} = 0. \quad (1.5.4)$$

The assumption that the fluid is behaving as an ideal gas is also inherent in the energy equation (1.5.3).

Converting the velocity and temperature fields into mean and fluctuating components

$$\begin{aligned} \text{i.e. } U &= \bar{u} + u' \\ V &= \bar{v} + v' \\ T_a &= \bar{T}_a + T_a' \\ P &= \bar{P} + P' \end{aligned}$$

and restricting the analysis to steady flow, after suitable manipulations and time-averaging, the equations become:-

In the x streamwise direction -

$$\bar{u} \frac{\partial \bar{u}}{\partial x} + \bar{v} \frac{\partial \bar{u}}{\partial y} + \frac{\partial}{\partial x}(\overline{u'^2}) + \frac{\partial}{\partial y}(\overline{u'v'}) = - \frac{1}{\rho} \frac{\partial \bar{P}}{\partial x} + \nu \left(\frac{\partial^2 \bar{u}}{\partial x^2} + \frac{\partial^2 \bar{u}}{\partial y^2} \right) \quad (1.5.5)$$

and in the y cross-stream direction -

$$\bar{u} \frac{\partial \bar{v}}{\partial x} + \bar{v} \frac{\partial \bar{v}}{\partial y} + \frac{\partial}{\partial x}(\overline{u'v'}) + \frac{\partial}{\partial y}(\overline{v'^2}) = - \frac{1}{\rho} \frac{\partial \bar{P}}{\partial y} + \nu \left(\frac{\partial^2 \bar{v}}{\partial x^2} + \frac{\partial^2 \bar{v}}{\partial y^2} \right). \quad (1.5.6)$$

Energy equation -

$$\bar{u} \frac{\partial \bar{T}_a}{\partial x} + \bar{v} \frac{\partial \bar{T}_a}{\partial y} + \frac{\partial}{\partial x}(\overline{u'T_a'}) + \frac{\partial}{\partial y}(\overline{v'T_a'}) = \alpha \left(\frac{\partial^2 \bar{T}_a}{\partial x^2} + \frac{\partial^2 \bar{T}_a}{\partial y^2} \right). \quad (1.5.7)$$

Continuity -

$$\frac{\partial \bar{u}}{\partial x} + \frac{\partial \bar{v}}{\partial y} = 0. \quad (1.5.8)$$

Applying the usual boundary layer approximations, and integrating (1.5.6) across the boundary layer, the equations become

$$\bar{u} \frac{\partial \bar{u}}{\partial x} + \bar{v} \frac{\partial \bar{u}}{\partial y} = - \frac{1}{\rho} \frac{\partial \bar{P}}{\partial x} + \nu \frac{\partial^2 \bar{u}}{\partial y^2} - \frac{\partial}{\partial y}(\overline{u'v'}) - \frac{\partial}{\partial x}(\overline{u'^2}) \quad (1.5.9)$$

$$\bar{P} = \bar{P}_s - \rho \overline{v'^2} \quad (1.5.10)$$

where \bar{P}_s is the imposed free stream pressure.

$$\bar{u} \frac{\partial \bar{T}_a}{\partial x} + \bar{v} \frac{\partial \bar{T}_a}{\partial y} = \alpha \frac{\partial^2 \bar{T}_a}{\partial y^2} - \frac{\partial}{\partial y}(\overline{v'T_a'}). \quad (1.5.11)$$

Now applying Bernoulli's equation at the edge of the boundary layer

$$\bar{P}_s + \rho U_s^2/2 = \text{constant} \quad (1.5.12)$$

and combining equations (1.5.9), (1.5.10) and (1.5.12) leaves

$$\bar{u} \frac{\partial \bar{u}}{\partial x} + \bar{v} \frac{\partial \bar{u}}{\partial y} = U_s \frac{dU_s}{dx} + \nu \frac{\partial^2 \bar{u}}{\partial y^2} - \frac{\partial}{\partial y}(\overline{u'v'}) - \frac{\partial}{\partial x}(\overline{u'^2} - \overline{v'^2}). \quad (1.5.13)$$

A further simplification, doubtful probably only near separation is that the normal stress term, i.e. the last term of equation (1.5.13), is negligible.

The set of equations to be solved are therefore

$$\bar{u} \frac{\partial \bar{u}}{\partial x} + \bar{v} \frac{\partial \bar{u}}{\partial y} = U_s \frac{dU_s}{dx} + \nu \frac{\partial^2 \bar{u}}{\partial y^2} - \frac{\partial}{\partial y}(\overline{u'v'}) \quad (1.5.14)$$

$$\bar{u} \frac{\partial \bar{T}_a}{\partial x} + \bar{v} \frac{\partial \bar{T}_a}{\partial y} = \alpha \frac{\partial^2 \bar{T}_a}{\partial y^2} - \frac{\partial}{\partial y}(\overline{v'T_a'}) \quad (1.5.15)$$

$$\frac{\partial \bar{u}}{\partial x} + \frac{\partial \bar{v}}{\partial y} = 0. \quad (1.5.16)$$

C Concept of eddy diffusivity - transformations and non-dimensionalizing

To form a closed set of equations, assumptions need only be made about the behaviour of the "Reynolds Stress" term $\overline{u'v'}$ and the turbulent flux $\overline{v'T_a'}$.

It is the nature of these assumptions which form the basis of the differences between many of the currently available calculation procedures for solving the boundary layer equations. In this present work, two methods of treatment for these turbulence terms are presented. The first relies on a "local" model based on the Prandtl Mixing Length concept, where the terms are related solely to the local mean flow field. The second allows turbulence "history" to some extent as it finds its basis in the Prandtl-Kolmogorov hypothesis where the turbulence terms are taken to be functions of the local turbulent kinetic energy structure.

Introducing the Boussinesq concept of an eddy diffusivity of momentum ϵ_m , defined as $-\overline{u'v'} = \epsilon_m \left(\frac{\partial \bar{u}}{\partial y} \right)$, analogous to laminar viscosity, and substituting in equation (1.5.14)

$$\bar{u} \frac{\partial \bar{u}}{\partial x} + \bar{v} \frac{\partial \bar{u}}{\partial y} = U_s \frac{dU_s}{dx} + \frac{\partial}{\partial y} \left[(\nu + \epsilon_m) \frac{\partial \bar{u}}{\partial y} \right]. \quad (1.5.17)$$

Defining a stream function ψ such that $\bar{u} = \frac{\partial \psi}{\partial y}$ then from the continuity equation (1.5.16) $\bar{v} = - \frac{\partial \psi}{\partial x}$.

If $\bar{u} = \bar{u}(x, y)$, $x = x(\xi, \eta)$ and $y = y(\xi, \eta)$ where x and y are independent, and ξ and η are independent,

$$\text{then } \bar{u} = \bar{u}(x, y) = \bar{u}(\xi, \eta).$$

The Von-Mises Transformation

Let $\xi = f(x)$ and choose $f(x) = x$

and $\eta = f(y)$ and choose $f(y) = y$

$$\text{then } \frac{\partial \bar{u}}{\partial x}(x, y) = \frac{\partial \bar{u}}{\partial \xi}(\xi, \eta) \frac{\partial \xi}{\partial x} + \frac{\partial \bar{u}}{\partial \eta}(\xi, \eta) \frac{\partial \eta}{\partial x}$$

$$\frac{\partial \bar{u}}{\partial x} = \frac{\partial \bar{u}}{\partial \xi} - \bar{v} \frac{\partial \bar{u}}{\partial \psi}.$$

$$\text{Similarly } \frac{\partial \bar{u}}{\partial y} = \frac{\partial \bar{u}}{\partial \xi} (\xi, \eta) \frac{\partial \xi}{\partial y} + \frac{\partial \bar{u}}{\partial \eta} (\xi, \eta) \frac{\partial \eta}{\partial y}$$

$$\frac{\partial \bar{u}}{\partial y} = \frac{\partial \bar{u}}{\partial \psi} \frac{\partial \psi}{\partial y}$$

$$\begin{aligned} \therefore \bar{u} \frac{\partial \bar{u}}{\partial x} + \bar{v} \frac{\partial \bar{u}}{\partial y} &= \bar{u} \left(\frac{\partial \bar{u}}{\partial \xi} - \bar{v} \frac{\partial \bar{u}}{\partial \psi} \right) + \bar{v} \frac{\partial \bar{u}}{\partial \psi} \frac{\partial \psi}{\partial y} \\ &= \bar{u} \frac{\partial \bar{u}}{\partial \xi}. \end{aligned}$$

Applying this transformation, equation (1.5.17) becomes

$$\bar{u} \frac{\partial \bar{u}}{\partial x} = U_s \frac{dU_s}{dx} + \bar{u} \frac{\partial}{\partial \psi} \left[(\nu + \epsilon_m) \bar{u} \frac{\partial \bar{u}}{\partial \psi} \right]. \quad (1.5.18)$$

Introducing the dimensionless parameters

$$R = \int \frac{U_s dx}{\nu} \quad \text{and} \quad Y = \frac{\psi}{\nu} = \int \frac{\bar{u} dy}{\nu}$$

and substituting in equation (1.5.18), dispensing with overbars and rearranging

$$\frac{\partial}{\partial R} \left(\frac{u}{U_s} \right)^2 = \frac{u}{U_s} \frac{\partial}{\partial Y} \left[\left(1 + \frac{\epsilon_m}{\nu} \right) \frac{\partial}{\partial Y} \left(\frac{u}{U_s} \right)^2 \right] + 2 \left[1 - \left(\frac{u}{U_s} \right)^2 \right] \frac{1}{U_s} \frac{dU_s}{dR}. \quad (1.5.19)$$

$$\text{Let } Z = \left(\frac{u}{U_s} \right)^2$$

$$p = \text{pressure gradient parameter} = \frac{2}{U_s} \frac{dU_s}{dR}$$

$$A = 1 + \frac{\epsilon_m}{\nu}$$

$$B = \frac{\partial}{\partial Y} \left(\frac{\epsilon_m}{\nu} \right).$$

Equation (1.5.19) becomes

$$\frac{\partial Z}{\partial R} = Z^{\frac{1}{2}} \left(A \frac{\partial^2 Z}{\partial Y^2} + B \frac{\partial Z}{\partial Y} \right) + (1 - Z)p \quad (1.5.20)$$

The energy equation (1.5.15) is similarly treated with the introduction of the flux law

$$-\overline{v'T_a'} = \epsilon_h \frac{\partial T_a}{\partial y}.$$

Using the Von-Mises Transformation and introducing the following dimensionless temperatures to deal with two distinct thermal boundary conditions,

(a) Constant wall temperature

$$T = \frac{\overline{T}_a - \overline{T}_{as}}{\overline{T}_{aw} - \overline{T}_{as}}$$

(b) Constant wall heat flux

$$T = \frac{\overline{T}_a - \overline{T}_{as}}{q_w / \rho C_p U_{si}}$$

equation (1.5.15) becomes, for either the constant wall temperature or constant heat flux case,

$$\frac{\partial T}{\partial R} = \frac{\partial}{\partial Y} \left[\left(\frac{1}{\sigma} + \frac{A-1}{\sigma_t} \right) Z^{\frac{1}{2}} \frac{\partial T}{\partial Y} \right] \quad (1.5.21)$$

Equations (1.5.20) and (1.5.21) are coupled, simultaneous, non-linear, parabolic partial differential equations and are solved numerically using a fully implicit form of the Crank and Nicholson [40] method. However, before any solution procedure is used, the terms A and B must be evaluated i.e. a turbulence model must be incorporated.

D Models of Turbulence

(i) Method 1 Prandtl Mixing Length Hypothesis

The consequence of the well-known mixing length hypothesis is that

$$\epsilon_m = \ell^2 \left| \frac{\partial \bar{u}}{\partial y} \right|. \quad (1.5.22)$$

Assumptions still have to be made about ℓ , the mixing length distribution. As the calculation is to be performed throughout the complete boundary layer, including the viscous sublayer, a hypothesis for ℓ is required which includes a sublayer effect. The hypothesis chosen is the well-known Van Driest [3] model where ℓ decays exponentially as the wall is approached.

The mixing length is given by

$$\ell = C_b y \left(1 - e^{-y^+/A_v} \right) \quad (1.5.23)$$

where C_b and A_v are constants.

For high values of y^+ , this hypothesis reduces to

$$\ell = C_b y.$$

The model so far described does not hold in the outer parts of the boundary layer. There is evidence that for equilibrium layers, the eddy diffusivity in the outer boundary layer is constant and can be related to global parameters of the flow such as displacement thickness and free stream velocity. Thus, in the outer layer, a model of the form

$$\epsilon_m = C_7 U_s \delta^* \quad (1.5.24)$$

is used. The turbulent shear stress has thus been related solely to the local mean flow field by a "two-zone" model of turbulence.

The turbulent Prandtl number σ_t is assumed constant.

The values of the constants used in the mixing length hypothesis were

$$\begin{aligned} C_b & 0.41 \\ A_v & 26.0 \\ C_\gamma & 0.018 \\ \sigma_t & 0.9 \end{aligned}$$

(ii) Method 2 Prandtl-Kolmogorov Turbulent Kinetic Energy Method

This approach may be classified as a "one-equation turbulence model" in the sense that one extra transport equation for turbulent kinetic energy is solved.

The basic hypothesis is that attributed to Prandtl [14] where the square root of the turbulent kinetic energy is used as the viscosity determining velocity scale.

$$\text{Hence } \epsilon_m = C_1 \cdot \ell_\mu \cdot k^{\frac{1}{2}} \quad (1.5.25)$$

$$\text{where } k = \frac{\overline{u'^2} + \overline{v'^2} + \overline{w'^2}}{2}$$

and C_1 is constant.

The length scale ℓ_μ is prescribed algebraically and the turbulent kinetic energy k is obtained from a solution of the turbulent kinetic energy equation.

The general, steady turbulence energy equation, in tensor notation, is

$$\overline{u}_j \frac{\partial k}{\partial x_j} = \underbrace{-\overline{u_i' u_j'}}_{\text{ADVECTION}} \frac{\partial \overline{u}_i}{\partial x_j} + \underbrace{-\frac{\partial}{\partial x_j} \left(\frac{\overline{u_j' u_i'^2}}{2} + \frac{\overline{u_j' P'}}{\rho} \right)}_{\text{TURBULENT DIFFUSION}} + \underbrace{\nu \frac{\partial^2 k}{\partial x_j^2}}_{\text{VISCOUS DIFFUSION}} - \underbrace{\nu \left(\frac{\partial \overline{u}_i}{\partial x_j} \right)^2}_{\text{DISSIPATION}} \quad (1.5.26)$$

This equation may be obtained directly from the Navier-Stokes equations by

- (i) Multiplying the momentum equation for each coordinate direction by its corresponding fluctuating velocity,
- (ii) time-averaging,
- (iii) summing the three equations and rearranging.

It should be noticed that because the turbulent kinetic energy equation comes from the Navier-Stokes equations before they are time-averaged, new turbulence information is gained from the equations.

For plane, two-dimensional boundary layer flow at high Reynolds' numbers, equation (1.5.26) becomes

$$\overline{u \frac{\partial k}{\partial x}} + \overline{v \frac{\partial k}{\partial y}} = -\overline{u'v'} \frac{\partial \bar{u}}{\partial y} - \frac{\partial}{\partial y} \left(\overline{v'k'} + \frac{\overline{v'P'}}{\rho} \right) + \nu \frac{\partial^2 \bar{k}}{\partial y^2} - \nu \sum_{i,j} \overline{\left(\frac{\partial u_i'}{\partial x_j} \right)^2}. \quad (1.5.27)$$

Before this equation can be solved, the unknown correlations on the right-hand-side must be approximated in terms of other dependent variables. The modelling technique used is that suggested by Emmons [12] among others.

Production term

$$-\overline{u'v'} = \epsilon_m \frac{\partial \bar{u}}{\partial y} = C_1 \cdot \ell_\mu \cdot k^{\frac{1}{2}} \cdot \frac{\partial \bar{u}}{\partial y}. \quad (1.5.28)$$

Turbulent diffusion term

$$-(\overline{v'k'} + \overline{P'v'}) = \text{constant} \cdot \ell_\mu \cdot k^{\frac{1}{2}} \cdot \frac{\partial \bar{u}}{\partial y} = \frac{\epsilon_m}{\sigma_k} \frac{\partial k}{\partial y} \quad (1.5.29)$$

where σ_k is constant.

σ_k cannot be expected to be unity as heat, mass, momentum and turbulent energy diffuse somewhat differently.

Dissipation term

Assuming local isotropy

$$\sum_{i,j} \overline{\left(\frac{\partial u_i}{\partial x_j}\right)^2} = \frac{C_2 \cdot k^{3/2}}{\ell_d}$$

where C_2 is constant.

ℓ_d , the dissipation length scale, must be prescribed.

Substituting the simulated terms in the turbulent energy equation (1.5.27)

$$\bar{u} \frac{\partial k}{\partial x} + \bar{v} \frac{\partial k}{\partial y} = \epsilon_m \left(\frac{\partial \bar{u}}{\partial y} \right)^2 + \frac{\partial}{\partial y} \left(\frac{\epsilon_m}{\sigma_k} \frac{\partial k}{\partial y} \right) + \nu \frac{\partial^2 k}{\partial y^2} - \frac{C_2 k^{3/2}}{\ell_d} \quad (1.5.28)$$

where $\epsilon_m = C_1 \cdot \ell_\mu \cdot k^{1/2}$.

Applying the Von-Mises transformation, as previously shown for the mean momentum equation, equation (1.5.28) transforms to

$$\bar{u} \frac{\partial k}{\partial x} = \epsilon_m \left(\bar{u} \frac{\partial \bar{u}}{\partial \psi} \right)^2 + \bar{u} \frac{\partial}{\partial \psi} \left(\frac{\epsilon_m}{\sigma_k} \frac{\partial k}{\partial \psi} \right) + \nu \bar{u} \frac{\partial}{\partial \psi} \left(\bar{u} \frac{\partial k}{\partial \psi} \right) - \frac{C_2 k^{3/2}}{\ell_d} \quad (1.5.29)$$

Non-dimensionalizing equation (1.5.29) gives

$$\begin{aligned} \left[\frac{\partial q}{\partial R} + p \cdot q \right] &= \left[\frac{(A-1)}{4Z^2} \left(\frac{\partial Z}{\partial Y} \right)^2 \right] + \left[Z^{\frac{1}{2}} \cdot \frac{B}{\sigma_k} \cdot \frac{\partial q}{\partial Y} + \frac{(A-1)}{2\sigma_k Z^{\frac{1}{2}}} \frac{\partial q}{\partial Y} \frac{\partial Z}{\partial Y} \right. \\ &\quad \left. + \frac{(A-1)Z^{\frac{1}{2}}}{\sigma_k} \frac{\partial^2 q}{\partial Y^2} \right] + \left[\frac{1}{2Z^{\frac{1}{2}}} \frac{\partial Z}{\partial Y} \frac{\partial q}{\partial Y} + Z^{\frac{1}{2}} \frac{\partial^2 q}{\partial Y^2} \right] - [d] \\ &\quad \text{ADVECTION} \quad \text{PRODUCTION} \quad \text{TURBULENT} \quad \text{DIFFUSION} \quad \text{VISCOUS DIFFUSION} \quad \text{DISSIPATION} \end{aligned} \quad (1.5.30)$$

where $q = \frac{k}{U_s^2}$,

$$R = \int \frac{U_s dx}{\nu}, \quad Z = \left(\frac{u}{U_s} \right)^2, \quad Y = \frac{\psi}{\nu} = \int \frac{\bar{u} dy}{\nu},$$

$$A = 1 + \frac{\epsilon_m}{\nu}, \quad B = \frac{\partial}{\partial Y} \left(\frac{\epsilon_m}{\nu} \right), \quad p = \frac{2}{U_s} \frac{dU_s}{dR}$$

$$d = \frac{C_2 \cdot \nu \cdot k^{3/2}}{Z^2 \cdot U_s^4 \cdot \ell_d}$$

$$\text{Thus } \frac{\partial q}{\partial R} + p \cdot q = C \cdot \frac{\partial q}{\partial Y} + D \cdot \frac{\partial^2 q}{\partial Y^2} + E \quad (1.5.31)$$

$$\text{where } C = \frac{Z^{\frac{1}{2}} \cdot B}{\sigma_k} + \frac{(A - 1)}{2Z^{\frac{1}{2}} \cdot \sigma_k} \frac{\partial Z}{\partial Y} + \frac{1}{2Z^{\frac{1}{2}}} \frac{\partial Z}{\partial Y}$$

$$D = (A - 1) \frac{Z^{\frac{1}{2}}}{\sigma_k} + Z^{\frac{1}{2}}$$

$$E = \frac{(A - 1)}{4Z^{\frac{1}{2}}} \left(\frac{\partial Z}{\partial Y} \right)^2 - d.$$

Equation (1.5.31) is parabolic and is in a form ready to be solved simultaneously with the momentum and energy equations (1.5.20 and 1.5.21), provided C, D and E are known.

N.B. Length scale distributions must still be specified.

The model suggested by Wolfshtein [39] was used where viscous action diminishes the length scale near the wall

$$\text{i.e. } \ell_\mu = y \left[1 - e^{-C_3 \cdot R_t} \right]$$

$$\text{and } \ell_d = y \left[1 - e^{-C_4 \cdot R_t} \right]$$

where $R_t = \frac{k^{\frac{1}{2}} y}{\nu}$, a turbulent Reynolds' number.

In the outer part of the boundary layer, these length scale distributions no longer apply. In this region, from experience with the mixing length method, it has been found that a constant eddy diffusivity is

reasonable. Thus, in this method, a constant eddy diffusivity was again used, but based on an integral of the turbulent kinetic energy across the boundary layer, rather than an integral property of the mean flow such as displacement thickness. The use of a viscosity determining parameter based on the integral of the turbulent kinetic energy was first suggested by Mellor and Herring [21].

Thus in the outer layer, a hypothesis of the form

$$\epsilon_m = C_5 \cdot U_s \cdot \int_0^\infty \left(\frac{k}{U_s^2} \right) dy \quad (1.5.32)$$

was used, where C_5 is constant.

N.B. The relation for the dissipation length scale ℓ_d given above was used in the outer part of the layer. This is of minor importance because of the probable negligible size of the dissipation term in this region.

Near wall region

The assumption of local isotropy used in modelling the dissipation term is perhaps not too good close to the wall. A Van-Driest mixing length expression was therefore used up to a value of y^+ of about 8, with the same constants as were used in the mixing length hypothesis.

Energy Equation

A constant value of turbulent Prandtl number was assumed.

The values of the constants used in the Prandtl-Kolmogorov turbulence hypothesis analysis were

| | |
|------------|-------|
| C_1 | 0.20 |
| C_2 | 0.416 |
| C_3 | 0.016 |
| C_4 | 0.263 |
| C_5 | 0.9 |
| σ_k | 1.49 |
| σ_t | 0.9 |

which are much the same as Wolfshtein [39] suggested.

1.6 External Flow - Numerical Analysis

A Summary

This section deals in detail with the solution of the equations. The procedure for solving the coupled parabolic partial differential equations of turbulent boundary layer flow using a fully implicit finite difference formulation is described.

The method of linearising the equations is discussed and also a technique allowing iteration of the equation of motion to establish the importance of the degree of non-linearity under certain conditions.

The incorporation of the boundary conditions, initial profile generation and the calculation of the usual boundary layer integral and wall parameters are included.

B Basic Requirements of Solution Procedure

At this stage in the analysis there remained a number of partial differential equations to be solved. If the Prandtl Mixing Length turbulence model was to be used there would only be the equations of motion and energy, but if the turbulent kinetic energy method was chosen, it was necessary to solve three equations. The following analysis, although concerned with the three differential equations, is inherently no different from the two equation solution, the only difference arising in the formulation of the eddy diffusivities. As the equations are parabolic they may be solved by a marching solution procedure. Boundary conditions must be specified on three sides and the solution marches towards the unknown side. Thus, for each dependent variable

i.e. Velocity u

Temperature T

and possibly Turbulent Kinetic Energy k

we need to specify (a) Initial starting profiles

(b) Wall boundary conditions

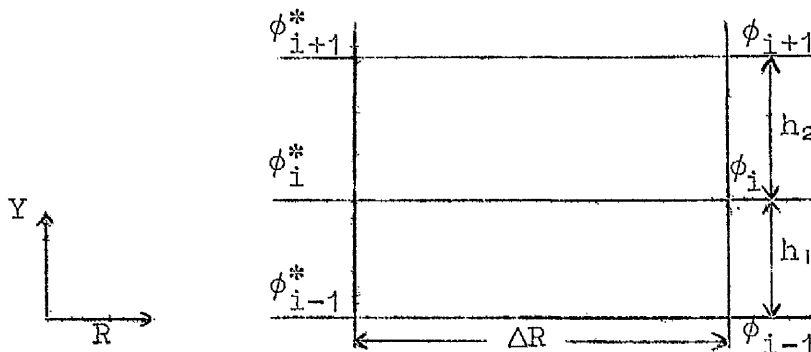
(c) Free Stream boundary conditions.

Due to the high gradients of the dependent variables close to the wall, small cross-stream steps in the Y-direction are required for accuracy to be maintained. Such small steps of ΔY are not required away from the wall so a geometric progression in step size was chosen, increasing in size with distance from the wall.

Complete variability of the streamwise step ΔR was necessary so a fully implicit solution procedure, with no stability restrictions, was chosen.

Finally, as no iterations were generally desired when stepping along the flow, the equations had to be linearised. This was generally accomplished by considering any non-linear terms to be, in fact, known and to have the values at the previous known station, unless of course they happened to be known at the current station under investigation.

C General Finite Difference Expressions



N.B. Starred quantities refer to known values.

The three differential equations are made up of combinations of three derivatives:-

$$\frac{\partial \phi}{\partial R}, \quad \frac{\partial^2 \phi}{\partial Y^2} \quad \text{and} \quad \frac{\partial \phi}{\partial Y}$$

where ϕ represents a general dependent variable.

Truncated Taylor series are used for the finite difference approximations to these derivatives. The truncation point implies that a quadratic equation is fitted to any three neighbouring points in the cross-stream direction and these are then differentiated analytically at the inner point to give the numerical values of the derivatives. The order of truncation in the streamwise direction is lower and therefore less accurate, so from point of view of accuracy, a small streamwise step gives a better approximation to the derivative than a larger value.

The finite difference representations of the derivatives are thus

$$\begin{aligned} \frac{\partial \phi}{\partial R} &\doteq \frac{\phi_i - \phi_{i-1}}{\Delta R} \\ \frac{\partial \phi}{\partial Y} &\doteq \frac{h_1^2 \phi_{i+1} + (h_2^2 - h_1^2) \phi_i - h_2^2 \phi_{i-1}}{h_1 h_2 (h_1 + h_2)} \\ \frac{\partial^2 \phi}{\partial Y^2} &\doteq \frac{2[h_1 \phi_{i+1} - (h_1 + h_2) \phi_i + h_2 \phi_{i-1}]}{h_1 h_2 (h_1 + h_2)} \end{aligned}$$

D Finite Difference Approximation to Equation of Motion

The equation of motion (1.5.20) may now be broken down using the above techniques.

Thus we have

$$\frac{\partial Z}{\partial R} = Z^{\frac{1}{2}} \left(A \frac{\partial^2 Z}{\partial Y^2} + B \frac{\partial Z}{\partial Y} \right) + (1 - Z)p \quad (1.6.1)$$

where $Z = \left(\frac{u}{U_s}\right)^2$ is the dependent variable, R and Y are independent variables, the turbulence quantities A and B are considered to be known at the current station and the pressure gradient parameter p is also a known parameter, being one of the boundary conditions.

Equation (1.6.1) then becomes

$$\frac{Z_i - Z_i^*}{\Delta R} = Z_i^{*\frac{1}{2}} \left\{ \frac{2A[h_1 Z_{i+1} - (h_1 + h_2)Z_i + h_2 Z_{i-1}]}{h_1 h_2 (h_1 + h_2)} + \frac{B[h_1^2 Z_{i+1} + (h_2^2 - h_1^2)Z_i - h_2^2 Z_{i-1}]}{h_1 h_2 (h_1 + h_2)} \right\} + p(1 - Z_i). \quad (1.6.2)$$

This equation may be written in the form

$$Z_{i-1} + b_i Z_i + c_i Z_{i+1} = d_i \quad (1.6.3)$$

where

$$b_i = \{h_1 h_2 (h_1 + h_2) - Z_i^{*\frac{1}{2}} \Delta R [-2A(h_1 + h_2) + B(h_2^2 - h_1^2)] + p h_1 h_2 (h_1 + h_2) \Delta R\} / [Z_i^{*\frac{1}{2}} \Delta R (B \cdot h_2^2 - 2A h_2)]$$

$$c_i = (2A h_2 - B \cdot h_2^2) / (2A h_1 + B h_1^2)$$

$$d_i = [Z_i^* \cdot h_1 h_2 (h_1 + h_2) + p \cdot h_1 h_2 (h_1 + h_2) \cdot \Delta R] / [Z_i^{*\frac{1}{2}} \cdot \Delta R (B \cdot h_2^2 - 2A h_2)].$$

Equation (1.6.3) is a tridiagonal matrix with known coefficients b_i , c_i and d_i and can be solved using the Thomas Algorithm (a Gaussian elimination procedure) and using the appropriate boundary conditions.

E Boundary Conditions and Solution Procedure for Equation of Motion

The boundary conditions for velocity which must be

built into the solution procedure are:-

In $u \sim y$ system

No slip, $u = 0, y = 0$

$$u = U_s, y = \infty$$

$$\frac{\partial u}{\partial y} = 0, y = \infty$$

or, in $Z \sim Y$ system $Z = 0, Y = 0$

$$Z = 1, Y = \infty$$

$$\frac{\partial Z}{\partial Y} = 0, Y = \infty.$$

Letting subscript "o" denote the wall mesh point and numbering consecutively away from the wall then $Z_0 = 0$.

∴ Equation (1.6.3) applied at the first mesh point, $i = 1$, gives

$$Z_0 + b_1 Z_1 + c_1 Z_2 = d_1.$$

But $Z_0 = 0$

$$\therefore Z_1 = \frac{d_1}{b_1} - \frac{c_1}{b_1} Z_2$$

$$Z_1 = \delta_1 - \gamma_1 Z_2 \quad (1.6.4)$$

where $\delta_1 = \frac{d_1}{b_1} \quad (1.6.5)$

and $\gamma_1 = \frac{c_1}{b_1} \quad (1.6.6)$

Now when $i = 2$ in equation (1.6.3)

$$Z_1 + b_2 Z_2 + c_2 Z_3 = d_2.$$

But $Z_1 = \delta_1 - \gamma_1 Z_2,$

$$\therefore Z_2 = \delta_2 - \gamma_2 Z_3$$

where $\delta_2 = \frac{d_2 - \delta_1}{b_2 - \gamma_1}$

and $\gamma_2 = \frac{c_2}{b_2 - \gamma_1}.$

Therefore a general expression for $i \geq 2$ can be written thus

$$Z_i = \delta_i - \gamma_i Z_{i+1} \quad (1.6.7)$$

where
$$\delta_i = \frac{a_i - \delta_{i-1}}{b_i - \gamma_{i-1}} \quad (1.6.8)$$

and
$$\gamma_i = \frac{c_i}{b_i - \gamma_{i-1}} \quad (1.6.9)$$

At the outer boundary, $Y = \infty$, then $Z_i = 1$ and $\frac{\partial Z}{\partial Y} = 0$.

∴ As only the boundary layer is to be calculated, the outer boundary condition is that

$$Z_{i+1} = Z_i = 1.$$

In equation (1.6.7) therefore, when $Z_{i+1} = Z_i$ then

$$Z_i = \frac{\delta_i}{1 + \gamma_i} \quad (1.6.10)$$

In actual fact, the outer boundary condition used was $1.0 \geq Z_i \geq 0.995$ because of the asymptotic behaviour of the velocity profile in this region.

The solution of the matrix at one R station thus consists of starting at the wall and calculating the groups δ_i and γ_i from equations (1.6.5) and (1.6.6) respectively. The general formulae (1.6.8 and 1.6.9) were used to calculate the remaining δ_i 's and γ_i 's. At every step, the relation (1.6.10) is tested to see if it was greater than 0.995. When this condition was satisfied equation (1.6.7) was used to back-substitute for all the other values of Z_i .

F Finite difference approximation to energy equation

The energy equation (1.5.21) is treated in a

similar way to the momentum equation. We have

$$\frac{\partial T}{\partial R} = \frac{\partial}{\partial Y} \left[\left(\frac{1}{\sigma} + \frac{A-1}{\sigma_t} \right) Z^{\frac{1}{2}} \frac{\partial T}{\partial Y} \right] \quad (1.6.11)$$

or, expanding,

$$\frac{\partial T}{\partial R} = \left[\frac{1}{\sigma} + \frac{(A-1)}{\sigma_t} \right] Z^{\frac{1}{2}} \frac{\partial^2 T}{\partial Y^2} + \frac{\partial T}{\partial Y} \frac{\partial}{\partial Y} \left[\left(\frac{1}{\sigma} + \frac{A-1}{\sigma_t} \right) Z^{\frac{1}{2}} \right] \quad (1.6.12)$$

where T is the dependent variable, R and Y are again the independent variables, and Z is considered known at the current station.

N.B. The group $\frac{\partial}{\partial Y} \left[\left(\frac{1}{\sigma} + \frac{A-1}{\sigma_t} \right) Z^{\frac{1}{2}} \right]$ is not broken down any further as numerical errors were propagated with the formation of the individual derivatives.

Equation (1.6.12) thus becomes

$$\begin{aligned} \frac{T_i - T_i^*}{\Delta R} &= 2Z_i^{\frac{1}{2}} \left[\frac{1}{\sigma} + \frac{(A-1)}{\sigma_t} \right] \left[\frac{h_1 T_{i+1} - (h_1 + h_2) T_i + h_2 T_{i-1}}{h_1 h_2 (h_1 + h_2)} \right] \\ &+ \frac{\partial}{\partial Y} \left\{ \left[\frac{1}{\sigma} + \frac{(A-1)}{\sigma_t} \right] Z_i^{\frac{1}{2}} \right\} \left[\frac{h_1^2 T_{i+1} + (h_2^2 - h_1^2) T_i - h_2^2 T_{i-1}}{h_1 h_2 (h_1 + h_2)} \right] \end{aligned} \quad (1.6.13)$$

This can again be written in tridiagonal matrix form as

$$T_{i-1} + b_i' T_i + c_i' T_{i+1} = d_i' \quad (1.6.14)$$

where

$$\begin{aligned} b_i' &= \left\{ h_1 h_2 (h_1 + h_2) + 2 \Delta R \cdot (h_1 + h_2) \cdot Z_i^{\frac{1}{2}} \left[\frac{1}{\sigma} + \frac{(A-1)}{\sigma_t} \right] \right. \\ &\quad \left. - \Delta R \cdot (h_2^2 - h_1^2) \cdot \frac{\partial}{\partial Y} \left[Z_i^{\frac{1}{2}} \left(\frac{1}{\sigma} + \frac{A-1}{\sigma_t} \right) \right] \right\} \\ &\quad / \left\{ -2 \Delta R \cdot h_2 Z_i^{\frac{1}{2}} \left(\frac{1}{\sigma} + \frac{A-1}{\sigma_t} \right) + \Delta R \cdot h_2^2 \frac{\partial}{\partial Y} \left[Z_i^{\frac{1}{2}} \left(\frac{1}{\sigma} + \frac{A-1}{\sigma_t} \right) \right] \right\} \end{aligned}$$

$$c_i' = \left\{ -2 \cdot \Delta R \cdot h_1 Z_i^{\frac{1}{2}} \left(\frac{1}{\sigma} + \frac{A-1}{\sigma_t} \right) - \Delta R \cdot h_1^2 \frac{\partial}{\partial Y} \left[Z_i^{\frac{1}{2}} \left(\frac{1}{\sigma} + \frac{A-1}{\sigma_t} \right) \right] \right\}$$

$$\left\{ -2 \cdot \Delta R \cdot h_2 Z_i^{\frac{1}{2}} \left(\frac{1}{\sigma} + \frac{A-1}{\sigma_t} \right) + \Delta R \cdot h_2^2 \frac{\partial}{\partial Y} \left[Z_i^{\frac{1}{2}} \left(\frac{1}{\sigma} + \frac{A-1}{\sigma_t} \right) \right] \right\}$$

$$d_i' = T_i^* \cdot h_1 h_2 (h_1 + h_2) / \left\{ -2 \cdot \Delta R \cdot h_2 Z_i^{\frac{1}{2}} \left(\frac{1}{\sigma} + \frac{A-1}{\sigma_t} \right) + \Delta R \cdot h_2^2 \frac{\partial}{\partial Y} \left[Z_i^{\frac{1}{2}} \left(\frac{1}{\sigma} + \frac{A-1}{\sigma_t} \right) \right] \right\} .$$

G Boundary Conditions and Solution Procedure for Energy Equation

The thermal boundary conditions which must again be incorporated in the solution procedure are:-

(i) Constant wall temperature

In $T_a \sim y$ system $T_a = T_{aw}$, $y = 0$

$$T_a = T_{as}, \quad y = \infty$$

$$\frac{\partial T_a}{\partial y} = 0, \quad y = \infty$$

or, in $T \sim Y$ system

$$T = 1, \quad Y = 0$$

$$T = 0, \quad Y = \infty$$

$$\frac{\partial T}{\partial Y} = 0, \quad Y = \infty.$$

Subscript "o" denotes the wall

$$\therefore T_o = 1.$$

Applying equation (1.6.14) at the first mesh point, $i = 1$, gives

$$T_o + b_1' T_1 + c_1' T_2 = d_1'.$$

But $T_o = 1$

$$\therefore T_1 = \frac{d_1' - 1}{b_1'} - \frac{c_1'}{b_1'} T_2$$

$$T_1 = \delta_1' - \gamma_1' T_2$$

$$\text{where } \delta_1' = \frac{d_1' - 1}{b_1'} \quad (1.6.15)$$

$$\text{and } \gamma_1' = \frac{c_1'}{b_1'}. \quad (1.6.16)$$

The general expressions for $i \geq 2$ are the same as for the momentum equation

$$\text{i.e. } T_i = \delta_i' - \gamma_i' T_{i+1} \quad (1.6.17)$$

$$\text{where } \delta_i' = \frac{d_i' - \delta_{i-1}'}{b_i' - \gamma_{i-1}'} \quad (1.6.18)$$

$$\text{and } \gamma_i' = \frac{c_i'}{b_i' - \gamma_{i-1}'} \quad (1.6.19)$$

The same procedure as for the outer boundary of the momentum equation is carried out with the energy equation as the boundary conditions are similar. The thermal boundary layer thickness is when $T|_{\text{outer boundary}} \leq 0.005$
i.e. the group

$$T_i = \frac{\delta_i'}{1 + \gamma_i'} \leq 0.005$$

is the outer boundary condition. Back-substitution with equation (1.6.17) up to $i = 1$ gives all the values of T at the current station.

(ii) Constant wall heat flux

$$\text{In } T_a \sim y \text{ system } \frac{\partial T_a}{\partial y} = \text{constant}, \quad y = 0$$

$$T_a = T_{as}, \quad y = \infty$$

$$\frac{\partial T_a}{\partial y} = 0, \quad y = \infty.$$

Now in the transformed $T \sim Y$ system the representation of the above three boundary conditions is a little more involved.

On the wall, the laminar flow relationship must hold

$$\text{i.e.} \quad \frac{\partial T_a^+}{\partial y^+} = \sigma \quad (1.6.20)$$

$$\text{where} \quad T_a^+ = \frac{T_{aw} - T_a}{q_w / \rho C_p u_\tau} \quad (1.6.21)$$

$$\text{Also} \quad T = \frac{T_a - T_{as}}{q_w / \rho C_p U_{si}} \quad (1.6.22)$$

$$\text{and} \quad \tau_w = \rho u_\tau^2.$$

Now for constant heat flux, i.e. q_w is constant, differentiating (1.6.21) and (1.6.22) with respect to y^+ and combining with relation (1.6.20) we get

$$\begin{aligned} \frac{\partial T}{\partial y^+} &= -\sigma \frac{U_{si}}{u_\tau} \\ \frac{\partial T}{\partial y^+} &= -\sigma \frac{U_{si}}{\sqrt{\tau_w / \rho}} \quad (1.6.23) \end{aligned}$$

Therefore the boundary conditions in the $T \sim Y$ system for constant wall heat flux may be given as

$$\begin{aligned} \frac{\partial T}{\partial y^+} &= -\sigma \frac{U_{si}}{\sqrt{\tau_w / \rho}}, \quad Y = 0 \\ T &= 0, \quad Y = \infty \\ \frac{\partial T}{\partial Y} &= 0, \quad Y = \infty. \end{aligned}$$

Subscript "o" denotes wall.

Applying equation (1.6.14) to the first mesh point

away from the wall, $i = 1$, gives

$$T_0 + b_1' T_1 + c_1' T_2 = d_1' . \quad (1.6.24)$$

But $\left. \frac{\partial T}{\partial y^+} \right|_0 = -\sigma \frac{U_{s1}}{\sqrt{\tau_w/\rho}} .$

°. Using a forward three point truncated Taylor series, the derivative $\left. \frac{\partial T}{\partial y^+} \right|_0$ may be written in terms of $T_1, T_2,$

y_1^+ and y_2^+ . y_0^+ is of course zero.

$$\therefore a_0' T_0 + b_0' T_1 + c_0' T_2 = -\sigma \frac{U_{s1}}{\sqrt{\tau_w/\rho}} \quad (1.6.25)$$

where

$$a_0' = -(y_1^+ + y_2^+) / (y_1^+ \cdot y_2^+)$$

$$b_0' = -y_2^+ / [y_1^+ (y_1^+ - y_2^+)]$$

$$c_0' = -y_1^+ / [y_2^+ (y_2^+ - y_1^+)] .$$

°. Eliminating T_0 between equations (1.6.24) and (1.6.25) we get

$$T_1 = \frac{d_1' + \frac{\sigma U_{s1}}{a_0' \sqrt{\tau_w/\rho}}}{-\frac{b_0'}{a_0'} + b_1'} - T_2 \left[\frac{c_1 - \frac{c_0'}{a_0'}}{b_1 - \frac{b_0'}{a_0'}} \right]$$

$$T_1 = \delta_1 - \gamma_1 T_2$$

where

$$\delta_1 = \left(d_1' + \frac{\sigma U_{s1}}{a_0' \sqrt{\tau_w/\rho}} \right) / \left(-\frac{b_0'}{a_0'} + b_1' \right)$$

and

$$\gamma_1 = \left(c_1 - \frac{c_0'}{a_0'} \right) / \left(b_1 - \frac{b_0'}{a_0'} \right) .$$

The general expressions (1.6.17), (1.6.18) and (1.6.19) as previously given for the constant wall temperature

case are the same for the constant wall heat flux case. The outer boundary condition is also the same. Care must be taken, however, with the back-substitution, as the general expression (1.6.17) will only hold up to and including $i = 1$. Either equation (1.6.24) or (1.6.25) must be used to evaluate T_0 .

H Finite Difference Approximation to the Turbulent Kinetic Energy Equation

Up to now it has been assumed that knowledge of the turbulence parameters A and B has been available when forming the coefficients and right-hand-side vectors of the tridiagonal matrices of the momentum and energy equations. This subsection deals with the solution of the turbulent energy equation, which, when combined with the turbulence hypothesis of Prandtl-Kolmogorov, will provide such information as we require. It must be re-emphasised that this equation is not considered when using a Prandtl Mixing Length hypothesis.

The turbulent kinetic energy equation (1.5.31) is

$$\frac{\partial q}{\partial R} + p \cdot q = C \frac{\partial q}{\partial Y} + D \frac{\partial^2 q}{\partial Y^2} + E \quad (1.6.26)$$

where
$$C = \frac{Z^{\frac{1}{2}} \cdot B}{\sigma_k} + \frac{(A - 1)}{2 \cdot Z^{\frac{1}{2}} \sigma_k} \frac{\partial Z}{\partial Y} + \frac{1}{2Z^{\frac{1}{2}}} \cdot \frac{\partial Z}{\partial Y}$$

$$D = (A - 1) \frac{Z^{\frac{1}{2}}}{\sigma_k} + Z^{\frac{1}{2}}$$

$$E = \frac{(A - 1)}{4Z^{\frac{1}{2}}} \left(\frac{\partial Z}{\partial Y} \right)^2 - d$$

and $q = \frac{k}{U_s^2}$ is the dependent variable, R and Y are the independent variables. Assuming p, C, D, E and the turbulence terms A and B are known. Thus, introducing the finite difference approximations, (1.6.26) becomes

$$\frac{q_i - q_i^*}{\Delta R} + p \cdot q_i = C \left[\frac{h_1^2 q_{i+1} + (h_2^2 - h_1^2) q_i - h_2^2 q_{i-1}}{h_1 h_2 (h_1 + h_2)} \right] + 2D \left[\frac{h_1 q_{i+1} - (h_1 + h_2) q_i + h_2 q_{i-1}}{h_1 h_2 (h_1 + h_2)} \right] + E.$$

This can also be written in the tridiagonal matrix form

$$q_{i-1} + b_i'' q_i + c_i'' q_{i+1} = d_i'' \quad (1.6.27)$$

where

$$b_i'' = [h_1 h_2 (h_1 + h_2) + p \cdot \Delta R \cdot h_1 h_2 (h_1 + h_2) - \Delta R \cdot C (h_2^2 - h_1^2) + 2 \cdot D \cdot \Delta R (h_1 + h_2)] / (h_2^2 \cdot \Delta R \cdot C - 2 \cdot D \cdot \Delta R \cdot h_2)$$

$$c_i'' = (-\Delta R \cdot C \cdot h_1^2 - 2D \cdot \Delta R \cdot h_1) / (h_2^2 \Delta R \cdot C - 2 \cdot D \cdot \Delta R \cdot h_2)$$

$$d_i'' = [q_i^* h_1 h_2 (h_1 + h_2) + E \cdot \Delta R \cdot h_1 h_2 (h_1 + h_2)] / (h_2^2 \cdot \Delta R \cdot C - 2 \cdot D \cdot \Delta R \cdot h_2).$$

I Boundary Conditions and Solution Procedure for Turbulent Kinetic Energy Equation

The turbulent kinetic energy boundary conditions are:-

In $k \sim y$ system $k = 0, y = 0$

$k = 0, y = \infty$

$\frac{\partial k}{\partial y} = 0, y = \infty$

and in $q \sim Y$ system $q = 0, Y = 0$

$q = 0, Y = \infty$

$\frac{\partial q}{\partial Y} = 0, Y = \infty.$

Now as stated previously, because of the assumption of local isotropy near the wall the dissipation model is probably a poor reflection of the true situation. It was therefore

decided not to solve the kinetic energy equation in this region but only to solve out from a y^+ of about 8. Thus, a new inner boundary condition is required instead of $q = 0, Y = 0$. A Van-Driest mixing length model is to be used in the near-wall region with the Prandtl-Kolmogorov hypothesis taking over at $y^+ = 8$. To give continuity of eddy diffusivity and shear stress, the two expressions are equated and solved for turbulent kinetic energy as the dependent variable in the near wall region.

i.e. Van Driest

$$\ell = C_b y \left(1 - e^{-\frac{y \sqrt{\tau_w} / \rho}{\nu A_v}} \right)$$

$$\epsilon_m = \ell^2 \left| \frac{\partial \bar{u}}{\partial y} \right|.$$

Prandtl-Kolmogorov

$$\epsilon_m = C_1 \ell_\mu \cdot k^{\frac{1}{2}}$$

$$\ell_\mu = y \left(1 - e^{-C_3 \cdot \frac{k^{\frac{1}{2}} y}{\nu}} \right).$$

°. In near wall region

$$\epsilon_m = \left[C_b \cdot y \left(1 - e^{-\frac{y \sqrt{\tau_w} / \rho}{\nu \cdot A_v}} \right) \right]^2 \frac{\partial \bar{u}}{\partial y} = C_1 \cdot y \left(1 - e^{-C_3 \frac{k^{\frac{1}{2}} y}{\nu}} \right) k^{\frac{1}{2}}. \quad (1.6.28)$$

Equation (1.6.28) is solved for k , and hence q using a Newton-Raphson technique. This analysis implies that the Prandtl-Kolmogorov hypothesis may be used right up to the wall and a continuous eddy diffusivity distribution will result. The value of q obtained at $y^+ = 8$ is that

used as the inner boundary condition. The boundary conditions to be used in solving the kinetic energy equation are therefore

$$q = q_t, \quad Y = Y_t$$

$$q = 0, \quad Y = \infty$$

$$\frac{\partial q}{\partial Y} = 0, \quad Y = \infty$$

where subscript t denotes the near wall position $y^+ = 8$. Subscript "o" again denotes the inner boundary (not the wall in this case)

$$\therefore q_o = q_t.$$

Applying equation (1.6.27) at the next mesh point i.e. $i = 1$ gives

$$q_o + b_1'' q_1 + c_1'' q_2 = d_1''.$$

But $q_o = q_t = \text{known}$

$$\therefore q_1 = \frac{d_1'' - q_t}{b_1''} - q_2 \frac{c_1''}{b_1''}$$

$$q_1 = \delta_1'' - \gamma_1'' q_2$$

where

$$\delta_1'' = \frac{d_1'' - q_t}{b_1''} \quad (1.6.29)$$

and

$$\gamma_1'' = \frac{c_1''}{b_1''}. \quad (1.6.30)$$

The general expressions for $i \geq 2$ are again the same as for the momentum equation.

i.e.

$$q_i = \delta_i'' - \gamma_i'' q_{i+1}$$

where

$$\delta_i'' = \frac{d_i'' - \delta_{i-1}''}{b_i'' - \gamma_{i-1}''}$$

and

$$\gamma_i'' = \frac{c_i''}{b_i'' - \gamma_{i-1}''}.$$

The outer boundary is treated a little differently than for the other two variables. The outer boundary for the turbulent kinetic energy is assumed to lie at the same point as for the velocity.

The quantity incorporating the two outer boundary conditions, similar to momentum and energy,

$$\text{i.e. } q_1 = \frac{\delta_1''}{1 + \gamma_1''}$$

gives the outer value of q_1 to start the back-substitution. Equation (1.6.27) is used for the back-substitution, only up to and including q_0 , the near wall region having been previously calculated.

J Models of Turbulence

In the analysis up to now the turbulence quantities $A \left[= 1 + \frac{\epsilon_m}{\nu} \right]$ and $B \left[= \frac{\partial}{\partial Y} \left(\frac{\epsilon_m}{\nu} \right) \right]$ have been assumed to be known. This subsection will deal with the numerical calculation of these quantities for both turbulence hypotheses.

(i) Prandtl Mixing Length

As stated previously, a Van Driest expression together with a constant eddy diffusivity in the outer layer is used.

i.e. Inner layer

$$\epsilon_m = \ell^2 \left| \frac{\partial u}{\partial y} \right| \quad (1.6.31)$$

$$\text{where} \quad \ell = C_b y \left(1 - e^{-y^+ / A_v} \right) \quad (1.6.32)$$

and outer layer

$$\epsilon_m = C_7 \cdot U_s \cdot \delta^* \quad (1.6.33)$$

where
$$\delta^* = \int_0^\delta \left(1 - \frac{u}{U_s}\right) dy.$$

In the inner layer, combining (1.6.31) and (1.6.32) we have

$$A = 1 + \frac{\epsilon_m}{\nu} = 1 + \frac{C_b^2 \cdot y^2}{\nu} \left(1 - e^{-y^+ / A_v}\right)^2 \left(\frac{\partial u}{\partial y}\right).$$

Making the usual transformations and non-dimensionalizing

$$\text{i.e. } Y = \int \frac{u dy}{\nu}, \quad Z = \left(\frac{u}{U_s}\right)^2$$

then

$$A = 1 + \frac{1}{2} \left(\frac{C_b y \cdot U_s}{\nu}\right)^2 \left[1 - e^{-\left(\frac{C_b y \cdot U_s}{\nu}\right) \frac{1}{C_b A_v} \sqrt{\frac{C_f}{2}}}\right]^2 \left(\frac{\partial Z}{\partial Y}\right)$$

$$A = 1 + \frac{1}{2} y'^2 \left[1 - e^{-\frac{y' \sqrt{C_f/2}}{C_b A_v}}\right] \left(\frac{\partial Z}{\partial Y}\right) \quad (1.6.34)$$

where $y' = \frac{C_b \cdot y \cdot U_s}{\nu}.$

Having the eddy diffusivity in this form requires the formation of the group $y' = \frac{C_b \cdot y \cdot U_s}{\nu}$ from knowledge of Y and u . This will be discussed at a later stage [section 1.6.N.]

In the outer layer,

$$\epsilon_m = C_\tau \cdot U_s \cdot \delta^*$$

$$\therefore A = 1 + \frac{\epsilon_m}{\nu} = 1 + \frac{C_\tau \cdot U_s}{\nu} \int_0^\delta \left(1 - \frac{u}{U_s}\right) dy$$

$$\therefore A = 1 + C_\tau \cdot R_\delta \quad (1.6.35)$$

where $R_\delta = \frac{U_s \delta^*}{\nu}$.

The calculation of R_δ will be discussed at a later stage [section 1.6.L]. No matching of slope at the changeover point is made with the eddy diffusivities. The Van Driest model is used until its numerical value becomes greater than the constant outer layer value, when the constant value takes over.

The derivative of eddy diffusivity with respect to Y , B , must also be found and these are found by differentiating analytically the expressions for A i.e. (1.6.34) and (1.6.35).

Obviously $B = 0$ for the outer layer, as A is constant. However differentiating (1.6.34), and with suitable manipulations, we obtain

$$B = \frac{\partial}{\partial Y} \left(\frac{\epsilon_m}{\nu} \right) = \frac{\partial Z}{\partial Y} \left[\frac{Y' \cdot C_b}{Z^{\frac{1}{2}}} \left(1 - e^{-\frac{Y' \sqrt{C_f}}{C_b A_v}} \right)^2 + \frac{Y'^2 \sqrt{\frac{C_f}{2}} e^{-\frac{Y' \sqrt{C_f}}{C_b A_v}}}{Z^{\frac{1}{2}} A_v} \left(1 - e^{-\frac{Y' \sqrt{C_f}}{C_b A_v}} \right) + \frac{\partial^2 Z}{\partial Y^2} \left[\frac{Y'^2}{2} \left(1 - e^{-\frac{Y' \sqrt{C_f}}{C_b A_v}} \right)^2 \right] \right]$$

$\frac{\partial Z}{\partial Y}$ and $\frac{\partial^2 Z}{\partial Y^2}$ are found numerically using truncated Taylor series.

(ii) Prandtl-Kolmogorov Hypothesis

The inner layer turbulence hypothesis is

$$\epsilon_m = C_1 \ell \mu^{\frac{1}{2}} k^{\frac{1}{2}}$$

where $l_\mu = y \left[1 - e^{-C_3 \cdot R_t} \right]$ and $R_t = \frac{k^{\frac{1}{2}} y}{\nu}$

$$\therefore \epsilon_m = C_1 \cdot y \left[1 - e^{-C_3 \cdot R_t} \right] k^{\frac{1}{2}}$$

$$\therefore A = 1 + \frac{\epsilon_m}{\nu} = 1 + C_1 \cdot R_t \left[1 - e^{-C_3 \cdot R_t} \right].$$

In the outer layer, a constant eddy diffusivity is chosen given by

$$\epsilon_m = C_5 \cdot U_s \int_0^\infty \left(\frac{k}{U_s^2} \right) dy$$

$$\therefore A = 1 + \frac{\epsilon_m}{\nu} = 1 + \frac{C_5}{C_6} \int_0^\delta q \, dy'.$$

This integral is formed numerically using a trapezoidal rule.

The eddy diffusivity derivatives, B, must also be obtained. Again, B = 0 in the outer layer.

In the inner layer,

$$B = \frac{\partial}{\partial Y} \left[C_1 \cdot R_t \left(1 - e^{-C_3 \cdot R_t} \right) \right]$$

$$\therefore B = C_1 \frac{\partial R_t}{\partial Y} \left(1 - e^{-C_3 \cdot R_t} \right) + C_1 C_3 R_t \frac{\partial R_t}{\partial Y} \cdot e^{-C_3 R_t}.$$

$\frac{\partial R_t}{\partial Y}$ is formed using a central difference truncated Taylor series.

K Generation of Initial Profiles

Initial profiles of velocity, temperature and, if being considered, turbulence kinetic energy must be supplied to start the calculation procedure.

(i) Initial velocity profile

The standard Van Driest hypothesis, derivable from a mixing length eddy diffusivity expression with the exponential length scale decay and the assumption of constant shear stress, is matched with a power law in the outer layer.

The Van Driest expression is

$$\frac{du^+}{dy^+} = \frac{2}{1 + \sqrt{1 + 4 \cdot C_b^2 \cdot y^{+2} \left(1 - e^{-y^+/A_v}\right)^2}} \quad (1.6.36)$$

with y^+ based on the local wall shear stress.

This ordinary differential equation is solved numerically using a Kutta-Merson technique. At sufficiently high values of y^+ , ($y^+ = 100$, say) this equation has the "law of the wall" as its solution.

$$\text{i.e.} \quad u^+ = \frac{1}{C_b} \ln y^+ + B' \quad (1.6.37)$$

where B' is a constant.

At $y^+ = 100$, B' is derivable from equations (1.6.36) and (1.6.37) having already assumed values for the constants C_b and A_v .

Thus, in the outer part of the boundary layer we require to match for value and slope, a power law

$$\frac{u}{U_s} = \left(\frac{y}{\delta}\right)^{1/n} \quad \text{and what has now become the universal law of the wall } u^+ = \frac{1}{C_b} \ln y^+ + B'.$$

Therefore we can write

$$\frac{u}{U_s} = \left(\frac{C_f}{2}\right)^{\frac{1}{2}} \left(\frac{1}{C_b} \ln y^+ + B'\right) \quad (1.6.38)$$

$$\frac{\partial(u/U_s)}{\partial y} = \left(\frac{C_f}{2}\right)^{\frac{1}{2}} \cdot \frac{1}{C_b y} \quad (1.6.39)$$

$$\frac{u}{U_s} = \left(\frac{y}{\delta}\right)^{1/n} \quad (1.6.40)$$

$$\frac{\partial(u/U_s)}{\partial y} = \frac{1}{ny} \left(\frac{y}{\delta}\right)^{1/n} \cdot \quad (1.6.41)$$

Equating for value and slope

i.e. equate (1.6.38) with (1.6.40)

and (1.6.39) with (1.6.41)

then equating the resulting two equations, there results

$$y^+ = e^{(n - C_b \cdot B')}$$

This is the value of y^+ at which the inner Van Driest law and the outer power law are equivalent in value and slope and is dependent solely on the chosen constants.

Having established the matching point, the velocity profile can be generated. In the inner layer, up to the matching point, to obtain the Z profile on the previously determined cross-stream Y mesh points, interpolation is necessary. As equation (1.6.36) had been solved previously for a large number of cross-stream points (of the order of 400), linear interpolation was considered to be accurate enough to establish the values of Z on the 30 or so Y mesh points over which this equation was used.

After the matching point, the power law, equation (1.6.40) came into use.

$$\text{Now} \quad dY = \int \frac{u dy}{\nu} \quad (1.6.42)$$

But
$$\frac{u}{U_s} = \left(\frac{y}{\delta}\right)^{1/n}. \quad (1.6.43)$$

At the matching point, from the Van Driest expression, $\frac{u}{U_s}$ and y are known, therefore δ , the boundary layer thickness can be evaluated using equation (1.6.43).

Combining (1.6.42) and (1.6.43)

$$dY = \frac{U_s}{\nu} \int \left(\frac{y}{\delta}\right)^{1/n} dy. \quad (1.6.44)$$

Integrating (1.6.44) between two consecutive mesh points, denoted by "o" and "1", say, where "o" is known, we get

$$y_1 = \left[y_o^{\frac{n+1}{n}} + \frac{\nu}{U_s} \cdot \Delta Y \cdot \delta^{1/n} \cdot \frac{n+1}{n} \right]^{\frac{n}{n+1}}$$

where $\Delta Y = Y_1 - Y_o$, a previously fixed step.

The $\left(\frac{u}{U_s}\right)$ profile, and hence the Z profile can then be evaluated using (1.6.43).

Therefore, summing up, the input data required to generate the velocity profile is

| | |
|-----------------|---|
| C_b and A_v | Constants in Van Driest hypothesis |
| n | Exponent in power law (generally 7 is used) |
| C_f | Friction factor, enabling the wall shear stress to be evaluated |
| U_s | Free stream velocity. |

(ii) Initial temperature profile

The initial temperature profile is constructed in a similar way to the velocity profile.

The inner layer is obtained from the following ordinary differential equation, again solved using a

Kutta-Merson technique.

$$\frac{dt^+}{dy^+} = \frac{2 \cdot \sigma}{1 + \sqrt{1 + 4 \cdot C_g^2 \cdot y^{+2} \cdot \sigma^2 \left(1 - e^{-y^+/A_t}\right)^2}} \quad (1.6.45)$$

A power law is again used in the outer layer,

$$\text{i.e.} \quad (1 - T) = \left(\frac{y}{\delta_t}\right)^{1/n'}$$

where T is the normalised dimensionless temperature, as is used for the constant wall temperature case. A value of 5.6 is generally assigned to n' .

Matching of the two profiles for value and slope is again performed. Interpolation and conversion from t^+ values to T for either thermal boundary condition must be done for the inner layer. For the outer layer, the power law profile is automatically correct for the constant wall temperature boundary condition but must be altered for the constant heat flux case. A knowledge of the local Stanton number is required to perform this operation

$$\text{e.g.} \quad T \left| \begin{array}{c} \text{const. heat} \\ \text{flux} \end{array} \right. = T \left| \begin{array}{c} \text{const. wall} \\ \text{temp.} \end{array} \right. / St$$

at the initial position.

Therefore, input data required to generate the temperature profile is

| | |
|-----------------|--|
| C_g and A_t | Constants in inner layer temperature profile |
| n' | Exponent in thermal power law |
| St | Local Stanton number. |

It may be noted that for the case of an unheated starting length, the dimensionless temperature will be zero everywhere and no thermal input data need be specified.

(iii) Initial turbulent kinetic energy profile

A turbulent kinetic energy profile is only required out to the velocity boundary layer thickness and knowledge of the previously generated velocity profile is used to determine the kinetic energy profile.

Assuming a velocity profile has already been generated, then using equation (1.6.35) the constant value of eddy diffusivity in the outer layer can be obtained by integration [section 1.6.L].

Equating the turbulence hypothesis of Prandtl-Kolmogorov and the Prandtl Mixing Length we obtain (as equation 1.6.28)

$$\left[C_5 \cdot y \left(1 - e^{-y^+ / A_v} \right) \right]^2 \frac{\partial \bar{u}}{\partial y} = C_1 \cdot y \left(1 - e^{-\frac{C_3 \cdot k^{\frac{1}{2}} \cdot y}{\nu}} \right) k^{\frac{1}{2}}. \quad (1.6.46)$$

Equation (1.6.46) is solved for $k^{\frac{1}{2}}$ using a Newton-Raphson iterative technique.

Let

$$r = \frac{C_5^2 y}{C_1} \left(1 - e^{-y^+ / A_v} \right)^2 \frac{\partial \bar{u}}{\partial y}$$

$$s = \frac{C_3 \cdot y}{\nu}$$

$$g = k^{\frac{1}{2}}.$$

Then equation (1.6.46) may be written

$$g \left(1 - e^{-sg} \right) = r$$

$$f(g) = g \left(1 - e^{-sg} \right) - r$$

$$f'(g) = 1 - e^{-sg} + gse^{-sg}.$$

∴ Iterative expression is

$$g_{n+1} = g_n - \left[\frac{g_n(1 - e^{-sg_n}) - r}{1 - e^{-sg_n} + g_n se^{-sg_n}} \right] \quad (1.6.47)$$

Equation (1.6.47) is used at each mesh point to solve for $k^{\frac{1}{2}}$ until $(g_{n+1} - g_n)$ is less than 1% of g_n .

This iterative technique is used to generate the turbulent kinetic energy profile up to the point where the eddy diffusivity reaches the previously determined constant value. The turbulent kinetic energy is then allowed to decay parabolically to zero at the edge of the boundary layer.

L Calculation of boundary layer displacement and momentum thickness

The dimensionless forms of these integral parameters are expressed as Reynolds' numbers

$$\text{i.e. } R_\delta = \frac{U_s \cdot \delta^*}{\nu} = \frac{U_s}{\nu} \int_0^\delta \left(1 - \frac{u}{U_s}\right) dy \quad (1.6.48)$$

$$\text{and } R_\theta = \frac{U_s \theta}{\nu} = \frac{U_s}{\nu} \int_0^\delta \frac{u}{U_s} \left(1 - \frac{u}{U_s}\right) dy. \quad (1.6.49)$$

(a) Displacement Thickness

$$\text{Now } dY = \frac{u dy}{\nu} \quad \text{and } Z = \left(\frac{u}{U_s}\right)^2.$$

∴ Combining with (1.6.48) we can write

$$R_\delta = \int_0^\delta \left(\frac{1}{Z^{\frac{1}{2}}} - 1\right) dY.$$

Formation of this integral will present difficulties on the wall where $Z = 0$. However, from the wall to the first mesh point i.e. from $Y = 0$ to $Y = \Delta Y$ the integral can be evaluated assuming laminar flow

$$\int_0^{\Delta Y} \left(\frac{1}{Z^2} - 1 \right) dY.$$

But $u^+ = y^+$

$$\therefore \int_0^{\Delta Y} \left(\frac{1}{Z^2} - 1 \right) dY = 2 \sqrt{\frac{\Delta Y}{Cf}} - \Delta Y.$$

The remainder of the integral is evaluated numerically using a trapezoidal rule up to the edge of the boundary layer.

(b) Momentum Thickness

From (1.6.49)

$$R_\theta = \int_0^\delta (1 - Z^2) dY.$$

No problems arise with the near-wall region and the integral is formed numerically using a trapezoidal rule.

N.B. Shape factor $H = \frac{R_\delta}{R_\theta}$.

M Friction factor and shear stress calculation

Friction factor is defined as

$$\frac{Cf}{2} = \frac{\tau_w}{\rho U_s^2}.$$

$$\text{Now } \tau_w = \mu \cdot \frac{\partial u}{\partial y} \Big|_{\text{wall}} \quad \text{and} \quad Z = \frac{u^2}{U_s^2}$$

$$\therefore Cf = \frac{\partial Z}{\partial Y} \Big|_{\text{wall}}.$$

$\frac{\partial Z}{\partial Y}$ at the wall is obtained from a forward three-

point differentiation formula.

Thus, if ΔY is the first step in the Y direction away from the wall and ω is the geometric progression increment, and the three steps are numbered 0, 1 and 2 where 0 is the wall then as $Z_0 = 0$

$$C_f = Z_1 \left(\frac{1 + \omega}{\omega \cdot \Delta y} \right) - \frac{Z_2}{\omega \cdot \Delta y (1 + \omega)}.$$

Calculation of total shear stress i.e. turbulent + laminar

$$\frac{\tau}{\tau_\omega} = \frac{\left(1 + \frac{\epsilon_m}{\nu} \right) \frac{\partial Z}{\partial Y}}{C_f}$$

$$\frac{\tau}{\tau_\omega} = \frac{A \cdot \frac{\partial Z}{\partial Y}}{C_f}$$

where A is $1 + \frac{\epsilon_m}{\nu}$.

$\frac{\partial Z}{\partial Y}$ is obtained from truncated Taylor series

C_f is found as previously explained.

The friction factor may also be found using the Van Karman two-dimensional momentum integral equation i.e.

$$\frac{C_f}{2} = \frac{dR}{dR} \theta + (H + 1) \frac{R}{U_s} \frac{dU}{dR} s. \quad (1.6.50)$$

The values of friction factor obtained from this expression were used as a guide to the forward step length. However the expression is not generally very useful because of its proneness to numerical error, especially in the formation of the derivative $\frac{dR}{dR} \theta$.

N Calculation of free stream velocity and true distances x and y

Calculation of true distance y

This is needed, for example, to evaluate the eddy

diffusivity when using the mixing length hypothesis.

It is generally formed as the dimensionless group y'

where
$$y' = \frac{C_b \cdot y \cdot U_s}{\nu}$$

As
$$Y = \int \frac{u dy}{\nu}$$

$$y' = C_b \int_0^Y \frac{1}{Z^2} dY. \quad (1.6.51)$$

Again assuming $u^+ = y^+$ near the wall

$$y_0' = 0$$

and
$$y_1' = C_b \sqrt{\frac{4\Delta Y}{C_f}}$$

where subscript "1" again denotes the first mesh point from the wall.

The remaining values of y' are found using the trapezoidal rule to integrate equation (1.6.51).

Calculation of true streamwise distance x and local free stream velocity

The free stream velocity variation is prescribed as a boundary condition as a variation of pressure gradient parameter, generally with Reynolds' number R .

The pressure gradient parameter is defined as

$$p = \frac{2}{U_s} \frac{dU_s}{dR} \quad (1.6.52)$$

where
$$dR = \frac{U_s dx}{\nu} \quad (1.6.53)$$

The pressure gradient parameter variation is usually of the general form

$$p = a + b \cdot R,$$

where a and b are constants.

i.e.
$$\frac{2}{U_s} \frac{dU_s}{dR} = a + b.R.$$

Letting U_s = current value of U_s i.e. the unknown value

U_{sp} = previous value of U_s i.e. the known value

ΔR = step in R between current and previous stations

R = current value of Reynolds' number

then

$$U_s = U_{sp} \cdot \exp \left[\frac{a \cdot \Delta R}{2} + \frac{b \cdot \Delta R}{4} (2.R - \Delta R) \right]. \quad (1.6.54)$$

This expression is used to find the free stream velocity variation from a knowledge of the pressure gradient.

The distance along the wall x is obtained from equation (1.6.53).

Letting x = current value of x i.e. the unknown value

x_p = previous value of x i.e. the known value

U_s = current value of U_s i.e. known

U_{sp} = previous value of U_s also known

then $x = x_p + \frac{2 \cdot \nu \cdot \Delta R}{U_{sp} + U_s}$, a trapezoidal rule approximation.

0 Calculation of Stanton Number

(i) Constant Wall Temperature Case

$$\begin{aligned} St &= \frac{q_w}{\rho C_p \cdot U_s (T_{aw} - T_{as})} \\ &= \frac{-k \frac{\partial T_a}{\partial y}}{\rho C_p \cdot U_s (T_{aw} - T_{as})} \end{aligned}$$

Now

$$T = \frac{T_a - T_{as}}{T_{aw} - T_{as}}$$

$$\therefore St = - \left. \frac{\partial T}{\partial y} \right|_w \cdot \sqrt{\frac{C_f}{2} \frac{1}{\sigma}}$$

$\frac{\partial T}{\partial y^+}$ at the wall is obtained from a forward 3 point differentiation formula. It should be noted that the expression for Stanton number is written in this form with $\frac{\partial T}{\partial y^+}$ instead of $\frac{\partial T}{\partial Y}$ because the latter expression is unusable due to the existence of the term $\frac{1}{u}$ which tends towards infinity at the wall.

(ii) Constant wall heat flux case

$$St = \frac{q_w}{\rho C_p U_s (T_{aw} - T_{as})} .$$

Now

$$T = \frac{T_a - T_{as}}{q_w / \rho C_p U_{si}} .$$

∴ Stanton number is immediately calculable as

$$St = \frac{1}{T_w} \cdot \frac{U_{si}}{U_s} .$$

P Iteration of equation of motion

The equations which were solved by the processes which have been described up to now have been non-linear. However, they have been linearised by considering the non-linear terms to have the values at the previous station. This linearising may not affect the solution unduly when the changes in variables from station to station tend to be small, but when the flow is accelerated suddenly, errors may be introduced due to this linearity. An attempt has been made to overcome this by solving the equation of motion in the normal way, but then using this solution as the first guess in an iterative solution procedure.

Returning to the equation of motion, equation (1.6.2), we have

$$\begin{aligned}
Z_i - Z_i^* - \frac{Z_i^{*\frac{1}{2}} \cdot \Delta R}{h_1 h_2 (h_1 + h_2)} & \left\{ 2A \left[h_1 Z_{i+1} - (h_1 + h_2) Z_i + h_2 Z_{i-1} \right] \right. \\
& + B \left[h_1^2 Z_{i+1} + (h_2^2 - h_1^2) Z_i - h_2^2 Z_{i-1} \right] \Big\} \\
& - p \cdot (1 - Z_i) \Delta R = 0. \quad (1.6.55)
\end{aligned}$$

In this case it is the term $Z_i^{*\frac{1}{2}}$ which is causing the non-linearity. The value used for $Z_i^{*\frac{1}{2}}$ should really be the value at the current station. The aim of the following analysis is to try and correct this error.

A Newton-Raphson technique was used to iterate with Z_i as the dependent variable. The term $Z_i^{*\frac{1}{2}}$ in the above equation is thus converted to $Z_i^{\frac{1}{2}}$.

Thus, we have

$$\begin{aligned}
f(Z_i) &= Z_i - Z_i^* - \frac{Z_i^{\frac{1}{2}} \Delta R}{h_1 h_2 (h_1 + h_2)} \left\{ 2A \left[h_1 Z_{i+1} - (h_1 + h_2) Z_i \right. \right. \\
& \quad \left. \left. + h_2 Z_{i-1} \right] + B \left[h_1^2 Z_{i+1} + (h_2^2 - h_1^2) Z_i - h_2^2 Z_{i-1} \right] \right\} \\
& \quad - p(1 - Z_i) \cdot \Delta R \\
f'(Z_i) &= 1 + p \cdot \Delta R - \frac{\Delta R}{2Z_i^{\frac{1}{2}} \cdot h_1 h_2 (h_1 + h_2)} \left\{ 2A \left[h_1 Z_{i+1} \right. \right. \\
& \quad \left. \left. - (h_1 + h_2) Z_i + h_2 Z_{i-1} \right] + B \left[h_1^2 Z_{i+1} + (h_2^2 - h_1^2) Z_i \right. \right. \\
& \quad \left. \left. - h_2^2 Z_{i-1} \right] \right\} - \frac{Z_i^{\frac{1}{2}} \cdot \Delta R}{h_1 h_2 (h_1 + h_2)} \left[B(h_2^2 - h_1^2) \right. \\
& \quad \left. - 2A(h_1 + h_2) \right].
\end{aligned}$$

The general iteration formula was then

$$Z_{i_{\text{new}}} = Z_{i_{\text{old}}} - \frac{f(Z_i)}{f'(Z_i)}.$$

A number of iterations were performed in the areas of very high pressure gradient and the results will be discussed in section [1.9.C].

1.7 Internal Flows - Basic Theory

A Introduction

Internal or confined flows form a particular class of boundary layer flow in which the stream velocity variation is not explicitly known but is itself a function of the boundary layer growth and the duct cross-sectional area. In many areas of confined flows, the boundary layers growing from opposite sides of the duct eventually meet and interfere; the flow development in a constant area passage is typical of this process. As has been seen in the preceding sections, when dealing with unconfined external flows, a physically correct description of the outer part of the boundary layer is usually of relatively minor importance. The inner layer description has a much greater influence on factors such as wall shear stress and heat transfer. For confined flows, however, it is much more important to use a reliable model for the outer part since it is this zone which determines the behaviour of the core flow and the position of the interference point. For a duct of uniform cross-sectional area, we may recognise three separate regions in the flow development. First, the growth of the wall boundary layers with a potential core flow until the interference point is reached. Secondly the region of readjustment from free boundary layer flow to the fully developed flow and third the developed flow itself. For a duct of varying cross-sectional area these regions are also present but the third region is one in which axial changes continue to occur. It is perhaps optimistic to expect that a turbulent flow model could be postulated that would give

reliable predictions for these very different flow regions.

B Flow before boundary layer interference

Only the major differences between the internal and external flows will be discussed in this section. In the entrance region of a parallel sided duct, before the boundary layers on the top and bottom walls meet, the major difference between the theories lies in the pressure gradient description. In the external flow situation, the pressure gradient variation with R or x must be prescribed as a boundary condition. However, in internal flows, the pressure gradient is itself a function of the boundary layer growth and the duct geometry.

Thus from continuity

$$U_{si} \cdot L_{ent} = U_s (L - 2\delta^*). \quad (1.7.1)$$

But
$$p = \frac{2}{U_s} \frac{dU_s}{dR}$$

∴
$$p = \frac{4\nu}{U_s \cdot L} \frac{dR}{dR} \delta - \frac{2}{L} \frac{dL}{dR} \cdot \quad (1.7.2)$$

Now in the cases considered, the ducts have either been parallel walled or a constant angle of divergence.

Therefore, in the general case, we can write

$$L = a' + b' \cdot x \quad (1.7.3)$$

where a' or b' are constants.

From equations (1.7.2) and (1.7.3) and the Reynolds Number definition

$$R = \int \frac{U_s dx}{\nu}$$

we can write

$$p = \frac{4\nu}{U_s \cdot L} \frac{dR}{dR} \delta + \frac{2\nu \cdot b'}{L \cdot U_s} \cdot \quad (1.7.4)$$

This relation holds up to the point where the boundary layers interfere.

C Flow after boundary layer interference

After boundary layer interference, major differences occur between the internal and external flow situations.

The assumption that Bernoulli's equation holds along the duct centre-line is not valid after interference.

Therefore, returning to the basic momentum equations (1.5.9) and (1.5.10) we have

$$\bar{u} \frac{\partial \bar{u}}{\partial x} + \bar{v} \frac{\partial \bar{u}}{\partial y} = - \frac{1}{\rho} \frac{\partial \bar{P}}{\partial x} + \nu \frac{\partial^2 \bar{u}}{\partial y^2} - \frac{\partial}{\partial y} (\bar{u}' \bar{v}') - \frac{\partial}{\partial x} (\bar{u}'^2) \quad (1.7.5)$$

$$\bar{P} = \bar{P}_s - \rho \bar{v}'^2. \quad (1.7.6)$$

Combining (1.7.5) and (1.7.6), neglecting the normal stress terms as before, introducing the eddy diffusivity of momentum concept and transforming leaves

$$\bar{u} \frac{\partial \bar{u}}{\partial x} = - \frac{1}{\rho} \frac{\partial \bar{P}_s}{\partial x} + \bar{u} \frac{\partial}{\partial \psi} \left[(\nu + \epsilon_m) \bar{u} \frac{\partial \bar{u}}{\partial \psi} \right] \quad (1.7.7)$$

c.f. equation (1.5.18).

Subscript "s" now refers to the duct centre-line conditions.

Letting $Z = \left(\frac{u}{U_m} \right)^2$ where U_m is the stream velocity at the point where the boundary layers first interfere i.e. U_m is constant for a particular case.

$$A = 1 + \frac{\epsilon_m}{\nu}$$

$$B = \frac{\partial}{\partial Y} \left(\frac{\epsilon_m}{\nu} \right)$$

where $R = \int \frac{U_m dx}{\nu}$ and $Y = \frac{\psi}{\nu} = \int \frac{\bar{u} dy}{\nu}$.

Thus, equation (1.7.7) becomes

$$\frac{\partial Z}{\partial R} = p' \cdot \frac{2\nu}{U_m^3} + Z^{\frac{1}{2}} \frac{\partial}{\partial Y} \left[A \frac{\partial Z}{\partial Y} \right]$$

$$\text{or } \frac{\partial Z}{\partial R} = Z^{\frac{1}{2}} \left(B \frac{\partial Z}{\partial Y} + A \frac{\partial^2 Z}{\partial Y^2} \right) + p' \cdot \frac{2\nu}{U_m^3} \quad (1.7.8)$$

$$\text{where } p' = - \frac{1}{\rho} \frac{\partial \bar{P}}{\partial x}$$

c.f. equation (1.5.20).

Continuity and pressure gradient after interference

From continuity, after interference, it must be true that

$$\int_0^{y_s} dy = \nu \int_0^{Y_s} \frac{dY}{u} = y_s$$

and this equation must be satisfied at all points down the duct. After interference, the pressure gradient was obtained from the duct flow momentum equation

$$\text{i.e. } p' = - \frac{1}{\rho} \frac{dP}{dx} = \frac{\tau_w \cdot s_d}{\rho A_d} - \frac{\dot{m} \cdot \bar{u}_1}{\rho A_d} \frac{dA_d}{dx}$$

$$\text{where } \bar{u}_1 = \frac{\int_0^{y_s} u^2 dy}{\int_0^{y_s} u dy}$$

No basic theoretical changes occur with the energy and turbulent kinetic energy equations, although the change of definition of the variable Z after interference necessitates some alterations to calculated parameters, but these will be discussed more fully in the following section [1.8].

1.8 Internal Flow - Numerical Analysis

A Solution of equations before boundary layer interference

The numerical solution of the internal flow equations contain a number of important differences to the previously described external flow situation. The outer (in this case the centre-line) boundary conditions will be different and the interference point will have to be considered with care.

Before interference the only difference between the internal and external flow calculation procedures lies in the prescribing of the pressure gradient. For the internal case, equation (1.7.4) is used.

$$\text{i.e.} \quad p = \frac{4\nu}{U_s \cdot L} \frac{dR}{dR} \delta + \frac{2\nu b'}{LU_s}.$$

This equation cannot be evaluated at the current station under investigation as, for instance, U_s appears which will only come from the solution of the equation of motion. To combat this possible non-linearity, the pressure gradient parameter is formed from known quantities at the previous station. The derivative $\frac{dR}{dR} \delta$ is formed from information at the previous two stations.

When dealing with internal flows, the formation of "bulk" quantities is generally more meaningful from point of view of comparing results. Thus, a bulk Stanton Number may be defined as

$$St_b = \frac{q_w}{\rho C_p U_b (T_{aw} - T_{ab})}$$

where T_{ab} is the bulk absolute temperature.

The bulk Stanton number may be obtained from the Stanton number based on centre-line velocity and

temperature using relation

$$St_b = \frac{St.L}{L_{ent} \frac{U_{si}}{U_s} - 2.x_h.St}$$

where x_h is the distance from the start of heating.

B Solution of equations after boundary layer interference

Finite difference approximation to equation of motion

Equation (1.7.8) is

$$\frac{\partial Z}{\partial R} = Z^{\frac{1}{2}} \left(B \frac{\partial Z}{\partial Y} + A \frac{\partial^2 Z}{\partial Y^2} \right) + p' \cdot \frac{2\nu}{U_m^3}$$

where $p' = -\frac{1}{\rho} \frac{dP}{dx} s.$

This is treated in a similar way to equation (1.6.1) and the equation again reduces to a tridiagonal matrix form

i.e. $Z_{i-1} + b_i Z_i + c_i Z_{i+1} = d_i$ (1.8.1)

where

$$b_i = \left\{ h_1 h_2 (h_1 + h_2) - Z_i^{*\frac{1}{2}} \cdot \Delta R \left[-2A(h_1 + h_2) + B(h_2^2 - h_1^2) \right] \right\} / \left[Z_i^{*\frac{1}{2}} \cdot \Delta R (B h_2^2 - 2.A.h_2) \right]$$

$$c_i = (2A h_2 - B h_2^2) / (2.A.h_1 + B h_1^2)$$

$$d_i = \left[Z_i^* \cdot h_1 h_2 (h_1 + h_2) + p' \cdot \frac{2\nu}{U_m^3} \cdot h_1 h_2 (h_1 + h_2) \Delta R \right] / \left[Z_i^{*\frac{1}{2}} \cdot \Delta R \cdot (B h_2^2 - 2A h_2) \right].$$

Now providing p' has been evaluated this equation can be solved in a similar way to that described for external flows. The boundary conditions after interference, in the $u \sim y$

system are

$$u = 0, y = 0$$

$$u = U_s, y = y_s$$

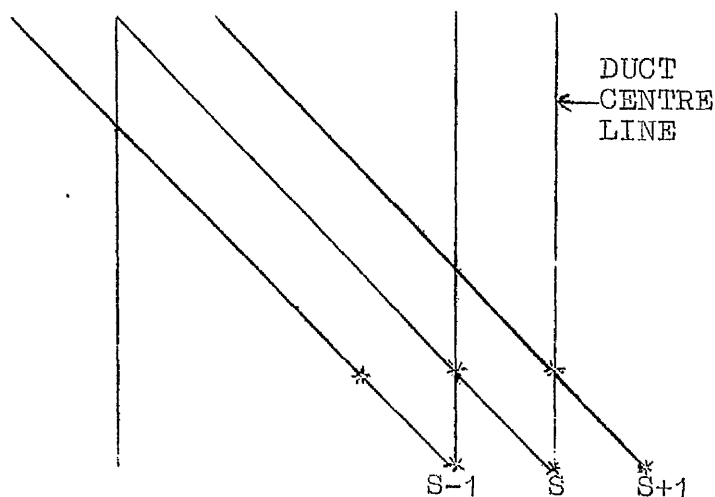
$$\frac{\partial u}{\partial y} = 0, y = y_s$$

and in $Z \sim Y$ system [remembering that Z is now defined by $Z = \left(u/U_m\right)^2$]

$$Z = 0, Y = 0$$

$$Z = Z_s, Y = Y_s$$

$$\frac{\partial Z}{\partial Y} = 0, Y = Y_s$$



OUTER BOUNDARY CONDITION

The general relationships relating Z_i to Z_{i+1} still hold i.e. Eqns. (1.6.7), (1.6.8) and (1.6.9) still hold.

In this case, however, Z_s , the centre-line value of Z , is unknown.

∴ We can write

$$Z_i = \delta_i - \gamma_i Z_{i+1} \quad (1.8.2)$$

where
$$\delta_i = \frac{d_i - \delta_{i-1}}{b_i - \gamma_{i-1}}$$

and
$$\gamma_i = \frac{c_i}{b_i - \gamma_{i-1}} \quad \text{as before.}$$

The general equation (1.8.1), when expressed at the centre-line, gives

$$Z_{s-1} + b_s Z_s + c_s Z_{s+1} = d_s. \quad (1.8.3)$$

But the outer boundary condition is that $\frac{\partial Z}{\partial Y} = 0$.

∴ The ΔY step from "s" to "s + 1" is made the same as that from "s - 1" to "s" and then we can say

$$Z_{s-1} = Z_{s+1}.$$

∴ Equation (1.8.3) becomes

$$Z_{s-1} = \frac{d_s}{1 + c_s} - \frac{b_s}{1 + c_s} Z_s. \quad (1.8.4)$$

But, from equation (1.8.2)

$$Z_{s-1} = \delta_{s-1} - \gamma_{s-1} Z_s. \quad (1.8.5)$$

Combining equations (1.8.4) and (1.8.5) we get

$$Z_s = \frac{\frac{d_s}{1 + c_s} - \delta_{s-1}}{\frac{b_s}{1 + c_s} - \gamma_{s-1}}. \quad (1.8.6)$$

Equation (1.8.6) can now be used to establish the value of Z on the duct centre-line, so giving the first value in the back-substitution using equation (1.8.2).

Recognition of duct centre-line

At every streamwise step, the boundary layer thickness is compared with the local duct half-width. When the boundary layer is equal to or greater than the duct half-width, interference is assumed to have occurred. The local boundary layer thickness at this point is then considered to be coincident with the duct half-width. This may cause an error due to the boundary layer over-

lapping the duct half width but the effects appear to be small. This point will be discussed more fully in the discussion [section 1.11].

Continuity after interference

After interference, there is no need to test for the edge of the boundary layer as the boundary layer thickness in terms of Y , a mass flow parameter, must remain constant and co-incident with the duct centre-line (or the fictitious duct centre-line as the case may be).

$$\text{i.e.} \quad \int_0^{y_s} dy = y_s = \nu \int_0^{Y_s} \frac{dY}{u} .$$

If necessary a constant multiple correction factor is introduced into the velocity profile to ensure this equation is satisfied. This correction factor is small, usually very much less than 1%.

Energy Equation

The interference point for the thermal boundary layers is probably not at the same point as the velocity boundary layers. However, recognition of the thermal interference point is accomplished in the same way as previously described for the motion.

The outer boundary condition after interference is obtained in a similar way as the velocity

$$\therefore \quad T_s = \frac{\frac{d'_s}{1 + c'_s} - \delta'_{s-1}}{\frac{s}{1 + c'_s} - \gamma'_{s-1}} .$$

Turbulent Kinetic Energy Equation

The outer boundary condition for the turbulent kinetic energy is given by

$$q_s = \frac{\frac{d''}{1 + c''} - \delta''}{\frac{b''}{1 + c''} - \gamma''} \cdot$$

1.9 Results and Discussion - External flow experiments and theory

In this section, the experimental results for the six tests performed by the author (denoted by the coding A1...A6) are discussed, together with their associated theoretical predictions. * The experimental results for these tests are tabulated in appendix 2. The following section (1.10.A) includes further theoretical predictions, and are compared with the experiments of Wolfendon [38]. The two tests performed by Wolfendon are denoted by the coding A7 and A8.

Fig. 2 shows the free stream velocity distributions for each of the six tests performed by the author.

A Constant Pressure Gradient Parameters

Friction factor and Stanton number variations with Reynolds number are displayed on fig. 3 for the constant pressure gradient parameter tests (A1, A2 and A3). The friction factors were obtained using Patel's [35] Preston tube calibration. Theoretical predictions using both the mixing length and turbulent kinetic energy turbulence hypotheses are also shown. All three pressure gradient situations are predicted well using either model of turbulence. Fig. 4 shows the variation, with Reynolds number, of the integral properties of the boundary layer, shape factor H and the momentum thickness Reynolds' number R_θ . Predictions using both turbulence hypotheses are given for comparison purposes. The zero and favourable pressure gradient situations are equally well predicted by either method. However the adverse pressure gradient case is less well predicted by the mixing length hypothesis. This is possibly to be expected because of

* N.B. THE EXPERIMENTAL - 85 - RESULTS OF TESTS A1, A2 AND A3 WERE PRESENTED IN THE AUTHORS MSc THESIS. [37]

the non-equilibrium nature of this flow. The adverse pressure gradient case is characterised by the higher values of shape factor and also higher R_θ than either of the other cases, and this observation is well predicted by both theories.

Figs. 5 and 6 illustrate typical velocity and temperature profiles respectively. The velocity profiles are plotted on the dimensionless $u^+ \sim y^+$ basis and one profile for each test case at similar values of Reynolds' number is shown on fig. 5. Agreement is good for the zero and favourable pressure gradient cases, with only fair agreement in the core of the adverse pressure gradient profile. The temperature profiles on fig. 6 are plotted in the dimensionless $t^+ \sim y^+$ form. Agreement between experiment and theory is reasonable.

Two-dimensionality checks on the boundary layer mean flow structure were made using the method described in appendix 4 and are illustrated on fig. 7. Agreement between the points and the lines denotes that the results fit the two-dimensional Von Karman momentum integral equation and valid comparisons can be made with the described two-dimensional theoretical analysis. Fig. 7 (a, b and c) show the two-dimensionality checks for tests A1, A2 and A3 respectively, and they exhibit the required character.

B Departure from two-dimensionality - test A4

As can be seen from fig. 7(d), the boundary layer for test A4 is not two-dimensional and the results of attempting to predict this three-dimensional situation using a two dimensional theory are illustrated on figs.

8 and 9. The departure from two-dimensionality is probably caused by the growth of side-wall boundary layers in this long adverse pressure gradient situation. Only the results of the theory using a turbulent kinetic energy hypothesis is illustrated. From fig. 7(d), the departure from two-dimensionality is seen to become significant at a distance of 0.9 m from the leading edge. Fig. 8 illustrates this further where a poor prediction of the friction factor is obtained from about 0.9 m onward. The effect on Stanton number is not so marked with only a slight over prediction being made in the region downstream of $x = 0.9$ m. The major discrepancies between theory and experiment occur with the integral parameters H and R_θ and these are illustrated on fig. 9. Errors of up to 90% are made in the prediction of the R_θ variation in the three-dimensional region. Although the shape of the H and R_θ variations is predicted, the magnitudes are in poor agreement. It would appear that these integral parameters are much more susceptible to any external influences than the wall parameters, C_f and St . Thus we may tentatively assume that the prediction of H and R_θ will be more difficult than C_f and St and external influences, such as pressure gradient, will have a more significant effect on their calculation. The results for this test are included principally to show the validity of the two-dimensionality checking procedure. The experimental results, being three-dimensional, cannot be justifiably compared with a two-dimensional theory. The predictions are included to show the possible errors which may be incurred by making such assumptions.

C Turbulent boundary layer laminarization

Tests A5 and A6 were concerned with the phenomenon of laminarization of a turbulent boundary layer under the influence of a high favourable pressure gradient. Both tests consisted of an initial adverse pressure gradient to give a thick boundary layer, then a severe acceleration to laminarize the layer, and finally a high adverse pressure gradient region.

The maximum values of the favourable pressure gradient parameter $\left(\frac{2\nu}{U_s^2} \frac{dU}{dx}\right)_s$ for tests A5 and A6 are 6.370×10^{-6} and 7.052×10^{-6} respectively. These values are higher than, for example, the experiments reported by Moretti and Kays [65] where the pressure gradient parameter had a maximum value of 6.0×10^{-6} , and partial laminarization occurred.

Fig. 7 (e and f) show the two-dimensionality of these flows which appear to be satisfactory. Too much reliance on the two-dimensionality check should perhaps not be made in these cases because of the severe changes of velocity gradient which occur. Because of the relatively few number of points which are available to describe the velocity distribution, the exact point at which the pressure gradient changes from adverse to favourable, or vice versa, may be difficult to determine. The consequent effect on the two-dimensionality parameters may be significant.

Fig. 10 shows the friction factor and Stanton number predictions and measurements for test A5. It should be noted that the friction factor results were obtained from Preston tube readings and as such must be

regarded with doubt in the region of high acceleration. The experimental Stanton number results exhibit the characteristic "dip and rise" associated with these high accelerations. The heat transfer coefficient h is also plotted and the high acceleration region is characterised by a rise in heat transfer coefficient. Thus the effect of the high free stream acceleration is to reduce the Stanton number below the fully turbulent value. When the pressure gradient is relaxed and changed to an adverse gradient, the Stanton number immediately rises back to its fully turbulent value. However the dimensional heat transfer coefficient, after falling initially, exhibits a sharp rise when the flow is accelerated.

A number of predictions of this situation are also given on fig. 10. The mixing length method and that based on the turbulent kinetic energy again give similar predictions of friction factor and Stanton number, with that based on the turbulent kinetic energy being only slightly better in that the dip of Stanton number is predicted earlier. Both methods agree very well with the Preston tube results for friction factor, the high acceleration producing a sharp rise in the local value. Removal of the acceleration is accompanied by a rapid fall in friction factor. Neither method manages to predict well the level to which the Stanton number drops under the influence of the acceleration. The effect of the modified sublayer hypothesis of Launder and Jones [10] is shown. From sink-flow boundary layer considerations, the modifications to A_v^+ , the "constant" on the Van Driest mixing length model were made as follows

$$A_v^+ = 26 \quad L \leq 1.9 \times 10^{-3}$$

$$A_v^+ = 11 + 7900L \quad L > 1.9 \times 10^{-3}$$

where L , an acceleration parameter, $= \frac{p}{2} Cf^{-3/2}$.

The effect of this artificial thickening of the sublayer on the calculation of the Stanton number, is to give much better agreement with experiment in the highly accelerated region. The friction factor results agree less well in the same region, but it is quite possible that these experimental values themselves may be larger than the true value because of the doubt surrounding the Preston tube readings.

The variation of shape factor and R_θ are shown on fig. 11. Both methods predict the behaviour of the shape factor H quite well but one point at a distance of 1.45 m from the leading edge has a relatively high value of shape factor and is not predicted by either of the theories. The high shape factor at this point could be explained by a partial laminarization of the boundary layer becoming turbulent again shortly afterwards. If this is true then both theoretical methods are unable to cope with this sudden reversion to laminar flow and back to turbulent again. More experimental evidence was required and this was the purpose of the following test A6. The experimental points of R_θ do not exhibit any apparently discontinuous behaviour such as is evident in the shape factor variation. It is noticeable that the high value of shape factor corresponds to the minimum value of R_θ . The momentum thickness Reynolds' number rises after this minimum, even though there is still a significant favourable pressure gradient being applied.

Good predictions of the R_θ variation were obtained by both turbulence hypotheses, with the mixing length appearing to give slightly better agreement with experiment.*

Detailed predictions and experiments of certain of the velocity and temperature profiles are made on figs. 12 and 13 respectively. The positions chosen for these comparisons are at distances of 1.029m, 1.45m, and 1.6m from the leading edge. The first of these corresponds to the end of the initial portion of adverse pressure gradient, the second is at the point of maximum acceleration and the third is at the end of the accelerating section. For clarity, only predictions using the turbulent kinetic energy method are presented for comparison. The velocity profiles on fig. 12 are plotted as $\left(1 - \frac{u}{U_s}\right)$ vs. $\left(y/\delta^*\right)$, a form of plotting which brings out the shape of the profile. It can be seen from fig. 12 that excellent predictions of the velocity profiles are made at the 1.029 m and 1.6 m positions but a rather poor prediction is made at the point 1.45 m (the point with the high shape factor value) from the leading edge. Similar results are obtained for the temperature profiles on fig. 13 with poor agreement again being obtained at this same point. The temperature profiles were plotted in a similar way to the velocity profiles with the conduction thickness δ^*_t used as the characteristic non-dimensionalizing length.

Figs. 14 to 17 inclusive contain the results of test A6 and the corresponding predictions. Experimental friction factor and Stanton number distributions are shown with a number of theoretical predictions on fig. 14. The friction factor experimental points must again be

Near the leading edge it is evident from fig.10 that the mixing length turbulence model predicts lower values of friction factor than the turbulent kinetic energy method. On fig.11, in the same region, the shape factor predictions are similar. Thus it would be expected that the streamwise variation of R_θ $\left(\text{i.e. } \frac{dR_\theta}{dx} \right)$ would be greater for the turbulent kinetic energy model. This observation is inconsistent with the predictions obtained. This inconsistency can only be due to the build-up of numerical error leading to poor agreement with the two-dimensional momentum integral equation. Alteration of the forward step length ΔR should produce better agreement.

regarded with doubt in the region of high acceleration. However, good predictions of the sharp rise in friction factor, then the severe drop in the strong adverse pressure gradient region, are obtained using both turbulence hypotheses. The modification of Launder and Jones previously described, was used and again it produced significantly lower values of friction factor than the experiment.

The experimental results of Stanton number distribution follow the same trend as in test A5 i.e. the "dip and rise" shape. The heat transfer coefficient again exhibits a rise in the accelerated region, falling away again in the final region of adverse pressure gradient. The "dip and rise" phenomena is predicted quite well by both theoretical methods, but again the minimum value of Stanton number is overpredicted. The Launder and Jones sublayer modification seems too severe in this case as it appears to come into operation at too early a stage.

Because of the rapid changes occurring in these high acceleration tests, the effects of non-linearity of the governing equations was overcome by iterating and the results of such iterations are displayed on fig. 14. Five iterations were carried out on the equation of motion at all stations in the favourable pressure gradient region with little effect on the predicted friction factors and Stanton numbers being obtained. It may thus be concluded that the steps chosen in the accelerated region were adequate and the treatment of the non-linear terms was satisfactory.

Fig. 15 shows the variation of the integral parameters, H and R_θ for test A6. Both theoretical methods give reasonable predictions of the shape factor variation. However the high value of shape factor of 1.725, a point which was evident in the previous test, can again be noticed at a point 1.42m from the leading edge. The following station at 1.57m also exhibits a rather high value of shape factor. The turbulent boundary layer appears to be partially laminarizing at a point approximately 1.35m from the leading edge and returning to a fully turbulent state at about 1.7m. This effect is not predicted by any of the theories. The agreement with experiment of the predictions of the R_θ variation are excellent. There is again no evidence of the behaviour of shape factor around the laminarization point being reflected in the R_θ measurements. *

Figs. 16 and 17 show certain of the profiles of velocity and temperature respectively, with their corresponding predictions using the turbulent kinetic energy method. Four velocity profiles around the laminarization region are illustrated on fig. 16. The first profile shown is at 1.293m from the leading edge and is at the start of the high acceleration. A good prediction of the shape of this profile was obtained. The prediction of the velocity profile at the next station 1.419m along the plate, in the high acceleration region, was not so good. At the start of the adverse pressure gradient section (1.566m) agreement had improved whilst at the final station in the strong adverse pressure gradient region, 1.864m from the leading edge,

The modified sublayer hypothesis of Launder and Jones, whilst having a significant effect on the wall parameter predictions, has a negligible effect on the predictions of H and R_0 . For this reason predictions using this modification are not shown on figs.11 and 15.

excellent agreement is again obtained between prediction and experiment. The temperature profiles shown on fig. 17 have similarities with the velocities in that excellent agreement is obtained before and after the laminarization region, but not so good agreement in the region itself.

1.10 Results and Discussion - External flow theory

In this section, the results of the theory, applied to the experiments of other workers, are discussed, with emphasis being placed on turbulence quantities.

A Comparison with results of Wolfendon [38]

Wolfendon worked on the same apparatus but examined different pressure gradient combinations. He also made detailed measurements of turbulent shear stress and turbulent kinetic energy using single straight and inclined hot wires.

The first comparison, shown on fig. 18, illustrates the ability to predict heated or unheated starting lengths. The tests compared are Wolfendon's tests (1) and (1A) with a severe adverse pressure gradient followed by an accelerating region. The velocity situation was the same in both tests, test (1A) having an unheated starting length. Reasonable predictions were made of the friction factor distributions in this difficult situation. The predictions of Stanton number variation, both with and without the unheated starting length were satisfactory. There was again little difference between the predictions of the turbulent kinetic energy and mixing length methods. It is possible that the slight rise in Stanton number shown in the results is caused by interference of the boundary layer on the tunnel roof with that on the heated floor. (c.f. internal flow results, figs. 44 and 45.)

One of the advantages of the turbulent kinetic energy method over the mixing length is that more turbulence information can be obtained from the solution of the equations. The agreement of this "extra" informa-

tion with experiment gives confidence in the reliability of the turbulence models incorporated in the solution procedure. Accordingly, because of the limited information with regard to turbulence, the mixing length method was not used in the remainder of cases for comparison to be presented in this section.

A detailed examination of Wolfendon's test 2 is now presented with, in addition to the mean flow quantities C_f , St , H and R_θ , the turbulent shear stress, turbulent kinetic energy and eddy diffusivity of momentum compared with experiment at all positions where experimental profiles were available.

Wolfendon's test 2 consisted of a fairly strong adverse pressure gradient followed by strong acceleration and a final adverse pressure gradient region. The favourable pressure gradient was not so high as to produce laminarization.

The predictions of the wall parameters C_f and St are illustrated on fig. 19. An indication as to the position of the particular experimental stations, particularly in relation to the free stream velocity distribution, is shown on fig. 19. Agreement between experiment and theory is very good as far as the friction factor variation is concerned. The Stanton number variation in the accelerated region is predicted less well, a slight rise instead of the observed fall being obtained. The integral parameters H and R_θ are shown on fig. 20. An excellent prediction of the R_θ variation is obtained but, although the general distribution of shape factor is very good, the magnitude of the high

shape factors in the initial strong adverse pressure gradient are underpredicted. Figs. 21, 22 and 23 compare predicted and measured turbulent shear stress profiles plotted against y^+ .

The station numbers and distances from the leading edge should be compared with the free stream velocity distributions on fig. 19 for information as to the local pressure gradient. Where two predictions are given it is because there was not one available at the particular point required for comparison. In these cases, the two predictions either side are displayed.

Fig. 21 shows the predicted and measured profiles of normalized turbulent shear stress for the first four experimental stations i.e. in the strong adverse pressure gradient. As can be seen, the initial agreement of predicted shear stress with experiment is not particularly good, although by the fourth station, agreement is improving. The initial theoretical profile of shear stress is that of a zero pressure gradient and time is required for it to develop to an adverse pressure gradient profile of the required magnitude. Stations 5, 7, 8 and 9 are illustrated on fig. 22. Good agreement between predicted and measured turbulent shear stress profiles is obtained by the fifth station, whilst at the seventh station, at the end of the adverse pressure gradient region, excellent agreement is observed between predicted and measured profiles. Stations 8 and 9 are in the favourable pressure gradient region and an immediate change is both measured and predicted in the shape of the profiles. The slope $\left. \frac{\partial \tau}{\partial y} \right|_{\text{wall}}$ changes sign and the peak magnitude of the shear stress, whilst

still occurring in the mid-boundary layer region, is reduced as the favourable pressure gradient has its effect. Excellent predictions of these effects are made at the eighth and ninth stations. Fig. 23 compares the predictions and measurements at the last 4 stations i.e. 10, 11, 12 and 13. By the tenth station, the favourable pressure gradient has increased and the peak shear stress now occurs at the wall. However, because of the sudden application of this pressure gradient to an adverse situation, the outer boundary layer still maintains the peaking associated with an adverse pressure gradient, although having been reduced in magnitude below the wall value. An excellent prediction of this effect is obtained at the tenth station. By the eleventh station, this outer layer peaking is markedly reduced and in the predicted profile, it has disappeared completely. At the final two stations the shear stress has a very steep slope at the wall, whilst maintaining a long section in the outer layer where the shear stress is practically constant at about $1/10$ th of the wall value. This phenomenon is again well predicted by the theory. There appears to be little evidence in the predicted and measured shear stress profiles that the pressure gradient has changed to adverse over these last two stations.

To summarise, the initial agreement between predicted and measured shear stress profiles is not good. However it is believed that the information obtained from supplying initial profiles which do not agree with experiment, and looking at the distance which must be traversed before agreement is obtained, is of

equal, if not more importance, than supplying the correct initial profile, as generally in a boundary layer prediction situation, no information will be available on initial conditions.

Thus it is apparent, from looking at the shear stress profiles, that agreement is obtained shortly after the fifth station i.e. about 0.85m from the leading edge.

Figs. 24, 25 and 26 compare predicted and measured profiles of turbulent kinetic energy at the same twelve stations as were considered previously. It is noticeable on fig. 24 that the initial theoretical profiles of turbulent kinetic energy are much smaller in magnitude than the measured values. The two profiles are approaching each other, however, and by the seventh station, on fig. 25, reasonable agreement is starting to be obtained. The favourable pressure gradient has started to take effect by the eighth station and the peak magnitude of the turbulent kinetic energy starts to fall under the influence of the pressure gradient. Good agreement between measurements and predictions is obtained at the eighth and ninth stations. Thus from considerations of turbulent kinetic energy, it would appear to take longer for agreement between predicted and measured profiles to be reached than was the case with the shear stress predictions. On fig. 26, by the tenth station, the general magnitude of the turbulent kinetic energy has fallen somewhat and this is well borne out by the theory. The last three stations (11, 12 and 13) show further evidence of turbulence being damped out, and the turbulent

kinetic energy profiles at these stations are well predicted both from shape and magnitude considerations. Predicted and measured profiles of eddy diffusivity of momentum are compared on figs. 27, 28 and 29. The first four stations on fig. 27 show that the assumption of a constant eddy diffusivity in the outer layer is reasonable, only becoming unrealistic, naturally, at the very edge of the boundary layer. Under the influence of the adverse pressure gradient, the eddy diffusivity in the outer layer continues to increase and, on fig. 28, at the seventh station, the predicted eddy diffusivity is significantly higher than the measured values. The favourable pressure gradient then tends to reduce the predicted level and quite good agreement is obtained at the tenth and eleventh stations on fig. 29. The final two stations on fig. 29 are poorly predicted. The possible sources of error involved in measuring the eddy diffusivity must be borne in mind before any conclusions can be drawn from these results.

Fig. 30 shows a comparison between the measured and predicted balance of turbulent kinetic energy at station 9, 1.438m from the leading edge, in the region of favourable pressure gradient. The general agreement between the predicted and measured turbulent kinetic energy transport quantities is good, bearing in mind the possible sources of error inherent in the measurement of these quantities. These errors are discussed by Wolfendon [38].

The main point for improvement in these predictions would appear to be a better description of the inlet

profile. The initial zero pressure gradient shear stress distribution is quite different from the measured profile. In a bid to improve this, the modified Van Driest hypothesis of Patankar [4] was tried such that shear stress variation in the near wall layer was accounted for according to the relation

$$\frac{\tau}{\tau_w} = 1 + p^+ y^+$$

where $p^+ = \mu/\tau_w^{3/2} \rho^{1/2} \frac{dp}{dx}$.

In this situation, use of this method produced no significant difference in the initial shear stress profile.

The initial turbulent kinetic energy distribution used to start the theoretical procedure lay well below the observed values, so the observed values were actually used as the starting point for the theory. This again had no effect as the turbulent energy was quickly reduced to its previous values. It appeared that a change in certain of the constants would be necessary to conserve the energy at its initial level. In view of the doubt which must surround the experiment in the neighbourhood of the leading edge, it was felt more evidence was needed before any constant changes were justified. *

B Comparison with the results of Schubauer and Klebanoff [21]

Fig. 31 shows the predictions obtained for C_f , H and R_θ variations for this standard test run (cf. Stanford [21]).

Excellent agreement between predictions and measurements is obtained except in the region approaching separation where the boundary layer approximations are invalid.

Although the discrepancies between experiment and theory near the leading edge have been explained in terms of the theory, the experimental results themselves must be regarded with some doubt in this thin boundary layer region. Errors in probe alignment, for example, will have a greater effect on shear stress and turbulent kinetic energy measurement in this region than in the thicker boundary layers which develop downstream. Wolfenden quotes typical errors in shear stress and turbulent kinetic energy measurement of 22% caused by a 4° error in probe alignment at the first measuring station.

No indication is given from the experimental shear stress profiles of fig.21, that the peak shear stress is occurring away from the wall and that the shear stress structure is characteristic of an adverse pressure gradient, although this has been assumed in the previous discussion of the results. If it were to be the case that the maximum levels of experimental shear stress shown on fig.21 are the values at the peak of the profile then it would appear that they have the structure of a severe adverse pressure gradient but it is doubtful whether this is possible in such a small development distance. This is probably due to measurement error and it would have been expected that the experiments would have a distribution typical of a zero pressure gradient with $\tau/\tau_w \approx 1$ near the wall.

C Comparison with results of Klebanoff [42]

One of the standard works as far as the measurement of turbulence quantities in a boundary layer is concerned is that of Klebanoff who performed his experiments in an artificially thickened boundary layer in zero pressure gradient. Among the turbulence quantities he measured were turbulent shear stress, turbulent kinetic energy and a balance of the turbulent energy transport quantities. Fig. 32(a) shows the comparison between theory and experiment of the mean velocity distribution plotted as a velocity defect. The mean velocity distribution is plotted on fig. 32(b) with the near wall region inserted at an expanded scale. As can be seen good predictions of these mean quantities were obtained. Fig. 32(c) shows the distribution of turbulent shear stress and turbulent kinetic energy across the boundary layer, together with their corresponding theoretical predictions. Good predictions of these turbulent quantities were obtained with, if anything, a slight overprediction of the turbulent kinetic energy and a slight underprediction of the turbulent shear stress being obtained. Fig. 33(a) shows the comparisons, in the near wall region, between the predicted and measured direct viscous dissipation and turbulent energy production. The predictions are in excellent agreement with the experimental values. Production, viscous diffusion and dissipation in the near wall region are plotted on fig. 33(b) with quite good agreement being obtained. The regions further away from the wall are plotted on fig. 34. The comparison between predicted and measured dissipation (fig. 34(a)) shows

that the size of the dissipation in this outer region has generally been overpredicted; consequently, the turbulent diffusion has been underpredicted, compared with experiment on fig. 34(b).

Comparison of the advection term in the outer layer is very good. Thus, on the whole, good agreement is obtained with the turbulence measurements of Klebanoff.

The fact that in the outer layer, the production and dissipation are much closer in magnitude than Klebanoff's measurements, suggests that the solution is tending more towards the "mixing-length" assumption than is apparent from experiment. i.e. The energy locally produced is locally dissipated.

D Effect of outer layer constant changes

Fig. 35 illustrates the effect of different values of the outer layer constant, C_5 on shape factor and friction factor predictions.

A Cole's correlation is provided for comparison purposes.

Three values of the constant were tried

0.5, 0.75 and 0.9.

The value of 0.5 underpredicted the friction factors whilst overpredicting the shape factor. There did not appear to be a great deal of difference between values of 0.75 and 0.9 but generally 0.9 was used for prediction purposes, being slightly better on friction factor prediction.

1.11 Results and Discussion - Internal Flow Theory

The duct used in the experiments consisted of two flat plates, width 0.82m, arranged initially as a parallel passage (Marriott [43]) and then as a diverging passage (Ellison [44]) giving a 1.3 area ratio from inlet to outlet. The separation distance was 0.051m in the parallel case, and varying from 0.051m to 0.153m over 3.94m. The sides of the passage were diverged by 5mm on each side to allow for the growth in side-wall boundary layers.

For further details of the apparatus and experiments, reference should be made to refs. [43], [44] and [45]. From the total head readings, it is evident that the interference point for both geometries occurs at $\frac{x}{2L}$ of about 15.

Figs. 36 and 37 show the comparisons between predicted and measured displacement and momentum thickness and shape factor for the parallel duct and the diverging case respectively. The results are encouraging and show that the theory is capable of reproducing in the parallel case, the unexpected way in which the parameters are observed to approach their fully developed values. This "overshoot" in approach occurs in the region where the shear stress is readjusting from a favourable pressure gradient boundary layer profile (in the parallel passage case) to the linear fully developed profile.

Results obtained for other Reynolds' numbers were equally as good. However it was found necessary to use different values for the constant C_5 (equation 1.5.32) for the two geometries. This constant exerts a strong influence on the interference position which, in turn,

has a governing effect on the subsequent flow development. The effect of changes in this constant in free boundary layer flows has already been discussed in section (1.10.D). It was found necessary to use value of 0.9 for the parallel passage (the same as for the free boundary layer flows) and 0.5 for the diverging passage.

Figs. 38 and 39 compare wall shear stress for several Reynolds' numbers for the parallel and diverging cases respectively. Good agreement is obtained in both cases with no guide to the position of interference being shown by theory or experiment.

Corresponding friction factor variations are shown on figs. 40 and 41 and the curves are only slightly dependent on Reynolds' number. For this reason, the scales have been shifted to separate the results for different Reynolds' numbers. The friction factors are based on the centreline velocity which is the usual practice in free boundary layer situations. For one of the diverging cases on fig. 41, the well-known empirical expression of Ludweig and Tillmann [41] is shown for comparison and is seen to give a reasonable approximation to the measured and predicted results. The interference point is recognisable by a gentle rise in friction factor on fig. 40 for the parallel case. This position and behaviour is borne out by the theory. A much more noticeable interference position occurs in the diverging situation (fig. 41) with quite a sharp increase in friction factor after interference. Also on fig. 41, the effect of changing the outer layer constant on the friction factor prediction is shown with an increase in value from

0.5 to 0.6 moving the interference point upstream and overpredicting the subsequent friction factor distribution. The results of a prediction using the standard mixing length procedure is also illustrated on fig. 41. Poor agreement is obtained with measured values of friction factor. Fig. 42 shows the ratio of the centreline to bulk velocity for three selected cases. Due to the changes of shape which take place in the velocity profile, the centreline velocity first rises then falls relative to the bulk velocity and the same behaviour is apparent in the theoretical prediction. Whilst the agreement here is satisfactory in the parallel wall passage, it is not so good in the diverging case, although the correct trend is obtained.

The predicted shear stress distributions show some interesting features in the parallel-wall duct. Some shear stress profiles calculated at various distances down the parallel duct are shown on fig. 43. In the initial region of the flow, the profiles have the typical form of a favourable pressure gradient boundary layer lying below the linear fully-developed distribution. Interference appears to cause the shear-stress profile to lie above the line, asymptoting to the line as distance increases. Measured and predicted Stanton numbers based on the bulk velocities are shown on figs. 44 and 45. The order of agreement in the diverging case is not very satisfactory after the interference has occurred. The rise in Stanton number which is apparent in the experimental results does take place in the prediction method but at a larger distance downstream. Adjustments of certain of the constants were tried but did not produce significant improvement.

1.12 Future Work - Turbulent Boundary Layer Flows

1. A problem which may face designers of turbomachine blades is that, given an overall pressure drop or rise, what is the optimum free stream velocity distribution to give, for example, minimum drag and maximum heat transfer? The examination of this problem, both experimentally and theoretically, should provide much useful information.
2. Although iterations were performed in the numerical procedure when calculating the highly accelerated external boundary layer situations, no check was made on the errors introduced by the linearizing of the equations when applied to internal flows. The non-linearity associated with the pressure gradient parameter, in addition to the non-linearities present in the equations, should be investigated, particularly in the region before boundary layer interference.
3. The incorporation of the mixing length outer layer turbulence model (based on displacement thickness) into the Prandtl-Kolmozorov solution procedure for the prediction of internal flows will produce some evidence as regards the reliability of the current technique where an integral of turbulent kinetic energy is used as the viscosity determining velocity scale in the outer layer.
4. Whilst the one-equation model of turbulence described in this thesis has been reasonably successful when applied to certain test situations, the degree of applicability would appear to be limited. The fact that changes have to be made in the outer layer constant for differing internal flow geometries does not enable one to place a great deal of reliance on the description of the turbulence.

in the outer part of the boundary layer. An initial attempt to rectify this situation might be to include a constant value of turbulence length scale l_μ in the outer layer, rather than the constant eddy viscosity which has been used up to the present. This should result in a decaying of the eddy viscosity as the edge of the boundary layer (or the centre-line of the duct) is approached. The importance of accurately predicting the interference point for the internal flows should then be lessened and the effect of the outer part of the boundary layer on the wall parameters will be reduced.

5. Greater generality of the solution procedure would be achieved if allowance were made for the transport of turbulence length scale, i.e. describe the length scale variation by means of a differential equation rather than the algebraic description which is used at present. A number of ideas have been suggested as to the actual nature of the dependent variable of such an equation, with, perhaps, the use of turbulent kinetic energy dissipation, ϵ , being among the most popular.

SECTION 2

RECIRCULATING FLOWS

2.1 Description of Section

This section is concerned with those flows where there is no predominant direction of flow and derivatives of velocity, temperature, etc., may be of equal importance in any direction. The basis of the theory and the use of an "upwind-difference" scheme in the solution procedure is discussed.

The calculations are applied to three distinct situations

- (i) Low-speed laminar combined natural and forced convection.
- (ii) Turbulent flow through a rotating radial turbomachine.
- (iii) Turbulent flow over a step.

The results in all three cases are compared with experiment. Cases (ii) and (iii) necessitated the incorporation of a model to account for the effects of turbulence and the results and implications of this model are discussed.

2.2 Introduction and Literature Survey

In addition to the description of the turbulence, the numerical analysis problems associated with the solution of the elliptic equations of two-dimensional viscous motion are by no means trivial. The possible high degree of non-linearity in the equations has perhaps contributed to the diversity of solution procedures which numerical analysts and engineers are constantly developing to solve elliptic equations in general. One of the major research groups in this field is at Imperial College, London, and the publication of the volume by Gosman et al [46] has been a significant stimulating factor in the study of such flows. This work highlighted the importance of taking "upwind differences" when modelling the convective terms in the transport equations, a process which was investigated and adopted in the development of the methods described in this thesis. Consideration was given to the incorporation of a matrix inversion technique developed by Benson et al [47] but a relaxation method was felt to have the advantage. This point is discussed in section (2.9).

In order to develop the computational techniques, the physical problems of turbulent flows were removed by considering constant viscosity laminar flow. An important problem chosen for these initial investigations was that of combined natural and forced convection. It was felt that this combined effect was more prominent in low-speed laminar flows, justifying the choice of problem. Having developed the solution procedure, the width of applicability was increased to cope with the flow through

a rotating radial turbomachine under various flow conditions. The flow rates and Reynolds' numbers for these cases were sufficiently high to invalidate the assumptions of laminar flow. The incorporation of a simple model of turbulence into the solution procedure, in order to account for these high Reynolds' number effects, was undertaken. Finally the implications of the chosen model of turbulence were studied with application to situations where more experimental data was available, namely that of the separation and reattachment of flow over a step.

Buoyancy forces may significantly affect the forced convection heat transfer in a number of practical situations. For example in high pressure boilers and in reactor cooling channels, with large temperature differences present, these effects may give rise to departures from the unheated flow pattern. This behaviour of the flow, in turn, causes significant errors if forced convection predictions are used.

Almost all of the previous theoretical studies have considered a forced convection situation in which the velocity profile was modified by the influence of the buoyancy forces, but in few cases was the study carried through to include flow reversal. Rao and Morris [48] considered a fully developed situation in a parallel wall channel and showed that the heat transfer with downward flow was reduced as the Rayleigh number increased. Acrivos [49] considered boundary layer solutions using profile assumptions and established limits for the parameter Gr/Re^2 outside which only one of the two

mechanisms would predominate. Gunness and Gebhart [50] describe a wedge flow solution and gave particular attention to the separation wedge case which was affected by buoyancy forces. Experimental studies were carried out by Brown and Gauvin [51] on upward and downward flow in pipes. They showed that with a downward turbulent flow the heat transfer increased with Rayleigh number - a contrary effect to that observed in laminar flow. They also pointed out the rapid transition to turbulence caused by the instability of the situation. Hatton et al [52] experimented with flows over horizontal cylinders and showed that with downward flow at the fixed Rayleigh number, the heat transfer first decreased then increased as the Reynolds' number increased. This, of course, was due to the flow change from upward by natural convection to downward by forced convection. Hall and Price [53] showed that heat transfer from a vertical plate by combined forced and free turbulent convection improves when the two components oppose each other, contrasting with the opposite effect which occurs in laminar convection. Byrne and Ejiogu [54] measured the heat transfer coefficient in upward flow in a vertical pipe, and showed a large decrease in the values expected for a horizontal pipe under certain conditions. A criteria was established for the influence of natural convection effects by considering the effect of buoyancy forces on turbulence production in the pipe. Transient flow solutions originated with the work of Fromm and Harlow [58] who investigated the development of a vortex street. Transient free convection problems have received attention

recently. Kettleborough [55] describes a numerical study relating to transient laminar free convection between two heated vertical plates. A number of different techniques for dealing with the time-dependent terms are considered, with a simple explicit treatment of the time-dependent term, in spite of its stability limitations, being adjudged the most promising. Szekely and Todd [56] studied theoretically and experimentally, transient laminar natural convection in a rectangular cavity. They used a combination of an alternating direction implicit variation of the Crank and Nicholson method for the vorticity transport equations, and successive over-relaxation for integration of the stream function equation. Churchill and Wilkes [57] studied the steady state and transient behaviour of fluids contained in rectangular cavities using an alternating direction implicit method.

Although the governing equations of free convection are the same as those of combined free and forced convection, all the theoretical analyses, for both the steady and transient solution of such equations, have only been concerned with the free convection situation. The important practical problem of combined natural and forced convection has received little attention from these recently developed solution procedures for solving such types of equations.

For many years the solution of the governing equations of turbomachinery have involved major limitations, with, almost without exception, the analysis being confined to inviscid flows. A number of workers have included boundary layer prediction methods in analyses of

turbomachine flows (e.g. Moore [63]) but these have generally been used in conjunction with inviscid calculations of the main flow. The author is aware of no solution procedure involving a numerical solution of the governing elliptic equations of fluid motion which includes the important effects of viscosity and turbulence.

At U.M.I.S.T., turbomachinery research has centred around radial machines. Flow visualization techniques have been developed whereby quantitative information can be obtained with regard to the flow in the rotating blade passages. These techniques are described by Benson et al [47] and Herath [64]. In addition to the experimental work, inviscid solution procedures (e.g. ref. [47]) have been developed. The main objects of the viscous solution procedure described in this work were to establish the effects of viscosity in predicting certain flow configurations and to assess the degree of success which could be obtained by incorporating a simple model to account for the effects of turbulence.

The flows in the blade passages, whilst not at first sight resembling those of combined natural and forced convection, have basic similarities in the structure of the governing equations. The solution procedure was originally developed for a cartesian coordinate system with body forces caused by buoyancy effects. These equations are very similar to the transformed polar equations of a rotating coordinate system, with body forces, in this case, due to the centrifugal and Coriolis accelerations. Thus, whilst two totally different problems

appear to have been investigated, the differences only amount to a change in geometry between the systems.

2.3 Nomenclature - Combined natural and forced convection

| | |
|--|---|
| C | Specific heat. |
| C _f | Friction factor $\left[= \frac{\tau_w}{\frac{1}{2}\rho_0 U^2} \right]$. |
| C _{ω, ψ, θ} | Leading diagonal of coefficients of equivalent matrices. |
| g | Acceleration due to gravity. |
| Gr | Grashof number $\left[= \frac{T_1 - T_0}{T_0} \frac{g l^3}{\nu^2} \right]$. |
| h | Local heat transfer coefficient. |
| h _a | Mean heat transfer coefficient. |
| k | Thermal conductivity. |
| l | Length of heated patch. |
| Nu _a | Mean Nusselt number $\left[= \frac{h_a l}{k} \right]$. |
| P | Pressure. |
| Pr | Prandtl number. |
| Re | Reynolds' number $\left[= \frac{U l}{\nu} \right]$. |
| R _{1, 2, 3} | Relaxation factors. |
| St | Stanton number $\left[= \frac{h}{\rho_0 C U} \right]$. |
| t | Time. |
| T | Local absolute temperature. |
| T ₀ | Ambient absolute temperature. |
| T ₁ | Absolute temperature of heated patch. |
| U | Characteristic inlet velocity. |
| u | Component of velocity in x direction. |
| v | Component of velocity in y direction. |
| x, y | Coordinate system directions. |
| α | Thermal diffusivity. |

| | |
|----------|-----------------------------|
| θ | Dimensionless temperature. |
| ν | Kinematic viscosity. |
| ρ | Local density. |
| ρ_0 | Ambient density. |
| τ_w | Wall shear stress. |
| ϕ | General dependent variable. |
| ψ | Stream function. |
| ω | Vorticity. |

Suffices

A prime denotes a dimensionless variable.

| | |
|------|--|
| n | Normalised variable. |
| m | Maximum value |
| exit | At the exit of the system. |
| * | "Known" quantity with respect to time. |
| s | At the start of the heated patch. |
| w | At the wall. |

2.4 Theory - Combined Natural and Forced Convection

A Basic equations - manipulations and non-dimensionalizing

Certain simplifying assumptions were applied to the basic Navier-Stokes equations.

These were:-

(i) The motion is two-dimensional.

(ii) The fluid is incompressible in the sense that the motion does not cause density variation and also that the density variations do not affect the motion except through the buoyancy force.

(iii) All other physical properties are assumed constant.

With these restrictions, the equations become

Momentum - in the x direction

$$\frac{\partial u}{\partial t} + u \frac{\partial u}{\partial x} + v \frac{\partial u}{\partial y} = - \frac{1}{\rho_0} \frac{\partial P}{\partial x} + g \left(\frac{\rho - \rho_0}{\rho_0} \right) + \nu \left(\frac{\partial^2 u}{\partial x^2} + \frac{\partial^2 u}{\partial y^2} \right) \quad (2.4.1)$$

- in the y direction

$$\frac{\partial v}{\partial t} + u \frac{\partial v}{\partial x} + v \frac{\partial v}{\partial y} = - \frac{1}{\rho_0} \frac{\partial P}{\partial y} + \nu \left(\frac{\partial^2 v}{\partial x^2} + \frac{\partial^2 v}{\partial y^2} \right) \quad (2.4.2)$$

Continuity

$$\frac{\partial u}{\partial x} + \frac{\partial v}{\partial y} = 0. \quad (2.4.3)$$

Energy (temperature)

$$\frac{\partial T}{\partial t} + u \frac{\partial T}{\partial x} + v \frac{\partial T}{\partial y} = \alpha \left(\frac{\partial^2 T}{\partial x^2} + \frac{\partial^2 T}{\partial y^2} \right) \quad (2.4.4)$$

Introducing a stream function ψ such that

$$u = \frac{\partial \psi}{\partial y} \quad (2.4.5)$$

$$\text{then from continuity (eqn. 2.4.3), } v = - \frac{\partial \psi}{\partial x} \quad (2.4.6)$$

Also introducing vorticity ω defined by

$$\omega = \frac{\partial v}{\partial x} - \frac{\partial u}{\partial y} . \quad (2.4.7)$$

Thus, substituting eqns. (2.4.5), (2.4.6) and (2.4.7) in eqns. (2.4.1) and (2.4.2) and eliminating the pressure gradient term by differentiating equation (2.4.1) with respect to y , equation (2.4.2) with respect to x and subtracting equation (2.4.2) from (2.4.1) yields

$$\frac{\partial \omega}{\partial t} + \frac{\partial \psi}{\partial x} \frac{\partial \omega}{\partial y} - \frac{\partial \psi}{\partial y} \frac{\partial \omega}{\partial x} = \frac{\partial}{\partial y} \left[g \left(\frac{\rho - \rho_0}{\rho_0} \right) \right] - \nu \left(\frac{\partial^2 \omega}{\partial x^2} + \frac{\partial^2 \omega}{\partial y^2} \right) .$$

The equations are non-dimensionalized by the following substitutions.

Let U be a characteristic velocity, e.g. the inlet velocity, and ℓ be a characteristic length, e.g. the length of the heated patch, and put $y' = y/\ell$, $x' = x/\ell$, $\psi' = \psi/U\ell$.

$$\psi_n = \text{normalized value of } \psi' = \frac{\psi'}{\psi_m'}$$

where ψ_m' is the maximum value of ψ' at the inlet

$$\omega' = \frac{\omega \ell}{U} .$$

$$\text{Dimensionless temperature } \theta = \frac{T - T_0}{T_1 - T_0}$$

$$\text{therefore } \frac{\rho - \rho_0}{\rho_0} = - \left(\frac{T - T_0}{T_0} \right) = - \theta \left(\frac{T_1 - T_0}{T_0} \right) .$$

$$\text{Dimensionless time } t' = t\ell/U.$$

$$\text{Defining Reynolds number } Re = \frac{U\ell}{\nu}$$

$$\text{and Grashof number } Gr = \frac{T_1 - T_0}{T_0} \cdot \frac{g\ell^3}{\nu^2} .$$

Omitting the primes for clarity, the equations then become

$$\frac{\partial \omega}{\partial t} + \psi_m \frac{\partial \psi}{\partial y} \frac{\partial \omega}{\partial x} - \psi_m \frac{\partial \psi}{\partial x} \frac{\partial \omega}{\partial y} = \frac{Gr}{Re^2} \frac{\partial \theta}{\partial y} + \frac{1}{Re} \left(\frac{\partial^2 \omega}{\partial x^2} + \frac{\partial^2 \omega}{\partial y^2} \right) \quad (2.4.8)$$

$$\omega = - \psi_m \left(\frac{\partial^2 \psi}{\partial x^2} + \frac{\partial^2 \psi}{\partial y^2} \right) \quad (2.4.9)$$

$$\frac{\partial \theta}{\partial t} + \psi_m \frac{\partial \psi}{\partial y} \frac{\partial \theta}{\partial x} - \psi_m \frac{\partial \psi}{\partial x} \frac{\partial \theta}{\partial y} = \frac{1}{Re \cdot Pr} \left(\frac{\partial^2 \theta}{\partial x^2} + \frac{\partial^2 \theta}{\partial y^2} \right). \quad (2.4.10)$$

These equations form a system of three coupled non-linear elliptic partial differential equations with dependent variables θ , ψ and ω and independent variables x , y and t .

It should be noted that the unsteady terms, $\frac{\partial \omega}{\partial t}$ and $\frac{\partial \theta}{\partial t}$, have been included for completeness. The solution procedure was in fact developed using the steady state equations where these two terms were absent. Only when the numerical techniques had been satisfactorily determined, were the unsteady terms included.

B Boundary Conditions

For the solution of elliptic P.D.E.'s, boundary conditions must be specified on all four sides of the solution domain indicated on fig. 46.

It is fairly simple to specify the boundary conditions at inlet and on each side of the domain. At the exit, however, the situation is not so straightforward. It was chosen to assume that the exit plane was sufficiently distant for the curvature of the streamlines and the decay rate of the temperature profile to be small and negligible. The choice of a uniform inlet velocity and a particular streamline parallel to the wall was intended to be an

approximation to boundary layer flow.

The original boundary conditions used were

$$\text{at } y = 0: \psi_n = \frac{\partial \psi_n}{\partial y} = 0$$

$$\theta = 1 \text{ on the heated patch}$$

$$\theta = 0 \text{ over the remainder}$$

$$\text{at } y = y_m: \psi_n = 1, \frac{\partial \psi_n}{\partial y} = \frac{1}{y_m}, \theta = 0$$

$$\text{at } x = 0: \psi_n = \frac{y}{y_m}, \theta = 0$$

$$\text{at } x = x_{\text{exit}}: \frac{\partial^2 \psi_n}{\partial x^2} = 0, \frac{\partial \theta}{\partial x} = 0.$$

This latter boundary condition was changed to see the effect on the solution and this will be discussed in section [2.10.A].

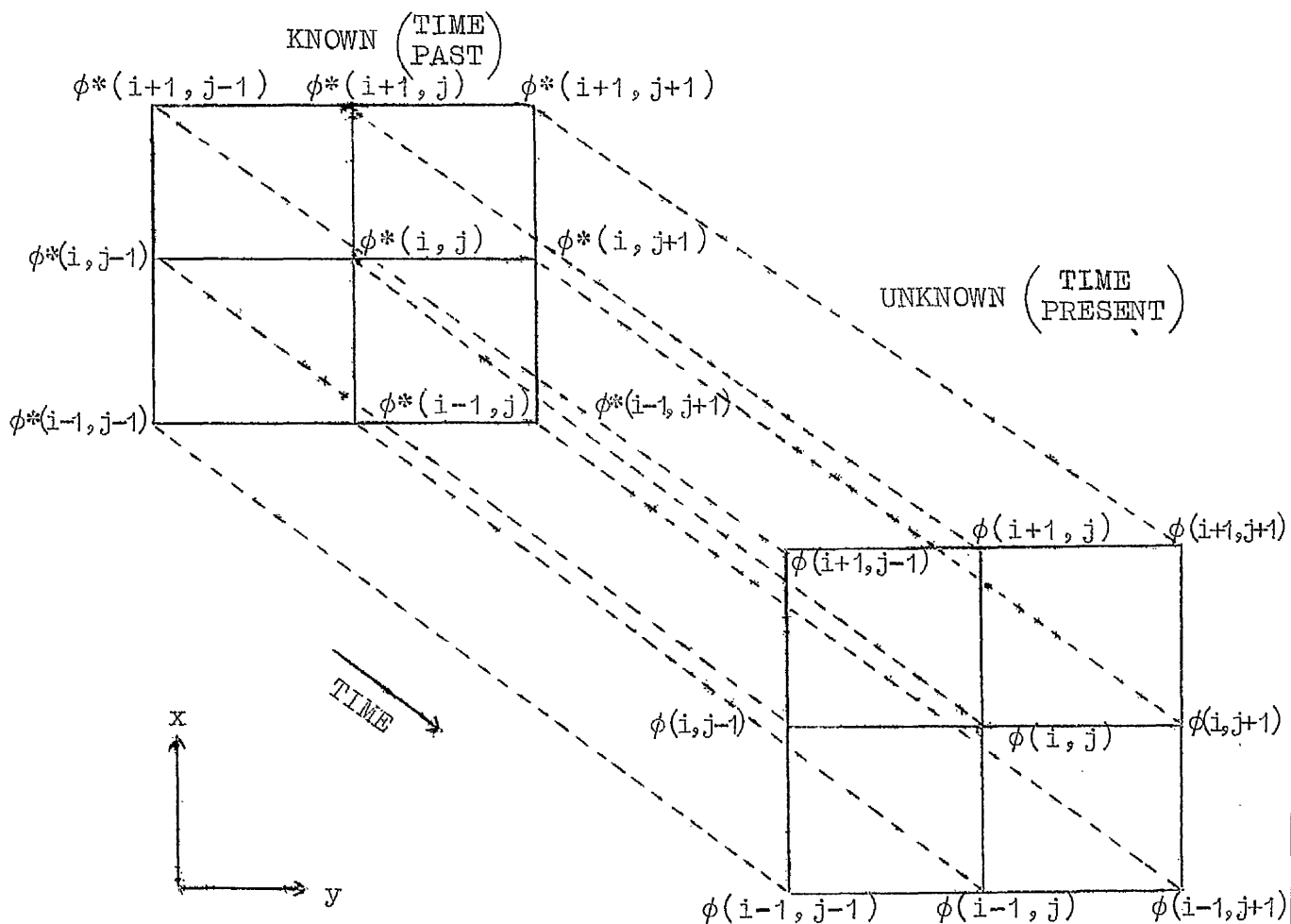
The buoyancy force was changed in sign for upward and downward flow, while for horizontal flow the buoyancy term in equation (2.4.8) was altered to $\left(\frac{Gr}{Re^2} \cdot \frac{\partial \theta}{\partial x}\right)$.

C General finite difference approximations

The conversion of the partial differential equations into algebraic equations was accomplished by using central, 3-point truncated Taylor series expansions for the second derivatives, whilst using a 2-point "upwind-difference" formulation for the first derivatives.

The unsteady terms $\frac{\partial \omega}{\partial t}$ and $\frac{\partial \theta}{\partial t}$ were represented by a two-point backward difference formula, i.e. backward in terms of time.

Solution of the resulting non-linear algebraic equations was obtained by means of a relaxation technique.



In terms of the above rectangular mesh, derivatives are expressed generally as

$$(i) \quad \frac{\partial \phi}{\partial x} \doteq (a), \frac{\phi(i+1, j) - \phi(i, j)}{\Delta x}$$

$$\text{or } (b), \frac{\phi(i, j) - \phi(i-1, j)}{\Delta x}$$

depending on the local flow direction at point (i, j) .

If the x component of velocity at point (i, j) is from point $(i+1, j)$, then the "upwind" expression (a) is used to represent $\frac{\partial \phi}{\partial x}$. On the other hand, if the same component of velocity is in the opposite direction, i.e. from point $(i-1, j)$, then the "upwind" expression in this case would be formulation (b).

A similar argument holds for the derivative $\frac{\partial \phi}{\partial y}$.

where $\frac{\partial \phi}{\partial y} \doteq$ either (a) $\frac{\phi(i, j+1) - \phi(i, j)}{\Delta y}$

or (b) $\frac{\phi(i, j) - \phi(i, j-1)}{\Delta y}$.

The component of velocity in the y direction must be evaluated to enable the above choice to be made. N.B. in determining the local flow direction, the first derivatives of ψ were obtained from a central difference expression $\left[\text{e.g. } \frac{\partial \psi}{\partial y} = \frac{\psi(i, j+1) - \psi(i, j-1)}{2\Delta y} \right]$.

The effect of this formulation technique is to ensure that all the coefficients of the dependent variable ϕ at point (i, j) have the same sign and consequently all add together. The equivalent matrix of coefficients of ϕ is thus diagonally dominant, an important criterion in securing stability of the iterative procedure.

$$(ii) \quad \frac{\partial^2 \phi}{\partial x^2} \doteq \frac{\phi(i+1, j) - 2\phi(i, j) + \phi(i-1, j)}{\Delta x^2}$$

$$\text{or } \frac{\partial^2 \phi}{\partial y^2} \doteq \frac{\phi(i, j+1) - 2\phi(i, j) + \phi(i, j-1)}{\Delta y^2}$$

$$(iii) \quad \frac{\partial \phi}{\partial t} \doteq \frac{\phi(i, j) - \phi^*(i, j)}{\Delta t}$$

where the starred value signifies a known quantity.

D Finite difference approximations to governing equations

Incorporating the above general expressions into the particular equations (2.4.8), (2.4.9) and (2.4.10) produces, respectively

$$\begin{aligned}
& \frac{\omega(i, j) - \omega^*(i, j)}{\Delta t} \\
& + \frac{\psi_m [\psi(i, j+1) - \psi(i, j-1)]}{2\Delta y} \cdot \frac{\left[\begin{array}{c} \omega(i+1, j) - \omega(i, j) \\ \text{or} \\ \omega(i, j) - \omega(i-1, j) \end{array} \right]}{\Delta x} \\
& - \frac{\psi_m [\psi(i+1, j) - \psi(i-1, j)]}{2\Delta x} \cdot \frac{\left[\begin{array}{c} \omega(i, j+1) - \omega(i, j) \\ \text{or} \\ \omega(i, j) - \omega(i, j-1) \end{array} \right]}{\Delta y} \\
& = \frac{Gr}{Re^2} \frac{[\theta(i, j+1) - \theta(i, j-1)]}{2\Delta y} \\
& + \frac{1}{Re} \left\{ \left[\frac{\omega(i+1, j) - 2\omega(i, j) + \omega(i-1, j)}{\Delta x^2} \right] \right. \\
& \left. + \left[\frac{\omega(i, j+1) - 2\omega(i, j) + \omega(i, j-1)}{\Delta y^2} \right] \right\} \quad (2.4.11)
\end{aligned}$$

$$\begin{aligned}
\omega(i, j) = - \psi_m \left\{ \left[\frac{\psi(i+1, j) - 2\psi(i, j) + \psi(i-1, j)}{\Delta x^2} \right] \right. \\
\left. + \left[\frac{\psi(i, j+1) - 2\psi(i, j) + \psi(i, j-1)}{\Delta y^2} \right] \right\} \quad (2.4.12)
\end{aligned}$$

$$\begin{aligned}
& \frac{\theta(i, j) - \theta^*(i, j)}{\Delta t} \\
& + \frac{\psi_m [\psi(i, j+1) - \psi(i, j-1)]}{2\Delta y} \cdot \frac{\left[\begin{array}{c} \theta(i+1, j) - \theta(i, j) \\ \text{or} \\ \theta(i, j) - \theta(i-1, j) \end{array} \right]}{\Delta x} \\
& - \frac{\psi_m [\psi(i+1, j) - \psi(i-1, j)]}{2\Delta x} \cdot \frac{\left[\begin{array}{c} \theta(i, j+1) - \theta(i, j) \\ \text{or} \\ \theta(i, j) - \theta(i, j-1) \end{array} \right]}{\Delta y} \\
& = \frac{1}{Re \cdot Pr} \left\{ \left[\frac{\theta(i+1, j) - 2\theta(i, j) + \theta(i-1, j)}{\Delta x^2} \right] \right. \\
& \left. + \left[\frac{\theta(i, j+1) - 2\theta(i, j) + \theta(i, j-1)}{\Delta y^2} \right] \right\}. \quad (2.4.13)
\end{aligned}$$

Equations (2.4.11), (2.4.12) and (2.4.13) can now be recast into relaxation equations solving for ω , ψ and θ respectively.

Thus, equation (2.4.11) can be written in the following form to give $\omega(i, j)$

$$\begin{aligned}
 \omega(i, j) \Big|_{\text{new}} &= \omega(i, j) + \frac{R_1}{-C_\omega} \left\{ \frac{\Delta x^2 \cdot \Delta y^2}{\Delta t} [\omega(i, j) - \omega^*(i, j)] \right. \\
 &+ \frac{\psi_m \Delta x \cdot \Delta y}{2} [\psi(i, j+1) - \psi(i, j-1)] \left[\begin{array}{c} \omega(i+1, j) - \omega(i, j) \\ \text{or} \\ \omega(i, j) - \omega(i-1, j) \end{array} \right] \\
 &- \frac{\psi_m \cdot \Delta x \Delta y}{2} [\psi(i+1, j) - \psi(i-1, j)] \left[\begin{array}{c} \omega(i, j+1) - \omega(i, j) \\ \text{or} \\ \omega(i, j) - \omega(i, j-1) \end{array} \right] \\
 &- \frac{Gr}{Re^2} \cdot \frac{\Delta x^2 \cdot \Delta y^2}{2} [\theta(i, j+1) - \theta(i, j-1)] \\
 &- \frac{\Delta y^2}{Re} [\omega(i+1, j) - 2\omega(i, j) + \omega(i-1, j)] \\
 &- \frac{\Delta x^2}{Re} [\omega(i, j+1) - 2\omega(i, j) + \omega(i, j-1)] \Big\} \quad (2.4.14)
 \end{aligned}$$

where R_1 is a relaxation factor, and C_ω is the coefficient of $\omega(i, j)$.

$$\begin{aligned}
 \text{i.e. } C_\omega &= \frac{\Delta x^2 \cdot \Delta y^2}{\Delta t} \pm \frac{\psi_m \cdot \Delta x \Delta y}{2} [\psi(i, j+1) - \psi(i, j-1)] \\
 &\pm \frac{\psi_m \cdot \Delta x \Delta y}{2} [\psi(i+1, j) - \psi(i-1, j)] + \frac{2}{Re} (\Delta x^2 + \Delta y^2). \quad (2.4.15)
 \end{aligned}$$

The choice of sign in the above expression for C_ω is determined by the derivative of ψ with which it is

associated. As the terms $\left(\frac{\Delta x^2 \Delta y^2}{\Delta t}\right)$ and $\left[\frac{2}{Re}(\Delta x^2 + \Delta y^2)\right]$ in (2.4.15) are always necessarily positive, then the matrix will be diagonally dominant if the signs of the other two terms in the equation are also positive. Thus taking the term $\pm \psi_m \cdot \Delta x \Delta y \left[\psi(i, j+1) - \psi(i, j-1) \right]$, the parameters ψ_m , Δx and Δy are always fixed as positive so the sign of the term as a whole is determined by $\psi(i, j+1) - \psi(i, j-1)$. If this difference is positive, then the positive sign comes into use to keep the term as a whole positive. If the difference were to be negative, the negative sign would be used, again keeping the term as a whole positive. It happens that the rules which must be followed for this to be true are those of an "upwind difference" formulation, which automatically ensures that all the requirements are met.

Equation (2.4.12) can be written as the following relaxation form to give $\psi(i, j)$

$$\begin{aligned} \psi(i, j) \Big|_{\text{new}} &= \psi(i, j) + \frac{R_2}{-C_\psi} \left\{ \Delta x^2 \Delta y^2 \cdot \omega(i, j) \right. \\ &+ \psi_m \cdot \Delta y^2 \left[\psi(i+1, j) - 2\psi(i, j) + \psi(i-1, j) \right] \\ &\left. + \psi_m \cdot \Delta x^2 \left[\psi(i, j+1) - 2\psi(i, j) + \psi(i, j-1) \right] \right\} \quad (2.4.16) \end{aligned}$$

where R_2 is a relaxation factor and C_ψ is the coefficient of $\psi(i, j)$.

$$\text{i.e.} \quad C_\psi = -2\psi_m(\Delta x^2 + \Delta y^2). \quad (2.4.17)$$

N.B. No upwind difference formulation appears in this equation. Equation (2.4.12) can also be used as a

definition of vorticity ω in order to obtain the value of vorticity at a particular point, usually on the boundary, where the value of ψ is fixed and known.

Finally equation (2.4.13) can be written in relaxation form to give $\theta(i, j)$

$$\begin{aligned}
 \theta(i, j) \Big|_{\text{new}} &= \theta(i, j) + \frac{R_3}{C_\theta} \left\{ \frac{\Delta x^2 \cdot \Delta y^2}{\Delta t} \left[\theta(i, j) - \theta^*(i, j) \right] \right. \\
 &+ \frac{\psi_m \cdot \Delta x \cdot \Delta y}{2} \left[\psi(i, j+1) - \psi(i, j-1) \right] \left[\begin{matrix} \theta(i+1, j) - \theta(i, j) \\ \text{or} \\ \theta(i, j) - \theta(i-1, j) \end{matrix} \right] \\
 &- \frac{\psi_m \cdot \Delta x \cdot \Delta y}{2} \left[\psi(i+1, j) - \psi(i-1, j) \right] \left[\begin{matrix} \theta(i, j+1) - \theta(i, j) \\ \text{or} \\ \theta(i, j) - \theta(i, j-1) \end{matrix} \right] \\
 &- \frac{\Delta y^2}{\text{Re} \cdot \text{Pr}} \left[\theta(i+1, j) - 2\theta(i, j) + \theta(i-1, j) \right] \\
 &\left. - \frac{\Delta x^2}{\text{Re} \cdot \text{Pr}} \left[\theta(i, j+1) - 2\theta(i, j) + \theta(i, j-1) \right] \right\} \quad (2.4.18)
 \end{aligned}$$

where R_3 is a relaxation factor and C_θ is the coefficient of $\theta(i, j)$.

$$\begin{aligned}
 \text{i.e. } C_\theta &= \frac{\Delta x^2 \Delta y^2}{\Delta t} \pm \frac{\psi_m \cdot \Delta x \Delta y}{2} \left[\psi(i, j+1) - \psi(i, j-1) \right] \\
 &\pm \frac{\psi_m \cdot \Delta x \cdot \Delta y}{2} \left[\psi(i+1, j) - \psi(i-1, j) \right] + \frac{2}{\text{Re} \cdot \text{Pr}} \left[\Delta x^2 + \Delta y^2 \right], \quad (2.4.19)
 \end{aligned}$$

The "upwind difference" formulation again leads to all the terms in equation (2.4.19) being positive.

The quantities $\omega(i, j) \Big|_{\text{new}}$, $\psi(i, j) \Big|_{\text{new}}$ and $\theta(i, j) \Big|_{\text{new}}$ are the new, updated values of $\omega(i, j)$, $\psi(i, j)$ and $\theta(i, j)$ respectively at one point in time.

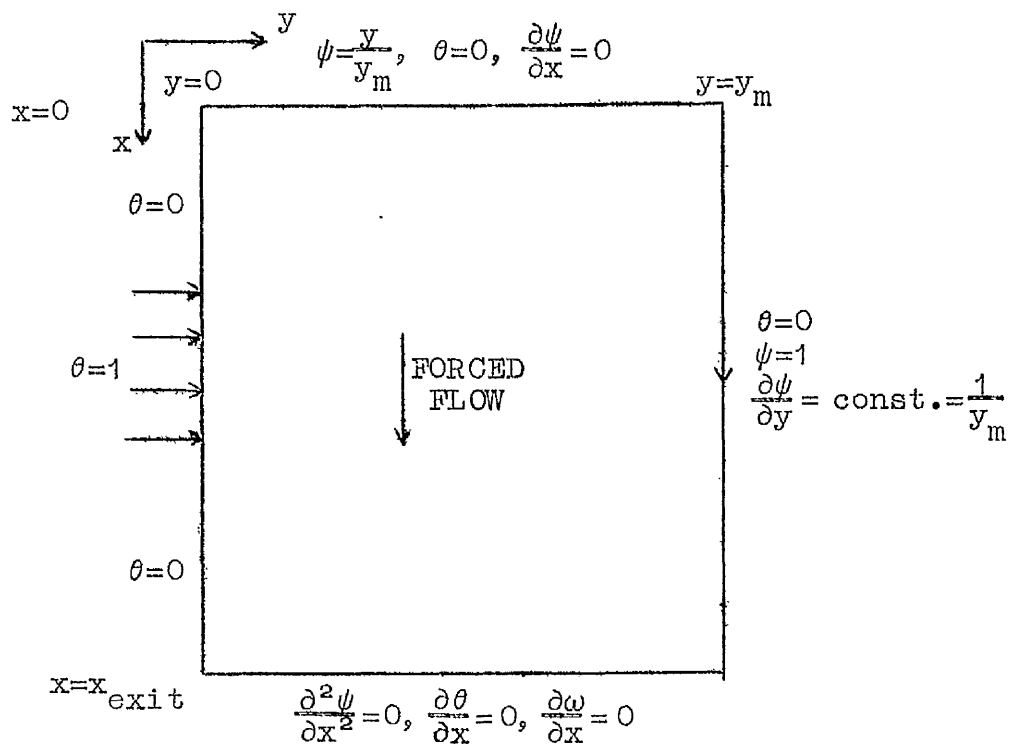
E Numerical Solution Procedure

(i) Steady state solutions

The steady state equations are the same as equations (2.4.14), (2.4.15), (2.4.16), (2.4.17), (2.4.18) and (2.4.19) with an infinite time step Δt .

i.e. all the terms involving Δt were absent.

The rectangular field of solution was divided into 21×21 mesh spaces. The current nodal point under investigation was always accessed by the argument (i, j).



Incorporation of derivative boundary conditions

Where derivatives of the dependent variables form part or all of the boundary conditions at any boundary, these derivatives are formed by incorporating a point outside the boundary. An example is shown below to clarify the situation. Suppose the boundary condition is that $\frac{\partial \psi}{\partial y} = 0$, as it is along $y = 0$, the wall.

Let the values of ψ at $y = -\Delta y$, 0 , and $+\Delta y$ be ψ_{-1} , ψ_0 and ψ_1 respectively.

Then, for the condition $\frac{\partial \psi}{\partial y} = 0$ to be satisfied at $y = 0$, then using a central difference expression, it is easily shown that $\psi_{-1} = \psi_1$. This condition is continuously updated as ψ_1 is changed.

The steps involved in a typical calculation can now be itemised. Assuming that the boundary conditions are the same as those stated in section (2.4.B) then the steps undertaken were:-

- (a) Generation of initial guesses of all three dependent variables, i.e. ω , ψ and θ :-

The starting values usually used were

ω - zero everywhere,

ψ - linear variation across field, corresponding to a constant velocity u ,

θ - zero everywhere except on the heated patch on the boundary where values of unity were used.

- (b) Incorporation of derivative boundary conditions:-

Values of ψ , θ and ω were calculated outside the boundary where required, in the manner indicated above and agreeing with the prescribed boundary conditions as shown on the above sketch. Wherever a derivative of a dependent variable is indicated in a direction normal to the boundary, then this technique was used.

- (c) Traversing the mesh of points:-

The points were considered in a direction (again referring to the sketch above) left to right and top to bottom.

Thus at a particular mesh point, the current value

of vorticity is updated using equation (2.4.14). At this same mesh point, a new value of stream-function ψ was obtained from equation (2.4.16). The new value of vorticity which had just been calculated was immediately available in this stream function calculation. The new temperature at this same mesh point was then obtained from equation (2.4.18). The general rule was that as soon as a variable has been recalculated, it was immediately available for use in the other equations. Equation (2.4.12) was used on certain boundaries (e.g. $y = 0$, the wall) to obtain the boundary value of vorticity, but this could only be used in this way if the value of stream function was fixed (e.g. $\psi = 0$ on the wall). The boundary derivatives were then recalculated and the mesh was traversed again. This procedure was repeated until the process converged.

(d) Convergence criterion

The calculation was considered to have converged to a solution when the maximum change of each variable during the course of one complete traverse was less than some arbitrary percentage of the current maximum value of that variable. This percentage was generally taken at between 0.1% and 0.5%.

(e) Calculation of wall parameters

Having obtained a converged solution to the equations, wall parameters such as friction factor, Stanton number and Nusselt number could be obtained.

Friction factor

For laminar flow, the friction factor C_f can easily be shown to have the relation

$$Cf = \frac{2}{Re} \cdot \psi_m \cdot \left. \frac{\partial^2 \psi_n}{\partial y^2} \right|_{wall}$$

The second derivative $\frac{\partial^2 \psi_n}{\partial y^2}$ at the wall were obtained from a central, 3 point difference formula

$$i.e. \quad Cf = \frac{2}{Re} \cdot \psi_m \cdot \frac{(\psi_{-1} - 2\psi_o + \psi_1)}{\Delta y^2}$$

where subscript "o" denotes the wall and "-1" and "1" denote the neighbouring mesh points on either side.

Stanton number

The Stanton number along the heated section is governed by the relation

$$St = - \frac{1}{Pr \cdot Re} \cdot \left. \frac{\partial \theta}{\partial y} \right|_{wall}$$

The first derivative $\frac{\partial \theta}{\partial y}$ at the wall was obtained from a forward 3 point difference formula i.e.

$$St = \frac{1}{Re \cdot Pr} \cdot \frac{(3\theta_o - 4\theta_1 + \theta_2)}{2 \cdot \Delta y}$$

Subscript "o" again denotes the wall.

Nusselt number

The Nusselt number was obtained as a mean heat transfer parameter, and was obtained by integrating the local Stanton number along the heated section using Simpson's rule.

(ii) Transient Solutions

The calculation of the transient solutions were similar to the steady solutions in that the iterative

procedures previously described were followed at each step in time. The time dependent state which has been examined up to the present time has consisted of a steady state solution for no heating at time equals zero, with the temperature of the heated patch being suddenly increased to unity (in non-dimensional terms). A study of the flow and temperature development with time followed.

Thus, the operation of the solution procedure was as follows:-

- (a) Steady state solution for no heating calculated in the manner previously described.
- (b) Increase temperature of heated patch to its constant value.
- (c) Step in time, from time = 0 to time = Δt .
- (d) Iterate around the equations (2.4.14), (2.4.16) and (2.4.18) until the system converges to some previously prescribed value, say 0.1% on the basis previously described.
- (e) Step in time to time = $2\Delta t$ and iterate again.

Eventually, depending on the flow and heating parameters, the flow either reached a steady state solution or else degenerated into large scale eddies with physical instabilities.

2.5 Nomenclature - Radial Turbomachine Flows

| | |
|--------------------|---|
| $C_{\omega, \psi}$ | Leading diagonal of coefficients of equivalent matrices. |
| h | Passage height in the axial direction. |
| H | Dimensionless passage height $\left[= \frac{h}{h_t} \right]$. |
| N | Number of blade passages in rotor. |
| p | Pressure |
| P | Dimensionless pressure $\left[= \frac{p}{\frac{1}{2}\rho U_t^2} \right]$. |
| r | Radius |
| R | Dimensionless radius $\left[= \frac{r}{r_t} \right]$. |
| Re | A flow Reynolds number $\left[= \frac{V_{ri} \cdot r_t}{\nu} \right]$. |
| Ro | A rotation Reynolds number $\left[= \frac{\Omega r_t^2}{\nu} \right]$. |
| R_1, R_2 | Relaxation factors. |
| u^+ | Dimensionless velocity $\left[= \frac{u}{\frac{\tau_w}{\rho}} \right]$. |
| U | Absolute velocity. |
| U'' | Dimensionless absolute velocity $\left[= \frac{U}{U_t} \right]$. |
| V | Velocity relative to the rotating coordinate system. |
| V'' | Dimensionless relative velocity $\left[= \frac{V}{U_t} \right]$. |
| η | Transformed coordinate in tangential direction. |
| θ | Polar coordinate angle. |
| ν | Effective kinematic viscosity (including the eddy diffusivity). |
| ξ | Transformed coordinate in the radial direction. |
| ρ | Density. |
| τ | Shear stress. |
| ψ | Stream function. |
| ψ' | Dimensionless stream function $\frac{\psi}{r_t h_t v_{ri}}$. |

ω Relative vorticity.
 ω' Dimensionless relative vorticity.
 Ω Angular velocity of system.

Suffixes

r in the radial direction.
 θ in the tangential direction.
t at the blade tip.
i at the inlet to the control surface.
o at the outlet from the control surface.
m maximum.
n normalised.
w at the wall.

2.6 Theory - Radial Turbomachine Flows

A Viscous flow in radial turbomachine blade passages - the problem considered

The situation considered is shown in fig. 60(a). The equations of motion and continuity in two-dimensional incompressible flow were used, although the passage height h was allowed to vary. In certain cases, the growth of the displacement thicknesses on the hub and shroud surfaces was included in this height variation using the calculation method for confined flows described in section (1.7). The blades of the rotor were assumed to be thin. The pressure and the magnitude and direction of the velocity were assumed constant over the entry and exit surfaces of the control volume. The direction of the exit velocity in both inflow and outflow was specified by considering the balance between the work done on the rotor blades and the change of absolute angular momentum through the rotor. The exit velocity direction was altered until these quantities become equal, guidance being obtained from experimental evidence.

On the open sides of the control surface formed by the extensions of the rotor blades, the conditions of magnitude and direction of velocity were assumed to be equal on each side at any particular radius.

On the blade surfaces themselves, a "slip" approximation was used in certain cases with the object of accounting for turbulence. With this approximation the flow was envisaged as the main flow having a high viscosity, augmented by turbulence, with a lower value, and hence a relatively lower shear stress on the wall. Whilst more

realistic models exist for the description of turbulence, they require a number of empirical constants to be determined and it is probable that in the very complex situation considered here, the simple approximation proposed will yield equally good results. The validity of the calculations are established by comparison with experiments carried out by Benson et al [47], and with a simple viscous rotating flow situation discussed by G. I. Taylor [60].

B Basic Theory

For two-dimensional constant property flow in polar coordinates, relative to a coordinate system rotating with angular velocity Ω , the equations of motion and continuity are:-

Momentum in r direction

$$V_r \cdot \frac{\partial V_r}{\partial r} + \frac{V_\theta}{r} \frac{\partial V_r}{\partial \theta} - \frac{V_\theta^2}{r} = \Omega^2 r + 2\Omega V_\theta - \frac{1}{\rho} \frac{\partial p}{\partial r} +$$

$$\nu \left[\frac{\partial^2 V_r}{\partial r^2} + \frac{1}{r} \frac{\partial V_r}{\partial r} - \frac{V_r}{r^2} + \frac{1}{r^2} \frac{\partial^2 V_r}{\partial \theta^2} - \frac{2}{r^2} \frac{\partial V_\theta}{\partial \theta} \right] \quad (2.6.1)$$

Momentum in θ direction

$$r \cdot V_r \frac{\partial V_\theta}{\partial r} + V_\theta \cdot \frac{\partial V_\theta}{\partial \theta} + V_r \cdot V_\theta = -2\Omega r \cdot V_r - \frac{1}{\rho} \frac{\partial p}{\partial \theta} +$$

$$\nu \left[r \frac{\partial^2 V_\theta}{\partial r^2} + \frac{\partial V_\theta}{\partial r} - \frac{V_\theta}{r} + \frac{1}{r} \frac{\partial^2 V_\theta}{\partial \theta^2} + \frac{2}{r} \frac{\partial V_r}{\partial \theta} \right] \quad (2.6.2)$$

Continuity

$$\frac{\partial}{\partial r} (V_r \cdot h \cdot r) + \frac{\partial}{\partial \theta} (V_\theta \cdot h) = 0 \quad (2.6.3)$$

The continuity equation includes, as a variable,

the passage height h . The effect of blade height variation and growth of boundary layers on hub and shroud could be accounted for by adjustments to this term. For constant passage height, of course, the parameter vanishes from the equation. h was considered to be only a function of radius i.e. to be constant in the tangential direction at a given radius. By differentiating equation (2.6.1) with respect to θ , and equation (2.6.2) with respect to r , and subtracting equation (2.6.2) from equation (2.6.1), the pressure term is eliminated.

The resulting equation was then transformed into coordinates ξ and η where

$$d\xi = \frac{dr}{r} \quad \text{and} \quad d\eta = d\theta. \quad (2.6.4)$$

The equations are thus transformed from polar to cartesian coordinates.

The vorticity ω , and stream function ψ were introduced where

$$\omega = \frac{V_\theta}{r} - \frac{1}{r} \frac{\partial V_r}{\partial \theta} + \frac{\partial V_\theta}{\partial r} \quad (2.6.5)$$

or, in transformed coordinates

$$\omega = \frac{V_\theta}{r} - \frac{1}{r} \frac{\partial V_r}{\partial \eta} + \frac{1}{r} \frac{\partial V_\theta}{\partial \xi}, \quad (2.6.6)$$

and ψ , to satisfy equation (2.6.3) is given by

$$V_r = \frac{1}{hr} \frac{\partial \psi}{\partial \theta} \quad \text{and} \quad V_\theta = -\frac{1}{h} \frac{\partial \psi}{\partial r}, \quad (2.6.7)$$

which, in transformed coordinates becomes

$$V_r = \frac{1}{hr} \frac{\partial \psi}{\partial \eta} \quad \text{and} \quad V_\theta = -\frac{1}{hr} \frac{\partial \psi}{\partial \xi}. \quad (2.6.8)$$

These manipulations, substitutions and coordinate transformations reduce equations (2.6.1), (2.6.2) and (2.6.3) to

$$\frac{1}{h} \left(\frac{\partial \omega}{\partial \xi} \frac{\partial \psi}{\partial \eta} - \frac{\partial \omega}{\partial \eta} \frac{\partial \psi}{\partial \xi} \right) - \frac{\omega}{h^2} \frac{\partial h}{\partial \xi} \frac{\partial \psi}{\partial \eta} = \frac{2\Omega}{h^2} \frac{\partial h}{\partial \xi} \frac{\partial \psi}{\partial \eta} + \nu \left(\frac{\partial^2 \omega}{\partial \xi^2} + \frac{\partial^2 \omega}{\partial \eta^2} \right) \quad (2.6.9)$$

$$\omega = - \frac{1}{hr^2} \left(\frac{\partial^2 \omega}{\partial \xi^2} + \frac{\partial^2 \psi}{\partial \eta^2} \right) + \frac{1}{h^2 r^2} \frac{\partial h}{\partial \xi} \frac{\partial \psi}{\partial \xi} . \quad (2.6.10)$$

These equations (2.6.9) and (2.6.10) are very similar to the equations developed for the combined natural and forced convection case [equations (2.4.8 and (2.4.9)], as one would expect for this transformed system.

Non-dimensional forms

The following substitutions were made

$$\psi' = \frac{\psi}{r_t h_t V_{ri}}$$

where V_{ri} is the radial velocity at the inlet to the system r_t and h_t are the radius and passage height at the blade tip.

ψ_n is the normalised value defined by $\frac{\psi'}{\psi'_m}$, where ψ'_m is the maximum value of ψ' .

$$\omega' = \omega \cdot \frac{r_t}{V_{ri}} , \quad R = \frac{r}{r_t} , \quad H = \frac{h}{h_t}$$

and two Reynolds numbers may be defined

$$(i) \quad \text{Flow } Re = \frac{V_{ri} \cdot r_t}{\nu}$$

$$(ii) \quad \text{Rotation } Ro = \frac{\Omega r_t^2}{\nu} .$$

Omitting the primes for clarity, equations (2.6.9) and

(2.6.10) become

$$\begin{aligned} \psi_m \cdot \frac{\partial \omega}{\partial \xi} \frac{\partial \psi_n}{\partial \eta} - \psi_m \frac{\partial \omega}{\partial \eta} \frac{\partial \psi_n}{\partial \xi} - \frac{\omega}{H} \psi_m \frac{\partial H}{\partial \xi} \frac{\partial \psi_n}{\partial \eta} \\ = \psi_m \cdot \frac{2}{H} \cdot \frac{Ro}{Re} \frac{\partial H}{\partial \xi} \frac{\partial \psi_n}{\partial \eta} + \frac{H}{Re} \left(\frac{\partial^2 \omega}{\partial \xi^2} + \frac{\partial^2 \omega}{\partial \eta^2} \right) \end{aligned} \quad (2.6.11)$$

$$\omega = - \frac{\psi_m}{H \cdot R^2} \left(\frac{\partial^2 \psi_n}{\partial \xi^2} + \frac{\partial^2 \psi_n}{\partial \eta^2} \right) + \frac{\psi_m}{H^2 R^2} \frac{\partial H}{\partial \xi} \frac{\partial \psi_n}{\partial \xi} . \quad (2.6.12)$$

C Boundary Conditions

Referring to fig. 60(a), the boundary conditions on the control surface were set as follows:-

(i) On the inner and outer radii, the chosen magnitudes and directions of the relative velocities were specified by the first derivative of ψ in the radial direction i.e. $\frac{\partial \psi}{\partial \xi}$. The values of the inlet components of velocity were obtained from experiment for a particular case, whilst the exit components were obtained from an angular momentum ~ torque balance as is dealt with in section (2.6.E).

The inlet and outlet streams were assumed to have zero absolute vorticity which implies a value relative to the rotating coordinate system of $-2Ro/Re$ in non-dimensional terms.

(ii) On the open sides the velocities at any given radius were made equal in magnitude and direction on each side and the mass flow was controlled to the correct value. This was done by equating vorticity values and $\frac{\partial \psi}{\partial \eta}$ values on each open side and also ensuring that the ψ_n values differed by unity.

(iii) On the blades, the ψ_n values were specified as zero on one side and unity on the other. The slip approximation

appears as a fixed relation, at any given radius, between $\frac{\partial \psi}{\partial \eta}$ and $\frac{\partial^2 \psi}{\partial \eta^2}$ as is shown in section 2.6.D.

D The Slip Approximation

In some flow situations it is possible for the viscosity close to the wall to be much lower than in the main flow; for example, if the wall is at a high temperature or if the main flow viscosity is augmented by a turbulent or eddy viscosity. Such situations can be dealt with by using a slip approximation in which a non-zero velocity is assumed on the wall. The slip approximation which is used here is loosely based on the familiar "law of the wall". Let the value of u^+ at the wall be fixed at u_w^+ where

$$u_w^+ = u_w \sqrt{\frac{\tau_w}{\rho}}.$$

Now $u_w = V_{rw}$ and introducing non-dimensional variables gives

$$\frac{\psi_m \cdot V_{r1}}{H \cdot R} \left(\frac{\partial \psi_n}{\partial \eta} \right)_w = u_w^+ \sqrt{\frac{\tau_w}{\rho}} \quad (2.6.13)$$

$$\text{also} \quad \frac{\tau_w}{\rho} = \frac{\nu}{r_t \cdot R} \left(\frac{\partial V_r}{\partial \eta} \right)_w = \frac{\nu}{r_t \cdot R} \frac{\psi_m \cdot V_{r1}}{H \cdot R} \left(\frac{\partial^2 \psi_n}{\partial \eta^2} \right)_w. \quad (2.6.14)$$

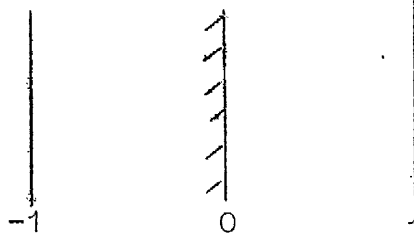
Equating equations (2.6.13) and (2.6.14) for τ_w/ρ yields

$$\left(\frac{\partial \psi_n}{\partial \eta} \right)_w^2 = \frac{(u_w^+)^2}{Re} \frac{H}{\psi_m} \left(\frac{\partial^2 \psi_n}{\partial \eta^2} \right)_w. \quad (2.6.15)$$

The Reynolds number Re is based on the main stream value of kinematic viscosity which will include both molecular and eddy components. Note that $u_w^+ = 0$ corresponds to the

boundary condition of no slip i.e. laminar flow and $u_w^+ \rightarrow \infty$ gives zero wall shear stress.

Now replacing the derivatives in the above expression by their finite difference form,



Subscript "0" denotes the wall

"1" is the first mesh point in the flow

"-1" is the mesh point required for the derivative boundary condition, we obtain

we obtain

$$\left[\frac{\psi_1 - \psi_{-1}}{2 \cdot \Delta\eta} \right]^2 = \left| \frac{u_w^{+2}}{\text{Re}} \cdot \frac{H}{\psi_m} \left[\frac{\psi_{-1} - 2\psi_0 + \psi_1}{\Delta\eta^2} \right] \right|.$$

Thus, solving the above equation for ψ_{-1} gives

$$\psi_{-1} = \frac{-b \pm \sqrt{b^2 - 4ac}}{2a}$$

where

$$a = 1$$

$$b = -2\psi_1 \pm \frac{4u_w^{+2}}{\text{Re} \cdot R \cdot \psi_m}$$

$$c = \pm \frac{4u_w^{+2}}{\text{Re} \cdot R \cdot \psi_m} \left[-2\psi_0 + \psi_1 \right] + \psi_1^2.$$

The optional signs in the above relations for b and c must be determined so as to give the required real solutions.

The correct choice of the real solutions is that value of ψ_{-1} which lies between ψ_1 and $-\psi_1$ i.e. between laminar and inviscid flow.

E Calculation of pressure, efficiency, torque and exit angle

As has already been mentioned, pressure had been removed as a dependent variable from the set of equations. Thus, to obtain the pressure distribution in the rotor passage, an integration of either equation (2.6.1) or (2.6.2) using the previously obtained solution for velocity will obtain the required pressures.

The pressure was assumed uniform at inlet along the radius, and pressures relative to this value were obtained by integration of equation (2.6.1) along the mid-blade radial line. Starting from these values, tangential integrations of equation (2.6.2) were carried out to the blades in each direction. It is possible for the pressure field to be established from only one of equations (2.6.1) or (2.6.2) but better numerical behaviour resulted when combinations of the two were used.

Thus taking equation (2.6.1) we have

$$\begin{aligned} \frac{1}{\rho} \frac{\partial p}{\partial r} = & -V_r \frac{\partial V_r}{\partial r} - \frac{V_\theta}{r} \frac{\partial V_r}{\partial \theta} + \frac{V_\theta^2}{r} + \Omega^2 r + 2\Omega V_\theta \\ & + \nu \left(\frac{\partial^2 V_r}{\partial r^2} + \frac{1}{r} \frac{\partial V_r}{\partial r} - \frac{V_r}{r^2} + \frac{1}{r^2} \frac{\partial^2 V_r}{\partial \theta^2} - \frac{2}{r^2} \frac{\partial V_\theta}{\partial \theta} \right) . \end{aligned}$$

Transforming in ξ, η coordinate system, and integrating with respect to ξ between inlet and the general position, non-dimensionalising the pressure and velocity using the tip speed U_t

$$\text{i.e. } V_r' = V_r/U_t, \quad V_\theta' = V_\theta/U_t$$

$$\frac{p - p_i}{\frac{1}{2}\rho U_t^2} = 2 \int_0^\xi f \, d\xi \quad (2.6.16)$$

$$\text{where } f = -V_r' \frac{\partial V_r'}{\partial \xi} - V_\theta' \frac{\partial V_r'}{\partial \eta} + V_\theta'^2 + R^2 + 2.R.V_\theta' \\ + \frac{1}{R.R_\theta} \left[\frac{\partial^2 V_r'}{\partial \xi^2} - V_r' + \frac{\partial^2 V_r'}{\partial \eta^2} - 2 \frac{\partial V_\theta'}{\partial \eta} \right]. \quad (2.6.17)$$

This function f may be evaluated at all points in the field using known values of V_r' , V_θ' etc. It is then integrated numerically along radial lines using a trapezoidal rule with the inlet conditions taken as the starting point for the integration. This method of establishing the pressure distribution was found to be satisfactory in the centre of the blade passage, but liable to numerical errors in the region near the blades where the velocities were changing more rapidly. To counteract this behaviour, the mid-blade radial line pressure distribution calculated as indicated above was used as the starting values for an integration in the tangential direction from the mid-blade position outwards to the blades.

i.e. from equation (2.6.2)

$$\frac{1}{\rho} \frac{\partial p}{\partial \theta} = -r.V_r \frac{\partial V_\theta}{\partial r} - V_\theta \frac{\partial V_\theta}{\partial \theta} - V_r.V_\theta - 2\Omega r.V_r \\ + \nu \left(r \frac{\partial^2 V_\theta}{\partial r^2} + \frac{\partial V_\theta}{\partial r} - \frac{V_\theta}{r} + \frac{1}{r} \frac{\partial^2 V_\theta}{\partial \theta^2} + \frac{2}{r} \frac{\partial V_r}{\partial \theta} \right). \quad (2.6.18)$$

Transforming in integrating with respect to η between mid-blade radial line and blades, we get

$$P = \frac{p - p_c}{\frac{1}{2}\rho U_t^2} = 2 \int f' d\eta \quad (2.6.19)$$

$$\text{where } f' = -V_r' \frac{\partial V_{\theta}'}{\partial \xi} - V_{\theta}' \frac{\partial V_{\theta}'}{\partial \eta} - V_r' V_{\theta}' - 2R \cdot V_r' + \frac{1}{R \cdot R_o} \left(\frac{\partial^2 V_{\theta}'}{\partial \xi^2} - V_{\theta}' + \frac{\partial^2 V_{\theta}'}{\partial \eta^2} + 2 \frac{\partial V_r'}{\partial \eta} \right). \quad (2.6.20)$$

A similar procedure as indicated above was carried out for this tangential integration.

Having thus obtained the pressure distribution in the rotor, it was necessary to check whether the chosen direction of the relative outlet velocity was correct. For no external forces other than the blade pressures acting on the fluid, the rate of change of absolute angular momentum must be equal to the rotor torque. This torque was obtained by a further radial integration of the pressure difference across the blade. If the values of these two quantities were not equal, the direction of the outlet velocity was changed and the whole calculation repeated.

The expressions used were

Rate of change of angular momentum

$$= \frac{2\pi H_1 R_1}{N} \rho \cdot r_t^2 h_t \cdot U_t V_{ri} \left(U_{\theta i}'' R_i - U_{\theta o}'' R_o \right). \quad (2.6.21)$$

$$\text{Torque} = \frac{1}{2} \cdot \rho \cdot r_t^2 h_t \cdot U_t^2 \int P \cdot H \cdot R \cdot dR \quad (2.6.22)$$

integrated over one blade (both sides included).

A rotor efficiency may be introduced to the balanced solution.

The change of total head through the rotor =

$$\left(p_i + \frac{\rho U_i^2}{2} \right) - \left(p_o + \frac{\rho U_o^2}{2} \right).$$

$$\therefore \text{Efficiency} = \frac{2(U_{\theta 1}'' R_i - U_{\theta 0}'' R_o)}{(p_i - p_o) + (V_{r i}''^2 - V_{r o}''^2) + (R_i - V_{\theta 1}''^2) - (R_o - V_{\theta 0}''^2)} \quad (2.6.23)$$

with care being taken over the signs of $V_{\theta 1}''$ and $V_{\theta 0}''$.

F Incorporation of passage height variation and calculation of normalizing factor

For the experimental cases considered, the flow area in the region between the blades remained constant

i.e. between the blades then $h r = \text{constant}$.

Thus in the region, in non-dimensional terms $H = \frac{1}{R}$

therefore $\frac{\partial H}{\partial \xi} = -\frac{1}{R}$.

In the region outside the blade passage, yet still in the system under investigation the passage height h was chosen to be constant.

Thus in the region outside the blade tip, the passage height was chosen to be equal to the height at the blade tip h_t .

i.e. in this region then $H = 1$ and thus $\frac{\partial H}{\partial \xi} = 0$.

In the region outside the blade eye, the passage height was chosen to be equal to the height of the blade at the eye,

thus $H = \text{constant}$ (dependent on radius of eye) and $\frac{\partial H}{\partial \xi} = 0$.

This last choice is perhaps a poor approximation to the true situation in the turbomachine where the flow turns through a right-angle soon after the rotor and flows out of the system axially.

Calculation of normalising factor ψ_m

From the previously defined radial velocity we have

$$V_r = \frac{\psi_m \cdot V_{r i}}{H \cdot R} \frac{\partial \psi_n}{\partial \eta}.$$

At inlet, $V_r = V_{ri}$ thus $\psi_m = \frac{H_i R_i}{\left. \frac{\partial \psi_n}{\partial \eta} \right|_i}$.

As a constant inlet velocity is used, then $\frac{\partial \psi_n}{\partial \eta}$ at inlet = $\frac{1}{\Delta \eta}$.

As the particular of the radial turbomachine had 10 radial blades then the angle between the "thin" blades was 36° (i.e. $\frac{\pi}{5}$ radians)

thus, as $H_i = 1$, then $\psi_m = R_i \cdot \frac{\pi}{5}$.

G Numerical Solution of Equations

The same solution procedure was used as previously described in section (2.4.E) for the combined natural and forced convection cases. The equations were reduced to their finite difference form using a uniform mesh in the ξ - η plane. This meant of course that in the $R \sim \theta$ plane, the mesh spacings were not equal. They were constant in the θ -direction and expanded with increased radius R . The dimensionless passage height variation H , as it is only a function of radius, is expressed in the finite difference form as the vector $H(i)$.

$\delta H(i)$ refers to $\frac{\partial H}{\partial \xi}$.

Thus, in finite difference form, equation (2.6.11) becomes

$$\begin{aligned}
& \psi_m \cdot \left[\frac{\psi(i, j+1) - \psi(i, j-1)}{2\Delta\eta} \right] \left[\frac{\omega(i+1, j) - \omega(i, j)}{\Delta\xi} \right. \\
& \quad \left. \text{or} \right. \\
& \quad \left. \frac{\omega(i, j) - \omega(i-1, j)}{\Delta\xi} \right] \\
& - \psi_m \cdot \left[\frac{\psi(i+1, j) - \psi(i-1, j)}{2\Delta\xi} \right] \left[\frac{\omega(i, j+1) - \omega(i, j)}{\Delta\eta} \right. \\
& \quad \left. \text{or} \right. \\
& \quad \left. \frac{\omega(i, j) - \omega(i, j-1)}{\Delta\eta} \right] \\
& - \frac{\omega(i, j)}{H(i)} \cdot \psi_m \cdot \delta H(i) \left[\frac{\psi(i, j+1) - \psi(i, j-1)}{2\Delta\eta} \right] \\
& = \frac{2\psi_m}{H(i)} \cdot \frac{R_0}{Re} \cdot \delta H(i) \left[\frac{\psi(i, j+1) - \psi(i, j-1)}{2\Delta\eta} \right] \\
& + \frac{H(i)}{Re} \left[\frac{\omega(i+1, j) - 2\omega(i, j) + \omega(i-1, j)}{\Delta\xi^2} \right. \\
& \quad \left. + \frac{\omega(i, j+1) - 2\omega(i, j) + \omega(i, j-1)}{\Delta\eta^2} \right] \quad (2.6.24)
\end{aligned}$$

and equation (2.5.12) becomes

$$\begin{aligned}
\omega(i, j) = & - \frac{\psi_m}{H(i)R(i)^2} \left[\frac{\psi(i, j+1) - 2\psi(i, j) + \psi(i, j-1)}{\Delta\eta^2} \right. \\
& + \frac{\psi(i+1, j) - 2\psi(i, j) + \psi(i-1, j)}{\Delta\xi^2} \left. \right] \\
& + \frac{\psi_m \delta H(i)}{H(i)^2 R(i)^2} \left[\frac{\psi(i+1, j) - \psi(i-1, j)}{2\Delta\xi} \right] \quad (2.6.25)
\end{aligned}$$

These equations can be rearranged in their relaxation form as

$$\omega'(i, j) = \omega(i, j)$$

$$\begin{aligned}
& + \frac{R_1}{C_\omega} \left\{ \frac{\psi_m \cdot \Delta \eta \Delta \xi^2}{2} \left[\psi(i, j+1) - \psi(i, j-1) \right] \left[\frac{\omega(i+1, j) - \omega(i, j)}{\omega(i, j) - \omega(i-1, j)} \right] \right. \\
& - \frac{\Delta \xi \Delta \eta \psi_m}{2} \left[\psi(i+1, j) - \psi(i-1, j) \right] \left[\frac{\omega(i, j+1) - \omega(i, j)}{\omega(i, j) - \omega(i, j-1)} \right] \\
& - \omega(i, j) \frac{\psi_m}{2} \frac{\delta H(i)}{H(i)} \cdot \Delta \xi^2 \Delta \eta \left[\psi(i, j+1) - \psi(i, j-1) \right] \\
& - \frac{\psi_m}{H(i)} \frac{R_0}{Re} \delta H(i) \Delta \xi^2 \Delta \eta \left[\psi(i, j+1) - \psi(i, j-1) \right] \\
& - H(i) \cdot \frac{\Delta \eta^2}{Re} \left[\omega(i+1, j) - 2\omega(i, j) + \omega(i-1, j) \right] \\
& \left. - \frac{H(i)}{Re} \Delta \xi^2 \left[\omega(i, j+1) - 2\omega(i, j) + \omega(i, j-1) \right] \right\} \\
& \hspace{15em} (2.6.26)
\end{aligned}$$

where C_ω , the coefficient of $\omega(i, j)$ is given by

$$\begin{aligned}
C_\omega = & \pm \frac{\psi_m \cdot \Delta \eta \cdot \Delta \xi^2}{2} \left[\psi(i, j+1) - \psi(i, j-1) \right] \\
& \pm \Delta \eta \cdot \Delta \xi \cdot \frac{\psi_m}{2} \left[\psi(i+1, j) - \psi(i-1, j) \right] \\
& - \frac{\psi_m}{2} \frac{\delta H(i)}{H(i)} \Delta \xi^2 \cdot \Delta \eta \left[\psi(i, j+1) - \psi(i, j-1) \right] \\
& + \frac{2H(i)}{Re} (\Delta \eta^2 + \Delta \xi^2) \hspace{10em} (2.6.27)
\end{aligned}$$

and also

$$\begin{aligned}
\psi'(i, j) = \psi(i, j) + \frac{R_2}{-C_\psi} \left\{ \Delta\eta^2 \Delta\xi^2 \cdot \omega(i, j) \right. \\
+ \frac{\psi_m \cdot \Delta\xi^2}{H(i) \cdot R(i)^2} \left[\psi(i, j+1) - 2\psi(i, j) + \psi(i, j-1) \right] \\
+ \frac{\psi_m \Delta\eta^2}{H(i) \cdot R(i)^2} \left[\psi(i+1, j) - 2\psi(i, j) + \psi(i-1, j) \right] \\
\left. - \frac{\psi_m \delta H(i) \Delta\xi \cdot \Delta\eta^2}{2H(i)^2 \cdot R(i)^2} \left[\psi(i+1, j) - \psi(i-1, j) \right] \right\}
\end{aligned}
\tag{2.6.28}$$

where C_ψ , the coefficient of $\psi(i, j)$ is given by

$$C_\psi = - \frac{2\psi_m}{H(i) \cdot R(i)^2} (\Delta\xi^2 + \Delta\eta^2) . \tag{2.6.29}$$

The upwind difference formulation as discussed in section (2.4.C) is used in a similar way for these equations in order to determine which finite difference approximation to the first derivative of ω is to be used.

H Method of Solution

The numerical solution procedure is identical to that described in section (2.4.E), in the setting up of the starting solutions, incorporation of derivative boundary conditions and the iteration procedure. It should be noted that for these turbomachine flows, there are only two dependent variables, ψ and ω . After the solution had converged to a criterion of 0.1% say, the velocities and hence the pressure distribution were calculated. A check on the balance between the change of angular momentum and the torque revealed if the exit angle chosen was correct. If this balance was poor, the exit angle was altered and

a new solution obtained. This process was continued until a balanced, converged solution was obtained. This usually meant a total of three runs to satisfy the required conditions.

I Calculation of hub and shroud boundary layer development

In order to ascertain the order of magnitude of the hub and shroud boundary layers, and their effect on the blade-to-blade viscous flow calculation described above, the method described in section (1.7) was used to give some estimation of blockage effect produced. As the boundary layer theory is two-dimensional then no effect could be taken of curved streamlines. The only case in which this method was applied was the near-design calculation illustrated on fig. 61. The severely off-design cases illustrated on figs. 62, 63, 64 were not considered because the existence of eddies in the blade-to-blade plane would give a considerable variation of parameters in the tangential direction.

The passage was considered as a variable area duct with, for the inflow case examined, an initial converging section followed by the rotor passage (considered as a parallel-walled section) and a final converging region. A duct of the same size as the rotor was examined in this way with the same mass flow rate as was passing through the turbomachine passage.

It was realised that only an order of magnitude accuracy could be ascribed to such a technique but it was felt that an indication of the probably important boundary layer effects in the hub-shroud plane was

necessary. The calculated displacement thicknesses were added to the local passage heights to give a new variation of blade height.

2.7 Nomenclature - Flow over a step

| | |
|-----------------|---|
| Cf | Local friction factor $\left(= \tau_w / \frac{1}{2} \rho U_s^2 \right)$. |
| C _p | Specific heat. |
| k | Thermal conductivity. |
| l | Characteristic length (chosen as step height). |
| Pr | Prandtl number |
| Pr _t | Turbulent Prandtl number. |
| q _w | Local wall heat flux. |
| Re | Reynolds number $\left(= \frac{U_s l}{\nu_t} \right)$. |
| St | Local Stanton number $\left[= q_w / \rho C_p U_s (T_w - T_s) \right]$. |
| T | Dimensional temperature. |
| u | Velocity component in streamwise direction. |
| u ⁺ | Dimensionless velocity $\left(= u / \sqrt{\tau_w / \rho} \right)$. |
| y | Independent variable. |
| θ | Dimensionless temperature $\left(= \frac{T - T_s}{T_\ell - T_s} \right)$. |
| ν | Kinematic viscosity. |
| ρ | Density. |
| τ _w | Local wall shear stress. |
| δ | Dimensional thickness of slip region. |
| ψ | Stream function. |
| ψ _m | Maximum value of stream function. |

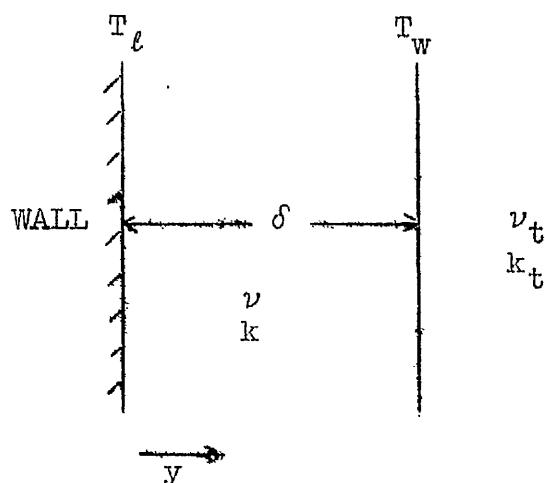
Subscripts

| | |
|---|---|
| l | At wall. |
| s | At free stream boundary. |
| t | Turbulent value. |
| w | At edge of region of slip (i.e. at a distance δ from the wall). |

2.8 Inclusion of Heat Transfer in Slip Approximation - Flow over a step

A Basic Theory

The introduction of heat transfer to the slip approximation means that, for instance, in the problem considered in section 2.4, for example, the temperature of the heated patch will no longer be unity, but some value less than unity but greater than zero. Thus some expression relating this wall temperature to the interior temperatures is required.



Let T_ℓ be the actual wall temperature and let δ be the thickness of the slip layer with kinematic viscosity ν and thermal conductivity k . Let T_w be the temperature at the edge of the slip layer (i.e. the boundary condition of temperature which it is required to determine). ν_t and k_t are the turbulent (enhanced) values of viscosity and conductivity respectively.

We can write an expression for the wall heat flux q_w such that

$$q_w = k \frac{(T_\ell - T_w)}{\delta} = -k_t \left. \frac{\partial T}{\partial y} \right|_w.$$

Non-dimensionalizing temperature gives

$$k \frac{(\theta_\ell - \theta_w)}{\delta} = -k_t \left. \frac{\partial \theta}{\partial y} \right|_w. \quad (2.8.1)$$

But $\frac{\tau_w}{\rho} = \nu \cdot \frac{u_w}{\delta}$ be definition

$$\therefore \delta = \frac{\nu \cdot u_w}{(\tau_w/\rho)} = \frac{\nu u_w^{+2}}{u_w}. \quad (2.8.2)$$

Substituting for δ in equation (2.8.1), introducing turbulent Prandtl number Pr_t , Prandtl number Pr , and replacing the derivative $\left. \frac{\partial \theta}{\partial y} \right|_w$ by a forward three point difference formula at points "0", "1" and "2" we obtain

$$\theta_0 = \frac{u_w^{+2} (4\theta_1 - \theta_2) + 2 \cdot \Delta y \cdot Re \cdot \frac{Pr_t}{Pr} \psi_m \left. \frac{\partial \psi}{\partial y} \right|_w}{3u_w^{+2} + 2 \Delta y \cdot Re \cdot \frac{Pr_t}{Pr} \psi_m \left. \frac{\partial \psi}{\partial y} \right|_w} \quad (2.8.3)$$

bearing in mind that $\theta_\ell = 1$.

Having reached a converged solution the friction factor and Stanton numbers can be easily obtained. Two expressions may be written down for Stanton number, and the results should be identical.

Friction factor calculation

Referring to the above sketch, the wall shear stress τ_w can be expressed as

$$\frac{\tau_w}{\rho} = \nu \frac{u_w}{\delta} = \nu_t \cdot \left. \frac{\partial u}{\partial y} \right|_w. \quad (2.8.4)$$

$$\text{But } Cf = \frac{\tau_w}{\frac{1}{2} \rho U_s^2} = \frac{2 \cdot \psi_m}{Re} \left. \frac{\partial^2 \psi}{\partial y^2} \right|_w \quad (2.8.5)$$

where $Re = \frac{U_s \cdot l}{\nu_t}$, based on the enhanced viscosity.

This is similar to the expression derived in section (2.4.E), part (i).

Stanton number calculation

(i) Using slip region

$$St = \frac{q_w}{\rho C_p \cdot U_s (T_w - T_s)} .$$

$$\text{But } q_w = k \frac{(T_\ell - T_w)}{\delta} .$$

∴ Introducing dimensionless temperature θ

$$St = \frac{k(1 - \theta_w)}{\rho C_p \cdot U_s \cdot \delta} .$$

$$\text{But } \delta = \nu \frac{u_w^{+2}}{u_w} \quad \text{from equation (2.8.2).}$$

$$\therefore St = \frac{(1 - \theta_w) \sqrt{\frac{Cf}{2}}}{Pr \cdot u_w^{+}} .$$

N.B. For this formula to be useful, the absolute value of the friction factor must be used as δ must be positive.

(ii) Using "turbulent" region

$$St = \frac{q_w}{\rho C_p \cdot U_s (T_w - T_s)} .$$

$$\text{But } q_w = -k_t \left. \frac{\partial T}{\partial y} \right|_w .$$

Introducing dimensionless temperature θ leaves

$$St = - \frac{1}{Pr_t \cdot Re} \left. \frac{\partial \theta}{\partial y} \right|_w$$

where Re is again based on the turbulent viscosity.

Slip approximation for velocity

The velocity slip approximation in this cartesian coordinate system is virtually identical to that previously described for the polar coordinate turbomachine situation.

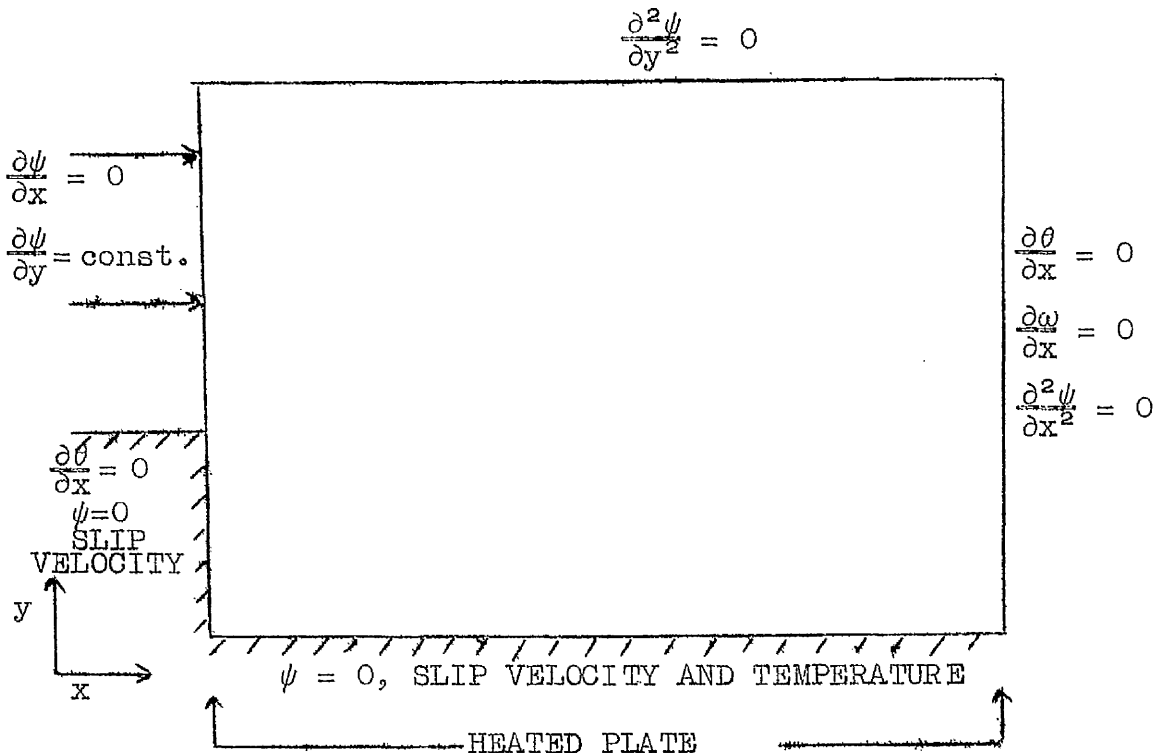
i.e. From equation (2.8.4)

$$\frac{u_w}{\delta} = \nu_t \cdot \frac{\partial u}{\partial y} \Big|_w$$

$$\therefore \frac{\partial \psi}{\partial y} \Big|_w^2 = \frac{u_w^2}{\text{Re} \cdot \psi_m} \frac{\partial^2 \psi}{\partial y^2} \Big|_w$$

The boundary derivative value of ψ (i.e. ψ_{-1}) may thus be obtained.

B Boundary Conditions



The control system for the flow over the step is illustrated above. A constant velocity flow is assumed to issue over the step, reattaching to the heated plate

at a position approximately midway along it. Slip approximations as previously described are used along the heated plate and also over the vertical part of the step. The exit plane is considered to be sufficiently far down the plate so that the curvature of the streamlines and the decay of the temperature profiles have become negligible. The velocity gradient normal to the plate is assumed to be zero at the outer flow boundary (i.e. $\frac{\partial u}{\partial y} = 0 = \frac{\partial^2 \psi}{\partial y^2}$).

2.9 General Discussion of Theory

In the initial stages of the work, the partial differential equations were converted into algebraic equations using three-point truncated Taylor series and central differences throughout. These equations were then solved by successive point iteration (relaxation). The advantage of the relatively low truncation errors was overcome by the fact that it was not possible to obtain convergence with this scheme, no matter if severe under-relaxation factors were used, at Reynolds numbers greater than 60. It was realized that increased Reynolds numbers resulted in larger values of the off-diagonal elements of the equivalent matrix, so reducing the "diagonal dominance" which is an important factor in securing convergence (certainly for linear equations). A more direct method of solution was therefore attempted which, it was hoped, would overcome this difficulty. Linear equations can be solved by direct matrix inversion without the necessity for diagonal dominance, and it was hoped that this method, when applied to the non-linear case, would enable convergence to be achieved at higher Reynolds numbers.

The equations were all written in the form

$$\nabla^2 \phi = K_\phi$$

where ϕ is a general dependent variable, and the vector K_ϕ is made up of all the terms in each equation with the exception of the Laplacian term $\nabla^2 \phi$.

Using five point central difference expressions for all derivatives to reduce truncation errors still

further, the equations were transformed into sets of algebraic equations of the form

$$A\phi = K_{\phi}$$

where A is a banded matrix of coefficients common to the three sets. Initial guesses of all the variables enabled the three K vectors (for vorticity, stream function and temperature) to be obtained and the solution of the ϕ variables carried out using the Thomas Algorithm (i.e. a form of Gaussian elimination). This enabled a new set of K vectors to be determined and this iteration was continued until the solution converged. This method, however, proved to be no more convergent and no faster than relaxation.

The incorporation of the convective terms in the matrix of coefficients was then attempted. This proved to be very time-consuming due to the fact that the matrix A had to be set up after every iteration, and proved no more successful than previous attempts.

Couette flow with no buoyancy was chosen as a simple test case for these different procedures. Generally, it was found that, when supplying the correct solution as the initial guess, and if the Reynolds number was below 60, then the solution remained with residuals, of the order of the round-off error of the machine, being obtained. However, the same procedures, with the Reynolds numbers increased above this value of 60, diverged, even when the correct solution was supplied as the initial guess.

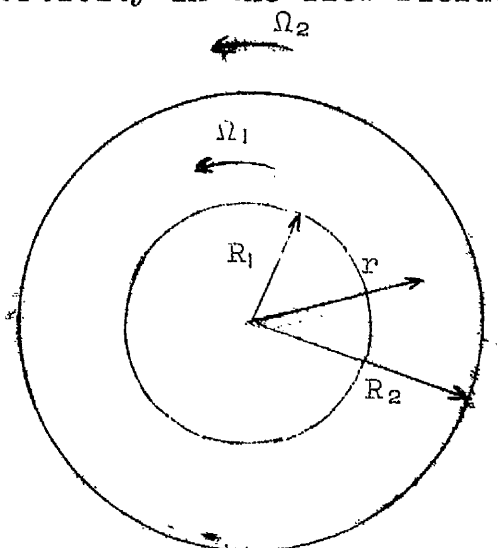
It was then realized that diagonal dominance must be a major factor in convergence whether matrix or

relaxation methods are used. The work of Gosman et al [46] has emphasised the importance of the "upwind difference" technique in securing stability. This method, in fact, has the property of ensuring the diagonal dominance of the equivalent matrix. The essential feature of this method, as used in this work, is that finite difference expressions for the first derivatives of ω and θ are formed from the values at two points only - the value at the point under consideration and the neighbouring upstream point. The local stream direction is determined from the ψ values around the point in question. This technique would be time-consuming to include in a matrix technique, owing to the necessity of setting up the matrix after each iteration but is simple to include in a point iteration procedure. This modification was thus made and the calculation was then found to converge rapidly, and apparently without any upper limit of Reynolds number (in the laminar flow regime of course). The disadvantage of this method is the possibly high truncation errors obtained by representing the first derivatives by two-point forward or backward difference formulae. This disadvantage may be overcome, to some extent, by the possibility of using many more mesh points to describe the field. Storage requirements of the relaxation techniques are of a relatively minor consideration, but for the matrix techniques, especially if different matrices have to be stored for each dependent variable, storage is a prime factor.

Comparison with simple solution - polar coordinates

It is useful to compare the numerical solution with

a known analytic solution to provide some check on the accuracy of the numerical method. One simple case is that of viscous flow between two rotating cylinders described by G. I. Taylor [60] where the analytic solution yields a constant vorticity in the flow field.



The tangential velocity distribution V in the region between the rotating cylinders, rotating with angular velocities Ω_1 and Ω_2 and radii R_1 and R_2 respectively, at any radius r , is given by

$$V = Ar + \frac{B}{r}$$

where

$$A = \frac{\Omega_1 R_1^2 - \Omega_2 R_2^2}{R_1^2 - R_2^2}$$

and

$$B = \frac{\Omega_1 R_1^2 \left(1 - \frac{\Omega_2}{\Omega_1}\right)}{1 - \frac{R_1^2}{R_2^2}} = \frac{\Omega_1 R_1^2 - \Omega_2 R_1^2}{1 - \frac{R_1^2}{R_2^2}} \dots$$

From the definition of vorticity previously used

$$\left[\text{i.e. } \omega = \frac{V_\theta}{r} - \frac{1}{r} \frac{\partial V}{\partial \theta} r + \frac{\partial V}{\partial r} \theta \right]$$

we obtain an expression for vorticity such that

$$\omega = 2A$$

i.e. Vorticity in the region between the cylinders is given by

$$\omega = \frac{2(\Omega_1 R_1^2 - \Omega_2 R_2^2)}{R_1^2 - R_2^2} .$$

The numerical calculation was carried out by specifying a value of stream function on the inner surface and adjusting the outer value of stream function until a converged solution with a constant vorticity was obtained. The resulting vorticity was within 0.3% of the analytic. This flow is strictly one-dimensional and is not ideal for test purposes. As a further check, on a cartesian coordinate grid, a comparison was made between the predicted variation of local friction factor and a zero pressure gradient laminar boundary layer Blasius distribution. A parabolic velocity profile at the inlet to the system was assumed. The numerical method tended to overpredict the Blasius value by approximately 10% at the exit to the field. It was felt that the Blasius solution must be regarded with some doubt in these low Reynolds number situations.

2.10 Results and Discussion of Theory

A Transient combined natural and forced convection

As has been mentioned previously, the numerical techniques for solution of the equations were established by considering steady state situations. Thus, unless stated otherwise, the results discussed refer to steady state calculations.

The coordinate system chosen for these calculations is shown on fig. 46.

The calculations of combined natural and forced convection were carried out for a range of Reynolds number from 6 to 2000, and Grashof number from zero to 5×10^6 . Only the case of Prandtl number unity was examined in detail. Particular attention was paid to determining the situations where buoyancy forces cause flow separation and recirculation. One such case ($Re = 1000$, $Gr = 3 \times 10^6$) is shown on fig. 51, in which isotherms and streamlines obtained from a contour plotting program are shown. It should be noted that these diagrams are not to the same scale in each direction. The cross-stream scale has been enlarged by a factor of 4. The boundary values of temperature chosen on the stationary wall were zero on the unheated mesh points and unity on the heated points. The contour plotting program interpolated values on the boundary over the finite step at each end of the heated portion. In the horizontal and upward flows the heating has little influence on the streamline shape although the acceleration caused by buoyancy is apparent in the upward case. The effect also causes the reduction in thickness of the

thermal boundary layer, which can be seen from the isotherms. For the particular conditions shown on fig. 51, the downflow case shows a recirculating region in which the buoyancy forces predominate. There are of course situations of lower Grashof number where there is no recirculation, but results were obtained which showed that separation may occur in horizontal flows.

The outer boundary condition for these cases was intended to be an approximation to boundary layer flow, i.e. the boundary was far enough away from the wall so that the streamline was parallel to the wall and the velocity, and hence $\frac{\partial \psi}{\partial y}$ was constant and equal to the inlet value. The loss of momentum associated with the "non-slip" influence of the wall can only be compensated for by an acceleration of the internal flow as the outer boundary is set at a fixed velocity. This accounts for the peaking of the velocity profiles on fig. 49. If the outer boundary was at an infinite distance from the wall, the velocity maxima would be removed and thus would then tend towards a zero pressure gradient boundary layer situation.

Figs. 47 and 48 show the local friction factor and Stanton number variations respectively for the same case as the contour plots. The friction factor is shown over the whole length of the region but the Stanton number has meaning over the heated patch only. Negative friction factors arise because of the flow reversal, and the flow separation and reattachment positions are indicated at the positions of zero friction factor. The local acceleration with upflow causes a considerable enhancement

of the wall shear stress.

Fig. 49 shows calculated profiles of temperature and velocity at the downstream edge of the heated patch where "downstream" refers to the main flow. The profiles do not show any unusual features apart from the distortions caused by the recirculating flow case. As an approximation to boundary layer flow, the chosen position of the straight streamline would appear to be adequate for horizontal and upward flow, but could be improved for downward flow as indicated by the non-asymptotic approach to the free-stream velocity. The decrease of velocity as the free-stream velocity is approached has already been commented on.

Mean Nusselt numbers versus Grashof number are shown on fig. 50 for a range of Reynolds number for two of the configurations. Horizontal flows are omitted for clarity and they lie between the curves for the other cases. Except at extremely low Reynolds number, the upflow curves do not exhibit any unusual features and the Nusselt number increases with Grashof number. At the very low Reynolds numbers, upstream conduction is significant and warm fluid is carried back over the heated portion thus reducing the wall temperature gradient. The downflow curves show a minimum Nusselt number in all cases as the influence of the natural convection overcomes the forced flow. It is not easy to locate exactly the onset of reversed flow unless a very fine mesh is used and a large number of combinations of Reynolds number and Grashof number are examined. The region in which separation occurs is marked as a shaded zone on the curves. The heat transfer continues to fall as the Grashof number increases after the flow reversal

has occurred. This is due to the growth of the recirculating eddy which results in wider spacing of the isotherms close to the wall. Eventually the increasing velocity of the recirculating flow causes the heat transfer to rise. The onset of flow reversal occurs, at the lower Reynolds numbers, when $Gr/Re^2 \sim 2.0$ and at the highest Reynolds number when $Gr/Re^2 \sim 0.5$. Some effects of changes of boundary conditions are shown on figs. 52, 53, and 54. It can be seen from fig. 52 that even with a variety of changes being made to the downstream boundary conditions of both velocity, temperature and position, the effects on the temperature profile at the exit of the field are indistinguishable. An extension of the cross-stream dimension by 50% does produce a significant change in the profile, but a further increase to double the initial cross-stream dimensions produces no further change. A similar effect on the velocity profiles is exhibited on fig. 53, where it can be seen that only an increase of the cross-stream dimension produces a change of velocity profile. The effects of this increase of the cross-stream dimension on the velocity profiles at the exit from the heated patch for the three flow cases are shown on fig. 54. The only case in which there is any effect is the downflow situation where the effect of change of boundary is only small.

In conjunction with the theoretical calculations, a rig had been constructed to investigate some of these interesting effects experimentally (see reference [66]). Fig. 56 shows a flow visualisation of a downflow case, $Re = 120$ with three Grashof numbers. The existence of a

stable recirculating eddy can clearly be seen for each of the three cases. A prediction of the streamlines for this case is included for comparison purposes. It should be noted that the outer boundary condition in the theory had to be changed somewhat to compare with this situation as it was a plane duct flow with heating on one side only. A comparison of the predicted and measured variation of mean Nusselt number with Grashof number is shown on fig. 55. The initial fall of Nusselt number then the rise as natural convection becomes increasingly important is well predicted by the theory.

The main point of interest of these buoyancy driven recirculating eddies is their physical stability. It can be seen from fig. 56 that the existence of a stable eddy is certainly possible under certain conditions. Figs. 57 and 58 are included, however, to demonstrate the effect of continuously increasing the Grashof number at a constant Reynolds number. The value of Reynolds number considered was 350. At Grashof numbers of 21.5×10^4 and 23.0×10^4 the existence of a stable eddy is clearly seen. When the heat flux is increased to give a Grashof number of 26×10^4 , an instability can be seen to be developing at the end of the eddy. Further increases of Grashof number cause these instabilities to expand till, at a Grashof number of 42.2×10^4 , a wholly unstable region is produced. The prediction of this breakdown of the stable situation was of course impossible with a calculation procedure based on the steady equations of motion and energy. The inclusion of the time-dependent terms in the equations enabled such situations to be predicted.

A situation in which physical instabilities in the flow have been predicted is shown on fig. 59(b). The flow case studied was that of a developing two-dimensional plane channel flow with a heated patch on one wall. Fig. 59(a) illustrates the case where the forcing flow is aiding the buoyancy forces and is thus referred to as upflow. The corresponding downflow situation (i.e. opposing flow) is shown on fig. 59(b). A constant velocity distribution was assumed at inlet. The true channel dimensions were 24:1, i.e. the lateral scale as shown on figs. 59(a) and (b) has been expanded. A Reynolds number of 2000 and a Grashof number of 3×10^7 were chosen for the initial test as the steady state solution procedure was found to be numerically unstable for these particular parameters. The starting conditions were a steady state solution of the equations of motion for this flow geometry, but with no buoyancy terms. At a time zero the heat was suddenly applied and the diagrams on figs. 59(a) and (b) show the subsequent development of the streamlines. The times quoted below are all dimensionless $\left[= \frac{Ut}{l} \right]$. For the downflow situation shown on fig. 59(b), almost immediately after the heating was started, a small recirculating eddy was generated. This eddy grew quickly as time advanced till at a time of 9.5 the eddy covered almost a quarter of the flow field. Further development of the flow with time shows the shedding of eddies and the breakdown of the flow into a number of smaller eddies. At large values of time (about 19.00) the flow reached a situation where it set up a periodic eddy shedding motion which was repeated with an apparent period of 2.6 units. Thus no

fully developed situation was reached for the chosen flow parameters. Smaller time intervals were chosen to arrive at the same point in time. The results compared favourably with those illustrated indicating that the original time intervals chosen were short enough.

The corresponding upflow situation shown on fig. 59(a) demonstrated the high degree of stability associated with this situation. A fully developed flow is obtained after a dimensionless time of approximately 10. Further increases of time showed no further changes in the streamlines or temperature contours. Thus an unsteady solution procedure has been used for the calculation of a steady state situation. The unsteady procedure has also been used for the predictions of steady state downflow situations where a stable recirculating eddy had been previously obtained by the steady calculation procedure (e.g. fig. 51). After a sufficient period of time, a steady fully developed solution was obtained.

B Radial turbomachinery flows

For given choices of the parameters (inlet angle, Reynolds numbers and u_w^+) the program had to be run several times until, by the torque-angular momentum change balance, the outlet angle was approximately correct. For this reason it was possible to examine only a limited number of cases and it was chosen to calculate those situations on which experimental evidence was available (reference [47]) or should be in the near future.

The rotor geometry shown on fig. 60(a) has a setment angle of 36° and radius ratio of 3:1. The passage height h varied to keep the cross-section area constant

although, in some calculations, the growth of displacement thicknesses on the hub and shroud surfaces was included. The control surface inner and outer radii were chosen at values which lay on the mesh and were sufficiently far from the rotor for conditions to be assumed uniform. These positions were $1.369r_t$ and $0.169r_t$, except for the outflow case where the inner value was taken at $0.285r_t$. Three inflow and one outflow cases were examined with the flow parameters given in appendix 3, table (i). Case 1 results in a flow which is nearly tangential to the blades at the rotor inlet and hence corresponds to a "near-design" condition. The other cases are severely off-design and include zones of separated flow.

Reynolds number and u_w^+ choices

The choice of $u_w^+ = 0$ and a moderate Reynolds number corresponds to a laminar flow whereas high values of both gives a close approximation to inviscid flow. Equation (2.6.15) is indeterminate for truly inviscid flow and the slip approximation on the blade surfaces was replaced in this case by a constant vorticity equal to the inlet relative value. Turbulent flows are approximated by values lying between the extremes but there is little evidence available on which to base realistic choices. In a parallel wall channel, Betts et al [61] showed that the effective viscosity is 100 times the laminar value when the Reynolds number is 1.5×10^5 (or 1500 when based on the effective viscosity). Estimations of the turbulent velocity profile on this basis show that it is well predicted by using the effective viscosity and a slip parameter $u_w^+ = 10$. The

use of this is supported by the value of $u_w^+ = 12$ used for the laminar sublayer thickness in the classic Prandtl-Taylor analogy for heat transfer. If the calculation method proposed here is to be useful then it will be necessary to examine the order of agreement obtained with experiments for a range of input parameters and, hopefully, a constant value of u_w^+ will emerge.

Values of u_w^+ used in these calculations were 2, 5 and 10. The former represents a flow of more viscous character whereas the latter tends towards the inviscid situation which is possibly a closer approximation to turbulent flow.

Comparisons of flow predictions

For comparison purposes, velocity profiles and streamline contour plots are shown together with some pressure distributions.

Figs. 60(b), 61 and 65 show predictions and measurements of Case 1, the near design situation. Fig. 65 shows the influence of the inclusion of boundary layers for Case 1(i) and these give increases in the magnitudes of the velocities of the order of 15%, producing possibly a better agreement with experiment. It was thought reasonable to account for boundary layer growth only in this case which contains no recirculating zone. However whilst this effect is not insignificant it is relatively much less important than the u_w^+ choice.

Predictions and measurements of the radial component of the relative velocity distribution are presented and four radii have been chosen for comparison purposes in this case. These radii are at values of r/r_t

of 1.2, 1.0, 0.633 and 0.367, thus corresponding to positions outside the rotor, at the inlet to the rotor, approximately mid-way along the blade passage and approaching the exit of the passage respectively.

Fig. 65 also shows the velocity distributions obtained for Cases 1(ii), 1(iii) and 1(iv) together with the inviscid solution for the same ratio U_t/V_{ri} . Case 1(iii) in which the Reynolds numbers are doubled and the u_w^+ increased by $\sqrt{2}$ keeps the same relation between $\frac{\partial \psi}{\partial y}$ and $\frac{\partial^2 \psi}{\partial y^2}$ in equation (2.6.15). Physically this corresponds to retaining the same thickness of the laminar layer at the wall whilst halving the effective viscosity in the main flow. Comparing 1(iii) with 1(i) we would conclude that, providing the eddy viscosity in the main stream is high, then the effect of changing its value (in this case from 50 to 100 times the laminar value) is very small.

The most important feature that is brought out on fig. 65 is the strong dependence of the velocity profile on the choice of the slip parameter u_w^+ . As the slip parameter is increased the profile changes regularly from the laminar towards the inviscid. This point is also apparent on the pressure variations shown on fig. 60(b). It is seen from the velocity predictions and measurements of fig. 65 that a viscous calculation procedure tends to give better agreement with the experimental evidence, bearing in mind the degree of scatter associated with the experimental results.

Fig. 66 gives results for an off-design case for which flow visualisation experiments and velocity measurements are reported in reference [47]. The inviscid

solutions shown on this figure were also presented in [47]. Looking at fig. 66 as a whole the viscous solutions appear to describe the flow parameters better than the inviscid solutions although the experimental evidence is again rather scattered. Again the importance of the choice of the value of u_w^+ is emphasized and $u_w^+ = 10$ appears to give a better prediction of the velocity variation whereas $u_w^+ = 2$ gives improved agreement for the pressure drop. However the two-dimensional theory described in this thesis cannot be expected to give good pressure drop predictions due to the large energy dissipation rates which must be present on the hub and shroud surfaces. Note that only three radii are illustrated for this case i.e. $r/r_t = 1.0, 0.633$ and 0.367 for the velocity distributions and slightly differing values of $0.967, 0.7$ and 0.367 for the pressures.

Figs. 61, 62, 63, 64 show the streamlines derived from the theory with $u_w^+ = 2$ compared with photographic evidence obtained by the method of ref. [47]. The experimental evidence was obtained by tracing photographs of streak lines from several rotor segments. Excellent agreement is obtained and it should be particularly noted that in all cases except Case 1, a recirculating eddy is both predicted and observed. The flow direction and direction of rotation of the rotor are indicated on the diagrams.

Fig. 67 shows predictions and measurements of the velocity variations for cases 3 and 4. Severe changes take place at the blade tip in Case 3 and the inviscid solution was found unreliable here: it is therefore not

shown. The most important feature of the calculations is seen on fig. 67, Case 4, where the inviscid analysis gives a markedly different variation from the viscous calculations and the experimental evidence, and fails to predict the presence of a recirculating eddy. This eddy is that indicated by the streamlines of fig. 64.

The overall parameters of the calculations are given in Table (ii), appendix 3. The efficiency values from this two dimensional calculation are obviously not reliable but their relative values should provide guidance on the influence of changing the input parameters on the rotor losses. In some of the cases - particularly 1(iv) and 2(iii) the balance between torque and change of angular momentum has not been achieved to a sufficient accuracy. In 1(iv) this has resulted in an inaccurate efficiency value in this design situation where all the values are close to 100%.

C Flow over a step

Figs. 68 and 69 respectively show predicted and measured friction factor and Stanton number distributions in the region downstream from a backward facing step. The limitations of the crude turbulence model are clearly shown when compared with the Preston tube results of Roussounelos [62]. The point of reattachment of the flow is not well predicted. Certain operations were performed on the numerical analysis such as a reduction in the mesh size by 50%, alteration of the wall slip parameter u_w^+ and allowing the flow to enter the control system with a linear velocity profile instead of the previously used constant velocity. These alterations had a negligible

effect on the point of reattachment of the flow, although producing significantly different predictions of the friction factor. These results are illustrated on fig. 68. No conclusions can be made from the friction factor results with regard to the best value of u_w^+ . The comparison of predicted and measured Stanton number distributions on fig. 69 show some interesting features. A value of u_w^+ of 2 gives good agreement with experiment up to the reattachment point. A value of $u_w^+ = 10$ gives a poor prediction of Stanton number. All the predictions exhibit the peaking associated with the Stanton number downstream from a step but then show a minimum value of Stanton number corresponding to predicted point of reattachment. There was no apparent experimental evidence for this predicted behaviour. The fact that this minimum does not appear in practice is probably because of the highly unstable nature of the flow in this region and the associated high levels of turbulence which have an overwhelming effect on the heat transfer.

2.11 Future Work - Recirculating Flows

1. At present, the theoretical solution procedure is limited to cases of small temperature differences. If the fluid density was allowed to be a general function of temperature and to appear in the equations (rather than just in the buoyancy term) then the applicability of the method would be greatly improved.

2. Applied to the turbomachinery situation, particular attention should be paid to the small radius region of the chosen control system. At present, in the region downstream from the blades for the inflow situation, the passage height of the system is assumed to be constant. Possibly a better reflection of the experimental rig would be obtained if the passage height was allowed to vary (as it does in the blade passage) in order to keep the cross-sectional area constant.

3. Further tests to establish the usefulness of the simple turbulence model should be performed. An extension of the theory to deal with curved blades will provide much more experimental evidence for comparison purposes than is available at present. The simplest case to consider is that of logarithmic spiral blades where the local tangent to the spiral makes a constant angle with the radial direction.

4. The transient calculation procedure is still in its relatively early stages of development. The most useful information from this program will come from a study of the point of instability with an investigation as to what particular combinations of Reynolds and Grashof

numbers promote unstable flow and what the characteristics of the flow are as the point of instability is approached. Further numerical experiments, particularly with regard to mesh sizes, are required. By increasing the number of mesh points and comparing with the original solutions, the influence of mesh size on indicated instability points may be investigated.

Conclusions

1. Predictions of velocity and temperature profiles, friction factor and Stanton number in constant pressure gradient parameter boundary layers showed good agreement with experiment. Equally reliable predictions were obtained by both a Prandtl mixing length hypothesis, and a turbulence model based on the Prandtl-Kolmogorov hypothesis.
2. A test consisting of a long adverse pressure gradient section showed poor agreement with experiment. A check on the two-dimensionality of this flow revealed the influence of side-wall boundary layers on the flow structure, thus invalidating predictions made by the methods described in this thesis.
3. Although the characteristic "dip and rise" of local Stanton number in a laminarized flow was predicted, the minimum level of Stanton number tended to be overpredicted. Alteration of the effective sublayer thickness parameter resulted in a better description, though not the complete answer. The implicit numerical formulation technique and the associated forward step appeared to be adequate as the results with iteration at each forward step did not appear to be significantly different from those of the non-iterative techniques which were generally used. Velocity and temperature profiles were well predicted, except in the region of very high favourable pressure gradient where there was evidence of boundary layer laminarization occurring.
4. Good agreement with the turbulent shear stress and turbulent kinetic energy measurements of Wolfenden [38] was obtained. Although the initial profiles of turbulent

kinetic energy and turbulent shear stress did not agree with experiment, a relatively short distance was necessary before good agreement between the predicted and measured turbulence quantities was obtained. This distance was of particular relevance because the starting conditions would generally not be known when applying the prediction procedure and the time taken for the shear stress and kinetic energy to adjust to the experimental values was consequently of more significance. The relative unimportance in a calculation procedure of the outer part of the boundary layer was emphasised by comparisons of predicted and measured values of eddy diffusivity of momentum. The crude assumption of a value of eddy diffusivity in the outer layer which remained constant at a particular station, although being allowed to vary in the streamwise direction, appeared to be sufficient in the prediction of both mean flow and turbulence quantities.

5. Comparison of the theory with the zero pressure gradient results of Klebanoff [42] exhibit good agreement with regard to both mean flow quantities and turbulence terms.

6. Extension of the theory to deal with developing internal flows has led to the prediction of some interesting features which have been observed experimentally. The existence of the three zones in the development of the internal flows and the associated non-asymptotic approach of the displacement and momentum thicknesses to their fully developed values is predicted and confirmed by experiment. It was found to be not possible to predict all the external and internal flows using the same

parameters. The diverging passage flow proved to be the exception where changes in the outer layer constant had to be made from the values used in external flows and parallel walled passages. Thus, in these internal flows, a correct description of the outer part of the boundary layer, i.e. the mid-duct flow, appears to be significantly more important than in external flows. Poor agreement was still obtained between predicted and measured Stanton numbers in the diverging duct case.

7. In moving forward from solutions of the governing parabolic partial differential equations of boundary layer and duct flows to those of the more general elliptic equations which cover separating boundary layers, an upwind difference formulation procedure was used. This method was directly analogous to the fully implicit techniques used for solutions of the parabolic equations.

8. Calculations were made on laminar steady-state combined natural and forced convection for a situation in which flow reversal may occur. The influence of the buoyancy effects on heat transfer and skin friction is considerable in laminar flows. The overall Nusselt number for downflow may be reduced to only 30% of the corresponding forced flow value.

9. The existence of a steady recirculating eddy has been shown by experiment (ref. [66]) to be possible and fair agreement between prediction and flow visualization was obtained. The predictions of overall Nusselt number variation with Grashof number agree well with observations.

10. The inclusion of time-dependent terms in the governing equations of laminar combined natural and forced

convection has shown physical instabilities in certain unsteady laminar flows. The apparently perfectly stable nature of an aiding flow situation, compared with the unstable behaviour of the corresponding opposing flow, illustrate the inherent differences between the two situations.

11. With certain combinations of Reynolds and Grashof number (e.g. opposing flow, $Re = 2000$, $Gr = 3 \times 10^7$) it was found impossible to obtain a converged solution by assuming the steady state equations described the situation. The unsteady equations had to be considered for a solution to be obtained. Use of the unsteady calculation method did not preclude a steady state solution being obtained if the conditions were suitable (e.g. opposing flow, $Re = 1000$, $Gr = 3 \times 10^6$).

12. The steady state solution method was extended to solve two-dimensional turbulent flow in a radial bladed rotor. A constant value of eddy diffusivity and a wall slip approximation were included. Laminar and inviscid flows formed special cases of the method.

13. Boundary layer development on the hub and shroud surfaces could be included and these may have a significant effect on the flows in the rotor.

14. The Reynolds number used in the calculations was based on the total effective viscosity and the comparisons made were based on choices of the ratio of eddy to molecular diffusivity of 50 and 100. The results were not greatly influenced by this choice.

15. The limited amount of experimental evidence was scattered so that no clear choice for the slip parameter

u_w^+ , which has a strong influence, could be made. Contour plots of streamlines based on the viscous solution, however, gave markedly better agreement than the inviscid. In one case an observed recirculating eddy was predicted by the viscous, but not by the inviscid calculation.

16. The method also includes predictions of pressure loss and efficiency but these were unreliable because of the presence of the hub and shroud surfaces. However the relative values should be useful in determining the influence of the design parameters on the losses and efficiency in radial bladed rotors.

17. The limitations of this simple model of turbulence as used in the turbomachinery calculations, are shown with predictions of separating and reattaching flow over a step. Poor agreement was obtained with experiment. It may thus be concluded that, for the case of the turbomachinery flows, where wall parameters are of secondary importance and the flow is highly turbulent, a constant value of eddy diffusivity is sufficient. However for the wall generated turbulence of the flow over a step, a much more accurate description of this wall turbulence is required.

Appendix 1

References

1. Prandtl, L. Bericht über Untersuchungen zur ausgebildeten Turbulenz. 1925, Zamm, 5, 136.
2. Boussinesq, J. Theorie de l'écoulement tourbillant. Mem. pres. Acad. Sci. XXIII, 46, Paris.
3. Van Driest, E.R. On turbulent flow near a wall. J. Aeronaut. Sci. 1956, 23, 1007.
4. Patankar, S.V. Wall shear stress and heat flux laws for turbulent boundary layer with a pressure gradient: Use of Van Driest's eddy viscosity hypothesis. 1966, Imp. Coll. Mech. Eng. Dept. TWF/TN/14.
5. Patankar, S.V. and Spalding, D.B. Heat and mass transfer in boundary layers. 1970, 2nd edit. (Intertext Books Ltd., London).
6. Byrne, J. and Hatton, A.P. Prediction and measurement of velocity and temperature profiles in turbulent boundary layers: 1970, 4th International Heat Transfer Conference, Versailles.
7. Clauser, F.H. Turbulent boundary layers in adverse pressure gradients. J. Aeronaut. Sci. 21(2), 91-108, 1954.
8. Mellor, G.L. and Gibson, D.M. Equilibrium turbulent boundary layers. 1966, J. Fluid Mech., 24 (225).
9. McEligot, D.M. and Bankston, C.A. Numerical predictions for circular tube laminarization by heating. 1969 A.S.M.E. 69-HT-52.
10. Launder, B.E. and Jones, W.P. On the prediction of laminarization. 1969, A.R.C. C.P. No. 1036.
11. Nee, V.W. and Kovasznay, S.G. Simple phenomenological theory of turbulent shear flows. Phys. of fluids, 12, 3, 1969, 473.
12. Emmons, H.W. Shear flow turbulence. 1954, Proc. of 2nd U.S. Nat. Congress of Appl. Mech.
13. Bradshaw, P., Ferriss, D.H. and Atwell, N.P. Calculation of boundary layer development using turbulent energy equation. J. Fluid Mech., 1967, 28 (593).

14. Prandtl, L. Über eine neues Formelsystem für
die ausgebildete Turbulenz.
Nachrichten der Akad. Wiss.,
Göttingen, Math. Phys. 1945, Van
den Loek and Ruprecht, Göttingen.
(On a new representation of fully
developed turbulence. J.P.L.
Publication No. 13 (1952), trans.
by D. Coles.)
15. Kolmogorov, A.N. Equations of turbulent motion of
an incompressible fluid. Izv.
Akad. Nauk. SSSR ser. phys. VI
No. 1-2 (1942). Eng. trans. Imp.
Coll., Mech. Eng. Dept. Rep. ON/6,
1968.
16. Ng, K.H. and Turbulence Model for Boundary
 Spalding, D.B. Layers near Walls. Phys. of Fluids,
1972, 15, 1, 20.
17. Rotta, J.C. Statistische Theorie nichthomogener
Turbulenz. Zeitsch für Physik,
1951, 129, 547 and 131, 51.
18. Gawain, T.H. and A unified Hueristic model of fluid
 Pritchard, J.W. turbulence. J. Comp. Physics,
385, 5, 1970.
19. Harlow, F.H. and Turbulence transport equations.
 Nakayama, P.T. Physics of Fluids, 1967, 10, 11, 2323.
20. Jones, W.P. and The prediction of laminarization
 Launder, B.E. with a two equation model of
turbulence. 1970. Imp. Coll. Mech.
Eng. Dept. Ref. BL/TN/A/40.
21. Kline, S.J., Computation of turbulent boundary
 Morkovin, M.V., layers - 1968. Proc. AFOSR-IFP
 Sovran, G. and Stanford Conf. 1 and 2. 1968.
 Cockrell, D.J. (Stanford University, California.)
22. Glushko, G.S. Turbulent boundary layer on a plane
plate in an incompressible fluid.
1965. Izv. Akad. Nauk. SSSR. Ser.
Mech. No. 4 (13).
23. Kearney, D. et al The effect of free stream turbulence
on heat transfer to strongly
accelerated turbulent boundary
layers. Proc. 1970 Heat transfer
and Fluid Mech. Institute, Stanford
U. Press.
24. Hanjalic, K. and A Reynolds stress model of turbulence
 Launder, B.E. and its application to thin shear
flows. J. Fluid Mech. 52, 609, 1972.

25. Daly, B.J. and Harlow, F.H. Transport equations in turbulence. Phys. of Fluids 1970, 13, 11, 2634.
26. Chung, P.M. Chemical reaction in a turbulent flow field with uniform velocity gradient. Phys. of Fluids, 1970, 13, 1153.
27. Lundgren, T.S. Model equation for non-homogeneous turbulence. Phys. of Fluids, 1969, 12, 485.
28. Tyldesley, J.R. and Silver, R.S. The prediction of the transport properties of a turbulent fluid. Int. J. Heat Mass Transfer, 1968, 11, 1325.
29. Deardorff, J.W. A numerical study of three dimensional turbulent channel flow at large Reynolds numbers. J. Fluid Mech. 1970, 41, 453.
30. Hatton, A.P. Heat transfer through the turbulent boundary layer on a flat plate. Int. J. Heat Mass Transfer, 1964, 7, 875.
31. Hatton, A.P. Heat transfer through the turbulent incompressible boundary layer in the presence of moderate pressure gradients. Int. J. Heat and Mass Transfer, 1965, 8, 1469.
32. Byrne, J., Hatton, A.P. and Marriott, P. Turbulent flow and heat transfer in the entrance region of a parallel wall passage. Proc. Instn. Mech. Engrs. 1969-70, 184 (Pt. 1), 697.
33. Reynolds, W.C. Computation of turbulent flows - State of the art, 1970. Thermosciences Div. Dept. of Mech. Eng. Stanford U., California. 1970 Report MD-27.
34. Bradshaw, P. The understanding and prediction of turbulent flow. Aeronautical Journal July 1972. 6th Reynolds-Prandtl Lecture - Munich, April 1972.
35. Patel, V.C. Calibration of the Preston tube and limitations on its use in pressure gradients. J. Fluid Mech. 1965, 23, 185.
36. Preston, J.H. The determination of turbulent skin friction by means of pitot tubes. J. Roy. Aero. Soc. 1954, 58, 109.

37. Woolley, N.H. Theoretical and experimental investigation of flow and heat transfer through turbulent boundary layers in internal, external and rotating flows. M.Sc. Thesis, Mech. Eng. Dept. U.M.I.S.T., 1969.
38. Wolfendon, S. Velocity, temperature and turbulence measurements in boundary layers. M.Sc. Dissertation, Mech. Eng. Dept., U.M.I.S.T., 1971.
39. Wolfshtein, M. Convection processes in a turbulent impinging jet. Ph.D. thesis, University of London, 1967.
40. Crank, J. and Nicholson, P. A practical method for numerical evaluation of solutions of partial differential equations of the heat conduction type. Proc. Cambridge Phil. Soc. 1947, 43, 50.
41. Ludwig, H. and Tillmann, W. Investigations of the wall shearing stress in turbulent boundary layers. N.A.C.A. T.M.1285, 1950.
42. Klebanoff, P.S. Characteristics of turbulence in a boundary layer with zero pressure gradient. N.A.C.A. Report 1247, 1954.
43. Marriott, P.G. Heat transfer in the entrance region of a parallel wall passage. M.Sc. Thesis, Mech. Eng. Dept., U.M.I.S.T., 1969.
44. Ellison, G.M. Flow and heat transfer in a straight sided diffuser. M.Sc. Dissertation, Mech. Eng. Dept., U.M.I.S.T., 1970.
45. Hatton, A.P. and Woolley, N.H. Heat transfer in two-dimensional turbulent confined flows. Instn. Mech. Engrs. Proc. 1972, 186, 53/72.
46. Gosman, A.D., Pun, W.M., Runchal, A.K., Spalding, D.B. and Wolfshtein, M. Heat and mass transfer in recirculating flows. 1968 (Academic Press Inc., New York and London.)
47. Benson, R.S., Cartwright, W.G. and Hill, M.J. Analytical and experimental studies of two dimensional flows in a radial bladed impellor. A.S.M.E. Paper 71-GT-20, 1971.
48. Rao, T.L.S. and Morris, W.D. Superimposed laminar forced and free convection between vertical parallel plates when one plate is uniformly heated and the other is thermally insulated. Thermodynamics and Fluid Mechanics. Conv. Proc. Inst. of Mech. Engrs., 1967-68, 182, Pt. 3H, 374.

49. Acrivos, A. Combined laminar free and forced convection heat transfer in external flows. A.I.Ch.E. Jl. 1958, 4 (No. 3), 285.
50. Gunness, R.C. jun. and Gebhart, B. Combined forced and natural convection flow for the wedge geometry. Int. J. Heat Mass Transfer 1965, 8 (No. 1, Jan.).
51. Brown, C.K. and Gauvin, W.H. Combined free and forced convection - Pt. 1. Heat transfer in aiding flow. Can. J. Chem. Engng. 1956, 43(6), 306; also Pt. 2, 1956, 43(6), 313.
52. Hatton, A.P., James, D.D., and Swire, W.H. Combined forced and natural convection with low speed air flow over horizontal cylinders. J. Fluid Mech. 1970, 42 (Pt. 1), 17.
53. Hall, W.B. and Price, P.H. Interaction between a turbulent free convection layer and a downward forced flow. Paper C113/71. Inst. Mech. E. Symposium. (Heat and mass transfer by combined forced and natural convection.) Manchester, 1971.
54. Byrne, J.E. and Ejiogu, E. Combined free and forced convection heat transfer in a vertical pipe. Paper C118/71. Inst. Mech. E. Symposium. (Heat and mass transfer by combined forced and natural convection.) Manchester, 1971.
55. Kettleborough, C.F. Transient laminar free convection between heated vertical plates including entrance effects. Int. J. Heat Mass Transfer 1972, 15 (883).
56. Szekely, J. and Todd, M.R. Natural convection in a rectangular cavity. Transient behaviour and two phase systems in laminar flow. Int. J. Heat Mass Transfer. 14, 3, 467, 1971.
57. Wilkes, J.O. and Churchill, S.W. The finite difference computation of natural convection in a rectangular enclosure. A.I.Ch.E. Jl. 1966, 12, 161.
58. Fromm, J.E. and Harlow, F.H. Numerical solution of the problem of vortex street development. Phys. of Fluids, 1963, 6, 975.
59. Hatton, A.P. and Woolley, N.H. Laminar combined natural and forced convection in a rectangular field. Paper C119/71. Inst. Mech. E. Symposium. (Heat and mass transfer by combined forced and natural convection.) Manchester 1971.

60. Taylor, G.I. Stability of a viscous liquid contained between two rotating cylinders. Phil. Trans. Roy. Soc. A. 223, 1923, 289.
61. Betts, C. and Hatton, A.P. The enhancement of turbulent diffusion in a parallel wall duct. Proc. Inst. Mech. E. 1971, 185.
62. Roussounelos, C. Heat transfer in separating and reattaching flows. M.Sc. Thesis, 1972, Mech. Eng. Dept. U.M.I.S.T.
63. Moore, J. The development of turbulent boundary layers in centrifugal machines. 1969, M.I.T. Gas Turbine Laboratory, report No. 99.
64. Herath, K. An investigation of relative velocities in a rotating cascade of radial blades. M.Sc. Dissertation, 1971, Mech. Eng. Dept., U.M.I.S.T.
65. Moretti, P.M. and Kays, W.M. Heat transfer through an incompressible turbulent boundary layer with varying free-stream velocity and varying surface temperature. Stanford University, Mech. Eng. Dept., Report No. PG-1.
66. Loy, A.W. Theoretical and experimental studies in combined natural and forced convection in parallel wall passages. M.Sc. Dissertation, 1972, Mech. Eng. Dept., U.M.I.S.T.

Appendix 2

Tables of results - boundary layer experiments

EXPT. A1

Zero pressure gradient, heating from leading edge.

| Stat. no. | x (m) | U_s (m/s) | $\delta^* \times 10^3$ (m) | R_θ | H | Cf $\times 10^3$ | St $\times 10^3$ | $\delta_t^* \times 10^3$ (m) |
|-----------|-------|-------------|----------------------------|------------|-------|------------------|------------------|------------------------------|
| 1 | 0.416 | 23.25 | 1.715 | 1820 | 1.401 | 3.668 | 3.448 | 2.165 |
| 2 | 0.721 | 23.20 | 2.193 | 2670 | 1.392 | 3.286 | 2.518 | 2.098 |
| 3 | 1.026 | 22.51 | 2.930 | 3270 | 1.387 | 3.186 | 2.361 | 3.125 |
| 4 | 1.330 | 23.00 | 3.703 | 4000 | 1.383 | 2.979 | 2.255 | 3.592 |
| 5 | 1.635 | 22.99 | 4.345 | 4700 | 1.369 | 2.939 | 2.063 | 4.350 |

Station no. 1

| y (m) | u/ U_s | y (m) | u/ U_s | y (m) | $\frac{T_{aw}-T_a}{T_{aw}-T_{as}}$ | y (m) | $\frac{T_{aw}-T_a}{T_{aw}-T_{as}}$ |
|----------|----------|----------|----------|----------|------------------------------------|----------|------------------------------------|
| 0.000152 | 0.3179 | 0.002083 | 0.7443 | 0.000127 | 0.4884 | 0.001549 | 0.7415 |
| 0.000178 | 0.3529 | 0.002464 | 0.7647 | 0.000178 | 0.5118 | 0.002057 | 0.7505 |
| 0.000203 | 0.3888 | 0.002972 | 0.7885 | 0.000229 | 0.5405 | 0.002565 | 0.7738 |
| 0.000229 | 0.4299 | 0.003480 | 0.8102 | 0.000279 | 0.5549 | 0.003073 | 0.8026 |
| 0.000254 | 0.4624 | 0.003988 | 0.8293 | 0.000356 | 0.5692 | 0.003835 | 0.8277 |
| 0.000279 | 0.4853 | 0.004623 | 0.8579 | 0.000432 | 0.6015 | 0.004597 | 0.8690 |
| 0.000330 | 0.5279 | 0.005131 | 0.8745 | 0.000533 | 0.6141 | 0.005867 | 0.9318 |
| 0.000381 | 0.5522 | 0.005893 | 0.8967 | 0.000660 | 0.6446 | 0.007137 | 0.9408 |
| 0.000457 | 0.5846 | 0.006655 | 0.9143 | 0.000787 | 0.6625 | 0.008915 | 0.9749 |
| 0.000533 | 0.6044 | 0.007417 | 0.9350 | 0.000991 | 0.6823 | 0.011455 | 1.0000 |
| 0.000635 | 0.6273 | 0.008179 | 0.9516 | 0.001245 | 0.7056 | | |
| 0.000787 | 0.6505 | 0.008941 | 0.9657 | | | | |
| 0.000940 | 0.6626 | 0.009703 | 0.9775 | | | | |
| 0.001143 | 0.6789 | 0.010719 | 0.9869 | | | | |
| 0.001397 | 0.7023 | 0.012500 | 0.9978 | | | | |
| 0.001702 | 0.7226 | 0.015037 | 1.0000 | | | | |

Station no. 2

| y (m) | u/ U_s | y (m) | u/ U_s | y (m) | $\frac{T_{aw}-T_a}{T_{aw}-T_{as}}$ | y (m) | $\frac{T_{aw}-T_a}{T_{aw}-T_{as}}$ |
|----------|----------|----------|----------|----------|------------------------------------|----------|------------------------------------|
| 0.000152 | 0.3153 | 0.003505 | 0.7509 | 0.000102 | 0.3089 | 0.001283 | 0.6739 |
| 0.000203 | 0.3617 | 0.004140 | 0.7740 | 0.000114 | 0.3398 | 0.001664 | 0.7035 |
| 0.000254 | 0.4229 | 0.004902 | 0.7991 | 0.000140 | 0.3787 | 0.002159 | 0.7330 |
| 0.000305 | 0.4740 | 0.005664 | 0.8182 | 0.000165 | 0.4203 | 0.002667 | 0.7558 |
| 0.000356 | 0.5072 | 0.006680 | 0.8439 | 0.000191 | 0.4458 | 0.003302 | 0.7813 |
| 0.000406 | 0.5293 | 0.007696 | 0.8726 | 0.000216 | 0.4579 | 0.004064 | 0.8001 |
| 0.000483 | 0.5549 | 0.008712 | 0.8999 | 0.000267 | 0.4900 | 0.005080 | 0.8363 |
| 0.000559 | 0.5673 | 0.009728 | 0.9160 | 0.000317 | 0.5371 | 0.006350 | 0.8712 |
| 0.000686 | 0.5912 | 0.010998 | 0.9422 | 0.000394 | 0.5491 | 0.008382 | 0.9195 |
| 0.000813 | 0.6055 | 0.012268 | 0.9589 | 0.000495 | 0.5773 | 0.010922 | 0.9745 |
| 0.001067 | 0.6312 | 0.013538 | 0.9739 | 0.000648 | 0.6109 | 0.013462 | 0.9879 |
| 0.001473 | 0.6614 | 0.014808 | 0.9887 | 0.000826 | 0.6216 | 0.018542 | 0.9919 |
| 0.001981 | 0.6874 | 0.019888 | 0.9991 | 0.001029 | 0.6471 | 0.026162 | 1.0000 |
| 0.002489 | 0.7089 | 0.027508 | 0.9989 | | | | |
| 0.002997 | 0.7328 | 0.040209 | 1.0000 | | | | |

Station no. 3

| y (m) | u/U _s | y (m) | u/U _s | y (m) | $\frac{T_{aw}-T_a}{T_{aw}-T_{as}}$ | y (m) | $\frac{T_{aw}-T_a}{T_{aw}-T_{as}}$ |
|----------|------------------|----------|------------------|----------|------------------------------------|----------|------------------------------------|
| 0.000152 | 0.2860 | 0.005537 | 0.7768 | 0.000102 | 0.3514 | 0.002108 | 0.6603 |
| 0.000203 | 0.3588 | 0.006426 | 0.7971 | 0.000127 | 0.3959 | 0.002616 | 0.7023 |
| 0.000254 | 0.4251 | 0.007442 | 0.8276 | 0.000152 | 0.4305 | 0.003124 | 0.7294 |
| 0.000305 | 0.4701 | 0.008585 | 0.8467 | 0.000178 | 0.4465 | 0.003759 | 0.7418 |
| 0.000381 | 0.5057 | 0.009855 | 0.8728 | 0.000229 | 0.4675 | 0.004648 | 0.7690 |
| 0.000483 | 0.5377 | 0.011125 | 0.8950 | 0.000279 | 0.4935 | 0.005664 | 0.7962 |
| 0.000610 | 0.5603 | 0.012395 | 0.9166 | 0.000356 | 0.5256 | 0.006934 | 0.8604 |
| 0.000864 | 0.5938 | 0.013665 | 0.9405 | 0.000432 | 0.5466 | 0.008204 | 0.8728 |
| 0.001219 | 0.6189 | 0.014935 | 0.9555 | 0.000533 | 0.5713 | 0.009728 | 0.8900 |
| 0.001600 | 0.6455 | 0.016205 | 0.9702 | 0.000635 | 0.5775 | 0.011506 | 0.9061 |
| 0.002108 | 0.6688 | 0.017729 | 0.9864 | 0.000838 | 0.5874 | 0.014046 | 0.9395 |
| 0.002616 | 0.6909 | 0.020269 | 0.9951 | 0.001092 | 0.6108 | 0.019126 | 0.9654 |
| 0.003251 | 0.7171 | 0.025349 | 0.9997 | 0.001346 | 0.6269 | 0.024206 | 1.0000 |
| 0.004013 | 0.7407 | 0.032970 | 0.9997 | 0.001727 | 0.6528 | | |
| 0.004775 | 0.7624 | 0.045668 | 1.0000 | | | | |

Station no. 4

| y (m) | u/U _s | y (m) | u/U _s | y (m) | $\frac{T_{aw}-T_a}{T_{aw}-T_{as}}$ | y (m) | $\frac{T_{aw}-T_a}{T_{aw}-T_{as}}$ |
|----------|------------------|----------|------------------|----------|------------------------------------|----------|------------------------------------|
| 0.000152 | 0.2431 | 0.006172 | 0.7650 | 0.000102 | 0.3671 | 0.002845 | 0.7120 |
| 0.000178 | 0.2963 | 0.007442 | 0.7998 | 0.000127 | 0.3880 | 0.003353 | 0.7283 |
| 0.000229 | 0.3678 | 0.008712 | 0.8236 | 0.000152 | 0.4077 | 0.004115 | 0.7410 |
| 0.000279 | 0.4232 | 0.009982 | 0.8429 | 0.000178 | 0.4147 | 0.005132 | 0.7689 |
| 0.000330 | 0.4634 | 0.011252 | 0.8632 | 0.000229 | 0.4507 | 0.006147 | 0.7968 |
| 0.000381 | 0.4872 | 0.012522 | 0.8818 | 0.000279 | 0.4704 | 0.007163 | 0.8142 |
| 0.000457 | 0.5140 | 0.013792 | 0.9031 | 0.000356 | 0.4995 | 0.008433 | 0.8467 |
| 0.000635 | 0.5553 | 0.015316 | 0.9251 | 0.000432 | 0.5227 | 0.010210 | 0.8630 |
| 0.000838 | 0.5799 | 0.016840 | 0.9444 | 0.000533 | 0.5517 | 0.012243 | 0.8862 |
| 0.001168 | 0.6063 | 0.018364 | 0.9622 | 0.000660 | 0.5680 | 0.014783 | 0.9141 |
| 0.001549 | 0.6309 | 0.019888 | 0.9737 | 0.000864 | 0.5912 | 0.017323 | 0.9443 |
| 0.002108 | 0.6574 | 0.021412 | 0.9868 | 0.001118 | 0.6237 | 0.019863 | 0.9640 |
| 0.002870 | 0.6821 | 0.023952 | 0.9955 | 0.001448 | 0.6528 | 0.023673 | 0.9803 |
| 0.003886 | 0.7138 | 0.031571 | 1.0000 | 0.001829 | 0.6644 | 0.028753 | 0.9930 |
| 0.004902 | 0.7138 | | | 0.002337 | 0.6911 | 0.036373 | 1.0000 |

Station no. 5

| y (m) | u/U _s | y (m) | u/U _s | y (m) | $\frac{T_{aw}-T_a}{T_{aw}-T_{as}}$ | y (m) | $\frac{T_{aw}-T_a}{T_{aw}-T_{as}}$ |
|----------|------------------|----------|------------------|----------|------------------------------------|----------|------------------------------------|
| 0.000152 | 0.2729 | 0.004648 | 0.7213 | 0.000102 | 0.3618 | 0.003708 | 0.7228 |
| 0.000178 | 0.3189 | 0.005664 | 0.7408 | 0.000127 | 0.3859 | 0.004470 | 0.7416 |
| 0.000229 | 0.3897 | 0.006934 | 0.7603 | 0.000152 | 0.4016 | 0.005359 | 0.7510 |
| 0.000279 | 0.4375 | 0.008204 | 0.7885 | 0.000203 | 0.4455 | 0.006375 | 0.7782 |
| 0.000330 | 0.4704 | 0.009474 | 0.8085 | 0.000254 | 0.4539 | 0.007391 | 0.7991 |
| 0.000381 | 0.4907 | 0.010998 | 0.8311 | 0.000305 | 0.4821 | 0.008661 | 0.8096 |
| 0.000457 | 0.5177 | 0.012522 | 0.8558 | 0.000356 | 0.4999 | 0.010191 | 0.83781 |
| 0.000559 | 0.5453 | 0.014046 | 0.8749 | 0.000432 | 0.5125 | 0.011963 | 0.8650 |
| 0.000686 | 0.5587 | 0.015570 | 0.8994 | 0.000533 | 0.5345 | 0.013995 | 0.8954 |
| 0.000940 | 0.5851 | 0.017602 | 0.9215 | 0.000635 | 0.5627 | 0.016027 | 0.9121 |
| 0.001346 | 0.6077 | 0.019634 | 0.9432 | 0.000762 | 0.5773 | 0.018567 | 0.9247 |
| 0.001854 | 0.6302 | 0.021666 | 0.9577 | 0.000914 | 0.5941 | 0.021107 | 0.9425 |
| 0.002362 | 0.6510 | 0.024206 | 0.9804 | 0.001168 | 0.6192 | 0.024155 | 0.9665 |
| 0.003124 | 0.6811 | 0.029286 | 0.9970 | 0.001549 | 0.6297 | 0.029235 | 0.9812 |
| 0.003886 | 0.7041 | 0.034366 | 1.0000 | 0.002057 | 0.6527 | 0.036855 | 0.9916 |
| | | | | 0.002565 | 0.6820 | 0.044475 | 1.0000 |
| | | | | 0.003073 | 0.6914 | | |

Expt. A2

Const. fav. pressure gradient, heating from leading edge.

| Stat. no. | x (m) | U_s (m/s) | $\delta^* \times 10^3$ (m) | R_σ | H | Cf $\times 10^3$ | St $\times 10^3$ | $\delta_t^* \times 10^3$ (m) |
|-----------|-------|-------------|----------------------------|------------|-------|------------------|------------------|------------------------------|
| 1 | 0.416 | 22.15 | 1.076 | 1190 | 1.377 | 4.326 | 3.229 | 1.259 |
| 2 | 0.721 | 24.61 | 1.311 | 1650 | 1.384 | 4.279 | 2.370 | 1.938 |
| 3 | 1.026 | 28.21 | 1.535 | 2130 | 1.347 | 3.757 | 1.960 | 2.339 |
| 4 | 1.330 | 32.97 | 1.492 | 2350 | 1.339 | 3.764 | 1.813 | 2.536 |
| 5 | 1.635 | 39.41 | 1.341 | 2600 | 1.36 | 3.763 | 1.707 | 2.436 |

Station no. 1

| y (m) | u/ U_s | y (m) | u/ U_s | y (m) | $\frac{T_{aw} - T_a}{T_{aw} - T_{as}}$ | y (m) | $\frac{T_{aw} - T_a}{T_{aw} - T_{as}}$ |
|----------|----------|----------|----------|----------|--|----------|--|
| 0.000152 | 0.3833 | 0.002310 | 0.8286 | 0.000102 | 0.4455 | 0.00651 | 0.7598 |
| 0.000178 | 0.4185 | 0.002692 | 0.8482 | 0.000127 | 0.4754 | 0.002032 | 0.7832 |
| 0.000203 | 0.4499 | 0.003073 | 0.8659 | 0.000152 | 0.4871 | 0.002540 | 0.8325 |
| 0.000254 | 0.5098 | 0.003454 | 0.8796 | 0.000203 | 0.5287 | 0.003048 | 0.8702 |
| 0.000305 | 0.5624 | 0.003962 | 0.8987 | 0.000254 | 0.5442 | 0.003810 | 0.8948 |
| 0.000356 | 0.6003 | 0.004471 | 0.9161 | 0.000330 | 0.5819 | 0.004572 | 0.9208 |
| 0.000406 | 0.6268 | 0.004978 | 0.9304 | 0.000432 | 0.6208 | 0.005334 | 0.9455 |
| 0.000457 | 0.6446 | 0.005486 | 0.9419 | 0.000559 | 0.6429 | 0.006096 | 0.9572 |
| 0.000533 | 0.6733 | 0.006248 | 0.9589 | 0.000762 | 0.6780 | 0.007366 | 0.9701 |
| 0.000660 | 0.6950 | 0.007010 | 0.9728 | 0.001016 | 0.7104 | 0.008636 | 1.0000 |
| 0.000787 | 0.7122 | 0.008026 | 0.9851 | 0.001270 | 0.7312 | | |
| 0.000965 | 0.7328 | 0.009805 | 0.9968 | | | | |
| 0.001168 | 0.7522 | 0.012344 | 0.9991 | | | | |
| 0.001372 | 0.7691 | 0.017425 | 0.9992 | | | | |
| 0.001626 | 0.7873 | 0.025045 | 1.0000 | | | | |
| 0.001930 | 0.8083 | | | | | | |

Station no. 2

| y (m) | u/ U_s | y (m) | u/ U_s | y (m) | $\frac{T_{aw} - T_a}{T_{aw} - T_{as}}$ | y (m) | $\frac{T_{aw} - T_a}{T_{aw} - T_{as}}$ |
|----------|----------|----------|----------|----------|--|----------|--|
| 0.000152 | 0.3487 | 0.002286 | 0.7881 | 0.000102 | 0.4067 | 0.001930 | 0.7160 |
| 0.000178 | 0.3904 | 0.002667 | 0.8062 | 0.000127 | 0.4375 | 0.002311 | 0.7435 |
| 0.000203 | 0.4237 | 0.003048 | 0.8254 | 0.000152 | 0.4496 | 0.002692 | 0.7644 |
| 0.000229 | 0.4617 | 0.003556 | 0.8437 | 0.000178 | 0.4760 | 0.003073 | 0.7743 |
| 0.000254 | 0.4930 | 0.004064 | 0.8661 | 0.000229 | 0.5046 | 0.003581 | 0.8096 |
| 0.000279 | 0.5148 | 0.004572 | 0.8824 | 0.000279 | 0.5289 | 0.004089 | 0.8239 |
| 0.000330 | 0.5624 | 0.005207 | 0.9004 | 0.000330 | 0.5289 | 0.004597 | 0.8393 |
| 0.000381 | 0.5882 | 0.005842 | 0.9193 | 0.000381 | 0.5322 | 0.005232 | 0.8800 |
| 0.000457 | 0.6201 | 0.006477 | 0.9344 | 0.000457 | 0.5564 | 0.005994 | 0.9009 |
| 0.000584 | 0.6491 | 0.007239 | 0.9500 | 0.000559 | 0.5850 | 0.006756 | 0.9086 |
| 0.000762 | 0.6742 | 0.008001 | 0.9647 | 0.000660 | 0.6070 | 0.007772 | 0.9329 |
| 0.001016 | 0.7043 | 0.008890 | 0.9792 | 0.000787 | 0.6180 | 0.009296 | 0.9736 |
| 0.001270 | 0.7248 | 0.009906 | 0.9896 | 0.000965 | 0.6345 | 0.011836 | 0.9890 |
| 0.001524 | 0.7431 | 0.011176 | 0.9978 | 0.001219 | 0.6555 | 0.016916 | 0.9967 |
| 0.001905 | 0.7655 | 0.013716 | 1.0000 | 0.001549 | 0.6852 | 0.024537 | 1.0000 |

Station no. 3

| y (m) | u/U _s | y (m) | u/U _s | y (m) | $\frac{T_{aw}-T_a}{T_{aw}-T_{as}}$ | y (m) | $\frac{T_{aw}-T_a}{T_{aw}-T_{as}}$ |
|----------|------------------|----------|------------------|----------|------------------------------------|----------|------------------------------------|
| 0.000152 | 0.3648 | 0.001981 | 0.7698 | 0.000102 | 0.3778 | 0.001930 | 0.6832 |
| 0.000178 | 0.4009 | 0.002413 | 0.7902 | 0.000127 | 0.4151 | 0.002311 | 0.6967 |
| 0.000203 | 0.4413 | 0.002870 | 0.8134 | 0.000152 | 0.4441 | 0.002819 | 0.7225 |
| 0.000229 | 0.4829 | 0.003378 | 0.8308 | 0.000203 | 0.4668 | 0.003327 | 0.7526 |
| 0.000254 | 0.5162 | 0.004013 | 0.8533 | 0.000254 | 0.4896 | 0.003962 | 0.7795 |
| 0.000279 | 0.5375 | 0.004648 | 0.8736 | 0.000330 | 0.5072 | 0.004597 | 0.8043 |
| 0.000305 | 0.5590 | 0.005283 | 0.8897 | 0.000406 | 0.5279 | 0.005359 | 0.8261 |
| 0.000356 | 0.5892 | 0.006045 | 0.9056 | 0.000483 | 0.5476 | 0.006375 | 0.8478 |
| 0.000406 | 0.6098 | 0.006807 | 0.9252 | 0.000584 | 0.5683 | 0.007645 | 0.8944 |
| 0.000483 | 0.6347 | 0.007569 | 0.9392 | 0.000711 | 0.5880 | 0.008915 | 0.9451 |
| 0.000584 | 0.6544 | 0.008585 | 0.9594 | 0.000889 | 0.6045 | 0.010185 | 0.9493 |
| 0.000762 | 0.6754 | 0.009601 | 0.9739 | 0.001092 | 0.6314 | 0.011963 | 0.9928 |
| 0.001016 | 0.7043 | 0.013411 | 0.9873 | 0.001295 | 0.6408 | 0.014503 | 1.0000 |
| 0.001270 | 0.7246 | 0.016078 | 0.9987 | | | | |
| 0.001600 | 0.7466 | 0.021158 | 1.0000 | | | | |

Station no. 4

| y (m) | u/U _s | y (m) | u/U _s | y (m) | $\frac{T_{aw}-T_a}{T_{aw}-T_{as}}$ | y (m) | $\frac{T_{aw}-T_a}{T_{aw}-T_{as}}$ |
|----------|------------------|----------|------------------|----------|------------------------------------|----------|------------------------------------|
| 0.000152 | 0.3605 | 0.002261 | 0.7989 | 0.000102 | 0.3684 | 0.002362 | 0.6564 |
| 0.000178 | 0.3997 | 0.002769 | 0.8219 | 0.000127 | 0.3929 | 0.002870 | 0.6931 |
| 0.000203 | 0.4510 | 0.003277 | 0.8420 | 0.000152 | 0.4118 | 0.003378 | 0.7131 |
| 0.000229 | 0.4975 | 0.003785 | 0.8561 | 0.000203 | 0.4385 | 0.004013 | 0.7587 |
| 0.000254 | 0.5339 | 0.004420 | 0.8761 | 0.000254 | 0.4596 | 0.004648 | 0.7843 |
| 0.000279 | 0.5589 | 0.005054 | 0.8919 | 0.000330 | 0.4885 | 0.005410 | 0.8054 |
| 0.000330 | 0.5964 | 0.005816 | 0.9096 | 0.000457 | 0.4996 | 0.006172 | 0.8154 |
| 0.000381 | 0.6216 | 0.006578 | 0.9270 | 0.000584 | 0.5252 | 0.007442 | 0.8599 |
| 0.000457 | 0.6431 | 0.007468 | 0.9430 | 0.000711 | 0.5541 | 0.008712 | 0.8999 |
| 0.000559 | 0.6618 | 0.008483 | 0.9580 | 0.000889 | 0.5652 | 0.010490 | 0.9411 |
| 0.000711 | 0.6872 | 0.009754 | 0.9747 | 0.001168 | 0.5897 | 0.012268 | 0.9833 |
| 0.000914 | 0.7072 | 0.011278 | 0.9879 | 0.001473 | 0.6164 | 0.014808 | 1.0000 |
| 0.001168 | 0.7341 | 0.013310 | 0.9980 | | | | |
| 0.001499 | 0.7575 | 0.018389 | 1.0000 | | | | |
| 0.001880 | 0.7813 | | | | | | |

Station no. 5

| y (m) | u/U _s | y (m) | u/U _s | y (m) | $\frac{T_{aw}-T_a}{T_{aw}-T_{as}}$ | y (m) | $\frac{T_{aw}-T_a}{T_{aw}-T_{as}}$ |
|----------|------------------|----------|------------------|----------|------------------------------------|----------|------------------------------------|
| 0.000152 | 0.4410 | 0.001956 | 0.8006 | 0.000102 | 0.3961 | 0.003861 | 0.7105 |
| 0.000178 | 0.4970 | 0.002286 | 0.8161 | 0.000152 | 0.4185 | 0.004496 | 0.7255 |
| 0.000203 | 0.5303 | 0.002667 | 0.8338 | 0.000229 | 0.4385 | 0.005258 | 0.7579 |
| 0.000229 | 0.5589 | 0.003175 | 0.8534 | 0.000356 | 0.4610 | 0.006020 | 0.7929 |
| 0.000254 | 0.5810 | 0.003683 | 0.8698 | 0.000483 | 0.4772 | 0.006782 | 0.8191 |
| 0.000305 | 0.6122 | 0.004318 | 0.8698 | 0.000686 | 0.5021 | 0.007544 | 0.8340 |
| 0.000356 | 0.6324 | 0.004318 | 0.8888 | 0.000940 | 0.5171 | 0.008560 | 0.8727 |
| 0.000432 | 0.6530 | 0.005080 | 0.9057 | 0.001321 | 0.5608 | 0.009576 | 0.8939 |
| 0.000533 | 0.6702 | 0.005842 | 0.9227 | 0.001702 | 0.5907 | 0.010592 | 0.9264 |
| 0.000660 | 0.6909 | 0.006731 | 0.9402 | 0.002083 | 0.6032 | 0.011862 | 0.9476 |
| 0.000813 | 0.7122 | 0.007747 | 0.9542 | 0.002591 | 0.6307 | 0.013132 | 0.9651 |
| 0.000965 | 0.7284 | 0.008890 | 0.9689 | 0.003226 | 0.6606 | 0.015672 | 1.0000 |
| 0.001143 | 0.7438 | 0.010414 | 0.9846 | | | | |
| 0.001397 | 0.7663 | 0.012954 | 0.9964 | | | | |
| 0.001651 | 0.7832 | 0.018034 | 1.0000 | | | | |

Expt. A3

Const. adverse pressure gradient, heating from leading edge.

| Stat. no. | x (m) | U_s (m/s) | $\delta^* \times 10^3$ (m) | R_θ | H | $C_f \times 10^3$ | $St \times 10^3$ | $\delta_L^* \times 10^3$ (m) |
|-----------|-------|-------------|----------------------------|------------|-------|-------------------|------------------|------------------------------|
| 1 | 0.568 | 23.91 | 2.541 | 2780 | 1.432 | 3.048 | 2.161 | 1.402 |
| 2 | 0.873 | 22.35 | 4.001 | 4030 | 1.450 | 2.644 | 1.945 | 2.241 |
| 3 | 1.178 | 20.72 | 6.476 | 5700 | 1.501 | 2.316 | 1.718 | 2.909 |
| 4 | 1.483 | 19.31 | 9.536 | 7250 | 1.545 | 1.931 | 1.719 | 4.050 |
| 5 | 1.788 | 18.07 | 2.319 | 8890 | 1.590 | 1.718 | 1.743 | 4.277 |

Station no. 1

| y (m) | u/U_s | y (m) | u/U_s | y (m) | $\frac{T_{aw}-T_a}{T_{aw}-T_{as}}$ | y (m) | $\frac{T_{aw}-T_a}{T_{aw}-T_{as}}$ |
|----------|---------|----------|---------|----------|------------------------------------|----------|------------------------------------|
| 0.000152 | 0.2825 | 0.004064 | 0.7538 | 0.000102 | 0.5047 | 0.001168 | 0.7441 |
| 0.000203 | 0.3366 | 0.004826 | 0.7805 | 0.000127 | 0.5286 | 0.001549 | 0.7668 |
| 0.000254 | 0.3978 | 0.005588 | 0.8068 | 0.000152 | 0.5626 | 0.002057 | 0.8311 |
| 0.000305 | 0.4459 | 0.006350 | 0.8327 | 0.000178 | 0.5765 | 0.002565 | 0.8424 |
| 0.000356 | 0.4803 | 0.007112 | 0.8548 | 0.000229 | 0.5979 | 0.003327 | 0.8702 |
| 0.000406 | 0.5053 | 0.007874 | 0.8746 | 0.000305 | 0.6446 | 0.004089 | 0.8903 |
| 0.000508 | 0.5308 | 0.008636 | 0.8958 | 0.000406 | 0.6471 | 0.005359 | 0.9483 |
| 0.000686 | 0.5649 | 0.009398 | 0.9102 | 0.000533 | 0.6710 | 0.007899 | 0.9445 |
| 0.000940 | 0.5907 | 0.010414 | 0.9312 | 0.000711 | 0.7126 | 0.010439 | 0.9761 |
| 0.001270 | 0.6196 | 0.011430 | 0.9549 | 0.000914 | 0.7252 | 0.012979 | 1.0000 |
| 0.001651 | 0.6463 | 0.012446 | 0.9705 | | | | |
| 0.002159 | 0.6718 | 0.014986 | 0.9916 | | | | |
| 0.002794 | 0.7019 | 0.020066 | 0.9993 | | | | |
| 0.003429 | 0.7331 | 0.027686 | 1.0000 | | | | |

Station no. 2

| y (m) | u/U_s | y (m) | u/U_s | y (m) | $\frac{T_{aw}-T_a}{T_{aw}-T_{as}}$ | y (m) | $\frac{T_{aw}-T_a}{T_{aw}-T_{as}}$ |
|----------|---------|----------|---------|----------|------------------------------------|----------|------------------------------------|
| 0.000152 | 0.2867 | 0.005918 | 0.7298 | 0.000102 | 0.4606 | 0.002134 | 0.7653 |
| 0.000203 | 0.3225 | 0.007188 | 0.7510 | 0.000127 | 0.4829 | 0.002896 | 0.7983 |
| 0.000279 | 0.3967 | 0.008712 | 0.7952 | 0.000152 | 0.5062 | 0.003658 | 0.8067 |
| 0.000330 | 0.4167 | 0.010236 | 0.8279 | 0.000203 | 0.5402 | 0.004928 | 0.8354 |
| 0.000406 | 0.4621 | 0.011760 | 0.8605 | 0.000254 | 0.5646 | 0.006198 | 0.8694 |
| 0.000483 | 0.4843 | 0.013030 | 0.8848 | 0.000305 | 0.5753 | 0.007468 | 0.8800 |
| 0.000584 | 0.5059 | 0.014300 | 0.9146 | 0.000381 | 0.6082 | 0.008738 | 0.9023 |
| 0.000711 | 0.5174 | 0.015570 | 0.9296 | 0.000457 | 0.6188 | 0.010262 | 0.9310 |
| 0.000965 | 0.5396 | 0.017094 | 0.9588 | 0.000584 | 0.6485 | 0.012802 | 0.9533 |
| 0.001473 | 0.5781 | 0.018618 | 0.9772 | 0.000737 | 0.6602 | 0.015342 | 0.9692 |
| 0.001981 | 0.5979 | 0.020142 | 0.9868 | 0.000991 | 0.6921 | 0.020422 | 0.9979 |
| 0.002743 | 0.6314 | 0.022682 | 0.9963 | 0.001245 | 0.7207 | 0.028042 | 1.0000 |
| 0.003632 | 0.6662 | 0.027762 | 1.0000 | 0.001626 | 0.7356 | | |
| 0.004648 | 0.6917 | | | | | | |

Station no. 3

| y (m) | u/U_s | y (m) | u/U_s | y (m) | $\frac{T_{aw}-T_a}{T_{aw}-T_{as}}$ | y (m) | $\frac{T_{aw}-T_a}{T_{aw}-T_{as}}$ |
|----------|---------|----------|---------|----------|------------------------------------|----------|------------------------------------|
| 0.000152 | 0.2423 | 0.013106 | 0.7782 | 0.000102 | 0.4425 | 0.002083 | 0.7510 |
| 0.000229 | 0.3021 | 0.014884 | 0.8155 | 0.000127 | 0.4705 | 0.002591 | 0.7693 |
| 0.000330 | 0.3763 | 0.016408 | 0.8383 | 0.000152 | 0.4923 | 0.003353 | 0.7955 |
| 0.000432 | 0.4153 | 0.018187 | 0.8635 | 0.000203 | 0.5229 | 0.004115 | 0.8104 |
| 0.000559 | 0.4397 | 0.019964 | 0.8936 | 0.000254 | 0.5500 | 0.005131 | 0.8366 |
| 0.000787 | 0.4700 | 0.021742 | 0.9153 | 0.000305 | 0.5753 | 0.006401 | 0.8462 |
| 0.001295 | 0.5054 | 0.023521 | 0.9406 | 0.000381 | 0.5972 | 0.007925 | 0.8646 |
| 0.001930 | 0.5395 | 0.025298 | 0.9630 | 0.000457 | 0.6155 | 0.010465 | 0.8960 |
| 0.002692 | 0.5607 | 0.027076 | 0.9769 | 0.000559 | 0.6374 | 0.013005 | 0.9196 |
| 0.003962 | 0.5959 | 0.029617 | 0.9934 | 0.000686 | 0.6575 | 0.016815 | 0.9450 |
| 0.005233 | 0.6201 | 0.034695 | 0.9986 | 0.000940 | 0.6811 | 0.024435 | 0.9825 |
| 0.007772 | 0.6756 | 0.042315 | 1.0000 | 0.001194 | 0.7064 | 0.034595 | 1.0000 |
| 0.009550 | 0.7073 | | | 0.001575 | 0.7248 | | |
| 0.011329 | 0.7425 | | | | | | |

| Station no. 4 | | | | | | | |
|---------------|------------------|----------|------------------|----------|--|----------|--|
| y (m) | u/U _s | y (m) | u/U _s | y (m) | $\frac{T_{aw} - T_a}{T_{aw} - T_{as}}$ | y (m) | $\frac{T_{aw} - T_a}{T_{aw} - T_{as}}$ |
| 0.000152 | 0.1835 | 0.017755 | 0.7643 | 0.000102 | 0.4412 | 0.002286 | 0.7357 |
| 0.000279 | 0.2735 | 0.019787 | 0.7960 | 0.000127 | 0.4738 | 0.002794 | 0.7487 |
| 0.000406 | 0.3578 | 0.021818 | 0.8192 | 0.000152 | 0.4828 | 0.004064 | 0.7700 |
| 0.000533 | 0.4014 | 0.023851 | 0.8519 | 0.000203 | 0.5138 | 0.005334 | 0.7952 |
| 0.000686 | 0.4169 | 0.025883 | 0.8806 | 0.000254 | 0.5448 | 0.006604 | 0.8165 |
| 0.000991 | 0.4392 | 0.027914 | 0.9106 | 0.000305 | 0.5676 | 0.007874 | 0.8417 |
| 0.001753 | 0.4832 | 0.029438 | 0.9304 | 0.000356 | 0.5758 | 0.009144 | 0.8507 |
| 0.003023 | 0.5232 | 0.030962 | 0.9365 | 0.000432 | 0.5897 | 0.011176 | 0.8785 |
| 0.005054 | 0.5604 | 0.033504 | 0.9653 | 0.000533 | 0.6125 | 0.013716 | 0.8907 |
| 0.007595 | 0.6040 | 0.035534 | 0.9781 | 0.000635 | 0.6370 | 0.016256 | 0.9029 |
| 0.009626 | 0.6440 | 0.038076 | 0.9846 | 0.000762 | 0.6517 | 0.020066 | 0.9266 |
| 0.011659 | 0.6653 | 0.043154 | 0.9985 | 0.000940 | 0.6639 | 0.025146 | 0.9535 |
| 0.014198 | 0.7133 | 0.050774 | 1.0000 | 0.001143 | 0.6919 | 0.032766 | 0.9780 |
| 0.016231 | 0.7556 | | | 0.001397 | 0.6933 | 0.042926 | 0.9967 |
| | | | | 0.001778 | 0.7161 | 0.055626 | 1.0000 |

| Station no. 5 | | | | | | | |
|---------------|------------------|----------|------------------|----------|--|----------|--|
| y (m) | u/U _s | y (m) | u/U _s | y (m) | $\frac{T_{aw} - T_a}{T_{aw} - T_{as}}$ | y (m) | $\frac{T_{aw} - T_a}{T_{aw} - T_{as}}$ |
| 0.000152 | 0.1256 | 0.019202 | 0.7104 | 0.000102 | 0.4480 | 0.001600 | 0.7286 |
| 0.000279 | 0.2441 | 0.021742 | 0.7267 | 0.000127 | 0.4682 | 0.001981 | 0.7465 |
| 0.000406 | 0.3191 | 0.024790 | 0.7808 | 0.000152 | 0.4899 | 0.002189 | 0.7590 |
| 0.000533 | 0.3652 | 0.027331 | 0.8071 | 0.000178 | 0.5055 | 0.003124 | 0.7792 |
| 0.000711 | 0.3821 | 0.029870 | 0.8328 | 0.000203 | 0.5280 | 0.003886 | 0.7885 |
| 0.001168 | 0.4198 | 0.032400 | 0.8736 | 0.000229 | 0.5420 | 0.004902 | 0.8126 |
| 0.001930 | 0.4582 | 0.034951 | 0.8975 | 0.000279 | 0.5568 | 0.005918 | 0.8219 |
| 0.003200 | 0.4827 | 0.037490 | 0.9173 | 0.000330 | 0.5871 | 0.007442 | 0.8359 |
| 0.005740 | 0.5303 | 0.041300 | 0.9471 | 0.000381 | 0.6004 | 0.009982 | 0.8562 |
| 0.007772 | 0.5504 | 0.043839 | 0.9676 | 0.000457 | 0.6252 | 0.013792 | 0.8818 |
| 0.010312 | 0.5908 | 0.046381 | 0.9819 | 0.000533 | 0.6377 | 0.017602 | 0.8974 |
| 0.012853 | 0.6242 | 0.054001 | 0.9987 | 0.000635 | 0.6610 | 0.022682 | 0.9269 |
| 0.015392 | 0.6534 | 0.061621 | 1.0000 | 0.000711 | 0.6688 | 0.027762 | 0.9487 |
| | | | | 0.000813 | 0.6843 | 0.032842 | 0.9720 |
| | | | | 0.000914 | 0.6952 | 0.040462 | 0.9782 |
| | | | | 0.001067 | 0.7061 | 0.045542 | 1.0000 |
| | | | | 0.001295 | 0.7201 | | |

Expt. A4

| Stat. no. | x (m) | U_s (m/s) | $\delta^* \times 10^3$ (m) | R_θ | H | Cf $\times 10^3$ | St $\times 10^3$ | $\delta_t^* \times 10^3$ (m) |
|--------------|------------|----------------|-------------------------------|------------|-------|---------------------|---------------------|---------------------------------|
| 1 | 0.267 | 20.98 | 2.039 | 1970 | 1.401 | 3.435 | 2.471 | 0.421 |
| 2 | 0.419 | 19.31 | 3.014 | 2590 | 1.449 | 2.862 | 2.159 | 1.633 |
| 3 | 0.566 | 18.25 | 4.267 | 3350 | 1.500 | 2.488 | 1.969 | 1.977 |
| 4 | 0.721 | 17.14 | 5.822 | 4170 | 1.539 | 2.150 | 1.868 | 2.492 |
| 5 | 0.869 | 16.22 | 8.016 | 5190 | 1.615 | 1.827 | 1.823 | 3.347 |
| 6 | 1.003 | 15.69 | 9.662 | 6000 | 1.631 | 1.629 | 1.718 | 3.563 |
| 7 | 1.126 | 15.35 | 11.308 | 6900 | 1.624 | 1.639 | 1.712 | 4.007 |
| 8 | 1.262 | 15.24 | 12.070 | 7420 | 1.598 | 1.556 | 1.702 | 4.347 |
| 9 | 1.411 | 15.54 | 13.167 | 8350 | 1.578 | 1.776 | 1.578 | 5.574 |
| 10 | 1.548 | 15.33 | 13.655 | 8850 | 1.526 | 1.929 | 1.577 | 4.893 |
| 11 | 1.687 | 15.67 | 12.771 | 8840 | 1.458 | 2.034 | 1.524 | 5.865 |
| 12 | 1.821 | 16.80 | 10.180 | 8180 | 1.348 | 2.783 | 1.458 | 5.454 |
| 13 | 1.963 | 18.90 | 6.401 | 6230 | 1.250 | 3.571 | 1.417 | 5.102 |

Expt. A5

| Stat. no. | x (m) | U_s (m/s) | $\delta^* \times 10^3$ (m) | R_θ | H | $C_f \times 10^3$ | $St \times 10^3$ | $\delta_t^* \times 10^3$ (m) |
|-----------|-------|-------------|----------------------------|------------|-------|-------------------|------------------|------------------------------|
| 1 | 0.419 | 15.93 | 2.106 | 1510 | 1.428 | 3.490 | 2.757 | 1.431 |
| 2 | 0.724 | 14.78 | 3.719 | 2440 | 1.447 | 2.946 | 2.369 | 2.284 |
| 3 | 1.029 | 13.96 | 5.060 | 3120 | 1.462 | 2.711 | 2.092 | 2.731 |
| 4 | 1.175 | 15.35 | 3.475 | 2570 | 1.336 | 3.657 | 1.916 | 2.873 |
| 5 | 1.313 | 22.06 | 1.033 | 1160 | 1.263 | 5.591 | 1.429 | 2.186 |
| 6 | 1.450 | 42.04 | 0.293 | 484 | 1.640 | 6.366 | 0.864 | 1.451 |
| 7 | 1.600 | 60.92 | 0.451 | 1200 | 1.477 | 4.059 | 1.078 | 1.767 |
| 8 | 1.753 | 46.86 | 2.170 | 4150 | 1.580 | 1.918 | 1.434 | 3.245 |

Station no. 1

| y (m) | u/U_s | y (m) | u/U_s | y (m) | $\frac{T_{aw} - T_a}{T_{aw} - T_{as}}$ | y (m) | $\frac{T_{aw} - T_a}{T_{aw} - T_{as}}$ |
|----------|---------|----------|---------|----------|--|----------|--|
| 0.000152 | 0.2800 | 0.003175 | 0.7556 | 0.000203 | 0.4986 | 0.001346 | 0.7625 |
| 0.000178 | 0.3080 | 0.003556 | 0.7830 | 0.000229 | 0.5195 | 0.001600 | 0.7780 |
| 0.000203 | 0.3429 | 0.004064 | 0.8004 | 0.000254 | 0.5482 | 0.001854 | 0.7950 |
| 0.000254 | 0.3912 | 0.004572 | 0.8170 | 0.000279 | 0.5675 | 0.002235 | 0.8267 |
| 0.000305 | 0.4427 | 0.005080 | 0.8375 | 0.000305 | 0.5930 | 0.002743 | 0.8429 |
| 0.000356 | 0.4832 | 0.005582 | 0.8581 | 0.000330 | 0.5961 | 0.003251 | 0.8662 |
| 0.000406 | 0.5074 | 0.006604 | 0.8811 | 0.000356 | 0.6271 | 0.003759 | 0.8793 |
| 0.000483 | 0.5347 | 0.007366 | 0.9020 | 0.000406 | 0.6395 | 0.004521 | 0.9010 |
| 0.000584 | 0.5694 | 0.008128 | 0.9203 | 0.000483 | 0.6480 | 0.005537 | 0.9226 |
| 0.000711 | 0.5953 | 0.008890 | 0.9383 | 0.000559 | 0.6874 | 0.006807 | 0.9435 |
| 0.000889 | 0.6181 | 0.009652 | 0.9516 | 0.000635 | 0.7006 | 0.008585 | 0.9605 |
| 0.001092 | 0.6391 | 0.010668 | 0.9694 | 0.000762 | 0.7091 | 0.010617 | 0.9799 |
| 0.001346 | 0.6594 | 0.011938 | 0.9850 | 0.000838 | 0.7246 | 0.014427 | 0.9954 |
| 0.001651 | 0.6804 | 0.013208 | 0.9938 | 0.000965 | 0.7308 | 0.019507 | 1.0000 |
| 0.002032 | 0.7015 | 0.018288 | 0.9998 | 0.001143 | 0.7516 | | |
| 0.002540 | 0.7241 | 0.025908 | 1.0000 | | | | |

Station no. 2

| y (m) | u/U_s | y (m) | u/U_s | y (m) | $\frac{T_{aw} - T_a}{T_{aw} - T_{as}}$ | y (m) | $\frac{T_{aw} - T_a}{T_{aw} - T_{as}}$ |
|----------|---------|----------|---------|----------|--|----------|--|
| 0.000152 | 0.2646 | 0.005131 | 0.7217 | 0.000203 | 0.3557 | 0.001448 | 0.7025 |
| 0.000178 | 0.3019 | 0.005893 | 0.7391 | 0.000229 | 0.4217 | 0.001829 | 0.7297 |
| 0.000203 | 0.3226 | 0.006909 | 0.7706 | 0.000254 | 0.4452 | 0.002337 | 0.7463 |
| 0.000254 | 0.3678 | 0.007926 | 0.8023 | 0.000279 | 0.4686 | 0.002845 | 0.7717 |
| 0.000305 | 0.4121 | 0.008687 | 0.8180 | 0.000305 | 0.4933 | 0.003480 | 0.7951 |
| 0.000381 | 0.4504 | 0.009449 | 0.8357 | 0.000330 | 0.5038 | 0.004242 | 0.8216 |
| 0.000508 | 0.4863 | 0.010465 | 0.8507 | 0.000356 | 0.5236 | 0.005512 | 0.8556 |
| 0.000686 | 0.5224 | 0.011735 | 0.8790 | 0.000406 | 0.5452 | 0.006782 | 0.8809 |
| 0.000940 | 0.5571 | 0.013005 | 0.9133 | 0.000457 | 0.5680 | 0.008052 | 0.9136 |
| 0.001194 | 0.5715 | 0.014275 | 0.9358 | 0.000508 | 0.5840 | 0.010592 | 0.9426 |
| 0.001575 | 0.5986 | 0.015545 | 0.9498 | 0.000584 | 0.6093 | 0.013132 | 0.9587 |
| 0.002083 | 0.6190 | 0.018085 | 0.9799 | 0.000686 | 0.6279 | 0.015672 | 0.9753 |
| 0.002845 | 0.6497 | 0.020625 | 0.9957 | 0.000813 | 0.6445 | 0.019482 | 0.9914 |
| 0.003607 | 0.6700 | 0.025679 | 0.9993 | 0.000991 | 0.6612 | 0.027102 | 1.0000 |
| 0.004369 | 0.6998 | 0.030785 | 1.0000 | | | | |

Station no. 3

| y (m) | u/U _s | y (m) | u/U _s | y (m) | $\frac{T_{aw}-T_a}{T_{aw}-T_{as}}$ | y (m) | $\frac{T_{aw}-T_a}{T_{aw}-T_{as}}$ |
|----------|------------------|----------|------------------|----------|------------------------------------|----------|------------------------------------|
| 0.000152 | 0.2021 | 0.007772 | 0.7268 | 0.000203 | 0.3866 | 0.002235 | 0.7407 |
| 0.000203 | 0.2581 | 0.009043 | 0.7604 | 0.000229 | 0.4320 | 0.002997 | 0.7655 |
| 0.000254 | 0.3058 | 0.010058 | 0.7834 | 0.000254 | 0.4516 | 0.003759 | 0.7943 |
| 0.000305 | 0.3546 | 0.011329 | 0.8037 | 0.000279 | 0.4779 | 0.004521 | 0.8088 |
| 0.000381 | 0.3995 | 0.012853 | 0.8241 | 0.000330 | 0.5098 | 0.005283 | 0.8330 |
| 0.000457 | 0.4368 | 0.014884 | 0.8692 | 0.000381 | 0.5232 | 0.006553 | 0.8479 |
| 0.000559 | 0.4711 | 0.016154 | 0.8909 | 0.000457 | 0.5408 | 0.007823 | 0.8681 |
| 0.000787 | 0.5047 | 0.017425 | 0.9103 | 0.000533 | 0.5773 | 0.009093 | 0.8753 |
| 0.001041 | 0.5250 | 0.018694 | 0.9295 | 0.000610 | 0.6021 | 0.010363 | 0.8959 |
| 0.001549 | 0.5607 | 0.019964 | 0.9450 | 0.000711 | 0.6212 | 0.011633 | 0.9134 |
| 0.002184 | 0.5928 | 0.021742 | 0.9583 | 0.000813 | 0.6413 | 0.013411 | 0.9526 |
| 0.002946 | 0.6164 | 0.023774 | 0.9785 | 0.000914 | 0.6547 | 0.015951 | 0.9577 |
| 0.003962 | 0.6453 | 0.026314 | 0.9935 | 0.001041 | 0.6706 | 0.018491 | 0.9727 |
| 0.005233 | 0.6786 | 0.031394 | 0.9997 | 0.001219 | 0.6882 | 0.021031 | 0.9835 |
| 0.006502 | 0.6974 | 0.039014 | 1.0000 | 0.001473 | 0.6995 | 0.026111 | 0.9990 |
| | | | | 0.001727 | 0.7170 | 0.033731 | 1.0000 |

Station no. 4

| y (m) | u/U _s | y (m) | u/U _s | y (m) | $\frac{T_{aw}-T_a}{T_{aw}-T_{as}}$ | y (m) | $\frac{T_{aw}-T_a}{T_{aw}-T_{as}}$ |
|----------|------------------|----------|------------------|----------|------------------------------------|----------|------------------------------------|
| 0.000152 | 0.2489 | 0.004166 | 0.7554 | 0.000203 | 0.3419 | 0.002007 | 0.7180 |
| 0.000203 | 0.3230 | 0.005436 | 0.7781 | 0.000229 | 0.3900 | 0.002515 | 0.7394 |
| 0.000254 | 0.3928 | 0.006706 | 0.7982 | 0.000254 | 0.4124 | 0.003023 | 0.7540 |
| 0.000305 | 0.4548 | 0.008230 | 0.8232 | 0.000305 | 0.4521 | 0.003785 | 0.7697 |
| 0.000356 | 0.4879 | 0.010008 | 0.8493 | 0.000356 | 0.4725 | 0.004547 | 0.7979 |
| 0.000406 | 0.5245 | 0.011786 | 0.8747 | 0.000406 | 0.4997 | 0.005563 | 0.8266 |
| 0.000457 | 0.5502 | 0.013564 | 0.8973 | 0.000457 | 0.5331 | 0.006833 | 0.8438 |
| 0.000533 | 0.5790 | 0.015342 | 0.9209 | 0.000533 | 0.5550 | 0.008357 | 0.8747 |
| 0.000635 | 0.6035 | 0.017120 | 0.9417 | 0.000635 | 0.5874 | 0.010389 | 0.9018 |
| 0.000762 | 0.6274 | 0.018898 | 0.9590 | 0.000737 | 0.6193 | 0.012929 | 0.9243 |
| 0.000914 | 0.6481 | 0.020676 | 0.9761 | 0.000864 | 0.6292 | 0.015469 | 0.9525 |
| 0.001245 | 0.6704 | 0.023216 | 0.9926 | 0.000991 | 0.6522 | 0.018009 | 0.9775 |
| 0.001753 | 0.6917 | 0.028296 | 0.9996 | 0.001168 | 0.6694 | 0.023089 | 0.9906 |
| 0.002388 | 0.7148 | 0.035915 | 1.0000 | 0.001372 | 0.6809 | 0.028169 | 0.9979 |
| 0.003150 | 0.7308 | | | 0.001626 | 0.6913 | 0.035789 | 1.0000 |

Station no. 5

| y (m) | u/U _s | y (m) | u/U _s | y (m) | $\frac{T_{aw}-T_a}{T_{aw}-T_{as}}$ | y (m) | $\frac{T_{aw}-T_a}{T_{aw}-T_{as}}$ |
|----------|------------------|----------|------------------|----------|------------------------------------|----------|------------------------------------|
| 0.000152 | 0.4016 | 0.000711 | 0.8294 | 0.000203 | 0.3041 | 0.001448 | 0.7119 |
| 0.000178 | 0.4570 | 0.000838 | 0.8453 | 0.000229 | 0.3631 | 0.001702 | 0.7440 |
| 0.000203 | 0.5048 | 0.001016 | 0.8564 | 0.000254 | 0.4026 | 0.002083 | 0.7606 |
| 0.000229 | 0.5474 | 0.001270 | 0.8670 | 0.000279 | 0.4187 | 0.002845 | 0.7875 |
| 0.000254 | 0.5910 | 0.001778 | 0.8838 | 0.000305 | 0.4433 | 0.003607 | 0.8099 |
| 0.000279 | 0.6351 | 0.002540 | 0.8993 | 0.000356 | 0.4800 | 0.004877 | 0.8408 |
| 0.000305 | 0.6676 | 0.003810 | 0.9144 | 0.000406 | 0.5126 | 0.006147 | 0.8603 |
| 0.000330 | 0.6977 | 0.005588 | 0.9310 | 0.000457 | 0.5327 | 0.007417 | 0.8883 |
| 0.000356 | 0.7141 | 0.008128 | 0.9517 | 0.000533 | 0.5647 | 0.008941 | 0.9147 |
| 0.000381 | 0.7329 | 0.010668 | 0.9729 | 0.000610 | 0.6020 | 0.010465 | 0.9347 |
| 0.000432 | 0.7611 | 0.013208 | 0.9897 | 0.000686 | 0.6277 | 0.011989 | 0.9628 |
| 0.000483 | 0.7816 | 0.015748 | 0.9997 | 0.000813 | 0.6426 | 0.014529 | 0.9817 |
| 0.000533 | 0.7956 | 0.020828 | 1.0000 | 0.000991 | 0.6821 | 0.017069 | 0.9948 |
| 0.000610 | 0.8136 | | | 0.001194 | 0.7039 | 0.022149 | 1.0000 |

Station no. 6

| y (m) | u/U _s | y (m) | u/U _s | y (m) | $\frac{T_{aw}-T_a}{T_{aw}-T_{as}}$ | y (m) | $\frac{T_{aw}-T_a}{T_{aw}-T_{as}}$ |
|----------|------------------|----------|------------------|----------|------------------------------------|----------|------------------------------------|
| 0.000152 | 0.4831 | 0.000356 | 0.8448 | 0.000203 | 0.3213 | 0.000338 | 0.7007 |
| 0.000178 | 0.5339 | 0.000381 | 0.8599 | 0.000229 | 0.3736 | 0.001016 | 0.7174 |
| 0.000191 | 0.5553 | 0.000432 | 0.8848 | 0.000254 | 0.3910 | 0.001219 | 0.7658 |
| 0.000203 | 0.5996 | 0.000483 | 0.9039 | 0.000279 | 0.4245 | 0.001473 | 0.7787 |
| 0.000216 | 0.6249 | 0.000533 | 0.9168 | 0.000305 | 0.4433 | 0.001956 | 0.7974 |
| 0.000229 | 0.6776 | 0.000660 | 0.9355 | 0.000356 | 0.4832 | 0.002718 | 0.8219 |
| 0.000241 | 0.6973 | 0.000838 | 0.9501 | 0.000406 | 0.5329 | 0.003734 | 0.8613 |
| 0.000254 | 0.7156 | 0.001092 | 0.9614 | 0.000457 | 0.5561 | 0.004750 | 0.8832 |
| 0.000267 | 0.7469 | 0.001600 | 0.9724 | 0.000508 | 0.5897 | 0.006020 | 0.9200 |
| 0.000279 | 0.7724 | 0.003124 | 0.9832 | 0.000559 | 0.6065 | 0.007290 | 0.9536 |
| 0.000292 | 0.7791 | 0.005664 | 0.9919 | 0.000635 | 0.6284 | 0.009068 | 0.9787 |
| 0.000305 | 0.7954 | 0.010744 | 1.0000 | 0.000711 | 0.6742 | 0.012878 | 1.0000 |
| 0.000330 | 0.8232 | | | | | | |

Station no. 7

| y (m) | u/U _s | y (m) | u/U _s | y (m) | $\frac{T_{aw}-T_a}{T_{aw}-T_{as}}$ | y (m) | $\frac{T_{aw}-T_a}{T_{aw}-T_{as}}$ |
|----------|------------------|----------|------------------|----------|------------------------------------|----------|------------------------------------|
| 0.000152 | 0.5477 | 0.000940 | 0.8365 | 0.000203 | 0.2156 | 0.001626 | 0.6072 |
| 0.000178 | 0.5677 | 0.001067 | 0.8588 | 0.000229 | 0.3182 | 0.002007 | 0.6921 |
| 0.000203 | 0.5953 | 0.001194 | 0.8774 | 0.000279 | 0.3512 | 0.002515 | 0.7275 |
| 0.000229 | 0.6260 | 0.001321 | 0.8948 | 0.000330 | 0.3843 | 0.003023 | 0.8290 |
| 0.000254 | 0.6437 | 0.001448 | 0.9107 | 0.000381 | 0.3984 | 0.003531 | 0.8761 |
| 0.000305 | 0.6757 | 0.001575 | 0.9260 | 0.000483 | 0.4240 | 0.004039 | 0.9045 |
| 0.000356 | 0.6984 | 0.001829 | 0.9478 | 0.000610 | 0.4550 | 0.005309 | 0.9575 |
| 0.000406 | 0.7141 | 0.002083 | 0.9645 | 0.000787 | 0.4657 | 0.009119 | 0.9693 |
| 0.000483 | 0.7378 | 0.002337 | 0.9755 | 0.001118 | 0.5553 | 0.016739 | 1.0000 |
| 0.000559 | 0.7581 | 0.002845 | 0.9865 | 0.001372 | 0.5836 | | |
| 0.000635 | 0.7759 | 0.005385 | 0.9955 | | | | |
| 0.000711 | 0.7922 | 0.010165 | 0.9999 | | | | |
| 0.000787 | 0.8079 | 0.018085 | 1.0000 | | | | |
| 0.000864 | 0.8236 | | | | | | |

Station no. 8

| y (m) | u/U _s | y (m) | u/U _s | y (m) | $\frac{T_{aw}-T_a}{T_{aw}-T_{as}}$ | y (m) | $\frac{T_{aw}-T_a}{T_{aw}-T_{as}}$ |
|----------|------------------|----------|------------------|----------|------------------------------------|----------|------------------------------------|
| 0.000152 | 0.3496 | 0.005055 | 0.8302 | 0.000203 | 0.4299 | 0.00546 | 0.7685 |
| 0.000203 | 0.3816 | 0.005563 | 0.8646 | 0.000381 | 0.4381 | 0.00673 | 0.8391 |
| 0.000279 | 0.4251 | 0.006071 | 0.8925 | 0.000635 | 0.4788 | 0.00800 | 0.8650 |
| 0.000356 | 0.4534 | 0.006579 | 0.9166 | 0.001143 | 0.5044 | 0.00927 | 0.9337 |
| 0.000610 | 0.4901 | 0.007087 | 0.9388 | 0.001651 | 0.5381 | 0.01181 | 0.9744 |
| 0.000991 | 0.5300 | 0.007849 | 0.9636 | 0.002159 | 0.6010 | 0.01435 | 0.9791 |
| 0.001499 | 0.5729 | 0.009119 | 0.9845 | 0.002921 | 0.6324 | 0.02197 | 1.0000 |
| 0.002007 | 0.6086 | 0.011659 | 0.9945 | 0.004191 | 0.6847 | | |
| 0.002769 | 0.6658 | 0.016739 | 0.9992 | | | | |
| 0.003531 | 0.7241 | 0.024359 | 1.0000 | | | | |
| 0.004293 | 0.7779 | | | | | | |

Expt. A6

| Stat. no. | x (m) | U_s (m/s) | $S^* \times 10^3$ (m) | R_o | H | $C_f \times 10^3$ | $St \times 10^3$ | $S_L^* \times 10^3$ (m) |
|-----------|-------|-------------|-----------------------|-------|-------|-------------------|------------------|-------------------------|
| 1 | 0.421 | 14.62 | 2.673 | 1790 | 1.400 | 3.437 | 2.865 | 1.195 |
| 2 | 0.569 | 13.73 | 3.810 | 2260 | 1.497 | 2.716 | 2.486 | 2.135 |
| 3 | 0.721 | 12.92 | 5.517 | 2980 | 1.543 | 2.502 | 2.339 | 2.705 |
| 4 | 0.874 | 11.84 | 7.224 | 3350 | 1.644 | 1.976 | 2.240 | 2.942 |
| 5 | 1.026 | 11.71 | 7.711 | 3820 | 1.523 | 2.182 | 2.093 | 3.497 |
| 6 | 1.170 | 12.82 | 5.029 | 3020 | 1.373 | 3.239 | 1.937 | 3.177 |
| 7 | 1.293 | 18.19 | 1.530 | 1450 | 1.238 | 5.134 | 1.483 | 2.390 |
| 8 | 1.419 | 36.09 | 0.326 | 440 | 1.727 | 6.617 | 0.826 | 1.500 |
| 9 | 1.566 | 51.97 | 0.369 | 774 | 1.595 | 4.660 | 0.614 | 1.321 |
| 10 | 1.716 | 40.02 | 1.603 | 2820 | 1.466 | 2.516 | 1.355 | 3.369 |
| 11 | 1.864 | 34.17 | 4.206 | 5750 | 1.615 | 1.526 | 1.374 | 5.230 |

Station no. 1

| y (m) | u/U_s | y (m) | u/U_s | y (m) | $\frac{T_{aw} - T_a}{T_{aw} - T_{as}}$ | y (m) | $\frac{T_{aw} - T_a}{T_{aw} - T_{as}}$ |
|----------|---------|----------|---------|----------|--|----------|--|
| 0.000152 | 0.3216 | 0.004471 | 0.7635 | 0.000203 | 0.4111 | 0.001016 | 0.7390 |
| 0.000203 | 0.3630 | 0.005486 | 0.7983 | 0.000229 | 0.4753 | 0.001143 | 0.7461 |
| 0.000254 | 0.4138 | 0.006757 | 0.8334 | 0.000254 | 0.4923 | 0.001397 | 0.7620 |
| 0.000330 | 0.4652 | 0.008026 | 0.8646 | 0.000279 | 0.5 53 | 0.001778 | 0.7895 |
| 0.000406 | 0.5044 | 0.009296 | 0.9027 | 0.000305 | 0.5466 | 0.002286 | 0.8059 |
| 0.000533 | 0.5448 | 0.010567 | 0.9209 | 0.000330 | 0.5542 | 0.003048 | 0.8415 |
| 0.000660 | 0.5685 | 0.011836 | 0.9433 | 0.000381 | 0.5800 | 0.003810 | 0.8805 |
| 0.000838 | 0.5974 | 0.013106 | 0.9670 | 0.000432 | 0.6063 | 0.004572 | 0.8854 |
| 0.001041 | 0.6157 | 0.014377 | 0.9801 | 0.000483 | 0.6272 | 0.005588 | 0.9210 |
| 0.001422 | 0.6439 | 0.016916 | 0.9959 | 0.000559 | 0.6540 | 0.006604 | 0.9479 |
| 0.001930 | 0.6731 | 0.021997 | 0.9990 | 0.000635 | 0.6694 | 0.009144 | 0.9666 |
| 0.002692 | 0.7059 | 0.029617 | 1.0000 | 0.000762 | 0.6995 | 0.011685 | 1.0000 |
| 0.003454 | 0.7310 | | | 0.000889 | 0.7089 | | |

Station no. 2

| y (m) | u/U_s | y (m) | u/U_s | y (m) | $\frac{T_{aw} - T_a}{T_{aw} - T_{as}}$ | y (m) | $\frac{T_{aw} - T_a}{T_{aw} - T_{as}}$ |
|----------|---------|----------|---------|----------|--|----------|--|
| 0.000152 | 0.2385 | 0.005004 | 0.7023 | 0.000203 | 0.4292 | 0.001702 | 0.7487 |
| 0.000229 | 0.2948 | 0.006274 | 0.7405 | 0.000229 | 0.4627 | 0.002210 | 0.7714 |
| 0.000305 | 0.3484 | 0.007544 | 0.7702 | 0.000254 | 0.4818 | 0.002972 | 0.8071 |
| 0.000432 | 0.4254 | 0.008814 | 0.8029 | 0.000279 | 0.5036 | 0.003734 | 0.8329 |
| 0.000559 | 0.4594 | 0.010084 | 0.8326 | 0.000330 | 0.5357 | 0.004750 | 0.8623 |
| 0.000686 | 0.4971 | 0.011354 | 0.8598 | 0.000381 | 0.5571 | 0.006020 | 0.8864 |
| 0.000864 | 0.5208 | 0.012624 | 0.8892 | 0.000457 | 0.5905 | 0.008560 | 0.9171 |
| 0.001067 | 0.5494 | 0.013894 | 0.9125 | 0.000559 | 0.6204 | 0.011100 | 0.9439 |
| 0.001448 | 0.5684 | 0.016434 | 0.9530 | 0.000686 | 0.6485 | 0.014910 | 0.9715 |
| 0.001956 | 0.6025 | 0.018974 | 0.9846 | 0.000864 | 0.6810 | 0.022530 | 0.9947 |
| 0.002718 | 0.6231 | 0.021514 | 0.9967 | 0.001067 | 0.6961 | 0.030150 | 1.0000 |
| 0.003734 | 0.6597 | 0.026594 | 1.0000 | 0.001321 | 0.7238 | | |

Station no. 3

| y (m) | u/U_s | y (m) | u/U_s | y (m) | $\frac{T_{aw}-T_a}{T_{aw}-T_{as}}$ | y (m) | $\frac{T_{aw}-T_a}{T_{aw}-T_{as}}$ |
|------------|---------|------------|---------|------------|------------------------------------|------------|------------------------------------|
| 0.000152 | 0.1630 | 0.008027 | 0.7154 | 0.000203 | 0.3152 | 0.001575 | 0.7161 |
| 0.000229 | 0.2210 | 0.009931 | 0.7491 | 0.000229 | 0.3897 | 0.002083 | 0.7476 |
| 0.000356 | 0.3164 | 0.012472 | 0.8125 | 0.000254 | 0.4192 | 0.002845 | 0.7756 |
| 0.000483 | 0.3811 | 0.015011 | 0.8651 | 0.000305 | 0.4570 | 0.004115 | 0.8110 |
| 0.000560 | 0.4356 | 0.017551 | 0.9012 | 0.000356 | 0.4999 | 0.005385 | 0.8386 |
| 0.000914 | 0.4691 | 0.019583 | 0.9348 | 0.000406 | 0.5314 | 0.007163 | 0.8756 |
| 0.001422 | 0.5040 | 0.021616 | 0.9645 | 0.000457 | 0.5550 | 0.009957 | 0.9059 |
| 0.002057 | 0.5424 | 0.024155 | 0.9904 | 0.000584 | 0.5924 | 0.015037 | 0.9484 |
| 0.003073 | 0.5745 | 0.026695 | 0.9960 | 0.000711 | 0.6228 | 0.020117 | 0.9819 |
| 0.004343 | 0.6110 | 0.031775 | 1.0000 | 0.000889 | 0.6606 | 0.025197 | 0.9965 |
| 0.005995 | 0.6578 | | | 0.001194 | 0.6775 | 0.032817 | 1.0000 |

Station no. 4

| y (m) | u/U_s | y (m) | u/U_s | y (m) | $\frac{T_{aw}-T_a}{T_{aw}-T_{as}}$ | y (m) | $\frac{T_{aw}-T_a}{T_{aw}-T_{as}}$ |
|------------|---------|------------|---------|------------|------------------------------------|------------|------------------------------------|
| 0.000152 | 0.0718 | 0.010186 | 0.6940 | 0.000203 | 0.3904 | 0.001727 | 0.7412 |
| 0.000279 | 0.1695 | 0.012725 | 0.7496 | 0.000229 | 0.4180 | 0.002489 | 0.7612 |
| 0.000533 | 0.3378 | 0.015265 | 0.7990 | 0.000254 | 0.4426 | 0.003251 | 0.7902 |
| 0.000787 | 0.3661 | 0.017806 | 0.8439 | 0.000305 | 0.4754 | 0.005029 | 0.8231 |
| 0.001041 | 0.4282 | 0.020345 | 0.8918 | 0.000356 | 0.5082 | 0.007569 | 0.8580 |
| 0.001803 | 0.4418 | 0.022885 | 0.9318 | 0.000432 | 0.5504 | 0.011125 | 0.8987 |
| 0.002565 | 0.4637 | 0.025426 | 0.9606 | 0.000508 | 0.5805 | 0.014935 | 0.9347 |
| 0.003835 | 0.5091 | 0.027965 | 0.9885 | 0.000610 | 0.6122 | 0.020015 | 0.9599 |
| 0.005105 | 0.5864 | 0.033046 | 0.9978 | 0.000737 | 0.6430 | 0.027635 | 0.9907 |
| 0.007645 | 0.6288 | 0.038124 | 1.0000 | 0.000965 | 0.6693 | 0.035255 | 1.0000 |
| | | | | 0.001346 | 0.7118 | | |

Station no. 5

| y (m) | u/U_s | y (m) | u/U_s | y (m) | $\frac{T_{aw}-T_a}{T_{aw}-T_{as}}$ | y (m) | $\frac{T_{aw}-T_a}{T_{aw}-T_{as}}$ |
|------------|---------|------------|---------|------------|------------------------------------|------------|------------------------------------|
| 0.000152 | 0.2133 | 0.011735 | 0.7105 | 0.000203 | 0.3411 | 0.002388 | 0.7471 |
| 0.000330 | 0.2954 | 0.013513 | 0.7307 | 0.000229 | 0.3910 | 0.003404 | 0.7725 |
| 0.000457 | 0.3633 | 0.015545 | 0.7690 | 0.000279 | 0.4377 | 0.005182 | 0.8057 |
| 0.000584 | 0.4123 | 0.017577 | 0.8055 | 0.000330 | 0.4674 | 0.007214 | 0.8402 |
| 0.000762 | 0.4512 | 0.019609 | 0.8372 | 0.000406 | 0.5060 | 0.009754 | 0.8766 |
| 0.001067 | 0.4824 | 0.022149 | 0.8756 | 0.000483 | 0.5350 | 0.012675 | 0.9004 |
| 0.001575 | 0.5072 | 0.024689 | 0.9102 | 0.000610 | 0.5769 | 0.017755 | 0.9356 |
| 0.002337 | 0.5337 | 0.027229 | 0.9408 | 0.000737 | 0.6120 | 0.025375 | 0.9684 |
| 0.003353 | 0.5583 | 0.029769 | 0.9651 | 0.000914 | 0.6388 | 0.032995 | 0.9939 |
| 0.004623 | 0.5876 | 0.032309 | 0.9835 | 0.001118 | 0.6594 | 0.040615 | 1.0000 |
| 0.005893 | 0.6045 | 0.037390 | 0.9974 | 0.001626 | 0.7045 | | |
| 0.007671 | 0.6363 | 0.047549 | 1.0000 | | | | |
| 0.009703 | 0.6683 | | | | | | |

Station no. 6

| y (m) | u/U _s | y (m) | u/U _s | y (m) | $\frac{T_{aw}-T_a}{T_{aw}-T_{as}}$ | y (m) | $\frac{T_{aw}-T_a}{T_{aw}-T_{as}}$ |
|----------|------------------|----------|------------------|----------|------------------------------------|----------|------------------------------------|
| 0.000152 | 0.1538 | 0.002591 | 0.6768 | 0.000203 | 0.3585 | 0.001575 | 0.7188 |
| 0.000229 | 0.2592 | 0.003861 | 0.7020 | 0.000229 | 0.3947 | 0.002210 | 0.7674 |
| 0.000279 | 0.3262 | 0.005639 | 0.7234 | 0.000305 | 0.4411 | 0.003480 | 0.7880 |
| 0.000330 | 0.3857 | 0.007417 | 0.7504 | 0.000356 | 0.4715 | 0.004750 | 0.8181 |
| 0.000381 | 0.4292 | 0.009195 | 0.7681 | 0.000432 | 0.5153 | 0.007290 | 0.8605 |
| 0.000432 | 0.4640 | 0.010973 | 0.7975 | 0.000508 | 0.5587 | 0.011481 | 0.9014 |
| 0.000483 | 0.4945 | 0.013005 | 0.8217 | 0.000584 | 0.5786 | 0.016561 | 0.9109 |
| 0.000559 | 0.5286 | 0.015545 | 0.8591 | 0.000686 | 0.6123 | 0.024181 | 0.9788 |
| 0.000635 | 0.5494 | 0.018085 | 0.8932 | 0.000813 | 0.6440 | 0.034341 | 0.9990 |
| 0.000737 | 0.5786 | 0.020625 | 0.9189 | 0.000991 | 0.6717 | 0.047041 | 1.0000 |
| 0.000914 | 0.5956 | 0.023165 | 0.9492 | 0.001194 | 0.6959 | | |
| 0.001041 | 0.6110 | 0.025705 | 0.9716 | | | | |
| 0.001321 | 0.6326 | 0.030785 | 0.9941 | | | | |
| 0.001829 | 0.6534 | 0.038405 | 1.0000 | | | | |

Station no. 7

| y (m) | u/U _s | y (m) | u/U _s | y (m) | $\frac{T_{aw}-T_a}{T_{aw}-T_{as}}$ | y (m) | $\frac{T_{aw}-T_a}{T_{aw}-T_{as}}$ |
|----------|------------------|----------|------------------|----------|------------------------------------|----------|------------------------------------|
| 0.000152 | 0.3464 | 0.000838 | 0.8198 | 0.000203 | 0.3261 | 0.001295 | 0.7268 |
| 0.000203 | 0.4181 | 0.001016 | 0.8342 | 0.000229 | 0.3594 | 0.001803 | 0.7565 |
| 0.000229 | 0.4588 | 0.001245 | 0.8453 | 0.000254 | 0.3884 | 0.002566 | 0.7898 |
| 0.000254 | 0.5029 | 0.001626 | 0.8588 | 0.000305 | 0.4302 | 0.003582 | 0.8170 |
| 0.000279 | 0.5430 | 0.002134 | 0.8706 | 0.000356 | 0.4688 | 0.004852 | 0.8464 |
| 0.000305 | 0.5807 | 0.002896 | 0.8865 | 0.000406 | 0.5024 | 0.007646 | 0.8800 |
| 0.000330 | 0.6068 | 0.003912 | 0.8898 | 0.000457 | 0.5219 | 0.010186 | 0.9204 |
| 0.000381 | 0.6604 | 0.005182 | 0.9019 | 0.000533 | 0.5696 | 0.015266 | 0.9589 |
| 0.000406 | 0.6812 | 0.006452 | 0.9108 | 0.000660 | 0.6199 | 0.020320 | 0.9883 |
| 0.000457 | 0.7145 | 0.008992 | 0.9298 | 0.000787 | 0.6525 | 0.027966 | 1.0000 |
| 0.000508 | 0.7357 | 0.011532 | 0.9496 | 0.000965 | 0.6786 | | |
| 0.000584 | 0.7666 | 0.014072 | 0.9688 | | | | |
| 0.000660 | 0.7838 | 0.016612 | 0.9855 | | | | |
| 0.000737 | 0.7995 | 0.021692 | 1.0000 | | | | |

Station no. 8

| y (m) | u/U _s | y (m) | u/U _s | y (m) | $\frac{T_{aw}-T_a}{T_{aw}-T_{as}}$ | y (m) | $\frac{T_{aw}-T_a}{T_{aw}-T_{as}}$ |
|----------|------------------|----------|------------------|----------|------------------------------------|----------|------------------------------------|
| 0.000152 | 0.3757 | 0.000483 | 0.9119 | 0.000203 | 0.3439 | 0.000749 | 0.7228 |
| 0.000178 | 0.4736 | 0.000533 | 0.9246 | 0.000241 | 0.4042 | 0.000991 | 0.7651 |
| 0.000203 | 0.5667 | 0.000610 | 0.9400 | 0.000267 | 0.4351 | 0.001245 | 0.7882 |
| 0.000229 | 0.6697 | 0.000686 | 0.9490 | 0.000318 | 0.4911 | 0.002007 | 0.8211 |
| 0.000254 | 0.7037 | 0.000813 | 0.9600 | 0.000368 | 0.5917 | 0.003277 | 0.8630 |
| 0.000279 | 0.7615 | 0.001067 | 0.9681 | 0.000419 | 0.5635 | 0.004928 | 0.9045 |
| 0.000305 | 0.7971 | 0.001524 | 0.9746 | 0.000495 | 0.6191 | 0.007468 | 0.9546 |
| 0.000330 | 0.8235 | 0.002286 | 0.9788 | 0.000572 | 0.6594 | 0.012548 | 0.9980 |
| 0.000356 | 0.8378 | 0.004826 | 0.9881 | 0.000648 | 0.6923 | 0.020168 | 1.0000 |
| 0.000381 | 0.8562 | 0.007391 | 0.9960 | | | | |
| 0.000432 | 0.8870 | 0.009906 | 1.0000 | | | | |

Station no. 9

| y (m) | u/U _s | y (m) | u/U _s | y (m) | $\frac{T_{aw}-T_a}{T_{aw}-T_{as}}$ | y (m) | $\frac{T_{aw}-T_a}{T_{aw}-T_{as}}$ |
|----------|------------------|----------|------------------|----------|------------------------------------|----------|------------------------------------|
| 0.000152 | 0.4798 | 0.000686 | 0.8684 | 0.000203 | 0.4006 | 0.001016 | 0.7424 |
| 0.000178 | 0.5137 | 0.000737 | 0.8777 | 0.000229 | 0.4123 | 0.001194 | 0.7671 |
| 0.000229 | 0.5809 | 0.000813 | 0.8970 | 0.000279 | 0.4366 | 0.001524 | 0.8073 |
| 0.000254 | 0.6150 | 0.000889 | 0.9078 | 0.000381 | 0.4777 | 0.002286 | 0.8467 |
| 0.000279 | 0.6423 | 0.000965 | 0.9230 | 0.000508 | 0.5489 | 0.003302 | 0.8693 |
| 0.000305 | 0.6493 | 0.001041 | 0.9333 | 0.000584 | 0.5937 | 0.004445 | 0.9020 |
| 0.000356 | 0.7009 | 0.001143 | 0.9435 | 0.000660 | 0.6214 | 0.006985 | 0.9535 |
| 0.000381 | 0.7213 | 0.001397 | 0.9600 | 0.000762 | 0.6607 | 0.012065 | 1.0000 |
| 0.000406 | 0.7376 | 0.001778 | 0.9749 | 0.000889 | 0.7060 | | |
| 0.000432 | 0.7503 | 0.002286 | 0.9848 | | | | |
| 0.000483 | 0.7881 | 0.004826 | 0.9937 | | | | |
| 0.000533 | 0.8126 | 0.009906 | 0.9998 | | | | |
| 0.000584 | 0.8384 | 0.017526 | 1.0000 | | | | |
| 0.000635 | 0.8498 | | | | | | |

Station no. 10

| y (m) | u/U _s | y (m) | u/U _s | y (m) | $\frac{T_{aw}-T_a}{T_{aw}-T_{as}}$ | y (m) | $\frac{T_{aw}-T_a}{T_{aw}-T_{as}}$ |
|----------|------------------|----------|------------------|----------|------------------------------------|----------|------------------------------------|
| 0.000152 | 0.4022 | 0.003302 | 0.7987 | 0.000203 | 0.3570 | 0.005080 | 0.7494 |
| 0.000178 | 0.4327 | 0.003683 | 0.8248 | 0.000254 | 0.4076 | 0.006096 | 0.7907 |
| 0.000203 | 0.4543 | 0.004064 | 0.8515 | 0.000330 | 0.4404 | 0.007112 | 0.8277 |
| 0.000254 | 0.5039 | 0.004445 | 0.8741 | 0.000508 | 0.4710 | 0.008255 | 0.8569 |
| 0.000381 | 0.5294 | 0.004826 | 0.8932 | 0.000762 | 0.4945 | 0.010795 | 0.9181 |
| 0.000508 | 0.5585 | 0.005207 | 0.9133 | 0.001270 | 0.5251 | 0.013335 | 0.9466 |
| 0.000762 | 0.5942 | 0.005715 | 0.9364 | 0.002032 | 0.5742 | 0.018415 | 0.9872 |
| 0.001016 | 0.6141 | 0.006223 | 0.9518 | 0.003048 | 0.6312 | 0.026035 | 1.0000 |
| 0.001397 | 0.6492 | 0.006985 | 0.9691 | 0.004064 | 0.6832 | | |
| 0.001778 | 0.6779 | 0.008255 | 0.9855 | | | | |
| 0.002159 | 0.7120 | 0.010795 | 0.9924 | | | | |
| 0.002540 | 0.7426 | 0.020955 | 1.0000 | | | | |
| 0.002921 | 0.7735 | | | | | | |

Station no. 11

| y (m) | u/U _s | y (m) | u/U _s | y (m) | $\frac{T_{aw}-T_a}{T_{aw}-T_{as}}$ | y (m) | $\frac{T_{aw}-T_a}{T_{aw}-T_{as}}$ |
|----------|------------------|----------|------------------|----------|------------------------------------|----------|------------------------------------|
| 0.000152 | 0.2816 | 0.008128 | 0.7688 | 0.000203 | 0.3703 | 0.004826 | 0.6587 |
| 0.000254 | 0.3519 | 0.009398 | 0.8168 | 0.000254 | 0.4264 | 0.006223 | 0.6895 |
| 0.000356 | 0.3796 | 0.010688 | 0.8591 | 0.000330 | 0.4665 | 0.008763 | 0.7474 |
| 0.000508 | 0.4196 | 0.011938 | 0.8940 | 0.000457 | 0.4911 | 0.011303 | 0.7942 |
| 0.001016 | 0.4462 | 0.013208 | 0.9304 | 0.000635 | 0.5096 | 0.013843 | 0.8577 |
| 0.001778 | 0.5090 | 0.014478 | 0.9558 | 0.000889 | 0.5336 | 0.016383 | 0.8940 |
| 0.003048 | 0.5636 | 0.015748 | 0.9757 | 0.001270 | 0.5589 | 0.018923 | 0.9242 |
| 0.004318 | 0.6128 | 0.018288 | 0.9955 | 0.001778 | 0.5810 | 0.024003 | 0.9642 |
| 0.005563 | 0.6665 | 0.023368 | 1.0000 | 0.002540 | 0.6082 | 0.031623 | 0.9945 |
| 0.006858 | 0.7175 | | | 0.003556 | 0.6248 | 0.039243 | 1.0000 |

Appendix 3

(i) Turbomachinery input data

Input data for the cases considered.

| Case | Flow Dirn. | R_e | R_o | Rel. Inlet Angle | u_w^+ |
|-------|---------------|-------|-------|------------------------|--------------|
| 1 (i) | In | - 975 | 2660 | -62.7 | 2 |
| (ii) | In | - 975 | 2660 | -62.7 | 0 laminar |
| (iii) | In | -1950 | 5320 | -62.7 | 2.83 |
| (iv) | In | - 975 | 2660 | -62.7 | 10 |
| 2 (i) | In | - 853 | 4670 | -79.9 | 2 |
| (ii) | In | -1706 | 9350 | -79.9 | 2.83 |
| (iii) | In | - 853 | 4670 | -79.9 | 10 |
| 3 | Out | 1367 | 4670 | 44.2 | 2 |
| 4 (i) | In | -1790 | 2450 | -10.9 | 2 |
| (ii) | In | -1790 | 2450 | -10.9 | 5 |
| (iii) | In | -1790 | 2450 | -10.9 | 10 |

(ii) Turbomachinery output data

Overall output parameters for the cases considered.

| Case | Dimensionless Torque | Dimensionless Change of Ang. Mom. | Effy. | Rel. Exit Angle |
|-------|----------------------|-----------------------------------|-------|-----------------|
| 1 (i) | 0.414 | 0.420 | 99.5 | 51.4 |
| (ii) | 0.426 | 0.420 | 94.8 | 51.4 |
| (iii) | 0.411 | 0.420 | 99.7 | 51.4 |
| (iv) | 0.402 | 0.420 | >100 | 51.4 |
| 2 (i) | 0.120 | 0.117 | 64.4 | 43.2 |
| (ii) | 0.120 | 0.117 | 60.8 | 43.2 |
| (iii) | 0.127 | 0.117 | 81.5 | 43.2 |
| 3 | 0.167 | 0.168 | 97.0 | 80.8 |
| 4 (i) | 1.539 | 1.548 | 82.6 | 52.1 |
| (ii) | | 1.548 | | 52.1 |
| (iii) | | 1.548 | | 52.1 |

$$\text{Dimensionless Torque} = \int \text{P.H.R. } dR.$$

$$\text{Dimensionless Change of Ang. Mom.} =$$

$$\frac{4\pi H_i R_i}{N} \cdot \frac{R_e}{R_o} \left[U'_{\theta i} R_i - U'_{\theta o} R_o \right]$$

Appendix 4

Two-Dimensionality Check - boundary layer experiments

The velocity boundary layers were checked for two-dimensionality by considering the Von-Karman momentum integral equation,

$$\frac{d\theta}{dx} = \frac{Cf}{2} - (H + 2) \frac{\theta}{U_s} \frac{dU_s}{dx}$$

or

$$\frac{dR_\theta}{dx} = \frac{U_s}{\nu} \frac{Cf}{2} - (H + 1) \frac{R_\theta}{U_s} \frac{dU_s}{dx} .$$

Integrating with respect to x between x_i and x , where x_i is the distance from the leading edge of the initial station, gives

$$\int_{x_i}^x \frac{dR_\theta}{dx} \cdot dx = \frac{1}{2\nu} \int_{x_i}^x U_s \cdot Cf \, dx - \int_{x_i}^x \frac{(H + 1)}{U_s} R_\theta \cdot \frac{dU_s}{dx} \cdot dx$$

$$\frac{R_\theta}{R_{\theta i}} - 1 = \frac{1}{2\nu R_{\theta i}} \int_{x_i}^x U_s \cdot Cf \, dx - \int_{x_i}^x \frac{H + 1}{U_s} \frac{R_\theta}{R_{\theta i}} \cdot \frac{dU_s}{dx} \cdot dx$$

(A.4.1)

Let ϕ_1 = Left hand side of equation (A.4.1) and

ϕ_2 = Right hand side.

Thus if $\phi_1 = \phi_2$ then the boundary layer is two-dimensional. Fig. 7 shows graphically the agreement between the two sides of the equation for each of the boundary layer tests.

Appendix 5

Boundary Layer and Duct Program (Language - Fortran 4)

Guide to symbols used in program

N.B. The symbols used to signify the meaning of the computer notation should be referred to the appropriate theoretical nomenclatures, e.g. for this appendix, refer to nomenclature, section 1.2.

| <u>Program Symbol</u> | <u>Meaning</u> |
|---------------------------|---|
| ADIS | Constant C_4 in the turbulent kinetic energy method dissipation length scale expression. |
| ADU | Constant a' in duct geometry description. |
| ADV | Dimensionless advection of turbulent kinetic energy $\left[\frac{\partial q}{\partial R} + p \cdot q \right]$. |
| ALPHA | Constant C_1 in Prandtl-Kolmogorov turbulence model. |
| AMU | Constant C_3 in the turbulent kinetic energy method length scale expression. |
| AP | Parameter describing the variation of pressure gradient parameter p with R . |
| AS | Constant A_v in Van Driest length scale hypothesis. |
| ASM | Constant A_t in Van Driest length scale hypothesis - used in generation of initial temperature profile. |
| BDS | Constant $1/\sigma_K$ in turbulent kinetic energy method diffusion term. |
| BDU | Constant b' in duct geometry description. |
| BL | Integer, in order to distinguish case considered between internal or external flows "BL" = 0 for internal flows "BL" = 1 for external boundary layer flows. |
| BP | Parameter describing the variation of pressure gradient parameter with R . |

| <u>Program Symbol</u> | <u>Meaning</u> |
|---------------------------|--|
| BT | Constant in logarithmic law for temperature. |
| BV | Constant B' in law of wall. |
| CASE | "CASE" = 0 for the thermal boundary condition of constant wall temperature "CASE" = 1 for a constant wall heat flux. |
| CF | Local friction factor Cf. |
| CFL | Friction factor Cf obtained from the Von Karman Momentum Integral Equation. |
| CL | $\left[= \frac{1}{\Delta R} \right]$. |
| CNTRL | Control of forward step length ΔR . If the number of steps needed to reach the outer edge of the boundary layer at two consecutive stations of R is less than "CNTRL" then the forward step length ΔR may be increased. |
| COUNT | Integer used in internal flows after interference. Determines whether a correction has been made or not to the velocity profile in order to make the limit of calculation coincide with the duct centre-line. "COUNT" = 0 - no correction made "COUNT" = 1 - correction has been made. |
| DELTA | Dimensional thickness of boundary layer, δ or δ_t . |
| DISS | Dimensionless dissipation of turbulent kinetic energy d. |
| DN | Coefficients of Thomas algorithm $\left[\gamma_i, \gamma_i', \gamma_i'' \right]$. |
| DNU | Parameter B $\left[= \frac{\partial}{\partial Y} \left(\frac{\epsilon_m}{\nu} \right) \right]$. |
| DQ | $\frac{\partial q}{\partial Y}$. |
| D2Q | $\frac{\partial^2 q}{\partial Y^2}$. |

| <u>Program Symbol</u> | <u>Meaning</u> |
|---------------------------|---|
| DR | Streamwise step ΔR . |
| DRT | $\frac{\partial}{\partial Y}(R_t)$. |
| DSTAR | Boundary layer displacement thickness δ^* . |
| DTBYP | $\frac{\partial T}{\partial y}^+$. |
| DY | Cross-stream step adjacent to wall. $[\Delta Y]$. |
| DZ | $\frac{\partial Z}{\partial Y}$. |
| EM | Value of eddy diffusivity in the inner layer from a mixing length hypothesis, used in generation of an initial profile of turbulent kinetic energy. |
| EMO | Eddy diffusivity in outer layer from mixing length hypothesis, used in initial k profile generation. |
| ERROR | Difference between duct centre line and assumed line of interference. |
| F | Integer which controls the position in the program where the turbulence information is evaluated so that the most up to date mean flow information is included, i.e. in main program at the first ΔR step and in subroutine "THERM" for all consequent steps. |
| FD | Integer used in internal flows "FD" = 0 before velocity boundary layers interfere "FD" = 1 after velocity boundary layers interfere. |
| FDT | Integer used in internal flows "FDT" = 0 before thermal boundary layer interference. "FDT" = 1 after thermal boundary layer interference. |
| FINAL | Value of R at which the calculations are desired to be terminated. |
| GAMA | Constant C_2 in turbulent kinetic energy method dissipation term. |

| <u>Program Symbol</u> | <u>Meaning</u> |
|---------------------------|--|
| H | Shape factor H. |
| HD | Arbitrary step ΔY in flow. |
| HY, HY2 | Neighbouring cross-stream steps of Y [h_1 , h_2 respectively]. |
| I | Dummy integer. |
| INCR | Incremental control of "OUT" i.e. determines when print outs of results will be obtained. |
| INCY | Geometric progression factor of cross- stream steps $\left[= \frac{h_2}{h_1} \right]$. |
| IND | Integer used in prescription of initial velocity and temperature profiles "IND" = 0 for velocity profile "IND" = 1 for temperature profile. |
| IND1 | Integer parameter. Marker as to whether the solution of the ordinary differential equation for the initial velocity and temperature profiles has ("IND1" = 1) or has not ("IND1" = 0) reached the straight line portion of the wall law. When it has then the constant B' can be determined. |
| INDYPI | Geometric progression increment of y^+ in initial velocity and temperature profile generation. |
| J | Integer used as argument for cross-stream steps. |
| JC | Number of cross-stream steps up to centre line for internal flows. Established from interference of velocity boundary layers. |
| JCT | Number of cross-stream steps up to centre line for internal flows. Established from interference of thermal boundary layers. |
| JUMP | Integer. "JUMP" = 0 for heating from leading edge "JUMP" = 1 for an unheated starting length. |
| K | Constant C_6 in the Van Driest length scale hypothesis. |

| <u>Program Symbol</u> | <u>Meaning</u> |
|---------------------------|--|
| K1 | Constant C_5 used in the description of the eddy diffusivity in the outer layer for the turbulent kinetic energy method. |
| KL | Constant C_7 in outer boundary layer, mixing length hypothesis. |
| KM | Constant C_8 used in initial temperature profile generation. |
| LD | Local duct height L (dimensional), internal flows. |
| LID | Local duct height at initial station. |
| M | Integer store of number of cross-stream steps required to calculate velocity boundary layer at current station. |
| MA | Integer used in turbulent kinetic energy equation method. Describes the number of cross-stream steps in the near-wall region when the Van Driest hypothesis is to be used before the turbulent kinetic energy equation takes over. |
| ML | Integer. "ML" = 0 for turbulent kinetic energy method. "ML" = 1 for mixing length method. |
| N | Maximum allowable number of cross-stream steps. |
| NEQ | Integer. "NEQ" = 1 for no heat transfer "NEQ" = 2 for heat transfer. |
| NTH | Constants n and n' . Exponents in power laws for initial velocity and temperature profile generation. |
| NU | $\left[1 + \frac{\epsilon_m}{\nu} \right]$. |
| NUBP | $\left[= Z^{\frac{1}{\sigma}} \left(\frac{1}{\sigma} + \frac{\epsilon_m}{\nu} \cdot \frac{1}{\sigma_t} \right) \right]$. Used in numerical evaluation of derivative with respect to Y of this expression. |
| NUL | Kinematic viscosity ν (dimensional). |

| <u>Program Symbol</u> | <u>Meaning</u> |
|---------------------------|---|
| NUO | $\left[1 + \frac{\epsilon_m}{\nu} \right]$ in the outer part of the boundary layer. Remains constant at a particular R station. |
| NUT | Turbulence group used in solution of energy equation $\left[= Z^{\frac{1}{2}} \left(\frac{1}{\sigma} + \frac{\epsilon_m}{\nu} \frac{1}{\sigma_t} \right) \right]$. |
| OUT | Value of R at which print outs of results are obtained. |
| PD | Pressure gradient p' , internal flows after interference. |
| PG | Pressure gradient parameter $p \left[= \frac{2}{U_s} \frac{dU_s}{dR} \right]$. |
| PL | Integer count of number of times subroutine "OUTPUT" entered. |
| PQ | $\left[\frac{1}{Z^{\frac{1}{2}}} - 1 \right]$. Used in integration to obtain displacement thickness. |
| PR | Prandtl number σ . |
| PROD | Dimensionless production of turbulent kinetic energy $\left[\frac{(A-1)}{4Z^{\frac{1}{2}}} \cdot \left(\frac{\partial Z}{\partial Y} \right)^2 \right]$. |
| PRT | Turbulent Prandtl number σ_t . |
| Q | Dimensionless turbulent kinetic energy $q \left[= \frac{k}{U_s^2} \right]$. |
| QP | "Q" at previous R station. |
| QT | Integer store for the number of cross-stream steps needed to solve the thermal energy equation. |
| R | Independent variable, Reynolds number R. |

| <u>Program Symbol</u> | <u>Meaning</u> |
|---------------------------|--|
| R1 | Parameter used in generation of initial turbulent kinetic energy profile $\left[= \frac{C_3}{C_6} \frac{y'}{U_s} \right]$. |
| R1I | 1st R station at which calculations are performed. |
| RD | Local duct Reynolds number $\left[\frac{L \cdot U_m}{\nu} \right]$. |
| RDEL1, RDEL2 | Displacement thickness Reynolds numbers R_θ at previous and current R stations respectively. |
| RDN | Duct Reynolds number $\left[\frac{U_{bi} \cdot L_i}{\nu} \right]$. |
| RN | Coefficients of Thomas Algorithm $[\gamma_i, \gamma_i', \gamma_i'']$. |
| RT | Turbulence Reynolds number R_t . |
| RTHE1, RTHE2 | Momentum thickness Reynolds number R_θ at previous and current R stations respectively. |
| SHEAR | Dimensionless total shear stress τ/τ_w . |
| SOLVE | Integer parameter used in solution of turbulent kinetic energy equation. "SOLVE" = 0 in near wall layer when a Van Driest hypothesis is used. "SOLVE" = 1 in remainder of boundary layer. |
| ST | Local Stanton number St . |
| STB | Bulk Stanton number St_b . |
| T | Dependent variable, temperature T . |
| TAU | Dimensionless total shear stress τ/τ_w . |
| TAUW | Dimensional wall shear stress τ_w/ρ . |
| TDIFF | Dimensionless turbulent diffusion of turbulent kinetic energy $\left[Z^{\frac{1}{2}} \frac{B}{\sigma_k} \frac{\partial q}{\partial Y} + \right.$ $\left. \frac{(A-1)}{2\sigma_k Z^{\frac{1}{2}}} \frac{\partial q}{\partial Y} \frac{\partial Z}{\partial Y} + \frac{(A-1)Z^{\frac{1}{2}}}{\sigma_k} \frac{\partial^2 q}{\partial Y^2} \right]$. |

| <u>Program Symbol</u> | <u>Meaning</u> |
|---------------------------|---|
| TEST | Parameter for testing the edge of the boundary layer $\left[\frac{\delta_i}{1 + \gamma_i} \right]$. |
| THIY | $\left[\frac{U_s - u_\tau}{u} \right]$. |
| THSTAR | Boundary layer momentum thickness θ . |
| TP | Values of t^+ as obtained from solution of ordinary differential equation before interpolation. |
| TS | Parameter used in integration to obtain momentum thickness $\left[= 1 - Z^{\frac{1}{2}} \right]$. |
| U | Reciprocal of dimensionless velocity $\left[= \frac{U_s}{u} \right]$. |
| UC | Centre-line velocity, internal flows. |
| UM | Centre-line velocity U_c at first interference point-internal flows. |
| US | Free stream velocity U_s . |
| US1 | U_s at previous station. |
| USI | Free stream velocity at initial station U_{si} . |
| UP | Values of u^+ obtained from solution of ordinary differential equation before interpolation. |
| UPR | Dimensionless velocity $\frac{U_s}{u}$ at previous R station. |
| UTAU | Friction velocity u_τ . |
| VDIFF | Dimensionless viscous diffusion of turbulent kinetic energy $\left[\frac{1}{2Z^{\frac{1}{2}}} \frac{\partial Z}{\partial Y} \frac{\partial q}{\partial Y} + Z^{\frac{1}{2}} \frac{\partial^2 q}{\partial Y^2} \right]$. |

| <u>Program Symbol</u> | <u>Meaning</u> |
|---------------------------|--|
| X | Dimensional streamwise distance x. |
| XD | $x/2L$ for internal flows. |
| XI | Distance x from leading edge of initial starting profiles. |
| Y | Independent variable Y. |
| YBCT | y/δ^*_t . |
| YD | Dimensional cross-stream distance y. |
| YDC | True distance y from wall to duct centre-line. |
| YDM | True distance y from wall to interference line (may be slightly different from duct centre-line due to overshoot on cross-stream steps). |
| YDT | True thickness of thermal boundary layer. |
| YI | Values of Y in initial profile generation before interpolation. |
| YIMAT | Value of Y at which initial velocity profiles in inner and outer region are matched for value and slope. |
| YL | Dimensionless true distance y' . |
| YLS | Value of y' at edge of boundary layer. |
| YP | Values of y^+ in initial profile generation before interpolation. |
| YP2, YP3 | Values of y^+ at 1st and 2nd steps of ΔY away from the wall. |
| YPI | Starting (wall) value of y^+ in solution of ordinary differential equation by Kutta-Merson technique. |
| YPL | Dimensionless cross-stream distance y^+ . |
| YPMAT | Value of y^+ at which the initial profile inner and outer laws are matched for value and slope. |
| YPMX | Maximum allowable limit of y^+ for initial profile generation. |
| YS | Value of Y at edge of boundary layer. |
| Z | Dependent variable, dimensionless velocity Z. |

| <u>Program</u> <u>Symbol</u> | <u>Meaning</u> |
|---------------------------------|--------------------------|
| ZP | Z at previous R station. |
| ZPR | Z at previous R station. |

Operation Notes

1. Specification of pressure gradient parameter variation (external flows)

The program has been developed assuming that the pressure gradient parameter variation can be described by the general relation

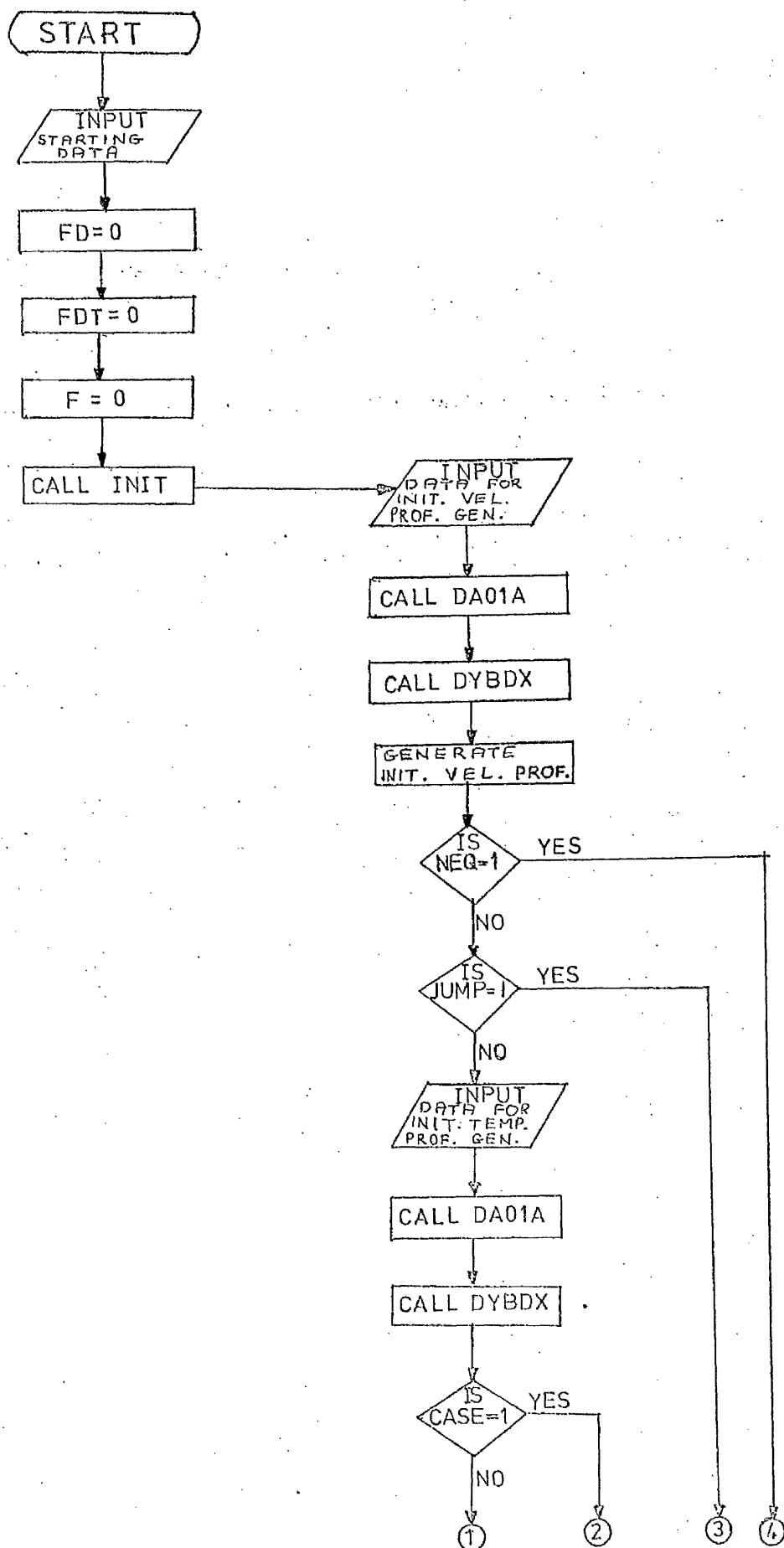
$$p = a + bR$$

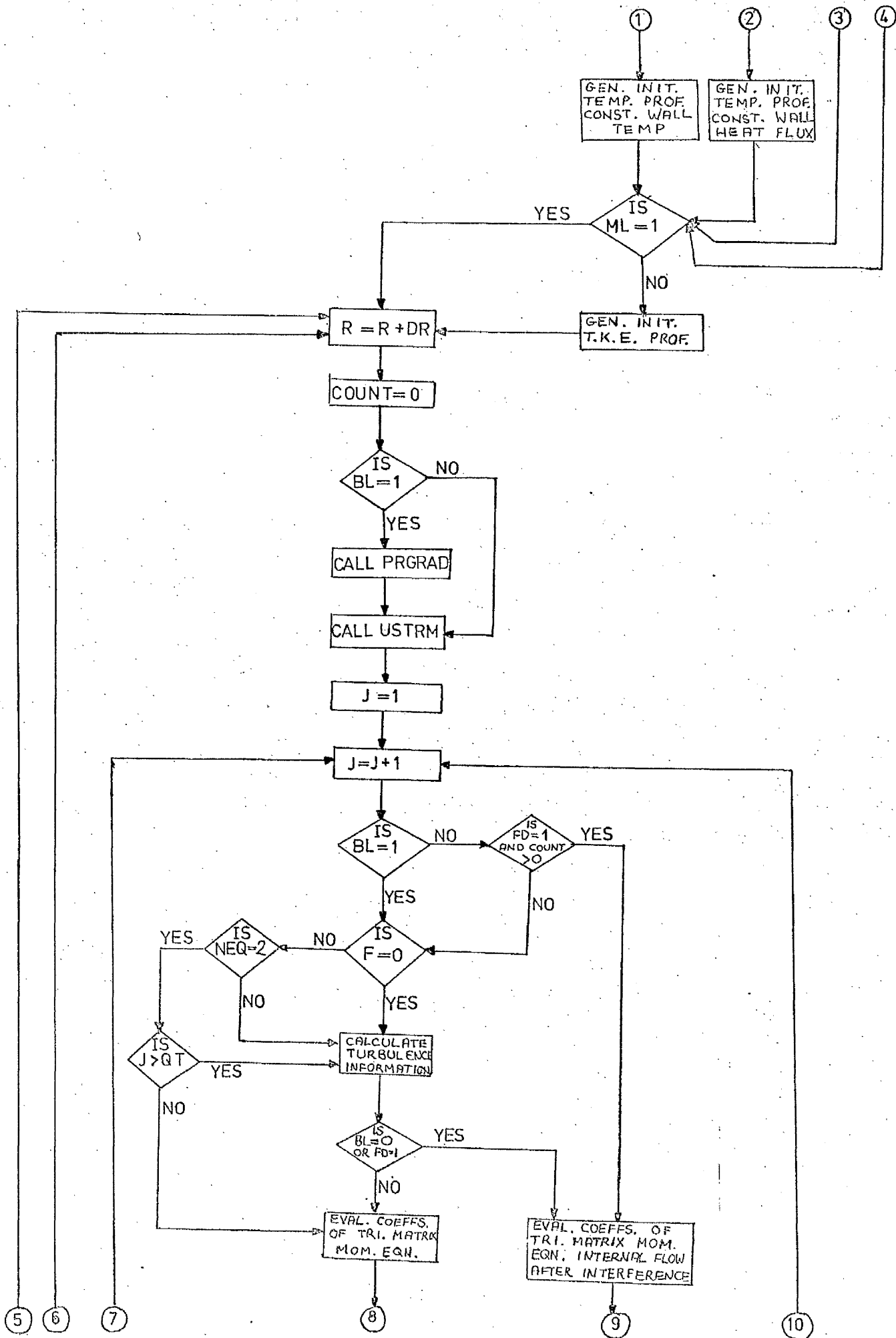
where a and b are constants. When the free stream velocity distributions are difficult to describe by a single analytic expression (e.g. tests A5 or A6) then the velocity distribution must be divided into suitable sections and an appropriate description made of the velocity in each section. Thus, subroutine "PRGRAD", in the following program listing, shows a typical description of the pressure gradient parameter in order to produce the free stream velocity variation of test A5.

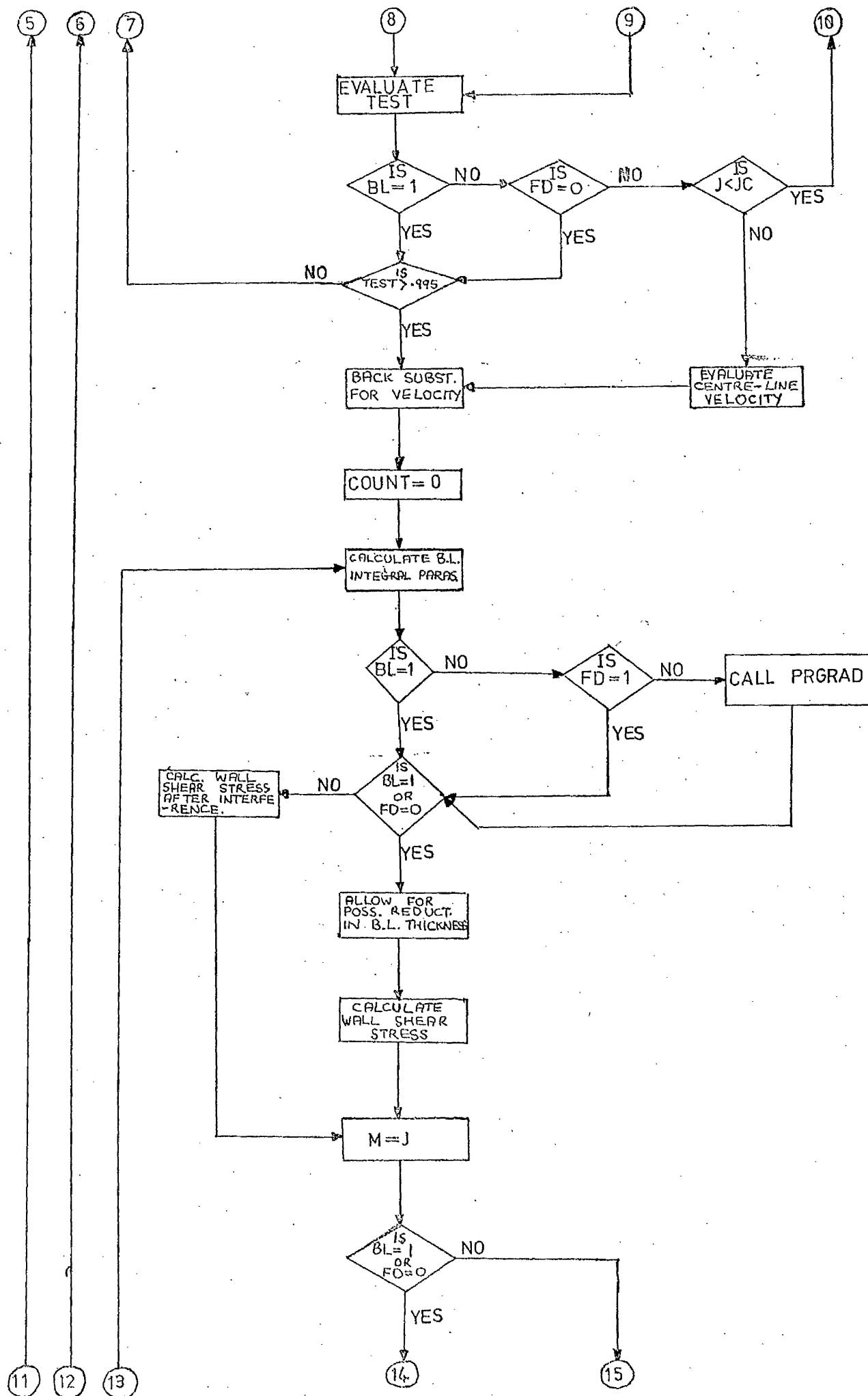
2. Run-times

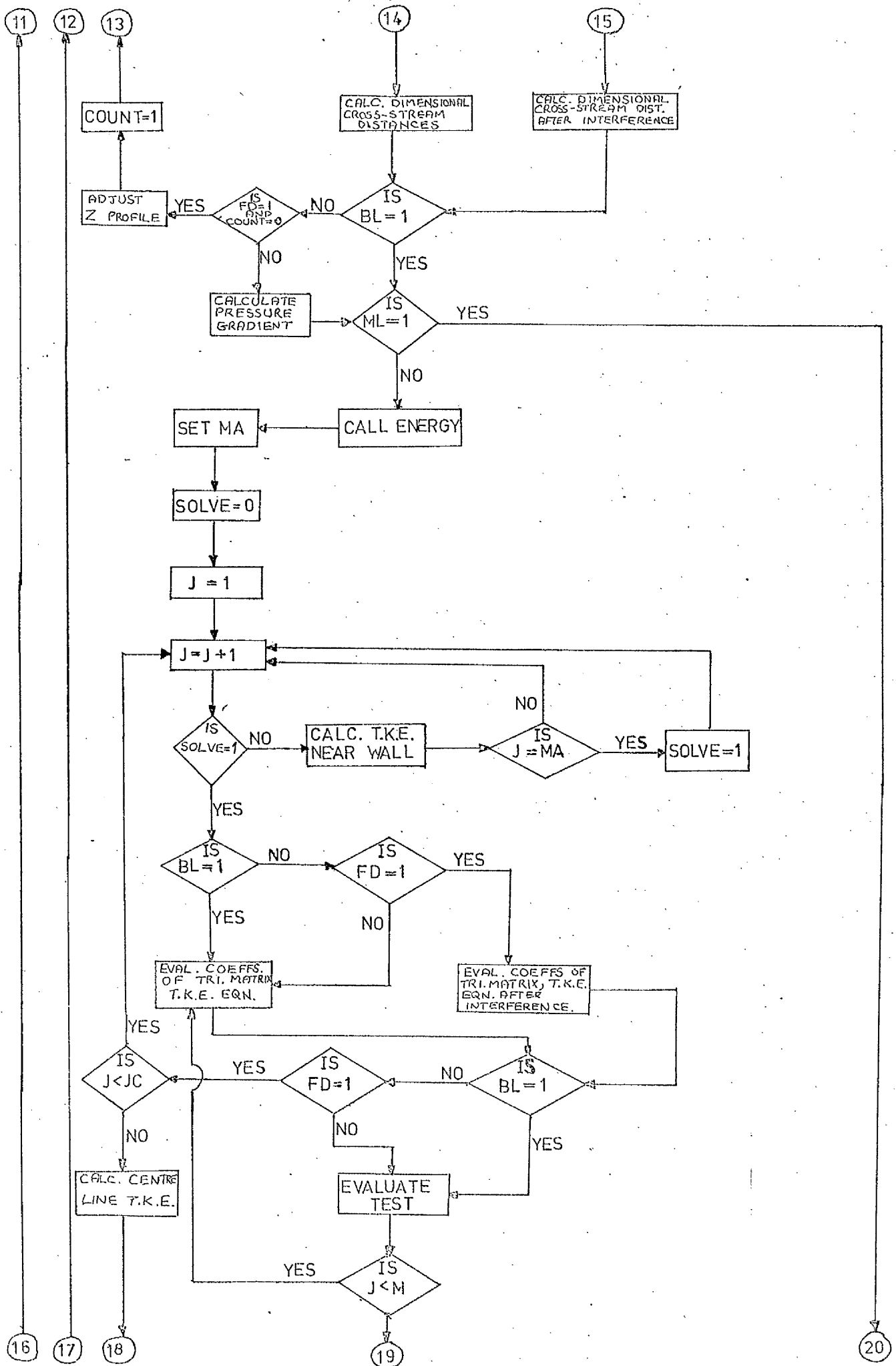
Although the run-times of the program are bound to depend on the chosen forward steps and the length of the test section, some typical figures may be of interest. Thus, for a typical boundary layer calculation, a complete solution, including print-outs of all required information, took 120 secs. on the U.M.R.C.C. 1906A computer (using 60 cross-stream steps, increasing with distance from the wall by a factor of 1.15, and 50 steps in the stream direction).

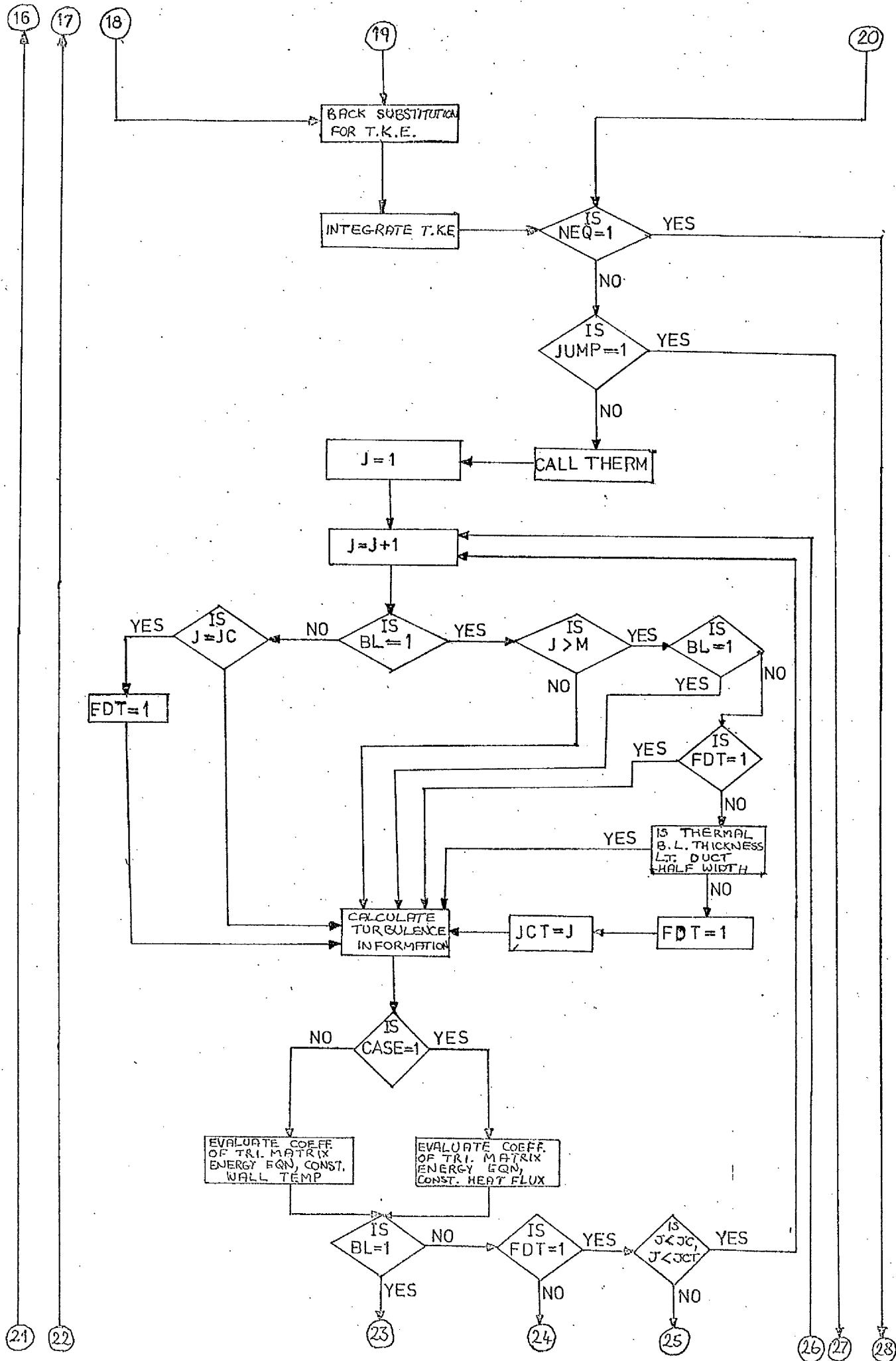
FLOW DIAGRAM OF TURBULENT BOUNDARY LAYER PROGRAM

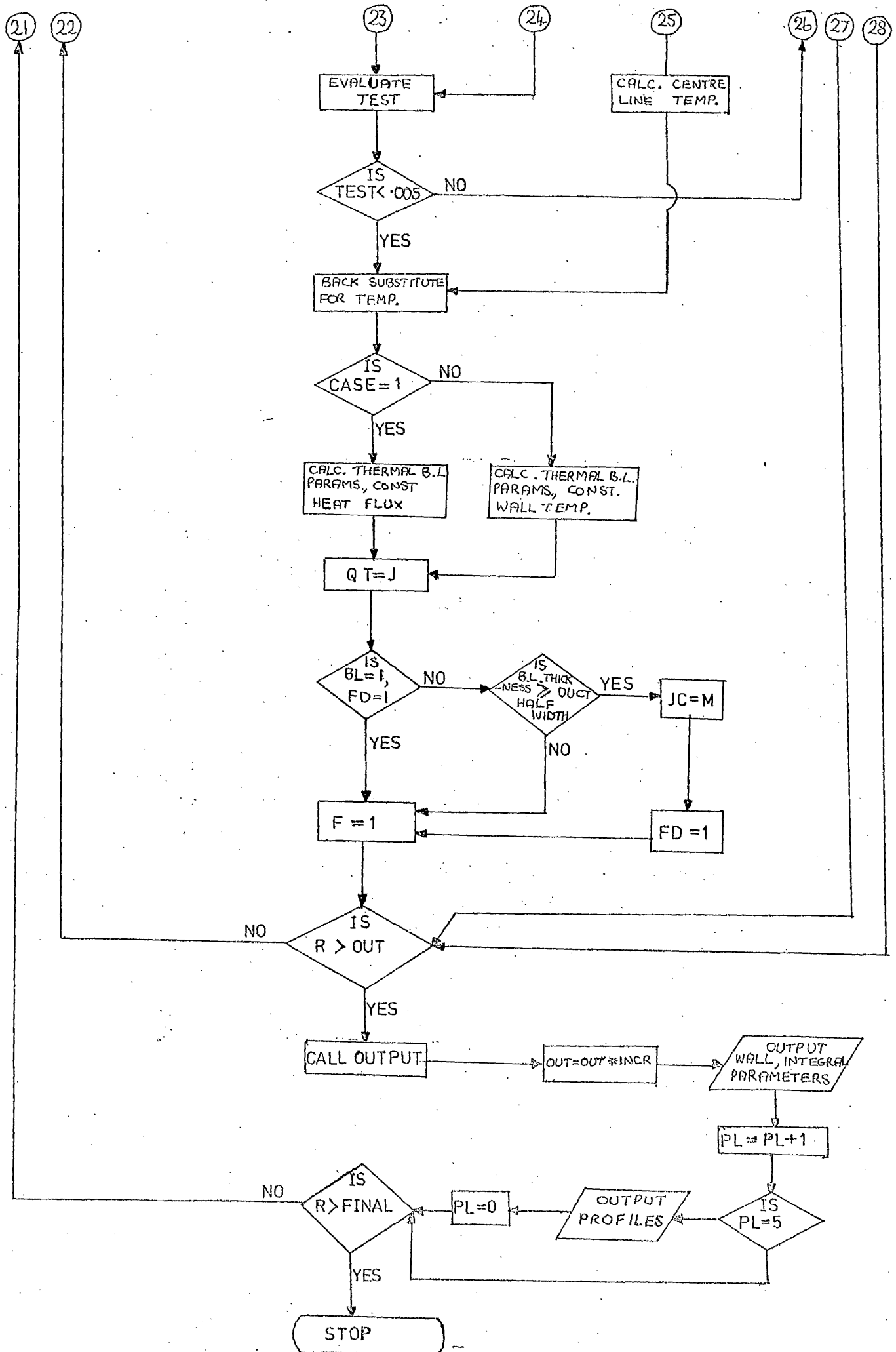












BOUNDARY LAYER AND DUCT PROGRAM

```

      REAL  NUO,KL,NU,NUT,K,NTH,KM,INCR,NUL,INCY,NUBP,K1,NR,LD,LID
      INTEGER F,W,CNTRL,CASE,QT,TAPE,FD,FDT,COUNT,BL
      DIMENSION RN(100),DN(100),TS(100),PQ(100),RS(100),TU(100),
1DZDR(100),VW(100),ZPR(100)
      COMMON K,AS,IND,PR,KM,ASM,H,RTHE2,CFL,INCY,Z(100),Q(100),
1      QP(100),TAU(100),K1,NUO,OUT,INCR,CF,R,US,X,NEQ,NL,
2      J,CASE,ST,USI,YL(100),T(100),U(100),NU(100),BDS,ML,
3      DNU(100),GAMA,ADIS,QT,DY,M,DR,RT(100),TAPE,TAUW,
4      DSTAR,THSTAR,UC,PD,STB,LD,HY2,HY,DZ,PRT,THETA,BL
5      ,CL,TH,KL,Y,YD(100),YPL(100),NTH,JUMP,NUL,N,YS,YLS
6      ,RDEL1,RDEL2,RTHE1,ALPHA,AMU,YP2,YP3,NUBP(100),ADU,
7      BDU,FD,RDN,LID,R1,JC,YDC,YDM,ZP(100),MARK,FDT,R11,
8      XI,UM,RD,UPR(100)
202 FORMAT (3I2,F7.4,2I2)
203 FORMAT (F6.3,F6.0,F4.1,I5,I3,2E10.3,F5.2/2F5.2,F6.3,E10.3,F6.3,
1F5.1/F7.4,F6.3,F7.4,F5.3,F6.3,F5.2,F7.4,F7.4)
204 FORMAT (1H ,6HALPHA=,E10.3,3X,4HAMU=,E10.3,3X,4HBDS=,E10.3,3X,
15HGAMA=,E10.3,3X,5HADIS=,E10.3)
205 FORMAT (1H0,13HINIT.REYN.NO=,E11.4,10X,13HINIT.STEP DR=,E11.4,
110X,13HINIT.STEP DY=,F6.3,10X,5HINCY=,F5.2)
206 FORMAT (1H0,11HK VELOCITY=,F6.3,10X,3HAS=,F6.2,10X,3HK1=,E10.3)
207 FORMAT (1H0,18HCONSTANT HEAT FLUX)
208 FORMAT (1H0,25HCONSTANT WALL TEMPERATURE)
209 FORMAT (1H0,12HPRANDTL NO.=,F5.2,10X,17HTURB.PRANDTL NO.=,F5.2,
110X,8HK TEMP.=,F6.3,10X,9HAS(TEMP)=,F6.2)
210 FORMAT (1H0,27HBOUNDARY LAYERS INTERFERING)
211 FORMAT (1H ,23HDUCT REYNOLD'S NUMBER= ,E11.4)
212 FORMAT(1H0,9HDUCT FLOW)
213 FORMAT(1H0,19HBOUNDARY LAYER FLOW)
214 FORMAT(1H0,24H MIXING-LENGTH HYPOTHESIS)
215 FORMAT(1H0,35HTURBULENT KINETIC ENERGY HYPOTHESIS)
C   READ IN STARTING DATA,CONSTANTS,ETC.
65  READ (1,202) NEQ,CASE,JUMP,X1,BL,ML
      READ (1,203) DY,DR,THETA,N,CNTRL,FINAL,OUT,INCR,PR,PRT,KL,NUL,
1K,AS,ALPHA,AMU,BDS,GAMA,ADIS,INCY,ADU,BDU
      WRITE (2,204) ALPHA,AMU,BDS,GAMA,ADIS
      FD=0
      FDT=0
      F=0
      TH=(1.-THETA)/THETA
CGENERATE REQUIRED INITIAL PROFILES IN SUBROUTINE INIT
      CALL INIT
      ERROR=0.0
      IF (ML.EQ.1) WRITE(2,214)
      IF (ML.EQ.0) WRITE(2,215)
      IF(BL.EQ.0) WRITE(2,212)
      IF(BL.EQ.1) WRITE (2,213)
      WRITE (2,205) R,DR,DY,INCY
      IF (BL.EQ.1) GO TO 10
      WRITE (2,211) RDN
10   WRITE (2,206) K,AS,K1
      IF (NEQ.EQ.1) GO TO 64
      IF (CASE.EQ.0) GO TO 100
      WRITE (2,207)
      GO TO 101
100  WRITE (2,208)
101  WRITE (2,209) PR,PRT,KM,ASM
C   MAJOR CONTROL LOOP STARTS
64  CL=1./DR
C   STEP IN R DIRECTION BY DISTANCE DR
      R=R+DR

```

```

COUNT=0
C CALCULATE EDDY DIFFUSIVITY OF MOMENTUM IN OUTER LAYER IF USING
C MIXING LENGTH HYPOTHESIS
  IF (ML.EQ.1) NUO=KL*RDEL1
C SUPPLY PRESSURE GRADIENT PARAMETER FOR EXTERNAL FLOWS
  IF (BL.EQ.1) CALL PRGRAD(PG,NUL,AP,BP,R,RDEL
    12,RDEL1,US,DR,LD,LID,USI,BDU,BL)
C CALCULATE FREE STREAM VELOCITY FOR EXTERNAL FLOWS AND CENTRE-LINE
C VELOCITY BEFORE INTERFERENCE FOR INTERNAL FLOWS
  CALL USTRM(US,PG,AP,BP,DR,X,NUL,XI,R,USI,LID,LD,RDEL1,ADU,BDU,R11,
    1FD,MARK,YDC,UM,RD,ERROR,BL)
77 YS=0.0
73 HY=DY
  J=1
  HY2=HY
C START OF CROSS-STREAM CALCULATION AT CURRENT R STATION
41 J=J+1
  HY=HY2
  HY2=HY*INCY
  IF (BL.EQ.1) GO TO 11
  IF (J.EQ.JC) HY2=HY
  IF (FD.EQ.1.AND.COUNT.GT.0) GO TO 74
11 IF (NU(J-1).EQ.NUO) GO TO 44
  IF (F.EQ.0) GO TO 45
  IF (NEQ.EQ.2) GO TO 46
45 IF (NU(J-1).EQ.NUO) GO TO 44
C CALCULATE DZ/DY FOR EXTERNAL AND INTERNAL FLOWS IN THE INNER REGION
C FOR THE SECOND STATION ONLY (I.E. THE FIRST CALCULATED STATION)
  DZ=(HY**2*(Z(J+1))+(HY2**2-HY**2)*Z(J)-HY2**2*Z(J-1))
  1/(HY*HY2*(HY+HY2))
  IF (ML.EQ.1) GO TO 17
C CALCULATE EDDY DIFFUSIVITY OF MOMENTUM IN INNER REGION-PRANDTL-
C -KOLMOGOROV HYPOTHESIS
  NU(J)=1.+ALPHA*RT(J)*(1.-EXP(-AMU*RT(J)))
  GO TO 18
17 EN=EXP(-YL(J)*SQRT(CF/2.)/(K*AS))
C CALCULATE EDDY DIFFUSIVITY OF MOMENTUM IN INNER REGION,
C PRANDTL MIXING LENGTH HYPOTHESIS
  NU(J)=1.+0.5*YL(J)**2*DZ*(1.0-EN)**2
18 IF (NUO.LT.NU(J)) GO TO 44
  IF (ML.EQ.1) GO TO 19
  DRT=(HY**2*(RT(J+1))+(HY2**2-HY**2)*RT(J)-HY2**2*RT(J-1))
  1/(HY*HY2*(HY+HY2))
C CALCULATE D/DY(NU) IN INNER REGION,PRANDTL-KOLMOGOROV
  DNU(J)=ALPHA*DRT*(1.-EXP(-AMU*RT(J)))+ALPHA*RT(J)*AMU*DRT*
  1EXP(-AMU*RT(J))
  GO TO 47
C CALCULATE D/DY(NU) IN INNER REGION,MIXING LENGTH
19 DNU(J)=DZ*(YL(J)*K*U(J)*(1.-EN)**2+YL(J)**2*SQRT(CF/2.)*U(J)*EN/AS
  1*(1.-EN))+(HY*Z(J+1)+HY2*Z(J-1)-(HY2+HY)*Z(J))/(HY*HY2*(HY+HY2))*C
  2YL(J)**2*(1.-EN)**2)
  GO TO 47
44 NU(J)=NUO
  DNU(J)=0.0
  GO TO 47
46 IF (J.GT.QT) GO TO 45
47 NUBP(J)=(1./PR+(NU(J)-1.)/PRT)/U(J)
C EVALUATE COEFFICIENTS OF TRIDIAGONAL MATRIX-MOMENTUM EQUATION
74 AA=1./(HY2*(2.*NU(J)-DNU(J)*HY2))
  AL=UPR(J)*AA*HY*HY2*(HY+HY2)/THETA
  A=2.*NU(J)*(HY+HY2)*AA
  B=(HY+HY2)*(HY2-HY)*DNU(J)*AA

```

```

C=(2.*NU(J)+HY*DNU(J))*HY*AA
P=AL*PG
AM=AL*CL
IF (BL.EQ.1) GO TO 12
IF (FD.EQ.1) GO TO 87
12 D=-TH*Z(J-1)+(TH*(A+B)-AM+P)*Z(J)-TH*C*Z(J+1)-P
88 B=-(A-B+AM)
147 IF (J.EQ.2) GO TO 48
RN(J)=1./(B-RN(J-1))
DN(J)=RN(J)*(D-DN(J-1))
RN(J)=RN(J)*C
GO TO 49
48 RN(2)=C/B
DN(2)=D/B
C EVALUATE TEST PARAMETER
49 TEST=DN(J)/(1.+RN(J))
YS=YS+HY
IF (BL.EQ.1) GO TO 85
IF (FD.EQ.0) GO TO 85
IF (FD.EQ.1.AND.J.LT.JC) GO TO 41
Z(J)=(D/(1.+C)-DN(J-1))/(B/(1.+C)-RN(J-1))
UC=UM*SQRT(Z(J))
GO TO 86
C TEST FOR EDGE OF VELOCITY BOUNDARY LAYER
85 IF (ABS(TEST-1.).GT.5.0E-03) GO TO 41
Z(J)=TEST
UC=US
IF (BL.EQ.1) UM=UC
86 I=J
C BACK SUBSTITUTION TO OBTAIN NEW VELOCITY PROFILE
50 I=I-1
Z(I)=DN(I)-RN(I)*Z(I+1)
IF (I-2) 51,51,50
51 Z(I)=0.0
COUNT=0
82 HD=DY
SUM=0.0
ADD=0.0
TS(1)=0.0
PQ(1)=2.*SQRT(DY/CF)-DY
C INTEGRATIONS FOR BOUNDARY LAYER INTEGRAL PARAMETERS
DO 52 I=2,J
TS(I)=1.-SQRT(Z(I))*UM/UC
PQ(I)=1./(SQRT(Z(I))*UM/UC)-1.
SUM=SUM+(TS(I)+TS(I-1))*HD/2.
ADD=ADD+(PQ(I)+PQ(I-1))*HD/2.
52 HD=HD*INCY
RDEL2=ADD
RTHE2=SUM
H=RDEL2/RTHE2
THSTAR=RTHE2*NUL/UC
DSTAR=RDEL2*NUL/UC
IF (BL.EQ.1) GO TO 90
IF (FD.EQ.1) GO TO 91
C CALL SUBROUTINE PRGRAD TO OBTAIN PRESSURE GRADIENT PARAMETER FOR
C INTERNAL FLOWS BEFORE INTERFERENCE
CALL PRGRAD(PG,NUL,AP,BP,R,RDEL2,RDEL1,US,DR,LD,LID,USI,BD
1U,BL)
90 CFL=2.*((RTHE2-RTHE1)/DR+(H+1)*PG/2.*RTHE2)
91 RTHE1=RTHE2
RDEL1=RDEL2
IF (BL.EQ.1) GO TO 13

```

```

    IF (FD.EQ.1) GO TO 54
13  I=J
53  I=I+1
    IF (Z(I).EQ.1.0) GO TO 54
    Z(I)=1.0
    GO TO 53
C   CALCULATE FRICTION FACTOR
54  CF=Z(2)*(1.+INCY)/(INCY*DY)-Z(3)/(DY*INCY*(1.+INCY))
    IF (BL.EQ.1) GO TO 14
    IF (FD.EQ.1) GO TO 55
    GO TO 56
55  CF=CF*UM**2/UC**2
56  TAUW=CF/2.*UC**2
14  IF (IABS(J-M).LT.CNTRL) GO TO 61
62  YD(1)=0.0
    YL(1)=0.0
    Y=0.0
    HY=DY
    M=J
    SUM=0.0
    DO 302 I=2,J
    Y=Y+HY
    IF (BL.EQ.1) GO TO 15
    IF (FD.EQ.1) GO TO 95
15  YL(I)=K*SQRT(4.*Y/CF)
    GO TO 96
C   CALCULATE DIMENSIONAL CROSS-STREAM STEPS
95  YL(I)=K*SQRT(4.*Y/(CF*UC**2/UM**2))
96  U(I)=1./SQRT(Z(I))
    SUM=SUM+0.5*(Z(I)+Z(I-1))*(YL(I)-YL(I-1))
    HY=HY*INCY
    IF (YL(I)*SQRT(CF/2.)/K.GT.2.0) GO TO 301
302 CONTINUE
301 IP=I+1
    DO 69 I=IP,J
    ZP(I)=Z(I)
    U(I)=1./SQRT(Z(I))
    YL(I)=YL(I-1)+0.5*HY*(U(I)+U(I-1))*K
    SUM=SUM+(Z(I)+Z(I-1))*(YL(I)-YL(I-1))*0.5
    HY=HY*INCY
69  CONTINUE
    IF (BL.EQ.1) GO TO 16
    YDM=NUL*YL(J)/(K*US)
    SUMB=SUM
    IF (FD.EQ.1.AND.COUNT.EQ.0) GO TO 93
    GO TO 94
93  DO 92 I=2,J
92  Z(I)=Z(I)*(YDM/YDC)**2
    UC=UM*SQRT(Z(J))
    COUNT=1
    GO TO 82
C   CALCULATE PRESSURE GRADIENT FOR INTERNAL FLOW,AFTER INTERFERENCE
94  PD=2.*CF*UC**2/(RD*UM**2)-4.*BDU*SUMB/(K*RD**2)
    1+4.*(SUMB-SUMA)/(DR*K*RD)
    SUMA=SUMB
16  YP2=YL(2)*SQRT(CF/2.)/K
    YP3=YL(3)*SQRT(CF/2.)/K
    YP4=YL(4)*SQRT(CF/2.)/K
    DO 75 I=1,J
    ZPR(I)=Z(I)
75  UPR(I)=U(I)
    IF (ML.EQ.1) GO TO 20

```

```

C   CALL SUBROUTINE ENERGY TO SOLVE TURBULENT KINETIC ENERGY EQUATION
C   WHEN USING PRANDTL-KOLMOGOROV HYPOTHESIS
      CALL ENERGY(PG)
20  YLS=YL(J)
      IF (NEQ.EQ.1) GO TO 63
C   CALL SUBROUTINE THERM TO SOLVE, IF REQUIRED, THE THERMAL ENERGY EQUATION
      CALL THERM
      IF (BL.EQ.1) GO TO 71
      IF (FD.EQ.1) GO TO 71
      IF ((LD-2.*YDM).LT.0.0) GO TO 70
71  F=1
63  IF (R.LT.OUT) GO TO 64
C   CALL OUTPUT TO PRINT OUT RESULTS
      CALL OUTPUT(PG)
      IF (R.GT.FINAL) GO TO 65
      GO TO 64
C   MAJOR CONTROL LOOP ENDS
      STOP
C   CONTROL OF FORWARD STEP LENGTH
61  IF( R.GT.6.50E+05) GO TO 62
      DR=2.*DR
      GO TO 62
70  WRITE (2,210)
      JC=M
      FD=1
      Z(JC)=1.0
      UM=US
      ERROR=YDM-YDC
      GO TO 71
87  D=-TH*ZPR(J-1)+(TH*(A+B)-AM)*ZPR(J)-TH*C*ZPR(J+1)-PD
      GO TO 88
      END

```

```

SUBROUTINE INIT
C  GENERATES INITIAL PROFILES OF VELOCITY,TEMPERATURE AND,IF REQUIRED,
C  TURBULENT KINETIC ENERGY
  REAL NUL,NTH,KM,K,INCR,NU,NUT,KL,NUO,INCY,INDYPI,NUBP,K1,LID,LD
  INTEGER CASE,W,COUNT,QT,TAPE,BL,FD,FDT
  DIMENSION YP(400),YI(400),UP(400),TP(400),YY(2),E(2),A(2),B(2)
  1,C(2),D(2),TPLU(100),YPLU(100),UPLU(100),YBDEL(100),YDL(100),
  2QL(100),TS(100),PQ(100),ADV(100),PROD(100),TDIFF(100),VDIFF(100),
  3DISS(100),SHEAR(100)
  COMMON K,AS,IND,PR,KM,ASM,H,RTHE2,CFL,INCY,Z(100),Q(100),
  1  QP(100),TAU(100),K1,NUO,OUT,INCR,CF,R,US,X,NEQ,NL,
  2  J,CASE,ST,USI,YL(100),T(100),U(100),NU(100),BDS,ML,
  3  DNU(100),GAMA,ADIS,QT,DY,M,DR,RT(100),TAPE
  4  ,TAUW,DSTAR,THSTAR,UC,PD,STB,LD,HY2,HY,DZ,PRT,THETA,BL
  5  ,CL,TH,KL,Y,YD(100),YPL(100),NTH,JUMP,NUL,N,YS,YLS
  6  ,RDEL1,RDEL2,RTHE1,ALPHA,AMU,YP2,YP3,NUBP(100),ADU,
  7  BDU,FD,RDN,LID,R1,JC,YDC,YDM,ZP(100),MARK,FDT,R1I,
  8  XI,UM,RD,UPR(100)
110 FORMAT (1H1,12HCF(INITIAL)=,E11.4)
111 FORMAT (1H+,25X,E11.4)
112 FORMAT (1H+,40X,E11.4)
113 FORMAT (1H ,3HST=,E11.4)
114 FORMAT (1H+,20X,E11.4)
202 FORMAT (I4)
201 FORMAT (E10.3,F6.3,F6.2,F7.2)
204 FORMAT (E10.3,F7.2,E10.3,F6.3,F6.2,F7.2,F5.2,F7.1)
203 FORMAT (F8.5,F9.6)
205 FORMAT (1H ,24HPOWER LAW CONSTANT(VEL)=,F5.2)
206 FORMAT (1H ,25HPOWER LAW CONSTANT(TEMP)=,F5.2)
207 FORMAT (1H ,24HINITIAL DISP. THICKNESS=,E10.3,28X,
123HINITIAL MOM. THICKNESS=,E10.3)
C  READ IN INPUT DATA FOR INITIAL PROFILE GENERATION
  READ (1,204) R,US,CF,KM,ASM,NTH,INDYPI,YPMX
  R1I=R+DR
  WRITE (2,205) NTH
  UTAU=US*SQRT(CF/2.)
  USI=US
  LID=ADU
  YPI=0.0
  DYPI=0.05
  JJ=0
  IND1=0
  IND=0
  YY(1)=0.0
  YY(2)=0.0
  I=1
  YP(1)=0.0
  YI(1)=0.0
  UP(1)=0.0
C  CALL SUBROUTINE DAO1A-A LIBRARY PROGRAM FOR THE SOLUTION OF ORDINARY
C  DIFFERENTIAL EQUATIONS BY THE KUTTA-MERSON METHOD
  1 CALL DAO1A(YY,E,A,B,C,D,2,YPI,DYPI)
  I=I+1
  YP(I)=YPI
  YI(I)=YY(1)
  UP(I)=YY(2)
  IF (IND1.EQ.0) GO TO 66
67 GO TO 98
  4 DYPI=INDYPI*DYPI
  IF (YP(I).LT.YPMX) GO TO 1
  Y=DY
  YH=DY
  I=0

```

```

      J=1
      YPL(1)=0.0
      U(1)=0.0
      YD(1)=0.0
5     I=I+1
      IF(Y.GT.YI(I))GO TO 5
      J=J+1
      YH=YH*INCY
C     INTERPOLATION TO ESTABLISH INITIAL VELOCITY PROFILE
7     YPL(J)=(Y-YI(I-1))*(YP(I)-YP(I-1))/(YI(I)-YI(I-1))+YP(I-1)
      U(J)=((Y-YI(I-1))*(UP(I)-UP(I-1))/(YI(I)-YI(I-1))+UP(I-1))*
      1UTAU/US
      YD(J)=YPL(J)*NUL/UTAU
      YT=Y
      Y=Y+YH
      IF(Y.LT.YIMAT)GO TO 5
      YF=YD(J)
      DELTA=YD(J)*EXP(-NTH*ALOG(U(J)))
      CON=NUL*EXP(1./NTH*ALOG(DELTA))*(NTH+1)/(NTH*US)
      YS=YT
8     J=J+1
      YD(J)=EXP(NTH/(NTH+1.)*(ALOG(CON*YH+EXP((NTH+1.)/NTH*ALOG(YD(J-1)
      1))))
      U(J)=EXP(1./NTH*ALOG(YD(J)/DELTA))
      YS=YS+YH
      YH=YH*INCY
10    IF(YD(J).LT.DELTA)GO TO 8
      M=J
      DO 11 I = J+1,N
      U(I)=1.0
      UPR(I)=1.0
11    Z(I)=1.0
      IF(NEQ.EQ.1)GO TO 29
      IF(JUMP.EQ.1)GO TO 13
C     READ IN DATA REQUIRED FOR GENERATION OF INITIAL TEMPERATURE PROFILE
      READ (1,201) STB,KM,ASM,NTH
      WRITE (2,206) NTH
      IF (BL.EQ.1) ST=STB
      IF (BL.EQ.1) GO TO 45
      ST=STB*LID/(LID+2.*XI*STB)
45    JJ=0
      YPI=0.0
      DYPI=0.05
      IND1=0
      IND=IND+1
      YY(1)=0.0
      YY(2)=0.0
      I=1
      TP(1)=0.0
C     CALL SUBROUTINE DAO1A FOR SOLUTION OF ORD. DIFF. EQNS.
14    CALL DAO1A(YY,E,A,B,C,D,2,YPI,DYPI)
      I=I+1
      TP(I)=YY(2)
      IF (IND1.EQ.0) GO TO 90
91    GO TO 99
16    DYPI=INDYPI*DYPI
      IF (YP(I).LT.YPMX) GO TO 14
      IF (YPMAT.LT.100) GO TO 50
      GO TO 51
50    DO 54 I=1,400
      IF (YPMAT-YP(I)) 53,53,54
54    CONTINUE

```



```

53 YIMAT=YI(I)
GO TO 51
51 Y=DY
YHS=YH
YH=DY
I=0
J=1
T(1)=1.0
19 I=I+1
IF(Y.GT.YI(I))GO TO 19
J=J+1
YH=YH*INCY
C INTERPOLATE TO OBTAIN INITIAL TEMPERATURE PROFILE
21 T(J)=1.-((Y-YI(I-1))*(TP(I)-TP(I-1))/(YI(I)-YI(I-1))+TP(I-1))*ST/S
1QRT(CF/2.)
Y=Y+YH
IF(J.GT.M)GO TO 150
149 IF(Y.LT.YIMAT)GO TO 19
DELTA=YD(J)*EXP(-NTH*ALOG(1.-T(J)))
I=J
22 I=I+1
IF(I.GT.M)GO TO 23
T(I)=1.-EXP(ALOG(YD(I)/DELTA)/NTH)
IF(YD(I).LT.DELTA)GO TO 22
DO 24 L = 1,N
24 T(L)=0.0
GO TO 25
23 J=M
94 J=J+1
U(J)=1.0
YD(J)=YD(J-1)+NUL*YHS/US
T(J)=1.-EXP(ALOG(YD(J)/DELTA)/NTH)
YHS=YHS*INCY
27 IF(YD(J).LT.DELTA)GO TO 94
599 DO 28 L = J+1,N
28 T(L)=0.0
25 IF(CASE.EQ.0)GO TO 29
DO 30 I = 1,N
30 T(I)=T(I)/ST
COA=(-SQRT(2.*DY)*(1.+SQRT(1.+INCY)))/(2.*DY*SQRT(1.+INCY))
COB=(SQRT(1.+INCY))/(SQRT(2.*DY)*(SQRT(1.+INCY)-1.))
COC=1./((SQRT(2.*DY*(1.+INCY)))*(SQRT(1.+INCY)-1.))
GO TO 29
13 DO 32 I = 1,N
32 T(I)=0.0
29 DO 33 I = 2,M
YL(I)=K*YD(I)*US/NUL
Z(I)=U(I)**2
U(I)=1./U(I)
33 UPR(I)=U(I)
YL(I)=0.0
Z(I)=0.0
YLS=YL(M)
YP2=YL(2)*SQRT(CF/2.)/K
YP3=YL(3)*SQRT(CF/2.)/K
I=1
Q(1)=0.0
RT(1)=0.0
800 IF (J-M) 999,998,998
999 MM=M
GO TO 997
998 MM=J
997 WRITE(2,110) CF

```

```

HD=DY
SUM=0.0
ADD=0.0
TS(1)=0.0
PQ(1)=2.*SQRT(DY/CF)-DY
DO 52 I=2,M
TS(I)=1.-SQRT(Z(I))
PQ(I)=1./SQRT(Z(I))-1.
SUM=SUM+(TS(I)+TS(I-1))*HD/2.
ADD=ADD+(PQ(I)+PQ(I-1))*HD/2.
52 HD=HD*INCY
RDEL1=ADD
RTHE1=SUM
H=RDEL1/RTHE1
DSTAR=NUL*RDEL1/US
THSTAR=NUL*RTHE1/US
RDN=2.*US*LID/NUL-4.*RDEL1
WRITE (2,207) DSTAR,THSTAR
CF=Z(2)*(1.+INCY)/(INCY*DY)-Z(3)/(DY*INCY*(1.+INCY))
WRITE(2,112) CF
EMO=KL*RDEL1
IF (ML.EQ.1) GO TO 38
C GENERATE INITIAL TURBULENT KINETIC ENERGY PROFILE IF REQUIRED
K1=0.0
HY=DY
HY2=DY
DO 41 I=2,M
HY=HY2
HY2=HY*INCY
R1=AMU*YL(I)/(K*US)
II=0
EN=1.-EXP(-YL(I)*SQRT(CF/2.)/(K*AS))
DZ=(HY**2*(Z(I+1))+(HY2**2-HY**2)*Z(I)-HY2**2*Z(I-1))
1/(HY*HY2*(HY+HY2))
EM=YL(I)**2/2.*DZ*EN**2
P1=YL(I)*K*US*EN**2*DZ/(2.*ALPHA)
IF (EM.GT.EMO) GO TO 72
IF (I.EQ.2) XN=0.03
IF (I.EQ.2) GO TO 42
43 XN=XNW
42 XNW=XN-(XN*(1.-EXP(-R1*XN))-P1)/(1.-EXP(-R1*XN)+XN*R1*EXP
1(-R1*XN))
II=II+1
IF (ABS(XNW-XN).GT.0.01*XN) GO TO 43
Q(I)=(XNW/US)**2
RT(I)=YL(I)*XNW/(US*K)
41 WRITE (2,44) Q(I),RT(I),II
44 FORMAT (1H ,E11.4,10X,E11.4,10X,I3)
72 MO=I
DO 73 I=MO,M
Q(I)=Q(MO-1)*(1.-YL(I)/YL(M))**2
RT(I)=SQRT(Q(I))*YL(I)/K
73 WRITE (2,74) Q(I),RT(I)
74 FORMAT (1H ,E11.4,10X,E11.4)
SUM=0.0
DO 75 I=2,M
75 SUM=SUM+(Q(I)+Q(I-1))/2.*(YL(I)-YL(I-1))
NUO=EMO
K1=K*(NUO-1.)/SUM
K1=0.5
DO 996 I=M,N
RT(I)=0.0

```

```

996 Q(I)=0.0
38 IF(NEQ.EQ.1)GO TO 39
WRITE(2,113) ST
IF(CASE.EQ.1)GO TO 40
DTBYP=T(1)*(-(YP2+YP3)/(YP2*YP3))+T(2)*(YP3/(YP2*(YP3-YP2
1))) - T(3)*YP2/(YP3*(YP3-YP2))
ST=-DTBYP*SQRT(CF/2.)/PR
WRITE(2,114) ST
GO TO 39
40 ST=USI/(US*T(1))
WRITE(2,114) ST
39 RETURN
3 YIMAT=YI(I)
JJ=1
GO TO 4
15 YIMAT=YI(I)
JJ=1
GO TO 16
66 IF (YP(I).LT.100.) GO TO 4
BV=UP(I)-1./KM*ALOG(YP(I))
YPMAT=EXP(NTH-BV*KM)
IND1=1
GO TO 67
150 YD(J)=YD(J-1)+NUL*YHS/US
YHS=YHS*INCY
GO TO 149
90 IF (YP(I).LT.100.) GO TO 16
BT=TP(I)-1./KM*ALOG(YP(I))
YPMAT=EXP(NTH-BT*KM)
IND1=1
GO TO 91
98 IF (JJ.EQ.1) GO TO 4
IF (YPMAT-YP(I)) 3,3,4
99 IF (JJ.EQ.1) GO TO 16
IF (YPMAT-YP(I)) 15,15,16
END

```

```

SUBROUTINE THERM
REAL NU,NUT,K,KL,KM,INCR,INCY,NUBP,NUO,K1,NTH,NUL,LD,LID
INTEGER CASE,QT,FD,FDT,BL,TAPE
DIMENSION RN(100),DN(100),TPLU(100),YPLU(100),UPLU(100)
COMMON K,AS,IND,PR,KM,ASM,H,RTHE2,CFL,INCY,Z(100),Q(100),
1 QP(100),TAU(100),K1,NUO,OUT,INCR,CF,R,US,X,NEQ,NL,
2 J,CASE,ST,USI,YL(100),T(100),U(100),NU(100),BDS,ML,
3 DNU(100),GAMA,ADIS,QT,DY,M,DR,RT(100),TAPE
4 ,TAUW,DSTAR,THSTAR,UC,PD,STB,LD
5 ,HY2,HY,DZ,PRT,THETA,BL,CL,TH,KL
6 ,Y,YD(100),YPL(100),NTH,JUMP,NUL,N,YS,YLS
7 ,RDEL1,RDEL2,RTHE1,ALPHA,AMU,YP2,YP3,NUBP(100),ADU,
8 BDU,FD,RDN,LID,R1,JC,YDC,YDM,ZP(100),MARK,FDT,R1I,XI,UM,RD
IF (ML.EQ.1) NUO=KL*RDEL2
J=1
HY=DY
HY2=DY
IF (JC.GT.0) JCT=0
100 FORMAT (1H,51HTHERMAL BOUNDARY LAYERS INTERFERING BEFORE VELOCITY
1)
COA=-(YP2+YP3)/(YP2*YP3)
COB=-YP3/(YP2*(YP2-YP3))
COC=-YP2/(YP3*(YP3-YP2))
COD=-PR*USI/(US*SQRT(CF/2.))
70 J=J+1
HY=HY2
HY2=HY*INCY
IF (BL.EQ.1) GO TO 72
IF (J.EQ.JC) HY2=HY
IF (J.EQ.JC) FDT=1
72 DZ=(HY**2*(Z(J+1))+(HY2**2-HY**2)*Z(J)-HY2**2*Z(J-1))/
1(HY*HY2*(HY+HY2))
IF (J.GT.M) GO TO 555
556 IF (NU(J-1).EQ.NUO) GO TO 73
IF (ML.EQ.1) GO TO 20
C UPDATE CALCULATION OF TURBULENCE QUANTITIES
NU(J)=1.+ALPHA*RT(J)*(1.-EXP(-AMU*RT(J)))
GO TO 21
20 EN=EXP(-YL(J)*SQRT(CF/2.)/(K*AS))
NU(J)=1.+0.5*YL(J)**2*DZ*(1.-EN)**2
21 IF (NU(J).GT.NUO) GO TO 73
IF (ML.EQ.1) GO TO 22
DRT=(HY**2*(RT(J+1))+(HY2**2-HY**2)*RT(J)-HY2**2*RT(J-1))/
1(HY*HY2*(HY+HY2))
DNU(J)=ALPHA*DRT*(1.-EXP(-AMU*RT(J)))+ALPHA*RT(J)*AMU*DRT*
1EXP(-AMU*RT(J))
GO TO 74
22 DNU(J)=DZ*(YL(J)*K*U(J)*(1.-EN)**2+YL(J)**2*SQRT(CF/2.)*U(J)*EN/AS
1*(1.-EN))+(HY*Z(J+1)+HY2*Z(J-1)-(HY+HY2)*Z(J))/(HY*HY2*(HY+HY2))*
2YL(J)**2*(1.-EN)**2)
GO TO 74
73 DNU(J)=0.0
NU(J)=NUO
74 NUT=(1./PR+(NU(J)-1.)/PRT)/U(J)
DNUT=(HY**2*(NUBP(J+1))+(HY2**2-HY**2)*NUBP(J)-HY2**2*NUBP
1(J-1))/(HY*HY2*(HY+HY2))
TAU(J)=NU(J)*DZ/CF
IF (BL.EQ.1) GO TO 10
IF (FD.EQ.1) TAU(J)=NU(J)*DZ*UM**2/(CF*UC**2)
C SOLVE ENERGY EQUATION
10 AA=1./(HY2*(2.*NUT-DNUT*HY2))

```

```

AL=AA*HY*HY2*(HY+HY2)/THETA
A=2.*NUT*(HY+HY2)*AA
B=(HY+HY2)*(HY2-HY)*DNUT*AA
C=(2.*NUT+HY*DNUT)*HY*AA
AM=AL*CL
D=-TH*T(J-1)+(TH*(A+B)-AM)*T(J)-TH*C*T(J+1)
B=-(A-B+AM)
IF (J.EQ.2) GO TO 75
RN(J)=1./(B-RN(J-1))
DN(J)=RN(J)*(D-DN(J-1))
RN(J)=RN(J)*C
GO TO 76
75 IF (CASE.EQ.1) GO TO 77
RN(2)=C/B
DN(2)=(D-1.)/B
GO TO 76
77 RN(2)=(C-COC/COA)/(-COB/COA+B)
DN(2)=(D+PR/COA*USI/(UC*SQRT(CF/2.)))/(-COB/COA+B)
76 IF (BL.EQ.1) GO TO 11
IF (FDT.EQ.1) GO TO 90
C CALCULATE TEST PARAMETER
11 TEST=DN(J)/(1.+RN(J))
IF (ABS(TEST).GT.(5.E-03*T(1))) GO TO 70
T(J)=TEST
I=J
GO TO 78
90 IF (J.LT.JC.OR.J.LT.JCT) GO TO 70
T(J)=(DN(J-1)*(1.+C)-D)/((1.+C)*RN(J-1)-B)
I=J
C BACK SUBSTITUTION TO OBTAIN TEMPERATURE PROFILE
78 I=I-1
T(I)=DN(I)-RN(I)*T(I+1)
IF (I-2) 79,79,78
79 IF (CASE.EQ.1) GO TO 80
T(1)=1.0
DTBYP=T(1)*(-(YP2+YP3)/(YP2*YP3))+T(2)*(YP3/(YP2*(YP3-YP2
1))) - T(3)*YP2/(YP3*(YP3-YP2))
C CALCULATE STANTON NUMBER-CONSTANT WALL TEMP. BOUNDARY CONDITION
ST=-DTBYP*SQRT(CF/2.)/PR
GO TO 81
80 T(1)=(-PR*USI/(UC*SQRT(CF/2.))-COB*T(2)-COC*T(3))/COA
C CALCULATE STANTON NUMBER-CONSTANT WALL HEAT FLUX BOUNDARY CONDITION
ST=1./T(1)*USI/UC
IF (BL.EQ.1) GO TO 81
STB=ST*LD/(LID*USI/UC-2.*X*ST)
900 FORMAT (1H ,10E11.4)
830 FORMAT (1H ,2E11.4)
81 QT=J
DO 83 I=1,J
83 NUBP(I)=NU(I)
DO 82 I=J+1,N
82 T(I)=0.0
RETURN
555 YL(J)=YL(J-1)+HY*K
IF (BL.EQ.1) GO TO 556
IF (FDT.EQ.1) GO TO 556
YDT=NUL*YL(J)/(K*US)
IF ((LD-2.*YDT).LT.0.0) GO TO 60
GO TO 556
60 WRITE (2,100)
FDT=1
JCT=J
GO TO 556
END

```

```

SUBROUTINE ENERGY(PG)
REAL NU,K,INCR,INCY,NUL,KM,NTH,NUO,K1,KL,NUBP,LD,LID
INTEGER FD,SOLVE,BL,CASE,QT,TAPE,FDT
DIMENSION RN(100),DN(100),PROD(100),ADV(100),DISS(100),
1VDIFF(100),SHEAR(100),ERROR(100),TDIFF(100),YPLU(100)
COMMON K,AS,IND,PR,KM,ASM,H,RTHE2,CFL,INCY,Z(100),Q(100),
1 QP(100),TAU(100),K1,NUO,OUT,INCR,CF,R,US,X,NEQ,NL,
2 J,CASE,ST,USI,YL(100),T(100),U(100),NU(100),BDS,ML,
3 DNU(100),GAMA,ADIS,QT,DY,M,DR,RT(100),TAPE
4 ,TAUW,DSTAR,THSTAR,UC,PD,STB,LD,HY2,HY,DZ,PRT,THETA,BL
5 ,CL,TH,KL,Y,YD(100),YPL(100),NTH,JUMP,NUL,N,YS,YLS
6 ,RDEL1,RDEL2,RTHE1,ALPHA,AMU,YP2,YP3,NUBP(100),ADU,BDU
7 ,FD,RDN,LID,R1,JC,YDC,YDM,ZP(100),MARK,FDT,R1I,XI,UM,RD
C SET UP SIZE OF NEAR WALL REGION
MA=10
SOLVE=0
DO 310 I=1,M
310 QP(I)=Q(I)
J=1
HY=DY
HY2=DY
51 J=J+1
HY=HY2
HY2=HY*INCY
IF (BL.EQ.1) GO TO 48
IF (J.EQ.JC) HY2=HY
48 DZ=(HY**2*(Z(J+1))+(HY2**2-HY**2)*Z(J)-HY2**2*Z(J-1))/
1(HY*HY2*(HY+HY2))
IF (SOLVE.EQ.1) GO TO 30
C CALCULATE TURBULENT KINETIC ENERGY IN NEAR WALL REGION
R1=AMU*YL(J)/(K*US)
EN=1.-EXP(-YL(J)*SQRT(CF/2.)/(K*AS))
EM=YL(J)**2/2.*DZ*EN**2
P1=YL(J)*K*US*EN**2*DZ/(2.*ALPHA)
IF (J.EQ.2) XN=0.005
IF (J.EQ.2) GO TO 42
43 XN=XNW
42 XNW=XN-(XN*(1.-EXP(-R1*XN))-P1)/(1.-EXP(-R1*XN
1)+XN*R1*EXP(-R1*XN))
IF (ABS(XNW-XN).GT.0.01*XN) GO TO 43
Q(J)=(XNW/US)**2
RT(J)=YL(J)*XNW/(US*K)
IF (J.EQ.MA) SOLVE=1
GO TO 51
C SOLVE TRIDIAGONAL MATRIX FOR TURBULENT KINETIC ENERGY EQUATION
30 C=BDS*SQRT(Z(J))*DNU(J)+BDS*(NU(J)-1.)*DZ/(2.*SQRT(Z(J)))+DZ
1/(2.*SQRT(Z(J)))
D=BDS*(NU(J)-1.)*SQRT(Z(J))+SQRT(Z(J))
IF (RT(J).EQ.0.0) GO TO 60
E=(NU(J)-1.)*DZ**2/(4.*SQRT(Z(J)))-K*GAMA*SQRT(Q(J)**3)/(SQRT
1(Z(J))*YL(J)*(1.-EXP(-ADIS*RT(J))))
61 CH=C*HY2**2-2.*D*HY2
IF (BL.EQ.1) GO TO 32
IF (FD.EQ.1) GO TO 54
32 AI=HY*HY2*(HY+HY2)/(DR*CH)+PG*HY*HY2*(HY+HY2)/CH-C*(
1HY2**2-HY**2)/CH+2.*D*(HY+HY2)/CH
55 BI=(-C*HY**2-2.*D*HY)/CH
CI=Q(J)*HY*HY2*(HY+HY2)/(DR*CH)+E*HY*(HY+HY2)*HY2/CH
IF (J.EQ.MA+1) GO TO 49
RN(J)=BI/(AI-RN(J-1))
DN(J)=(CI-DN(J-1))/(AI-RN(J-1))

```

```

50 IF (BL.EQ.1) GO TO 31
   IF (FD.EQ.1) GO TO 20
31 TEST=DN(J)/(1.+RN(J))
   IF (J.LT.M) GO TO 51
   Q(J)=ABS(TEST)
   RT(J)=SQRT(Q(J))*YL(J)/K
   I=J
   GO TO 52
20 IF (J.LT.JC) GO TO 51
C  CALCULATE CENTRE-LINE VALUE OF T.K.E. FOR INTERNAL FLOWS
   Q(J)=(DN(J-1)*(1.+BI)-CI)/((1.+BI)*RN(J-1)-AI)
   Q(J)=ABS(Q(J))
   RT(J)=SQRT(Q(J))*YL(J)/K
   I=J
52 I=I-1
   Q(I)=DN(I)-RN(I)*Q(I+1)
   IF (Q(I).LT.0.0) GO TO 633
634 RT(I)=SQRT(Q(I))*YL(I)/K
   IF (I-(MA+1)).53,53,52
53 Q(I)=0.0
   RT(I)=0.0
503 FORMAT (1H ,10E11.4)
   SUM=0.0
   DO 70 I=2,J
70 SUM=SUM+(Q(I)+Q(I-1))/2.*(YL(I)-YL(I-1))
   NUO=1.+K1*SUM/K
   RETURN
54 AI=HY*HY2*(HY+HY2)/(DR*CH)-C*(HY2**2-HY**2)/CH+2.*D*(HY+HY2)/CH
   GO TO 55
633 Q(I)=ABS(Q(I))
   WRITE (2,255)
255 FORMAT (1H ,15HNEGATIVE ENERGY)
   GO TO 634
49 DN(MA+1)=(CI-Q(MA))/AI
   RN(MA+1)=BI/AI
   GO TO 50
60 E=(NU(J)-1.)*DZ**2/(4.*SQRT(Z(J)))
   GO TO 61
   END

```

```

SUBROUTINE DAO1A(YY,E,A,B,C,D,NO,XO,DX)
CA RUNGE-KUTTA-MERSON (5 ENTRIES TO DYBDX) WITH EST. TRUNC. ERR. E(I)
CCALLS S/R DYBDX(Y,F,N,X) TO SET UP F(J)=FUNC(Y(I),X), I,J=1,N
C FEB. 1963MCVICAR HARWELL
DIMENSION YY(2),E(2),A(2),B(2),C(2),D(2)
N=NO
Z=XO
H=DX/3.
DO 1 I=1,N
D(I)=YY(I)
1 CONTINUE
X=Z
DO 41 J=1,5
CALL DYBDX(YY,E,N,X)
DO 21 I=1,N
GO TO (11,12,13,14,15),J
11 A(I)=H*E(I)
YY(I)=D(I)+A(I)
GO TO 21
12 B(I)=H*E(I)
YY(I)=D(I)+(A(I)+B(I))*0.5
GO TO 21
13 B(I)=H*E(I)
YY(I)=D(I)+(A(I)+B(I)*3.)*0.375
GO TO 21
14 C(I)=H*E(I)
YY(I)=D(I)+(A(I)-B(I)*3.+C(I)*4.)*1.5
GO TO 21
15 Z =D(I)
D(I)=H*E(I)
YY(I)=Z+(A(I)+C(I)*4.+D(I))*0.5
E(I)=(A(I)*2.-B(I)*9.+C(I)*8.-D(I))/10.
21 CONTINUE
GO TO (31,41,33,34,41),J
31 X=Z+H
GO TO 41
33 X=Z+DX*0.5
GO TO 41
34 X=Z+DX
41 CONTINUE
XO=X
RETURN
END

```



```

SUBROUTINE DYBDX(YY,F,N,X)
  REAL K,KM
  DIMENSION YY(2),F(2)
  COMMON K,AS,IND,PR,KM,ASM
  IF (IND.EQ.1) GO TO 2
  F(1)=YY(2)
C  VAN-DRIEST EXPRESSION FOR INITIAL VELOCITY PROFILE GENERATION
  F(2)=2./(1.+SQRT(1.+4.*K**2*X**2*(1.-EXP(-X/AS))**2))
  GO TO 1
  2 F(1)=YY(2)
C  EQUIVALENT VAN-DRIEST EXPRESSION FOR TEMP. PROFILE GENERATION
  F(2)=2.*PR/(1.+SQRT(1.+4.*KM**2*X**2*PR**2*(1.-EXP(-X/ASM))**2))
  1 RETURN
  END

```

```

SUBROUTINE OUTPUT(PG)
  REAL K, KM, INCR, INCY, NU, NUC, LD, NUO, KL, NTH, NUL, NUBP, K1, LID
  INTEGER CASE, PL, QT, TAPE, BL, FD, FDT
  DIMENSION TH1Y(100), TDIFF(100), VDIFF(100), ADV(100), PROD(100),
  1 DISS(100)
  COMMON K, AS, IND, PR, KM, ASM, H, RTHE2, CFL, INCY, Z(100), Q(100),
  1 QP(100), TAU(100), K1, NUO, OUT, INCR, CF, R, US, X, NEQ, NL,
  2 J, CASE, ST, USI, YL(100), T(100), U(100), NU(100), BDS, ML,
  3 DNU(100), GAMA, ADIS, QT, DY, M, DR, RT(100), TAPE,
  4 TAUW, DSTAR, THSTAR, UC, PD, STB, LD, HY2, HY, DZ, PRT, THETA, BL
  5, CL, TH, KL, Y, YD(100), YPL(100), NTH, JUMP, NUL
100 FORMAT (1H0, 3HCF=, E11.4, 5X, 2HR=, E11.4, 5X, 3HUS=, E11.4, 5X, 2HX=, E11.4,
  1)
101 FORMAT (1H+, 75X, 3HST=, E11.4)
102 FORMAT (1H , 23HYPLUS UPLUS)
103 FORMAT (1H+, 33X, 5HTPLUS, 10X, 5HSHEAR, 9X, 6HYBYC.T, 10X, 4HTEMP
  1, 10X, 7HDEF.VEL, 10X, 11HYBYDEF.DIS)
104 FORMAT (1H , E11.4, 6X, E11.4)
105 FORMAT (1H+, 30X, E11.4, 4X, E11.4, 4X, E11.4, 4X, E11.4, 4X, E11.4,
  14X, E11.4)
106 FORMAT (1H , 2HH=, E11.4, 5X, 7HRTHETA=, E11.4, 5X, 8HCF(MOM)=, E11.4)
107 FORMAT (1H0, 4HPROD, 13X, 6HT.DIFF, 9X, 6HV.DIFF, 9X, 4HDISS, 11X, 5HT.K.E,
  111X, 7HED.VISC, 10X, 4HU/US, 9X, 5HY(FT))
108 FORMAT (1H , E11.4, 4X, E11.4, 4X, E11.4, 4X, E11.4, 4X, E11.4, 4X, E11
  1.4, 4X, E11.4, 4X, E11.4)
114 FORMAT (1H , 11HWALL SHEAR=, E11.4, 5X, 24HDISPLACEMENT THICKNESS= ,
  1E11.4, 5X, 15HMOM.THICKNESS= , E11.4)
115 FORMAT (1H , 22HCENTRE-LINE VELOCITY= , E10.3, 5X, 27HFULLY-DEVELOPED
  1CRITERION= , E10.3, 5X, 10HST(BULK)= , E10.3, 5X, 6HX/2L= , E10.3)
  IF (BL.EQ.1) GO TO 20
  XD=X/(2.*LD)
20 WRITE (2,100) CF,R,US,X
  OUT=OUT*INCR
  IF (NEQ.EQ.1) GO TO 82
  WRITE (2,101) ST
  WRITE (2,106) H,RTHE2,CFL
  WRITE (2,114) TAUW,DSTAR,THSTAR
  IF (BL.EQ.1) GO TO 82
  WRITE (2,115) UC,PD,STB,XD
82 PL=PL+1
C CONTROL ON PROFILE PRINT OUT
  IF (PL.LT.5) GO TO 84
  WRITE (2,102)
  WRITE (2,103)
60 HY=DY
  HY2=DY
  IF (ML.EQ.1) GO TO 61
  DO 315 I=2,J
  HY=HY2
  HY2=HY*INCY
C CALCULATION AND PRINT OUT OF PROFILES OF TURBULENT KINETIC
C ENERGY AND ASSOCIATED TRANSPORT PROPERTIES
313 DZ=(HY**2*(Z(I+1))+(HY2**2-HY**2)*Z(I)-HY2**2*(Z(I-1)))/
  1(HY*HY2*(HY+HY2))
  DQ=(HY**2*(Q(I+1))+(HY2**2-HY**2)*Q(I)-HY2**2*(Q(I-1)))/
  1(HY*HY2*(HY+HY2))
  D2Q=2.*(HY*Q(I+1)-(HY+HY2)*Q(I)+HY2*Q(I-1))/(HY*HY2*(HY+HY2))
  ADV(I)=-((Q(I)-QP(I))/DR-PG*Q(I)
  PROD(I)=(NU(I)-1.)*DZ**2/(4.*SQRT(Z(I)))
  TDIFF(I)=BDS*SQRT(Z(I))*DNU(I)*DQ+BDS*(NU(I)-1.)*DQ*DZ/(2.*SQRT(
  1Z(I)))+BDS*(NU(I)-1.)*SQRT(Z(I))*D2Q

```

```

VDIFF(I)=DZ*DQ/(2.*SQRT(Z(I)))+D2Q*SQRT(Z(I))
IF (RT(I).EQ.0.0) GO TO 316
DISS(I)=-K*GAMA*SQRT(Q(I)**3)/(SQRT(Z(I))*YL(I)*(1.-EXP(-ADIS
I*RT(I))))
315 CONTINUE
61 IF (CASE.EQ.1) GO TO 91
93 CT=0.0
DO 2 I=1,QT
2 CT=CT+(T(I)+T(I+1))*(YL(I+1)-YL(I))/2.
THI=0.0
THIY(I)=(1.-SQRT(CF/2.))*(2.*SQRT(DY/CF)-DY+1.)
DO 3 I=2,M
THIY(I)=U(I)*(1.-SQRT(CF/2.))
3 THI=THI+(THIY(I)+THIY(I-1))*(YL(I)-YL(I-1))/2.
DO 88 I=2,J
YPLUSC=YL(I)*SQRT(CF/2.)*UC/(US*K)
UPLUSC=1./(U(I)*SQRT(CF/2.))*US/UC
WRITE (2,104) YPLUSC,UPLUSC
DEF=1./SQRT(CF/2.)-UPLUSC
YBCT=YL(I)/CT
TEMP=1.-T(I)
IF (CASE.EQ.1) T(I)=T(I)*USI/(US*ST)
SHEAR=TAU(I)
YBTHI=YL(I)/THI
IF (NEQ.EQ.1) GO TO 88
IF (CASE.EQ.1) GO TO 89
TPLUSC=(1.-T(I))*SQRT(CF/2.)/ST
GO TO 95
89 TPLUSC=(1.-T(I)*UC*ST/USI)*SQRT(CF/2.)/ST
95 WRITE (2,105) TPLUSC,SHEAR,YBCT,TEMP,DEF,YBTHI
88 CONTINUE
IF (ML.EQ.1) GO TO 62
WRITE (2,107)
DO 90 I=2,J
PRODC=PROD(I)
TDIFFC=TDIFF(I)
VDIFFC=VDIFF(I)
DISSC=DISS(I)
QC=Q(I)
NUC=NU(I)
RTC=SQRT(Z(I))
ADVC=YL(I)*NUL/(K*US)
WRITE (2,108) PRODC,TDIFFC,VDIFFC,DISSC,QC,NUC,RTC,ADVC
90 CONTINUE
62 PL=0
84 RETURN
91 DO 92 I=1,J
92 T(I)=T(I)*ST*US/USI
GO TO 93
316 DISS(I)=0.0
GO TO 315
END

```

```

SUBROUTINE PRGRAD(PG,NUL,AP,BP,R,RDEL2,RDEL1,US,DR,LD,LID,USI,
(BDU,BL)
  (REAL NUL,LD,LID
  INTEGER BL
  IF (BL.EQ.1) GO TO 21
  IF (FD.EQ.1) GO TO 1
C  CALCULATE PRESSURE GRADIENT PARAMETER FOR INTERNAL FLOWS BEFORE
C  INTERFERENCE
  AA=4.*NUL*(RDEL2-RDEL1)/(US*DR*LD)
  BB=2.*NUL*BDU/(US*LD)
  PG=AA-BB
  1 PG=PG
  GO TO 20
C  PRESCRIPTION OF PRESSURE GRADIENT PARAMETER AS A FUNCTION OF R FOR
C  EXTERNAL BOUNDARY LAYER FLOWS
  21 IF (R.LT.8.887E+05) GO TO 15
  IF (R.LT.1.152E+06) GO TO 2
  IF (R.LT.1.296E+06) GO TO 4
  IF (R.LT.1.350E+06) GO TO 10
  IF (R.LT.1.440E+06) GO TO 9
  IF (R.LT.1.536E+06) GO TO 6
  IF (R.LT.1.728E+06) GO TO 3
  IF (R.LT.1.872E+06) GO TO 11
  IF (R.LT.2.060E+06) GO TO 12
  IF (R.LT.2.260E+06) GO TO 13
  IF (R.LT.2.682E+06) GO TO 7
  PG=-125.41E-08
  8 PG=AP+BP*R
  20 RETURN
  15 AP=-65.0E-08
  BP=0.0
  GO TO 8
  13 AP=100.0E-08
  BP=0.0
  GO TO 8
  2 BP=24.781E-13
  AP=-28.548E-07
  GO TO 8
  3 AP=450.0E-08
  BP=0.0
  GO TO 8
  7 AP=-100.0E-08
  BP=0.0
  GO TO 8
  4 AP=50.0E-08
  BP=0.0
  GO TO 8
  6 AP=600.0E-08
  BP=0.0
  GO TO 8
  10 AP=100.0E-08
  BP=0.0
  GO TO 8
  9 AP=250.0E-08
  BP=0.0
  GO TO 8
  11 AP=370.0E-08
  BP=0.0
  GO TO 8
  12 AP=200.0E-08
  BP=0.0
  GO TO 8
  END

```

```

SUBROUTINE USTRM(US,PG,AP,BP,DR,X,NUL,XI,R,USI,LID,LD,RDEL1
1,ADU,BDU,R11,FD,MARK,YDC,UM,RD,ERROR,BL)
  REAL NUL,LID,LD
  INTEGER BL,FD
  IF (BL.EQ.1) GO TO 5
  IF (FD.EQ.1) US=UM
5 US1=US
  IF (BL.EQ.1) GO TO 3
  IF (FD.EQ.1) GO TO 2
  IF (R.LT.(R11+1000.)) GO TO 1
C  CALCULATE CENTRE-LINE VELOCITY VARIATION FOR INTERNAL
C  FLOWS BEFORE INTERFERENCE
  US=USI*LID/LD+2.*NUL*RDEL1/LD
  IF (BL.EQ.0) GO TO 2
C  CALCULATE FREE STREAM VELOCITY VARIATION FOR EXTERNAL BOUNDARY L/
3 US=US*EXP(AP/2.*DR+BP/4.*DR*(2.*R-DR))
  GO TO 2
1 US=USI
2 X=XI+NUL*DR*2./(US1+US)
  XI=X
  IF (BL.EQ.1) GO TO 4
  LD=ADU+BDU*X
  YDC=LD/2.+ERROR
  UM=US
  RD=LD*UM/NUL
4 RETURN
  END

```

TYPICAL INPUT DATA

```

2 1 0 0.419 1 0
1.000 1000. 1.0 100 2 6.500E+06 5.000E+05 1.1
0.71 0.9 0.018 1.670E-04 0.410 26.0
0.200 0.016 0.670 0.416 0.263 1.15 0.1667 0.0
4.632E+05 50.00 3.937E-03 0.410 26.0 7.0 1.023000.
3.465E-03 0.6 26.0 5.6

```

Appendix 6

Transient combined natural and forced convection program (Language - Fortran 4)

The following section lists the important variables in the program. The definitions should be related to the appropriate nomenclature, i.e. section 2.3.

| <u>Program</u> <u>Symbol</u> | <u>Meaning</u> |
|---|--|
| C1, C2X, C2Y, C3, C4, C5, C6, C7, CFS | Groups which remain constant for a particular case. |
| CVS | Contour values for stream function ψ_n . |
| CVT | Contour values for temperature θ . |
| ERS, ERT, ERW | Convergence criteria for stream function, temperature and vorticity respectively. |
| GR | Grashof number Gr |
| HT | Dimensionless time step $\Delta t' (= \frac{\ell}{U} \cdot \Delta t)$. |
| HX, HY | Step lengths in x and y directions respectively. |
| ITMX | Maximum allowable number of iterations. |
| KOPY | "KOPY" = 0 for no hard copy of contour plot. = 1 for a hard copy of contour plot. |
| M | Number of mesh spaces in x direction. |
| N | Number of mesh spaces in y direction. |
| NCVS, NCVT | Number of contour values of stream function and temperature respectively. |
| PR | Prandtl number, Pr. |
| RE | Reynolds number, Re. |
| RFS, RFT, RFW | Relaxation factors for stream function, temperature and vorticity respectively. |
| RSMX, RTMX, RWMX | Maximum residuals at each iteration for stream function, temperature and vorticity respectively. |
| S | Dimensionless stream function ψ_n . |
| SMX | Maximum value of stream function ψ_m . |

| <u>Program Symbol</u> | <u>Meaning</u> |
|---------------------------|---------------------------------------|
| T | Dimensionless temperature θ . |
| TIM | Dimensionless time t' . |
| TL | Temperature at previous step in time. |
| W | Dimensionless vorticity ω . |
| WL | Vorticity at previous step in time. |
| YMX | Maximum value of y' . |

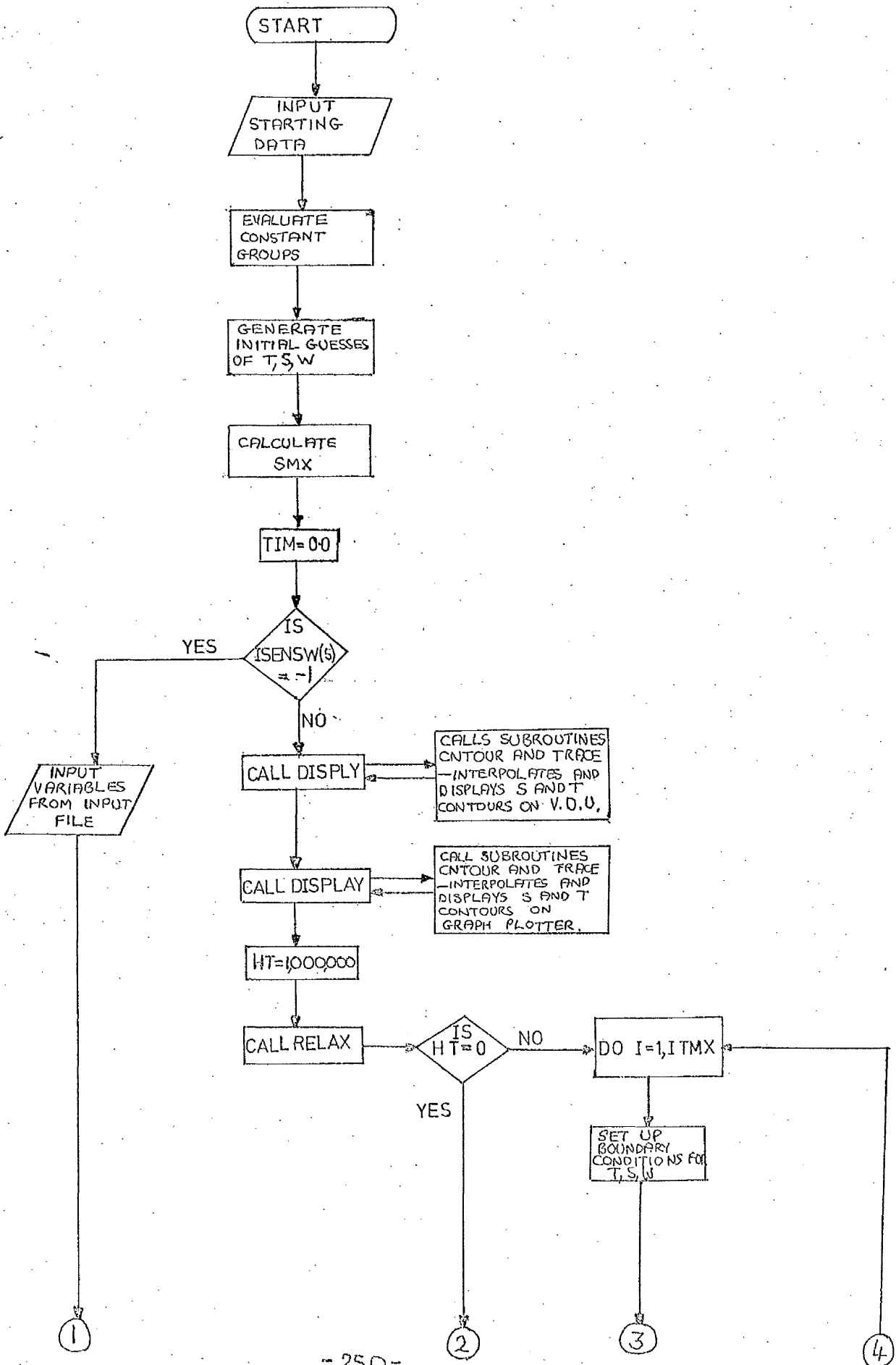
Operation Notes

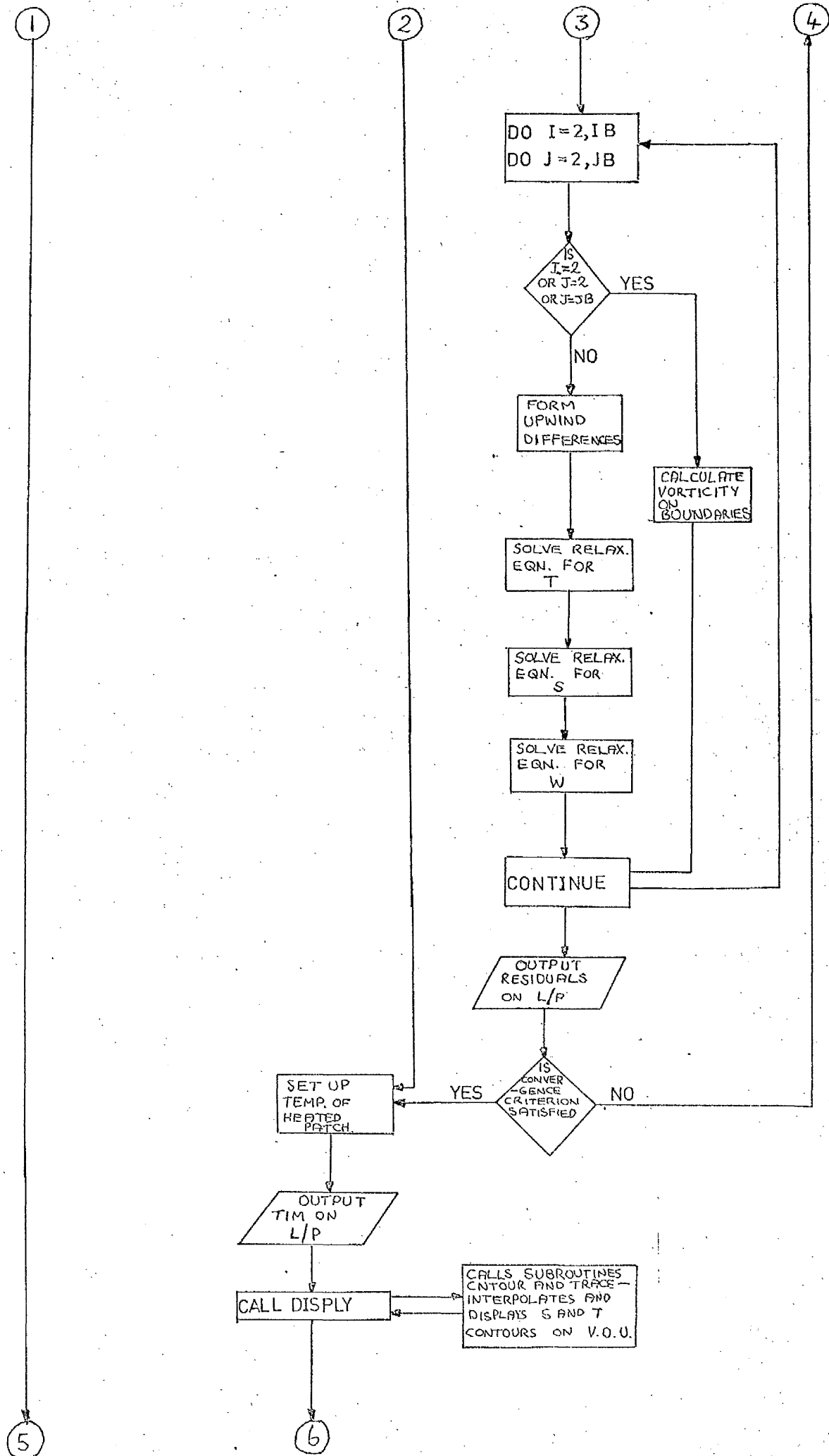
1. It should be noted that this program has been written specifically for the Department's PDP 15/40 computer, and consequently contains a number of machine instructions which make use of the available peripherals.
2. For convergence criteria of 0.1% for temperature, stream-function and vorticity, each iteration took 2 secs. The following table shows the number of iterations performed for each step in time to produce the result of fig. 59(b). It can be seen from the table that, in order to obtain the results of fig. 59(b), it requires 1531 iterations, taking a total run time of approximately 3060 secs.

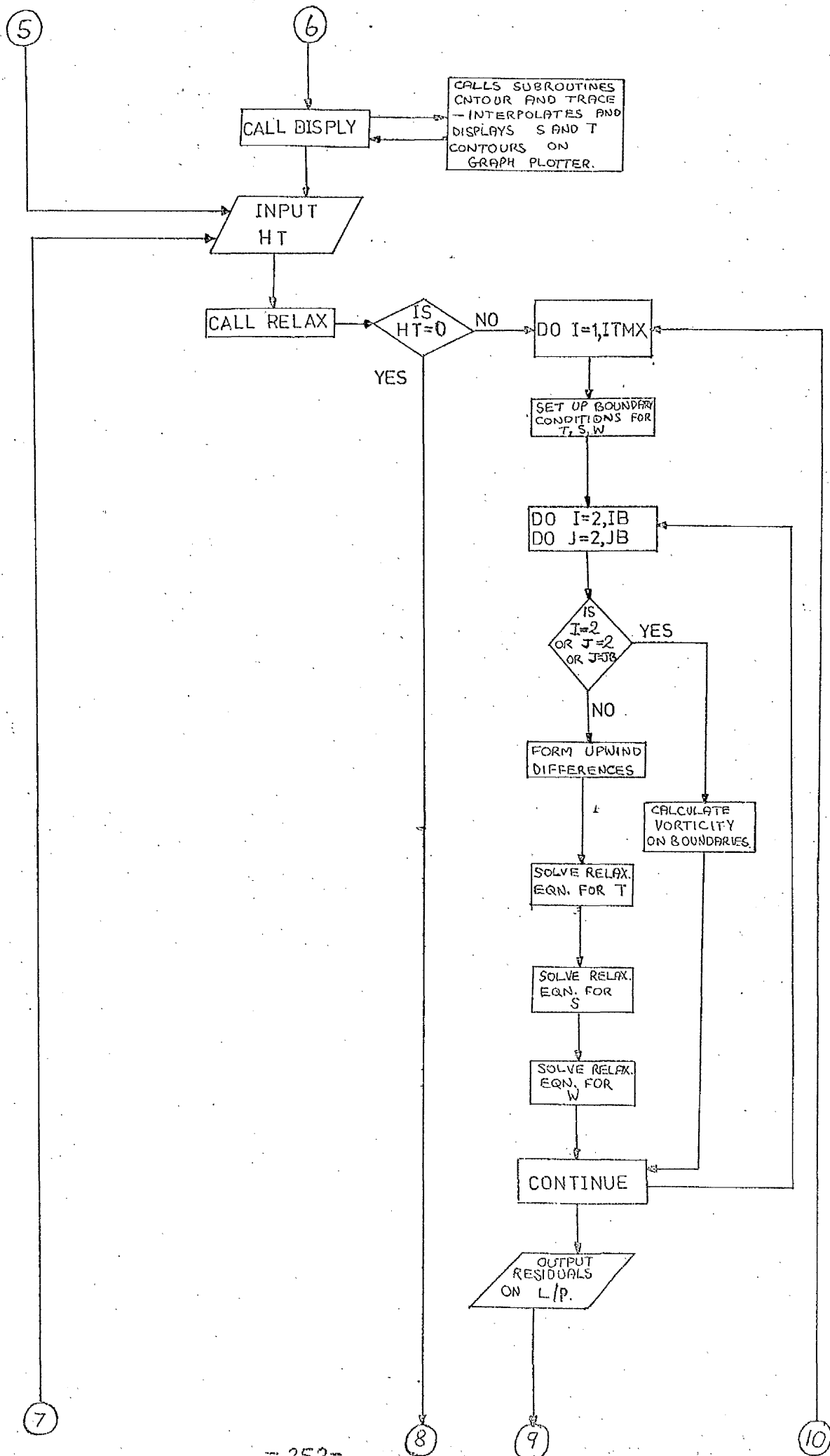
| Is current situation shown on fig. 5.9(b) | Dimensionless time $\frac{Ut}{l}$ | No. of itns. from previous time step | Total no. of itns. to current stage |
|---|---|---|--|
| ✓ | 0.2 | 21 | 21 |
| | 0.4 | 31 | 52 |
| ✓ | 0.6 | 38 | 90 |
| | 0.8 | 35 | 125 |
| ✓ | 1.0 | 37 | 162 |
| | 1.3 | 43 | 205 |
| ✓ | 1.6 | 44 | 249 |
| | 2.0 | 40 | 289 |
| | 2.5 | 36 | 325 |
| | 3.0 | 37 | 362 |
| ✓ | 3.5 | 37 | 399 |
| | 4.0 | 35 | 434 |
| | 4.5 | 34 | 468 |
| | 5.0 | 40 | 508 |
| ✓ | 5.5 | 41 | 549 |
| | 6.0 | 42 | 591 |
| | 6.5 | 38 | 629 |
| | 7.0 | 38 | 667 |
| ✓ | 7.5 | 40 | 707 |
| | 8.0 | 39 | 746 |
| ✓ | 8.5 | 36 | 782 |
| | 9.0 | 36 | 818 |
| ✓ | 9.5 | 34 | 852 |
| | 10.0 | 31 | 883 |
| ✓ | 10.5 | 29 | 912 |
| | 11.0 | 27 | 939 |
| ✓ | 11.5 | 27 | 966 |
| | 12.0 | 25 | 991 |
| ✓ | 12.5 | 24 | 1015 |
| | 13.0 | 24 | 1039 |
| ✓ | 13.5 | 23 | 1062 |
| | 13.75 | 5 | 1067 |
| ✓ | 14.0 | 4 | 1071 |
| ✓ | 14.25 | 15 | 1086 |
| | 14.35 | 3 | 1089 |
| | 14.5 | 3 | 1092 |
| | 14.75 | 4 | 1096 |
| ✓ | 15.0 | 4 | 1100 |
| | 15.1 | 3 | 1103 |
| ✓ | 15.2 | 3 | 1106 |
| | 15.25 | 2 | 1108 |
| | 15.3 | 2 | 1110 |
| ✓ | 15.4 | 3 | 1113 |
| | 15.5 | 3 | 1116 |
| | 15.6 | 3 | 1119 |
| | 15.8 | 3 | 1122 |
| ✓ | 16.0 | 17 | 1139 |
| | 16.2 | 5 | 1144 |
| ✓ | 16.4 | 5 | 1149 |
| ✓ | 16.6 | 16 | 1165 |
| | 16.8 | 5 | 1170 |
| ✓ | 17.0 | 15 | 1185 |
| | 17.2 | 5 | 1190 |

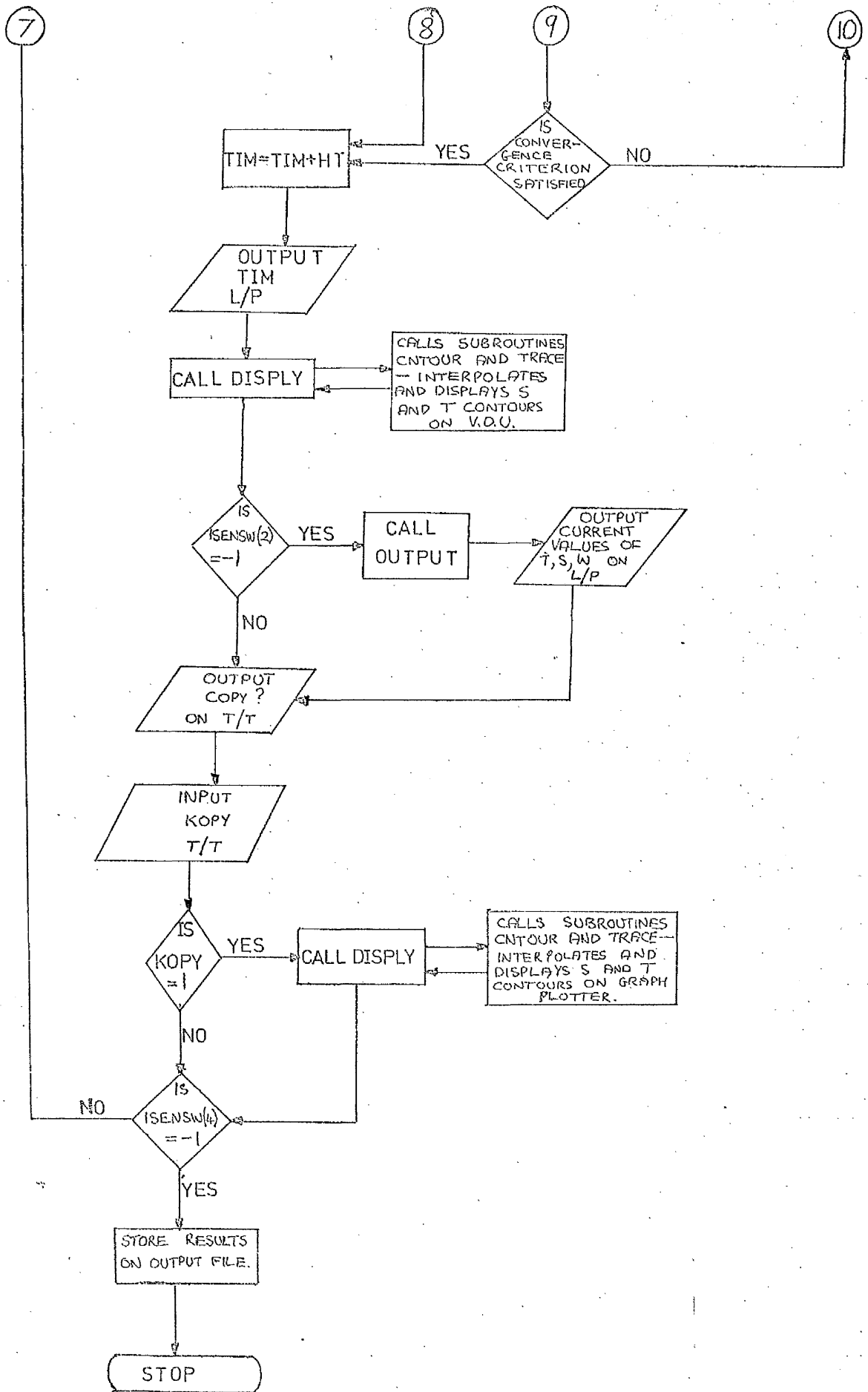
| Is current situation shown on fig. 5.9(b) | Dimensionless time $\frac{Ut}{l}$ | No. of itns. from previous time step | Total no. of itns. to current stage |
|---|---|---|--|
| | 17.4 | 15 | 1205 |
| | 17.6 | 6 | 1211 |
| ✓ | 17.8 | 15 | 1226 |
| | 18.0 | 7 | 1233 |
| | 18.2 | 17 | 1250 |
| ✓ | 18.4 | 7 | 1257 |
| | 18.6 | 17 | 1274 |
| | 18.8 | 14 | 1288 |
| ✓ | 19.0 | 15 | 1303 |
| | 19.2 | 17 | 1320 |
| | 19.4 | 16 | 1336 |
| | 19.6 | 17 | 1353 |
| ✓ | 19.8 | 16 | 1369 |
| | 20.0 | 18 | 1387 |
| | 20.2 | 15 | 1402 |
| ✓ | 20.4 | 18 | 1420 |
| | 20.6 | 18 | 1438 |
| | 20.8 | 19 | 1457 |
| | 21.0 | 16 | 1473 |
| ✓ | 21.2 | 21 | 1494 |
| | 21.4 | 21 | 1515 |
| ✓ | 21.6 | 16 | 1531 |

FLOW DIAGRAM OF TRANSIENT COMBINED NATURAL AND FORCED CONVECTION PROGRAM.









TRANSIENT COMBINED NATURAL AND FORCED
CONVECTION PROGRAM

```

C      UNSTEADY CASE TEST
      DIMENSION FILOUT(2),FILIN(2)
      COMMON /SET1/ T(23,23),S(23,23),W(23,23),TL(23,23),WL(23,23)
      COMMON /SET2/ HXSQ,HYSQ,C1,C2X,C2Y,C3,C4,C5,C6,C7,CFS
      COMMON RE,PR,GR,RFS,RFT,RFW,HX,HY,HT,M,N,IMX,IB,JMX,JB,DSF,SM
      COMMON ITMX,ALFA,ERT,ERS,ERW
      COMMON FRX(5),FRY(5),CVS(16),CVT(16),NCVS,NCVT
      READ(1,101)M,N,ITMX
101  FORMAT(3I2)
      READ(1,100) RE,PR,GR
      READ(1,100) RFT,RFS,RFW
      READ(1,100) ERT,ERS,ERW
      READ(1,100) HX,HY,ALFA
100  FORMAT (8F10.0)
      READ(1,101) NCVS
      READ(1,100) (CVS(I),I=1,NCVS)
      READ(1,101) NCVT
      READ(1,100) (CVT(I),I=1,NCVT)
      WRITE(2,210)M,N,ITMX
210  FORMAT(1X,3I5)
      WRITE(2,211)RE,PR,GR
      WRITE(2,211)RFT,RFS,RFW
      WRITE(2,211) ERT,ERS,ERW
      WRITE(2,211)HX,HY,ALFA
211  FORMAT(1X,3E15.6)
      HXSQ=HX*HX
      HYSQ=HY*HY
      C1=SMX/(2.0*HY*HX)
      C2X=GR/(RE*RE*2.0*HX)*COS(ALFA)
      C2Y=GR/(RE*RE*2.0*HY)*SIN(-ALFA)
      C3=1.0/(RE*HYSQ*HXSQ)
      C4=C3*2.0*(HYSQ+HXSQ)
      C5=C3/PR
      C6=C5*2.0*(HYSQ+HXSQ)
      C7=SMX/(HYSQ*HXSQ)
      C8=1.0/HT
      CFS=2.0*(HYSQ+HXSQ)*C7
      IB=M+2
      JB=N+2
      FRX(1)=0.0
      FRY(1)=0.0
      FRX(2)=0.0
      FRY(2)=N
      FRX(3)=M
      FRY(3)=N
      FRX(4)=M
      FRY(4)=0.0
      FRX(5)=0.0
      FRY(5)=0.0
      IMX=IB+1
      JMX=JB+1

C
C      GENERATE INITIAL GUESSES OF T,W AND S
C
      DO 1 I=1,IMX
      DO 1 J=1,JMX
      T(I,J)=0.0
      W(I,J)=0.0
      TL(I,J)=0.0

```



```

      WL(I,J)=0.0
1  CONTINUE
      DSF=1.0/FLOAT(N)
      SF=0.0
      DO 3 J=2,JB
      DO 4 I=2,IB
      S(I,J)=SF
4  CONTINUE
      SF=SF+DSF
3  CONTINUE
      YMX=HY*FLOAT(N)
      SMX=YMX
      TIM=0.0
      IF(ISENSW(5).EQ.-1) GOTO 9
      CALL DISPLY(T,S,TIM,8)
      CALL DISPLY(T,S,TIM,9)
      HT=1000000.0

C
C      CALL SUBROUTINE RELAX TO OBTAIN INITIAL STEADY STATE SOLUTION
C      WITH NO HEATING. THIS SOLUTION THEN FORMS THE STARTING
C      CONDITIONS FOR THE TIME DEPENDENT PROCEDURE.
C

      CALL RELAX(T,S,W,TL,WL)
      DO 2 I=6,8
      T(I,2)=1.0
2  CONTINUE
      WRITE(2,212) TIM
212  FORMAT(/8H TIME = F10.2/)
      CALL DISPLY(T,S,TIM,8)
      CALL DISPLY(T,S,TIM,9)
      GOTO 8
9  WRITE(4,404)
404  FORMAT(13H INPUT FILE ?)
      READ(4,405) FILIN
405  FORMAT (A5,A4)
      CALL SEEK(7,FILIN)
      READ(7) TIM,T,S,W
      CALL CLOSE(7)

C
C      STORE VALUES OF T AND W AT PREVIOUS TIME STEP
C

8  DO 6 I=1,IMX
      DO 6 J=1,JMX
      TL(I,J)=T(I,J)
      WL(I,J)=W(I,J)
6  CONTINUE
      WRITE(4,400)
400  FORMAT (4H HT?)
      READ(4,100) HT
      CALL RELAX(T,S,W,TL,WL)
      TIM=TIM+HT
      WRITE(2,212) TIM
      CALL DISPLY(T,S,TIM,8)
      IF(ISENSW(2).EQ.-1) CALL OUTPUT(S,3)
      WRITE(4,401)
401  FORMAT(6H COPY?)
      READ(4,402) KOPY
402  FORMAT(I1)
      IF(KOPY.EQ.1) CALL DISPLY(T,S,TIM,9)
      IF(ISENSW(4).EQ.-1) GOTO 7

```

```
GOTO 8
7 WRITE(4,406)
406 FORMAT (14H OUTPUT FILE ?)
READ(4,405) FILOUT
CALL ENTER(7,FILOUT)
WRITE(7) TIM,T,S,W
CALL CLOSE(7)
STOP
END
```

```

SUBROUTINE RELAX(T,S,W,TL,WL)
DIMENSION T(1,1),S(1,1),W(1,1),TL(1,1),WL(1,1)
COMMON /SET2/ HXSQ,HYSQ,C1,C2X,C2Y,C3,C4,C5,C6,C7,CFS
COMMON RE,PR,GR,RFS,RFT,RFW,HX,HY,HT,M,N,IMX,IB,JMX,JB,DSF,SMX
COMMON ITMX,ALFA,ERT,ERS,ERW
IF(HT.EQ.0.0) RETURN
C8=1.0/HT
DO 3 IT=1,ITMX
RTMX=0.0
RSMX=0.0
RWMX=0.0

```

```

C
C SET UP REQUIRED BOUNDARY CONDITIONS FOR S,T AND W
C

```

```

DO 4 I=2,IB
S(I,1)=S(I,3)
S(I,JMX)=S(I,JMX-2)
4 CONTINUE
DO 5 J=2,JB
T(IMX,J)=T(IMX-2,J)
S(1,J)=S(3,J)
S(IMX,J)=2.0*S(IB,J)-S(IMX-2,J)
W(IMX,J)=W(IB-1,J)
5 CONTINUE
DO 1 I=2,IB
DO 1 J=2,JB
IF(I.EQ.2.OR.J.EQ.2.OR.J.EQ.JB) GOTO 2
T0=T(I,J)
S0=S(I,J)
W0=W(I,J)
T1=T(I,J+1)
S1=S(I,J+1)
W1=W(I,J+1)
T2=T(I+1,J)
S2=S(I+1,J)
W2=W(I+1,J)
T3=T(I,J-1)
S3=S(I,J-1)
W3=W(I,J-1)
T4=T(I-1,J)
S4=S(I-1,J)
W4=W(I-1,J)

```

```

C
C FORM UPWIND DIFFERENCES
C

```

```

DSY=S1-S3
IF(DSY) 100,100,101
100 TIS=T2
WIS=W2
GOTO 102
101 TIS=T4
WIS=W4
102 DSY=ABS(DSY)
DSX=S4-S2
IF(DSX) 103,103,104
103 TJS=T1
WJS=W1
GOTO 105
104 TJS=T3
WJS=W3

```

```

105 DSX=ABS(DSX)
    GOTO 17
C
C   SOLVE RELAXATION EQUATION FOR TEMPERATURE
C
    CFT=C1*(DSY+DSX)+C6+C8
    RT=TO-(C8*TL(I,J)+C1*(DSY*TIS+DSX*TJS)
1+C5*(HYSQ*(T2+T4)+HXSQ*(T1+T3)))/CFT
    T(I,J)=TO-RFT*RT
    RTMX=AMAX1(RTMX,ABS(RT))
17 CONTINUE
C
C   SOLVE RELAXATION EQUATION FOR STREAM FUNCTION
C
    RS=SO-(W0+C7*(HYSQ*(S2+S4)+HXSQ*(S1+S3)))/CF5
    S(I,J)=SO-RFS*RS
    RSMX=AMAX1(RSMX,ABS(RS))
C
C   SOLVE RELAXATION EQUATION FOR VORTICITY
C
    CFW=C1*(DSY+DSX)+C4+C8
    RW=W0-(C8*WL(I,J)+C1*(DSY*WIS+DSX*WJS)+C2X*(T2-T4)+C2Y*(T1-T3)
1+C3*(HYSQ*(W2+W4)+HXSQ*(W1+W3)))/CFW
    W(I,J)=W0-RFW*RW
    RWMX=AMAX1(RWMX,ABS(RW))
    GOTO 1
C
C   CALCULATE VORTICITY DIRECTLY ON BOUNDARIES. THIS EQUATION MAY
C   ONLY BE USED WHEN THE STREAM FUNCTION IS EXPLICITLY KNOWN
C   ON THE PARTICULAR BOUNDARY.
C
    2 W(I,J)=-C7*(HYSQ*(S(I+1,J)+S(I-1,J))+HXSQ*(S(I,J+1)+S(I,J-1))
    1-2.0*(HYSQ+HXSQ)*S(I,J))
    1 CONTINUE
    WRITE(2,200) IT,RTMX,RSMX,RWMX
200 FORMAT(1X,I5,3(5X,E13.6))
C
C   SUPPLY CONVERGENCE CRITERION
C
    IF(RTMX.LT.ERT.AND.RSMX.LT.ERS.AND.RWMX.LT.ERW) RETURN
3 CONTINUE
    RETURN
    END

```

```

SUBROUTINE OUTPUT (A,NDP)
C THIS ROUTINE ORGANISES THE OUTPUT OF T,S, AND W ARRAYS
C INTO BLOCKS. NECESSARY WHEN THE ARRAYS ARE LARGE.
C PROVIDES A CHOICE OF NO. OF DECIMAL PLACES.
  DIMENSION A(1,1)
  COMMON RE,PR,GR,RFS,RFT,RFW,HX,HY,HT,M,N,IMX,IB,JMX,JB,DSF,SMX
  JF=1
  1 JS=JF+1
    JF=MIN0(JB,JS+20)
    DO 2 I=2,IB
      GOTO (3,4,5),NDP
    3 WRITE(2,220) (A(I,J),J=JS,JF)
220  FORMAT(1X,21F6.1)
      GOTO 2
    4 WRITE(2,221) (A(I,J),J=JS,JF)
221  FORMAT(1X,21F6.2)
      GOTO 2
    5 WRITE(2,222) (A(I,J),J=JS,JF)
222  FORMAT(1X,21F6.3)
    2 CONTINUE
      WRITE(2,223)
223  FORMAT(/)
      IF(JF.NE.JB) GOTO 1
      WRITE(2,224)
224  FORMAT(//)
      RETURN
  END

```

```

SUBROUTINE DISPLY(T,S,TIM,IDV)
C THIS ROUTINE ORGANISES THE DISPLAY OF THE 2 CONTOUR
C DIAGRAMS FOR T AND S. ON THE INCREMENTAL PLOTTER ONLY
C THE S CONTOURS ARE DRAWN.
  DIMENSION T(1,1),S(1,1),A(23,23),BCD(1)
  COMMON RE,PR,GR,RFS,RFT,RFW,HX,HY,HT,M,N,IMX,IB,JMX,JB,DSF,SMX
  COMMON ITMX,ALFA,ERT,ERS,ERW
  COMMON FRX(5),FRY(5),CVS(16),CVT(16),NCVS,NCVT
  DATA BCD/4HTIME/
C CLEAR SCREEN
  CALL PLOTS(IDV)
  IF(IDV.EQ.9) CALL FACTOR(0.5)
C DRAW FRAME
  CALL LINE(FRX,FRY,5,0,0,0,0,1,0,0,0,2,0)
  TP=FLOAT(N)/2.0+0.5
  CALL SYMBOL(0.0,TP,0.5,BCD,0.0,4)
  CALL NUMBER(2.5,TP,0.5,TIM,0.0,2)
  DO 3 I=2,IB
  DO 3 J=2,JB
  A(I-1,J-1)=S(I,J)
3 CONTINUE
  MK=0
  DO 1 I=1,NCVS
  CALL CNTOUR(A,M+1,N+1,CVS(I),MK,1.0,2.0)
1 CONTINUE
  IF(IDV.EQ.9) GOTO 5
C SHIFT ORIGIN
  CALL PLOT(0.0,15.0,-3)
C DRAW FRAME
  CALL LINE(FRX,FRY,5,0,0,0,0,1,0,0,0,2,0)
  DO 4 I=2,IB
  DO 4 J=2,JB
  A(I-1,J-1)=T(I,J)
4 CONTINUE
  MK=0
  DO 2 I=1,NCVT
  CALL CNTOUR(A,M+1,N+1,CVT(I),MK,1.0,2.0)
2 CONTINUE
C RETURN ORIGIN
  CALL PLOT(0.0,-15.0,-3)
C CLEAR BUFFER & RETURN
5 CALL PLOT(0.0,0.0,999)
  RETURN
  END

```

```

SUBROUTINE CNTOUR(AR,M,N,Z,MK,SCX,SCY)
C   THIS ROUTINE SEARCHES FOR STARTING POINTS FOR A PARTICULAR
C   CONTOUR VALUE ASSUMING LINEAR INTERPOLATION.
C   ENTER WITH MK=0 1'ST TIME CALL
C           MK>0 SUBSEQUENT CALLS
C MK=1  NORMAL EXIT
C MK=-1 LN OVERFLOW (20)
C MK=-2 NC OVERFLOW (20)
C MK=-3 NP OVERFLOW (100)
      DIMENSION AR(1,1),LX(20),LY(20),BCD(1)
      COMMON /TRA/I,J,MRX,MD
      IF(MK.GT.0)GOTO 200
C SEARCH FOR MAXIMA,MINIMA & SADDLE POINTS
      LN=0
      NN=N-1
      DO 100 J=2,NN
        MRX=-1
        IF(AR(2,J)-AR(1,J))10,20,30
30      MRX=MRX+1
20      MRX=MRX+1
10      DO 100 I=3,M
        IF(AR(I,J)-AR(I-1,J))50,100,70
50      IF(MRX.LT.0)GOTO 100
        MRX=-1
55      IF(AR(I-1,J).LE.AR(I-1,J-1).AND.AR(I-1,J).LT.AR(I-1,J+1))GOTO 61
        IF(AR(I-1,J).GE.AR(I-1,J-1).AND.AR(I-1,J).GT.AR(I-1,J+1))GOTO 62
        GOTO 100
61      K=-1
        IF(MRX.LT.0)GOTO 64
        K=-7
        GOTO 60
62      K=-1
        IF(MRX.GT.0)GOTO 64
        K=-2
60      LN=LN+1
        IF(LN.GT.20)GOTO 65
        LX(LN)=I-1
        LY(LN)=J
64      X=FLOAT(I-2)
        Y=FLOAT(J-1)
        GOTO 100
65      MK=-1
        RETURN
70      IF(MRX.GT.0)GOTO 100
        MRX=1
        GOTO 55
100      CONTINUE
C CHECK EACH MAXIMUM & MINIMUM FOR POSSIBLE CLOSED CONTOURS
200      IF(LN.LT.1)GOTO 400
        MK=0
        DO 300 K=1,LN
          II=LX(K)+1
          J=LY(K)
          MRX=-1
          IF(AR(II-1,J)-Z)210,220,230
230      MRX=MRX+1
220      MRX=MRX+1
210      DO 300 I=II,M
          IF(AR(I,J)-Z)260,270,280

```

```

260 IF(MRX.LT.0)GOTO 300
    MRX=-1
290 MD=5
    CALL TRACE(AR,M,N,Z,MK,SCX,SCY)
    IF(MK.LT.0)RETURN
    GOTO 300
270 MRX=0
    GOTO 300
280 IF(MRX.GT.0)GOTO 300
    MRX=1
    GOTO 290
300 CONTINUE
C CHECK PERIPHERY FOR OPEN CONTOURS
400 MRX=-1
    MD=0
    MK=0
    IF(AR(1,1)-Z)410,420,430
430 MRX=MRX+1
420 MRX=MRX+1
410 J=1
    JD=0
    I=2
    ID=1
455 MD=MD+1
435 IF(AR(I,J)-Z)440,450,460
440 IF(MRX.LT.0)GOTO 500
    MRX=-1
    CALL TRACE(AR,M,N,Z,MK,SCX,SCY)
    IF(MK.LT.0)RETURN
    GOTO 500
450 MRX=0
    GOTO 500
460 IF(MRX.GT.0)GOTO 500
    MRX=1
500 I=I+ID
    J=J+JD
    GOTO(510,520,530,540),MD
510 IF(I.LE.M)GOTO 435
    I=M
    ID=0
    JD=1
    GOTO 455
520 IF(J.LE.N)GOTO 435
    J=N
    JD=0
    ID=-1
    GOTO 455
530 IF(I.GT.0)GOTO 435
    I=1
    ID=0
    JD=-1
    GOTO 455
540 IF(J.GT.0)GOTO 435
    MK=1
    RETURN
    END

```



```

SUBROUTINE TRACE(AR,M,N,Z,MK,SCX,SCY)
C   GIVEN STARTING POINTS THIS ROUTINE TRACES THE VARIOUS
C   CONTOURS BY LINEAR INTERPOLATION AND A MAZE-SEARCHING
C   TYPE ALGORITHM. THE POINTS WHERE A PARTICULAR CONTOUR
C   INTERSECTS THE MESH GRID ARE PLOTTED CONNECTED BY
C   STRAIGHT LINES ONLY.
C   ENTER WITH:  MK=0 1'ST TIME FOR CLOSED CONTOURS
C                MD=5 CLOSED CONTOUR
C                MD=1,2,3,4 OPEN CONTOUR ON SIDE 'MD'
      DIMENSION AR(1,1),X(100),Y(100),S(20,2)
      COMMON /TRA/II,JJ,MRX,MD
      NP=0
      I=II
      J=JJ
      IF(MK.NE.0)GOTO 5
      MK=1
      NC=0
5    IF(MRX.LT.0)GOTO 10
20   IF(I.EQ.1)GOTO 600
      I=I-1
      IF(AR(I,J).GE.Z)GOTO 20
      GOTO 300
10   GOTO(100,200,300,400,100),MD
100  IF(I.EQ.1)GOTO 600
      IF(AR(I-1,J).LT.Z)GOTO 150
      IF(NP.EQ.100)GOTO 660
      NP=NP+1
      X(NP)=FLOAT(I-2)+(Z-AR(I-1,J))/(AR(I,J)-AR(I-1,J))
      Y(NP)=FLOAT(J-1)
      IF(MD.NE.5)GOTO 400
      NZ=1
80   IF(NC.EQ.0)GOTO 180
      DO 175 K=1,NC
      IF(ABS(S(NC,1)-X(NP)).LT.1E-5.AND.ABS(S(NC,2)-Y(NP)).LT.1E-5)
1    RETURN
175  CONTINUE
180  IF(NP.EQ.1)GOTO 185
      IF(ABS(X(NP)-X(1)).LT.1E-5.AND.ABS(Y(NP)-Y(1)).LT.1E-5)GOTO 630
185  GOTO(400,300,200,100),NZ
400  IF(J.EQ.N)GOTO 600
      IF(AR(I,J+1).LT.Z)GOTO 450
      IF(NP.EQ.100)GOTO 660
      NP=NP+1
      X(NP)=FLOAT(I-1)
      Y(NP)=FLOAT(J-1)+(Z-AR(I,J))/(AR(I,J+1)-AR(I,J))
      IF(MD.NE.5)GOTO 300
      NZ=2
      GOTO 80
300  IF(I.EQ.M)GOTO 600
      IF(AR(I+1,J).LT.Z)GOTO 350
      IF(NP.EQ.100)GOTO 660
      NP=NP+1
      X(NP)=FLOAT(I-1)+(Z-AR(I,J))/(AR(I+1,J)-AR(I,J))
      Y(NP)=FLOAT(J-1)
      IF(MD.NE.5)GOTO 200
      NZ=3
      GOTO 80
200  IF(J.EQ.1)GOTO 600
      IF(AR(I,J-1).LT.Z)GOTO 250
      IF(NP.EQ.100)GOTO 660
      NP=NP+1
      X(NP)=FLOAT(I-1)
      Y(NP)=FLOAT(J-2)+(Z-AR(I,J-1))/(AR(I,J)-AR(I,J-1))

```

```

      IF(MD.NE.5)GOTO 100
      NZ=4
      GOTO 80
150   I=I-1
      GOTO 200
450   J=J+1
      GOTO 100
350   I=I+1
      GOTO 400
250   J=J-1
      GOTO 300
600   IF(MD.EQ.5)RETURN
      IF(NP.EQ.0)RETURN
625   CALL LINE(X,Y,NP,0.0,0.0,SCX,0.0,SCY)
      RETURN
630   NC=NC+1
      IF(NC.GT.20)GOTO 650
      S(NC,1)=X(1)
      S(NC,2)=Y(1)
      GOTO 625
650   MK=-2
      RETURN
660   MK=-3
      RETURN
      END

```

Appendix 7

Turbomachinery Program (Language - Fortran 4)

Nomenclature, section (2.5), should be used with the following list of program symbols.

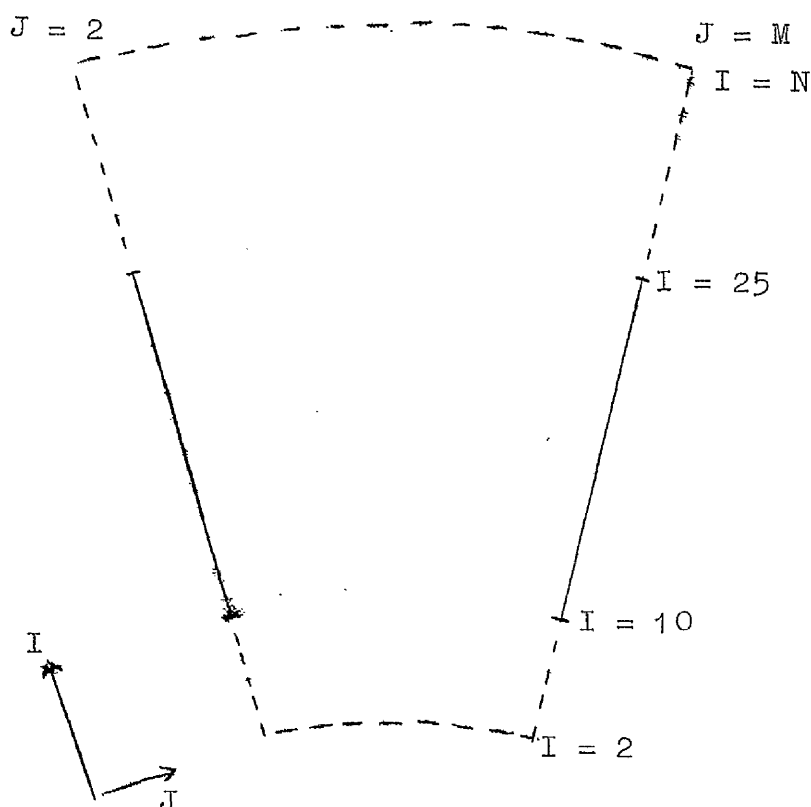
| <u>Program Symbol</u> | <u>Meaning</u> |
|---------------------------|---|
| AA | Maximum residual (sometimes expressed as a percentage) of the iterations for ω . |
| AI | Group a used in slip approximation. |
| ANGB | Angle in degrees between local streamline and radial directions. |
| BDX, BDY | Integers denoting upwind direction and first derivative approximation to be used e.g. "BDX" = 1, backward difference formula in ξ direction. "BDY" = 1, backward difference formula in η direction. |
| BI | Group b used in slip approximation. |
| BL | Integer. "BL" = 0 for no hub-shroud boundary layers. "BL" = 1 for hub-shroud boundary layers to be included. |
| CI | Group c used in slip approximation. |
| COMP | Integer. "COMP" = 0 for inflow (turbine). "COMP" = 1 for outflow (pump). |
| COT1, COT2 | ± 1 depending on local component of flow direction in ξ and η directions respectively. |
| DIF1, DIF2 | Parameters which determine the correct solution ("SOL1" or "SOL2") for the slip approximation. |
| DH | Derivative with respect to ξ of the passage height, $\frac{\partial H}{\partial \xi}$. |
| F | Parameter f' [see eqns. (2.6.17) and (2.6.20)] used in integration to obtain pressure distribution. |
| FDX, FDY | Integers denoting upwind direction and first derivative approximation to be used e.g. "FDX" = 1, forward difference in ξ direction. "FDY" = 1, forward difference in η direction. |

| <u>Program Symbol</u> | <u>Meaning</u> |
|---------------------------|--|
| H | Dimensionless passage height H. |
| HX, HY | Step lengths in ξ ($\Delta\xi$) and η ($\Delta\eta$) directions respectively. |
| I | Dummy integer for streamwise ξ direction. |
| INCR | Increment used in generation of initial stream function distribution ($= 1/"M"$). |
| J | Dummy integer for cross-stream η direction. |
| M | Number of steps in cross-stream η direction. |
| N | Number of steps in streamwise ξ direction. |
| OM | Dimensionless relative vorticity ω' . |
| OMAX | Maximum value of vorticity along a boundary. |
| OMAXDF | Maximum difference between vorticities calculated along boundaries from one iteration to the next. (Maximum value of "OMDIF".) |
| OMDIF | Difference between vorticities at a mesh point from one iteration to the next. |
| OMPR | Value of vorticity ω before an iteration. |
| P | Dimensionless pressure P. |
| P1 | Maximum residual (sometimes expressed as a percentage) of the iterations for ψ . |
| PAR | Group, $b^2 - 4ac$, used in slip approximation. |
| PER | Maximum value of vorticity on all mesh points which are relaxed. |
| PERCEN | Percentage change of relaxed vorticity (i.e. $\frac{"AA"}{"PER"} \times 100$). |
| R | Radius ratio $R \left(= \frac{r}{r_t} \right)$. |
| RE | Flow Reynolds number Re . |
| RSI | Relaxation factor R_2 . |
| RTHETA | Rotation Reynolds number Ro . |

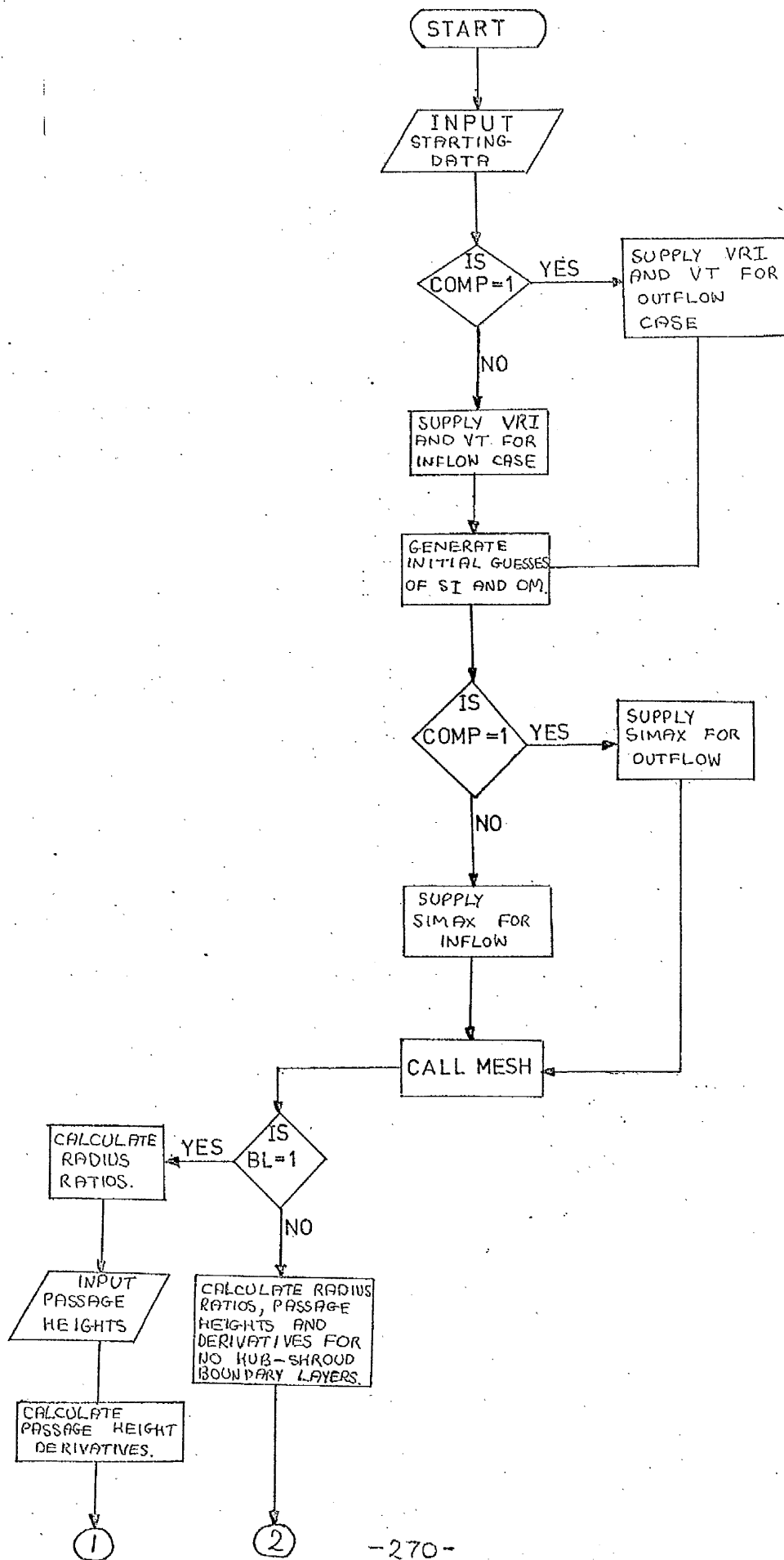
| <u>Program Symbol</u> | <u>Meaning</u> |
|---------------------------|---|
| RV | Relaxation factor R_1 . |
| SI | Dimensionless normalised stream function ψ_n' . |
| SIMAX | Maximum value of ψ (ψ_m). |
| SLIP | Integer. "SLIP" = 0 for no slip on wall. "SLIP" = 1 for wall slip approximation to be incorporated. |
| SOL1, SOL2 | Solutions for ψ_{-1} , i.e. the slip approximation. |
| U | Dimensionless radial component of relative velocity $\left(= \frac{V^r}{U_t}\right)$. |
| UI | $\psi(i, j + 1) - \psi(i, j - 1)$ used in determining the local ξ component of flow direction. |
| UPLUS | Slip parameter u_w^+ . |
| V | Dimensionless tangential component of relative velocity $(= V_\theta/U_t)$. |
| VI | $-\left[\psi(i + 1, j) - \psi(i - 1, j)\right]$ used in determining the local η component of flow direction. |
| VRI | Dimensional radial component of velocity, V_{r1} , at inlet to system. |
| VT | Dimensional tangential velocity of rotor tip U_t . |
| VY | Residual of vorticity iterations $[\omega'(i, j) - \omega(i, j)]$. |
| X | Inner value of radius ratio (R/r_t) . |
| Y | Difference between new and old values of ψ over one iteration. |
| Z | Integer count of number of iterations performed. |

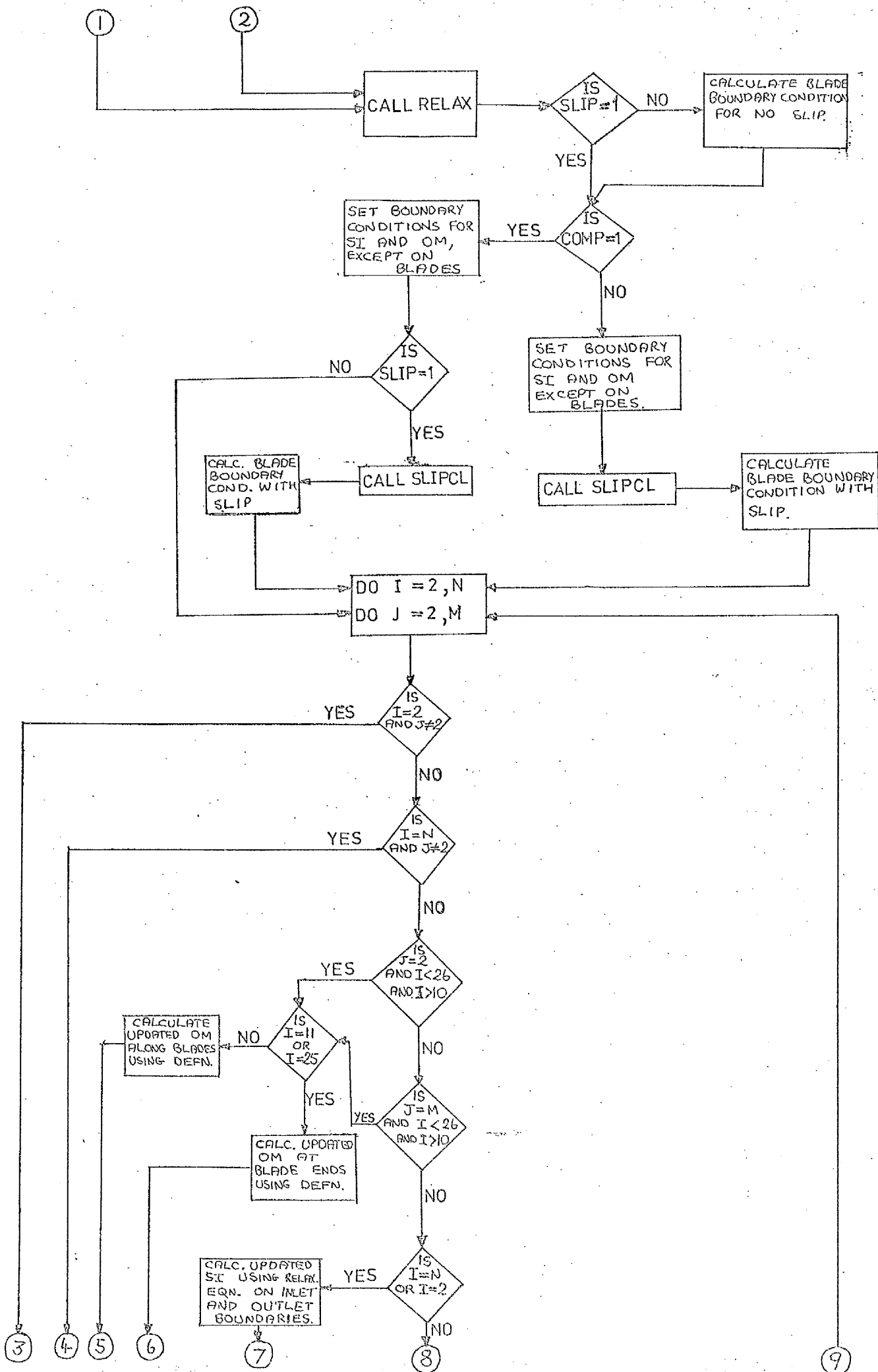
Operation Notes

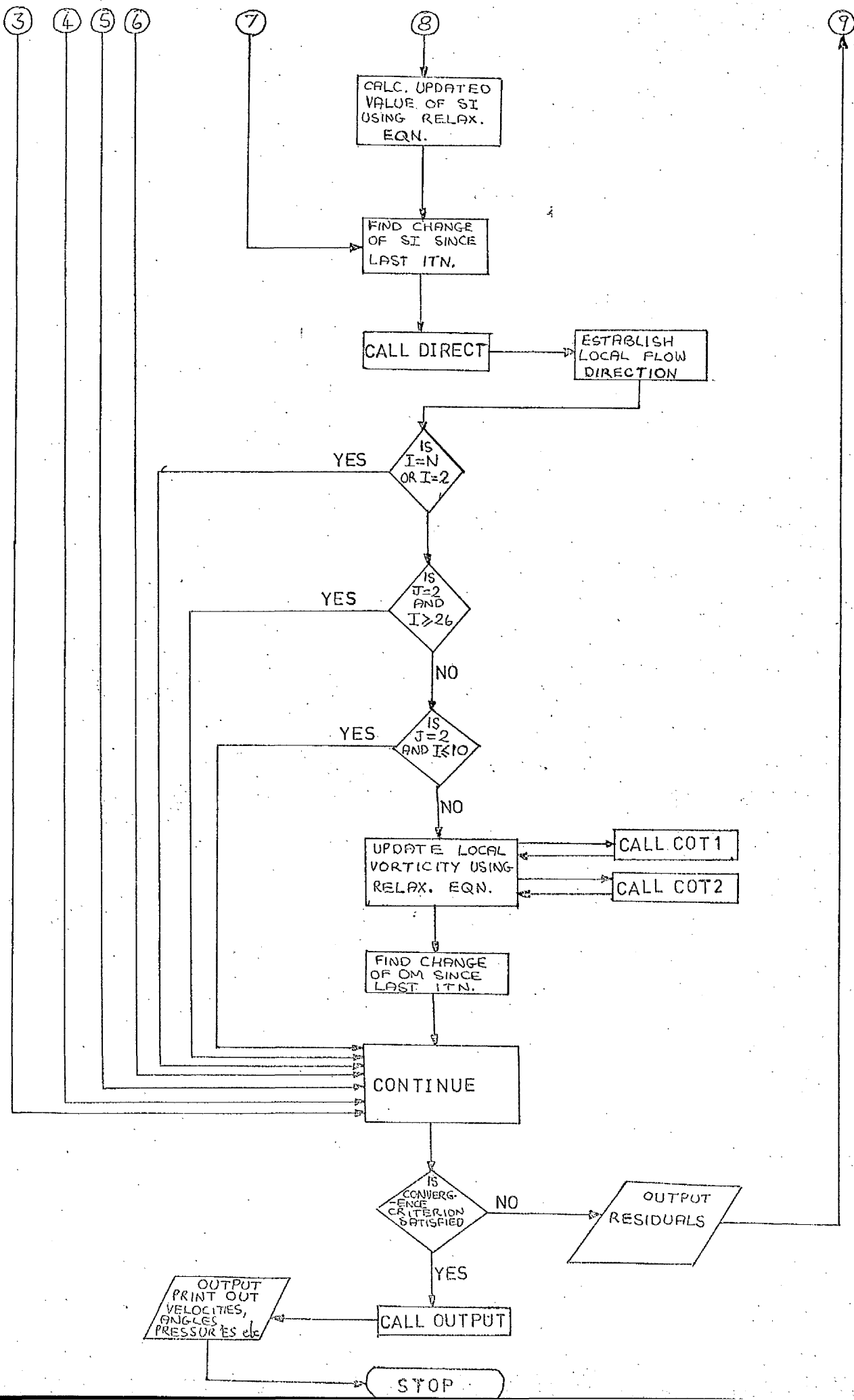
1. The time required to obtain a satisfactory converged solution obviously depends on the desired convergence criterion. For the examples given in this thesis, the solution was assumed to have converged when the maximum change of each dependent variable from one complete iteration to the next, was less than 0.1% of the maximum value of that particular dependent variable over the whole mesh. Typically each iteration takes 5-6 secs. and generally 150-200 iterations are required for satisfactory convergence to be obtained.
2. In the program, the control system is numbered according to the diagram below.



FLOW DIAGRAM OF TURBOMACHINERY PROGRAM







TURBOMACHINERY PROGRAM

```

REAL INCR
INTEGER FDX,FDY,BDX,BDY,BL,COMP,SLIP
COMMON M,N,RSI,RV,HX,HY,RE,RTHETA,OM(30,23),SI(30,23),SIMAX,DSI,
1 R(30),H(30),DH(30),FDX,FDY,BDX,BDY,I,J,SLIP,UPLUS
2 ,UC(30,23),V(30,23),ANGB(30,23),P(30,23),VRI,BL,COMP,VT
100 FORMAT (2I3,2F6.3,2F9.6,2E10.3,3I2,F5.0)
C READ IN INPUT DATA (SEE LIST FOR DETAILS)
  READ (1,100) M,N,RSI,RV,HX,HY,REX,RTHETX,BL,COMP,SLIP,UPLUS
C DIVIDE REYNOLDS NUMBERS BY CHOSEN VISCOSITY ENHANCEMENT FACTOR
  RE=REX/100.
  RTHETA=RTHETX/100.
C SUPPLY RADIAL COMPONENT OF VELOCITY AT INLET
  VRI=0.9664
  IF (COMP.EQ.1) VRI=1.974
C SUPPLY TIP SPEED
  VT=11.783
  IF (COMP.EQ.1) VT=-6.75
  BB=-2.*RTHETA/RE
  INCR=0.05
  STRFN=0.0
C GENERATE INITIAL GUESSES OF STREAM FUNCTION,SI,AND VORTICITY,OM
  DO 3 J=2,M
  DO 4 I=2,N
    OM(I,J)=BB
    IF (COMP.EQ.1) GO TO 7
    SI(I,J)=1.0-STRFN
    GO TO 4
  7 SI(I,J)=STRFN
  4 CONTINUE
  3 STRFN=STRFN+INCR
C SUPPLY MAXIMUM VALUE OF SI
  SIMAX=-1.532
  IF (COMP.EQ.1) SIMAX=0.537
  6 CALL MESH
  CALL RELAX
  STOP
  END

```

```

SUBROUTINE MESH
  INTEGER FDX,FDY,BDX,BDY,BL,COMP,SLIP
  COMMON M,N,RSI,RV,HX,HY,RE,RTHETA,OM(30,23),SI(30,23),SIMAX,1
1    R(30),H(30),DH(30),FDX,FDY,BDX,BDY,I,J,SLIP,UPLUS
2    ,UC(30,23),V(30,23),ANGB(30,23),P(30,23),VRI,BL,COMP,VT
  IF (BL.EQ.1) GO TO 5
C  FOR THE CHOSEN MESH SPACINGS HX,OBTAIN THE CORRESPONDING RADIUS
C  RATIOS,PASSAGE HEIGHTS AND PASSAGE HEIGHT DERIVATIVES
  X=-3.32992
  DO 1 I=2,N
    R(I)=EXP(X*0.342)
    GO TO 2
    IF (I.GT.25.OR.I.LT.11) GO TO 2
    H(I)=1./R(I)
    DH(I)=-1./R(I)
    GO TO 3
2  DH(I)=0.0
  H(I)=1.0
3  X=X+HX
1  CONTINUE
  GO TO 8
  DO 4 I=2,10
4  H(I)=H(11)
  GO TO 8
C  OBTAIN RADIUS RATIOS,PASSAGE HEIGHT AND DERIVATIVES FOR INCLUSION
C  OF HUB-SHROUD BOUNDARY LAYERS
5  X=-1.80484
  DO 6 I=2,N
    R(I)=EXP(X)
    X=X+HX
C  READ IN THE PASSAGE HEIGHT TAKING INTO ACCOUNT BOUNDARY LAYER
C  BLOCKAGE EFFECTS
  READ (1,100) H(1)
100 FORMAT (F5.3)
6  CONTINUE
  DH(2)=0.0
  DH(N)=0.0
  K=N-1
  DO 7 I=3,K
7  DH(I)=(H(I+1)-H(I-1))/(2.*HX)
8  RETURN
  END

```

```

SUBROUTINE DIRECT
  INTEGER FDX,FDY,BDX,BDY,BL,COMP,SLIP
  COMMON M,N,RSI,RV,HX,HY,RE,RTHETA,OM(30,23),SI(30,23),SIMAX,DSI,
1      R(30),H(30),DH(30),FDX,FDY,BDX,BDY,I,J,SLIP,UPLUS
2      ,U(30,23),V(30,23),ANGB(30,23),P(30,23),VRI,BL,COMP,VT
C  ESTABLISHES THE LOCAL COMPONENTS OF THE FLOW DIRECTION
  FDX=0
  FDY=0
  BDX=0
  BDY=0
  UI=SI(I,J+1)-SI(I,J-1)
  IF (UI.GE.0.0) BDX=1
  IF (UI.LT.0.0) FDX=1
  VI=-(SI(I+1,J)-SI(I-1,J))
  IF (VI.GE.0.0) BDY=1
  IF (VI.LT.0.0) FDY=1
  RETURN
END

```

```

FUNCTION COT1(FDX,FDY,BDX,BDY)
  INTEGER FDX,FDY,BDX,BDY
C  ASSIGNS VALUES OF +1,-1 TO THE FUNCTION COT1,DEPENDING ON FLOW
C  DIRECTION
  IF (FDX.EQ.1) COT1=-1.0
  IF (BDX.EQ.1) COT1=1.0
  RETURN
END

```

```

FUNCTION COT2(FDX,FDY,BDX,BDY)
  INTEGER FDX,FDY,BDX,BDY
C  ASSIGNS VALUES OF +1,-1 TO THE FUNCTION COT2,DEPENDING ON FLOW
C  DIRECTION
  IF (FDY.EQ.1) COT2=-1.0
  IF (BDY.EQ.1) COT2=1.0
  RETURN
END

```

```

SUBROUTINE RELAX
REAL INCR
INTEGER FDX,FDY,BDX,BDY,Z,BL,COMP,SLIP
COMMON M,N,RSI,RV,HX,HY,RE,RTHETA,OM(30,23),SI(30,23),SIMAX,DSI,
1 R(30),H(30),DH(30),FDX,FDY,BDX,BDY,I,J,SLIP,UPLUS
2 ,U(30,23),V(30,23),ANGB(30,23),P(30,23),VRI,BL,COMP,VT
10 P1=0.0
AA=0.0
OMAXDF=0.0
OMAX=0.0
IF (SLIP.EQ.1) GO TO 13
C SET UP BLADE BOUNDARY CONDITIONS FOR NO SLIP
DO 1 I=4,18
SI(I,1)=SI(I,3)
1 SI(I,M+1)=SI(I,M-1)
13 IF (COMP.EQ.1) GO TO 22
C SET UP BOUNDARY CONDITIONS FOR INFLOW CASE
C SET BOUNDARY CONDITIONS FOR SI AND OM IN REGION DOWNSTREAM FROM
C BLADE PASSAGE EXIT. I.E. FOR RADIUS RATIOS LESS THAN 0.333
DO 2 I=2,10
OM(I,1)=OM(I,M-1)
OM(I,M+1)=OM(I,3)
SI(I,1)=SI(I,M-1)+1.0
2 SI(I,M+1)=SI(I,3)-1.0
C SET BOUNDARY CONDITIONS FOR SI AND OM IN REGION UPSTREAM FROM
C BLADE PASSAGE. I.E. FOR RADIUS RATIOS GREATER THAN 1.0
DO 3 I=26,29
SI(I,1)=SI(I,M-1)+1.0
SI(I,M+1)=SI(I,3)-1.0
OM(I,1)=OM(I,M-1)
3 OM(I,M+1)=OM(I,3)
C SET FLOW DIRECTION AT INLET AND EXIT TO FIELD
DO 4 J=2,M
SI(N,J+1)=SI(N,J)-0.05
SI(2,J+1)=SI(2,J)-0.05
SI(1,J)=SI(3,J)+4.094*HX
4 SI(N+1,J)=SI(N-1,J)+0.4841*HX
C CALL SUBROUTINE SLIPCL TO CALCULATE THE BLADE BOUNDARY CONDITIONS
DO 90 I=11,25
90 CALL SLIPCL
GO TO 23
C SET UP BOUNDARY CONDITIONS FOR OUTFLOW CASE
22 DO 24 I=2,3
OM(I,1)=OM(I,M-1)
OM(I,M+1)=OM(I,3)
SI(I,1)=SI(I,M-1)-1.0
24 SI(I,M+1)=SI(I,3)+1.0
IF (SLIP.NE.1) GO TO 15
C CALL SUBROUTINE SLIPCL TO CALCULATE THE BLADE BOUNDARY CONDITIONS
DO 14 I=4,18
14 CALL SLIPCL
C SET BOUNDARY CONDITIONS IN EXIT REGION. I.E. FOR RADIUS RATIOS
C GREATER THAN 1.0
15 DO 25 I=19,22
SI(I,1)=SI(I,M-1)-1.0
SI(I,M+1)=SI(I,3)+1.0
OM(I,1)=OM(I,M-1)
25 OM(I,M+1)=OM(I,3)
DO 26 J=2,M
C SET FLOW DIRECTION AT INLET AND EXIT TO FIELD
SI(N,J+1)=SI(N,J)+0.05

```

```

SI(2,J+1)=SI(2,J)+0.05
SI(1,J)=SI(3,J)-3.100*HX
26 SI(N+1,J)=SI(N-1,J)+5.0*HX
23 DO 5 I=2,N
DO 6 J=2,M
IF (I.EQ.2.AND.J.NE.2) GO TO 6
IF (I.EQ.N.AND.J.NE.2) GO TO 6
IF (J.EQ.2.AND.I.LT.26.AND.I.GT.10) GO TO 7
IF (J.EQ.M.AND.I.LT.26.AND.I.GT.10) GO TO 7
IF (I.EQ.N) GO TO 12
IF (I.EQ.2) GO TO 12
C RELAXATION EQUATION TO OBTAIN NEW VALUE OF SI
DD=RSI/(2.*SIMAX*(HX**2+HY**2)/(H(I)*R(I)**2))
Y=DD*(SIMAX*HY**2/(H(I)*R(I)**2)*(SI(I-1,J)-2.*SI(I,J)+SI(I+1,J))+
1SIMAX*HX**2/(H(I)*R(I)**2)*(SI(I,J-1)-2.*SI(I,J)+SI(I,J+1))+HX**2*
2HY**2*OM(I,J)-SIMAX*HX*HY**2/(H(I)*R(I)**2)*DH(I)*(SI(I+1,J)-SI(I-
31,J))/(2.*H(I)))
GO TO 11.
C RELAXATION EQUATION TO OBTAIN NEW VALUE OF SI ON THE INLET AND
C OUTLET BOUNDARIES.
12 DD=RSI/(2.*SIMAX*HY**2/(H(I)*R(I)**2))
Y=DD*(SIMAX*HY**2/(H(I)*R(I)**2)*(SI(I-1,J)-2.*SI(I,J)
1+SI(I+1,J))+HX**2*HY**2*OM(I,J))
11 SI(I,J)=SI(I,J)+Y
C FIND MAXIMUM CHANGE OF SI OVER ONE ITERATION
IF (P1.GE.(ABS(Y))) GO TO 8
P1=ABS(Y)
GO TO 8
7 OMPR=OM(I,J)
IF (I.EQ.11.OR.I.EQ.25) GO TO 30
C DEFINITION OF VORTICITY.CAN BE USED IF VALUE OF SI IS KNOWN
C AT A PARTICULAR POINT
OM(I,J)=SIMAX/(H(I)*R(I)**2)*((SI(I,J+1)-2.*SI(I,J)+SI(I,J-1))
1/(HY**2)+(SI(I+1,J)-2.*SI(I,J)+SI(I-1,J))/
2(HX**2)-DH(I)/H(I)*(SI(I+1,J)-SI(I-1,J))/(2.*HX))
GO TO 31
30 OM(I,J)=SIMAX/(H(I)*R(I)**2)*(SI(I,J+1)-2.*SI(I,J)+SI(I,J-1))/(HY*
1*2)
31 OM(I,J)=-1.0*OM(I,J)
OMDIF=OMPR-OM(I,J)
OMDIF=ABS(OMDIF)
IF (OMAXDF.LT.OMDIF) OMAXDF=OMDIF
OMAXD=ABS(OM(I,J))
IF (OMAX.LT.OMAXD) OMAX=OMAXD
GO TO 6
8 CALL DIRECT
9 IF (I.EQ.N) GO TO 6
IF (I.EQ.2) GO TO 6
IF (J.EQ.2.AND.I.GE.26) OM(I,2)=OM(I,M)
IF (J.EQ.2.AND.I.GE.26) GO TO 6
IF (J.EQ.2.AND.I.LE.10) OM(I,2)=OM(I,M)
IF (J.EQ.2.AND.I.LE.10) GO TO 6
C RELAXATION EQUATION TO OBTAIN NEW VALUE OF OM
COV=4.*H(I)/RE*(HX**2+HY**2)+COT1(FDX,FDY,BDX,BDY)*SIMAX*HX*HY*(SI
1(I,J+1)-SI(I,J-1))-COT2(FDX,FDY,BDX,BDY)*SIMAX*HX*HY*(SI(I+1,J)-SI
2(I-1,J))
IF (FDX.EQ.1) DIFWX=OM(I+1,J)-OM(I,J)
IF (BDX.EQ.1) DIFWX=OM(I,J)-OM(I-1,J)
IF (FDY.EQ.1) DIFWY=OM(I,J+1)-OM(I,J)
IF (BDY.EQ.1) DIFWY=OM(I,J)-OM(I,J-1)
VY=RV/(-COV)*(SIMAX*HX*HY*(SI(I,J+1)-SI(I,J-1))*DIFWX-SIMAX*HX*HY*
1(SI(I+1,J)-SI(I-1,J))*DIFWY-2.*HY**2*H(I)/RE*(OM(I-1,J)-2.*OM(I,J)

```

```

2+OM(I+1,J))-2.*HX**2*H(I)/RE*(OM(I,J-1)-2.*OM(I,J)+OM(I,J+1))-SIMA
3X*HX**2*HY*OM(I,J)*DH(I)*(SI(I,J+1)-SI(I,J-1))/H(I)
4-2.*SIMAX*HX**2*HY*R
5THETA*DH(I)*(SI(I,J+1)-SI(I,J-1))/(H(I)*RE))
  OM(I,J)=OM(I,J)+VY
  IF (AA.GE.(ABS(VY))) GO TO 6
  AA=ABS(VY)
6 CONTINUE
5 CONTINUE
  OMDIF=100.0*OMAXDF/OMAX
  Z=Z+1
  P1=100.*P1/RSI
  AA=AA/RV
  PER=0.0
  DO 20 I=2,N
  DO 21 J=2,M
    IF (PER.GE.(ABS(OM(I,J)))) GO TO 21
    PER=ABS(OM(I,J))
  21 CONTINUE
  20 CONTINUE
  PERCEN=100.*AA/PER
  WRITE (2,101) Z,AA,PER,PERCEN,OMDIF,P1
101 FORMAT (1H,I3,3X,E11.4,3X,F7.2,3X,F7.3,3X,F7.3,3X,F7.4)
C  SUPPLY DESIRED CONVERGENCE CRITERION
  IF (Z.EQ.200) CALL OUTPUT
102 FORMAT (1H0,18HCONVERGED SOLUTION)
  GO TO 10
  RETURN
  END

```



```

SUBROUTINE SLIPCL
REAL INCR
INTEGER FDX,FDY,BDX,BDY,BL,COMP,SLIP
COMMON M,N,RSI,RV,HX,HY,RE,RTHETA,OM(30,23),SI(30,23),SIMAX,DSI,
1      R(30),H(30),DH(30),FDX,FDY,BDX,BDY,I,J,SLIP,UPLUS
2      ,U(30,23),V(30,23),ANGB(30,23),P(30,23),VRI,BL,COMP,VT
C SOLVES THE QUADRATIC SLIP EQUATION SUPPLYING THE REQUIRED SOLUTION
C AND DISCARDING THE OTHER
  J=2
  AI=1.0
  IF (SI(I,2).LT.SI(I,3)) CO=4.
  IF (SI(I,2).GE.SI(I,3)) CO=-4.
  BI=-2.*SI(I,3)-CO*UPLUS**2/(RE*100.*SIMAX*R(I))
  CI=-CO*UPLUS**2*(-2.*SI(I,2)+SI(I,3))/(RE*100.*SIMAX*R(I))
  CI=CI+SI(I,3)**2
  GO TO 2
1 J=M
  AI=1.0
  IF (SI(I,M).LT.SI(I,M-1)) CO=4.
  IF (SI(I,M).GE.SI(I,M-1)) CO=-4.
  BI=-2.*SI(I,M-1)-CO*UPLUS**2/(RE*100.*SIMAX*R(I))
  CI=-CO*UPLUS**2*(-2.*SI(I,M)+SI(I,M-1))/(RE*100.*SIMAX*R(I))
  CI=CI+SI(I,M-1)**2
2 PAR=BI**2-4.*AI*CI
  IF (PAR.LT.0.0) WRITE(2,100)
100 FORMAT(1H ,18HPARAMETER NEGATIVE)
  SOL1=(-BI+SQRT(PAR))/(2.*AI)
  SOL2=(-BI-SQRT(PAR))/(2.*AI)
  IF (J.EQ.M) GO TO 3
  DIF1=ABS(SI(I,3)-SOL1)
  DIF2=ABS(SI(I,3)-SOL2)
  IF (DIF1.GE.DIF2) SI(I,1)=SOL2
  IF (DIF2.GE.DIF1) SI(I,1)=SOL1
  GO TO 4
3 DIF1=ABS(SI(I,M-1)-SOL1)
  DIF2=ABS(SI(I,M-1)-SOL2)
  IF (DIF1.GE.DIF2) SI(I,M+1)=SOL2
  IF (DIF2.GE.DIF1) SI(I,M+1)=SOL1
4 IF (J.EQ.2) GO TO 1
  RETURN
END

```

```

SUBROUTINE OUTPUT
INTEGER FDX,FDY,BDX,BDY,BL,COMP,SLIP
DIMENSION F(30)
COMMON M,N,RSI,RV,HX,HY,RE,RTHETA,OM(30,23),SI(30,23),SIMAX,DSI,
1      R(30),H(30),DH(30),FDX,FDY,BDX,BDY,I,J,SLIP,UPLUS
2      ,U(30,23),V(30,23),ANGB(30,23),P(30,23),VRI,BL,COMP,VT
C PRINTS OUT THE DESIRED OUTPUT DATA
100 FORMAT (1H ,12HREYNOLDS NO=,F9.1)
101 FORMAT (1H ,7HRTTHETA=,E10.3)
102 FORMAT (1H0,13HRADIUS-RATIOS)
103 FORMAT (1H ,F7.4)
104 FORMAT (1H0,15HSTREAM-FUNCTION)
105 FORMAT (1H ,21F6.3)
106 FORMAT (1H0,9HVORTICITY)
107 FORMAT (1H ,21F6.1)
108 FORMAT (1H0,10HVELOCITY-U)
109 FORMAT (1H ,21F6.3)
110 FORMAT (1H0,10HVELOCITY-V)
111 FORMAT (1H0,7HANGLE-B)
112 FORMAT (1H ,14F8.2)
113 FORMAT (1H ,10F7.4)
114 FORMAT (1H ,10F7.2)
115 FORMAT (1H0,14HPRESSURE-RATIO)
116 FORMAT (1H ,10F8.3)
WRITE (2,100) RE
WRITE (2,101) RTHETA
WRITE (2,102)
DO 1 I=2,N
1 WRITE (2,103) R(I)
WRITE (2,104)
I=N
2 WRITE (2,105) (SI(I,J),J=2,M)
I=I-1
IF (I.GE.2) GO TO 2
WRITE (2,106)
I=N
3 WRITE (2,107) (OM(I,J),J=2,M)
I=I-1
IF (I.GE.2) GO TO 3
121 FORMAT (1H ,9F7.4)
I=N
90 WRITE (5,121) (SI(I,J),J=2,M)
I=I-1
IF (I.GE.2) GO TO 90
DO 4 I=2,N
DO 5 J=2,M
U(I,J)=((SI(I,J+1)-SI(I,J-1))*SIMAX*VRI)/(2.*HY*R(I)*H(I)*VT)
U(I,J)=-1.0*U(I,J)
V(I,J)=-((SI(I+1,J)-SI(I-1,J))*SIMAX*VRI)/(2.*HX*R(I)*H(I)*VT)
V(I,J)=-1.0*V(I,J)
ANGB(I,J)=ATAN2V(I,J),-U(I,J))*180./3.142
5 CONTINUE
4 CONTINUE
WRITE (2,108)
I=N
6 WRITE (2,109) (U(I,J),J=2,M)
I=I-1
IF (I.GE.2) GO TO 6
WRITE (2,110)
I=N
7 WRITE (2,109) (V(I,J),J=2,M)

```

```

      I=I-1
      IF (I.GE.2) GO TO 7
      WRITE (2,111)
      I=N
      8 WRITE (2,112) (ANGB(I,J),J=2,M)
      I=I-1
      IF (I.GE.2) GO TO 8
C   INTEGRATIONS TO OBTAIN PRESSURE DISTRIBUTION
      DO 12 I=11,25
      U(I,1)=U(I,3)
      V(I,1)=-V(I,3)
      U(I,M+1)=U(I,M-1)
      12 V(I,M+1)=-V(I,M-1)
      DO 13 I=2,10
      U(I,1)=U(I,M-1)
      V(I,1)=V(I,M-1)
      U(I,M+1)=U(I,3)
      13 V(I,M+1)=V(I,3)
      DO 14 I=26,N
      U(I,1)=U(I,M-1)
      V(I,1)=V(I,M-1)
      U(I,M+1)=U(I,3)
      14 V(I,M+1)=V(I,3)
      WRITE(2,115)
C   INTEGRATE IN RADIAL DIRECTION
      DO 10 J=2,M
      FO=-U(N,J)*(U(N,J)-U(N-1,J))/HX
      FO=FO+V(N,J)**2+R(N)**2+2.0*R(N)*V(N,J)
      FO=FO-U(N,J)/(R(N)*RTHETA)
      F(N)=FO
      FN=-U(2,J)*(U(3,J)-U(2,J))/HX
      FN=FN+V(2,J)**2+R(2)**2
      FN=FN+2.*R(2)*V(2,J)
      FN=FN-U(2,J)/(R52)*RTHETA)
      F(2)=FN
      I=N-1
      16 IF (I.EQ.11.AND.J.EQ.2.OR.J.EQ.M) GO TO 30
      IF (I.EQ.25.AND.J.EQ.2.OR.J.EQ.M) GO TO 31
      IF (I.EQ.26.AND.J.EQ.2.OR.J.EQ.M) GO TO 30
      IF (I.EQ.10.AND.J.EQ.2.OR.J.EQ.M) GO TO 31
      F(I)=-U(I,J)*(U(I+1,J)-U(I-1,J))/(2.0*HX)
      GO TO 32
      31 F(I)=-U(I,J)*(U(I,J)-U(I-1,J))/HX
      GO TO 32
      30 F(I)=-U(I,J)*(U(I+1,J)-U(I,J))/HX
      32 IF (J.EQ.2) GO TO 21
      IF (J.EQ.M) GO TO 22
      F(I)=F(I)-V(I,J)*(U(I,J+1)-U(I,J-1))/(2.0*HY)
      GO TO 23
      21 F(I)=F(I)-V(I,2)*(-U(I,4)+4.*U(I,3)-3.*U(I,2))/(2.0*HY)
      GO TO 23
      22 F(I)=F(I)-V(I,M)*(3.*U(I,M)-4.*U(I,M-1)+U(I,M-2))/(2.0*HY)
      23 F(I)=F(I)+V(I,J)**2+R(I)**2+2.*R(I)*V(I,J)
      F(I)=F(I)+1.0/(R(I)*RTHETA)*(U(I+1,J)-2.*U(I,J)+U(I-1,J))/(HX**2)
      F(I)=F(I)-U(I,J)/(R(I)*RTHETA)
      IF (J.EQ.2) GO TO 24
      IF (J.EQ.M) GO TO 25
      F(I)=F(I)+(U(I,J+1)-2.*U(I,J)+U(I,J-1))/(HY**2*R(I)*RTHETA)
      GO TO 26
      24 F(I)=F(I)+(U(I,2)-2.*U(I,3)+U(I,4))/(HY**2*R(I)*RTHETA)
      GO TO 26

```

```

25 F(I)=F(I)+(U(I,M)-2.*U(I,M-1)+U(I,M-2))/(HY**2*R(I)*RTHETA)
26 IF (J.EQ.2) GO TO 27
   IF (J.EQ.M) GO TO 28
   F(I)=F(I)-2.*(V(I,J+1)-V(I,J-1))/(2.*HY*R(I)*RTHETA)
   GO TO 29
27 F(I)=F(I)-2.*(-V(I,4)+4.*V(I,3)-3.*V(I,2))/(2.*HY*R(I)*RTHETA)
   GO TO 29
28 F(I)=F(I)-2.*(3.*V(I,M)-4.*V(I,M-1)+V(I,M-2))/(2.*HY*R(I)*RTHETA)
29 I=I-1
   IF (I.GE.3) GO TO 16
   P(N,J)=0.0
   I=N
17 I=I-1
   P(I,J)=P(I+1,J)+(F(I)+F(I+1))*HX
   IF (I.EQ.2) GO TO 10
   GO TO 17
10 CONTINUE
   I=N
20 WRITE(2,116) (P(I,J),J=2,M)
   I=I-1
   IF (I.GE.2) GO TO 20
C  INTEGRATE IN TANGENTIAL DIRECTION TO OBTAIN A MORE ACCURATE
C  PRESSURE CALCULATION, ESPECIALLY ON BLADES
   DO 33 I=2,N
     J=2
51 IF (I.EQ.11.AND.J.EQ.2.OR.J.EQ.M) GO TO 37
   IF (I.EQ.25.AND.J.EQ.2.OR.J.EQ.M) GO TO 38
   IF (I.EQ.26.AND.J.EQ.2.OR.J.EQ.M) GO TO 37
   IF (I.EQ.10.AND.J.EQ.2.OR.J.EQ.M) GO TO 38
   IF (I.EQ.2) GO TO 34
   IF (I.EQ.N) GO TO 35
   F(J)=-U(I,J)*(V(I+1,J)-V(I-1,J))/(2.*HX)
   GO TO 36
34 F(J)=-U(I,J)*(-V(4,J)+4.*V(3,J)-3.*V(2,J))/(2.*HX)
   GO TO 36
35 F(J)=-U(I,J)*(3.*V(N,J)-4.*V(N-1,J)+V(N-2,J))/(2.*HX)
   GO TO 36
37 F(J)=-U(I,J)*(V(I+1,J)-V(I,J))/HX
   GO TO 36
38 F(J)=-U(I,J)*(V(I,J)-V(I-1,J))/HX
36 IF (J.EQ.2) GO TO 39
   IF (J.EQ.M) GO TO 40
   F(J)=F(J)-V(I,J)*(V(I,J+1)-V(I,J-1))/(2.*HY)
   GO TO 41
39 F(J)=F(J)-V(I,J)*(-V(I,4)+4.*V(I,3)-3.*V(I,2))/(2.*HY)
   GO TO 41
40 F(J)=F(J)-V(I,J)*(3.*V(I,M)-4.*V(I,M-1)+V(I,M-2))/(2.*HY)
41 F(J)=F(J)-U(I,J)*V(I,J)-2.*U(I,J)*R(I)
   F(J)=F(J)-V(I,J)/(R(I)*RTHETA)
   IF (I.EQ.2) GO TO 42
   IF (I.EQ.N) GO TO 43
   F(J)=F(J)+(V(I+1,J)-2.*V(I,J)+V(I-1,J))/(R(I)*RTHETA*HX**2)
   GO TO 44
42 F(J)=F(J)+(V(2,J)-2.*V(3,J)+V(4,J))/(R(I)*RTHETA*HX**2)
   GO TO 44
43 F(J)=F(J)+(V(N,J)-2.*V(N-1,J)+V(N-2,J))/(R(I)*RTHETA*HX**2)
44 IF (J.EQ.2) GO TO 45
   IF (J.EQ.M) GO TO 46
   F(J)=F(J)+(V(I,J-1)-2.*V(I,J)+V(I,J+1))/(R(I)*RTHETA*HY**2)
   GO TO 47
45 F(J)=F(J)+(V(I,2)-2.*V(I,3)+V(I,4))/(R(I)*RTHETA*HY**2)

```

```

GO TO 47
46 F(J)=F(J)+(V(I,M)-2.*V(I,M-1)+V(I,M-2))/(R(I)*RTHETA*HY**2)
47 IF (J.EQ.2) GO TO 48
   IF (J.EQ.M) GO TO 49
   F(J)=F(J)+2.*(U(I,J+1)-U(I,J-1))/(2.*HY*R(I)*RTHETA)
   GO TO 50
48 F(J)=F(J)+2.*(-U(I,4)+4.*U(I,3)-3.*U(I,2))/(2.*HY*R(I)*RTHETA)
   GO TO 50
49 F(J)=F(J)+2.*(3.*U(I,M)-4.*U(I,M-1)+U(I,M-2))/(2.*HY*R(I)*RTHETA)
50 J=J+1
   IF (J.LE.M) GO TO 51
   DO 52 J=13,M
52 P(I,J)=P(I,J-1)-(F(J)+F(J-1))*HY
   J=11
53 P(I,J)=P(I,J+1)+(F(J)+F(J+1))*HY
   J=J-1
   IF (J.GE.2) GO TO 53
33 CONTINUE
   I=N
54 WRITE(2,116) (P(I,J),J=2,M)
   I=I-1
   IF (I.GE.2) GO TO 54
   RETURN
   END

```

TYPICAL INPUT DATA

```

22 29 1.00  1.00  0.078471 0.03143 -9.750E+04 2.660E+05 0 0 1  20.

```

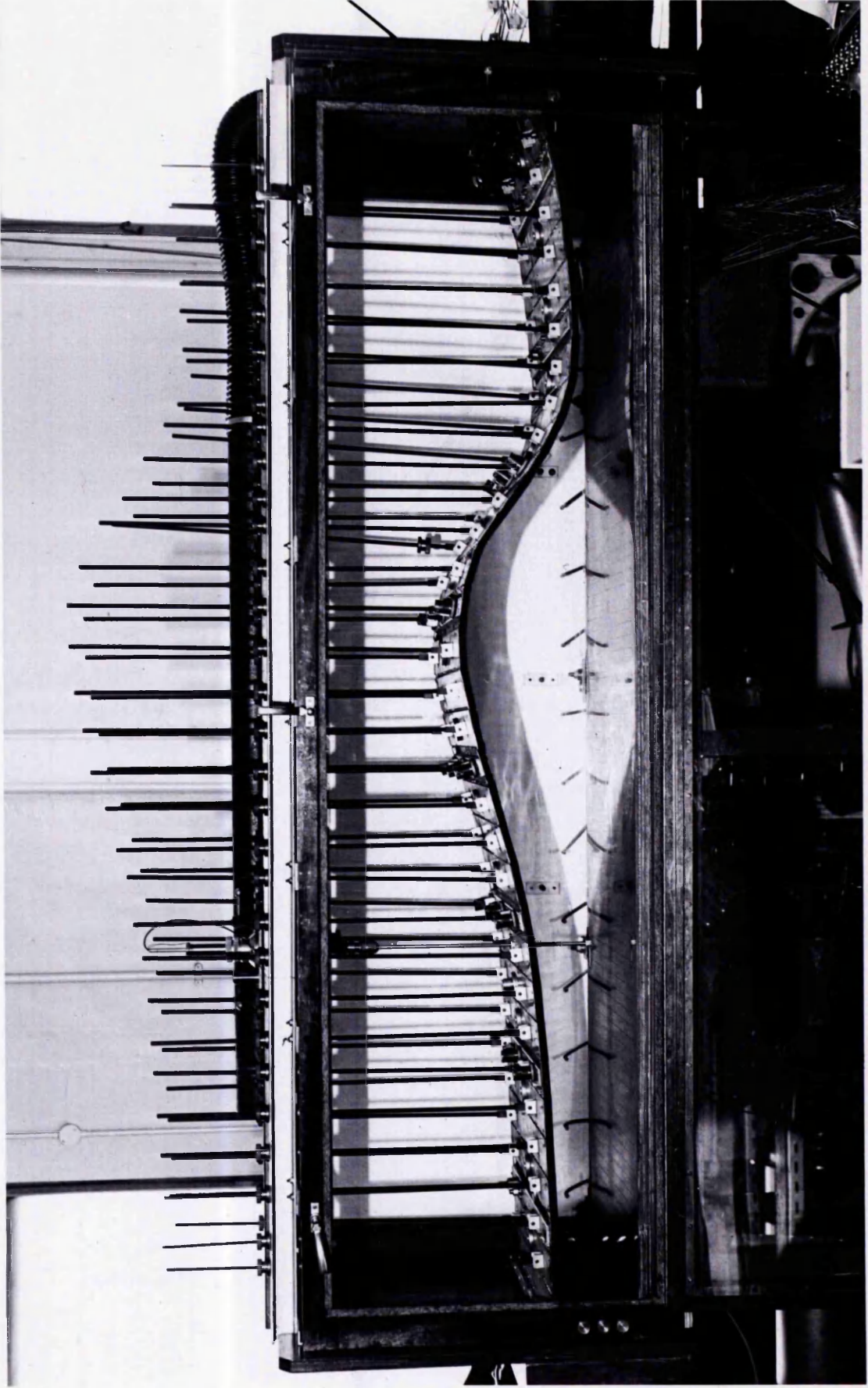


FIG 1 WIND-TUNNEL WORKING SECTION

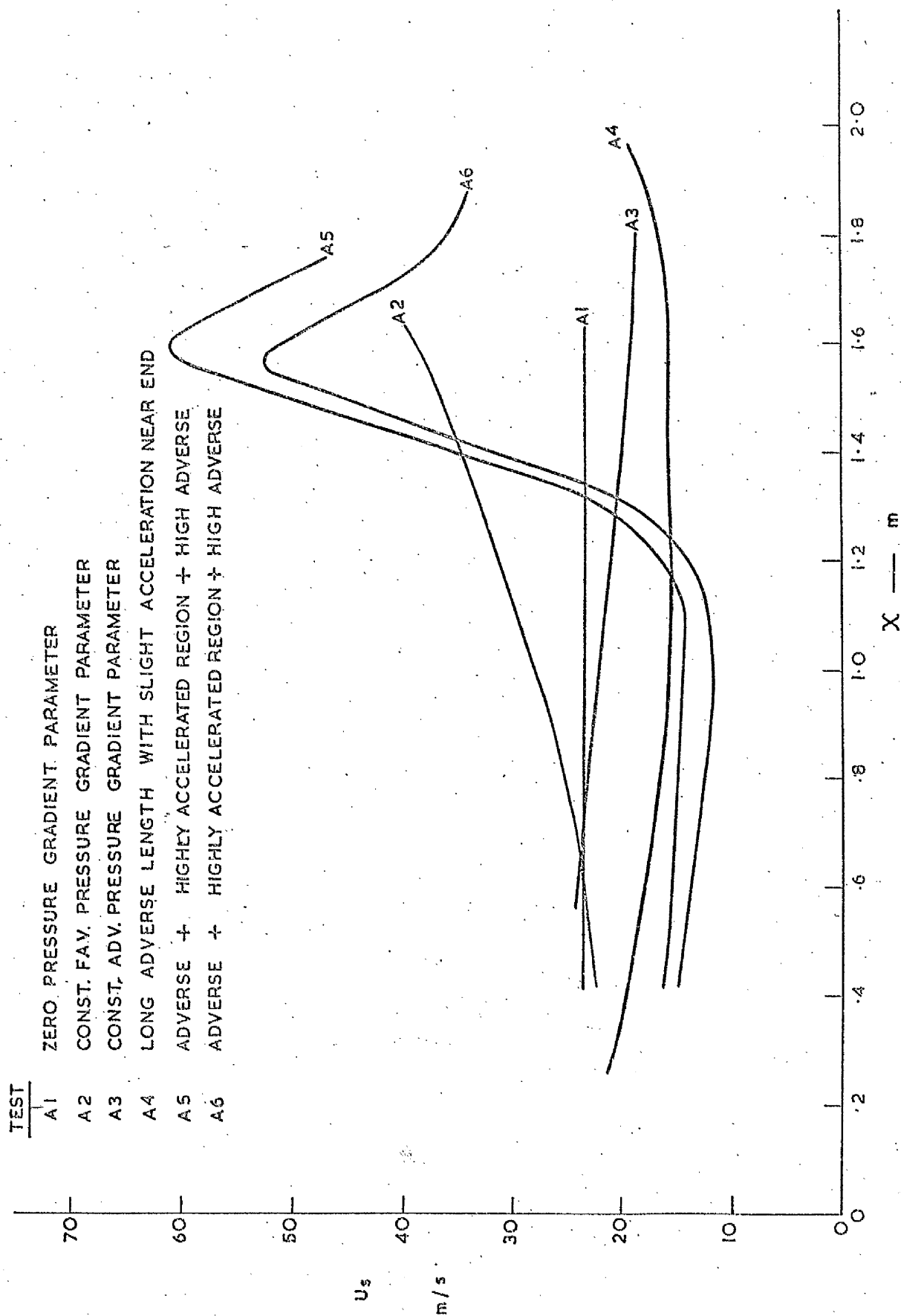
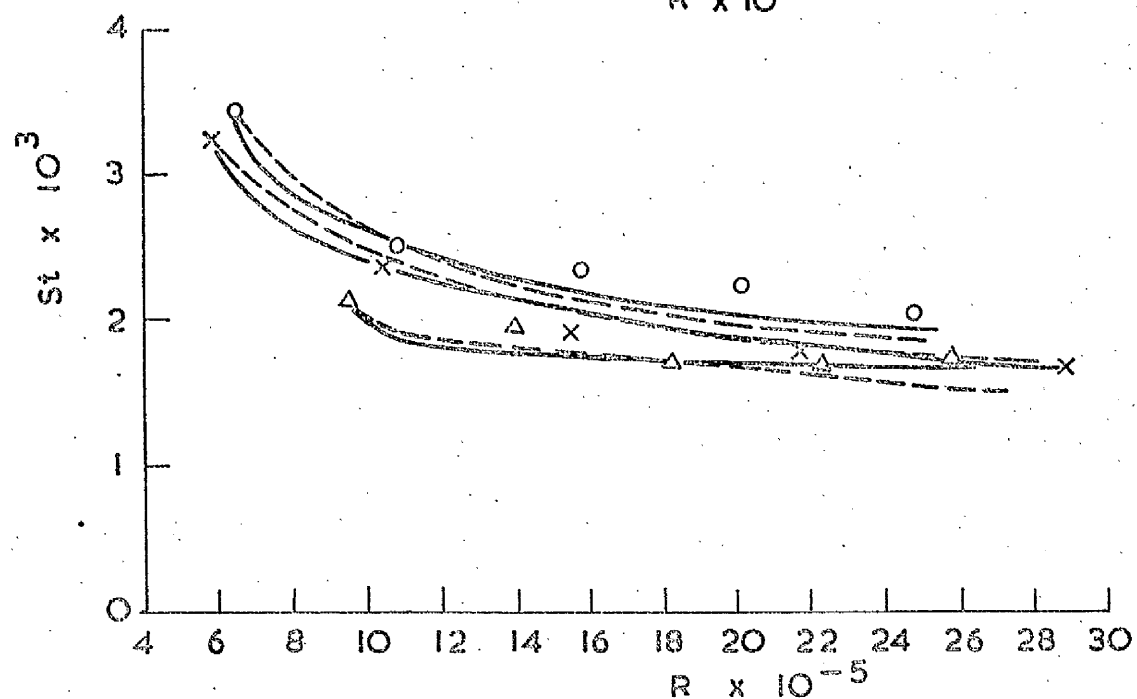
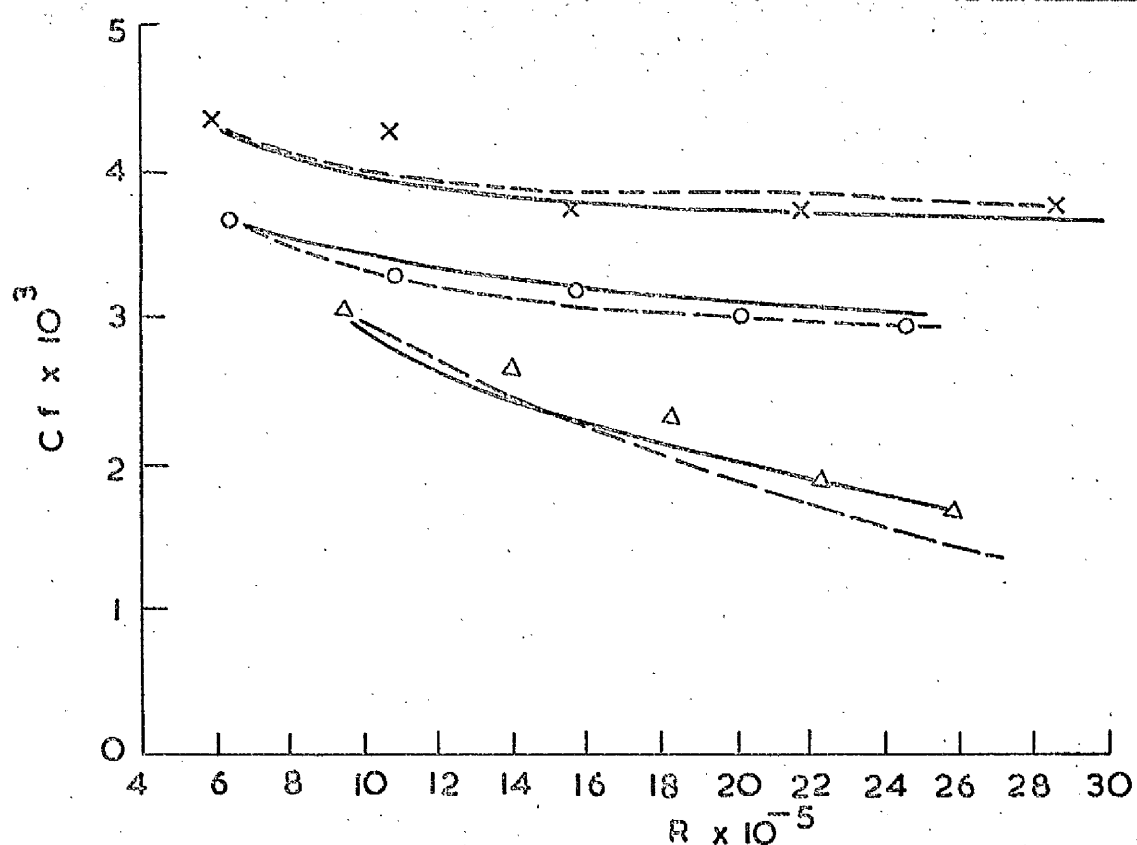


FIG. 2 EXPERIMENTAL FREE STREAM VELOCITY DISTRIBUTIONS



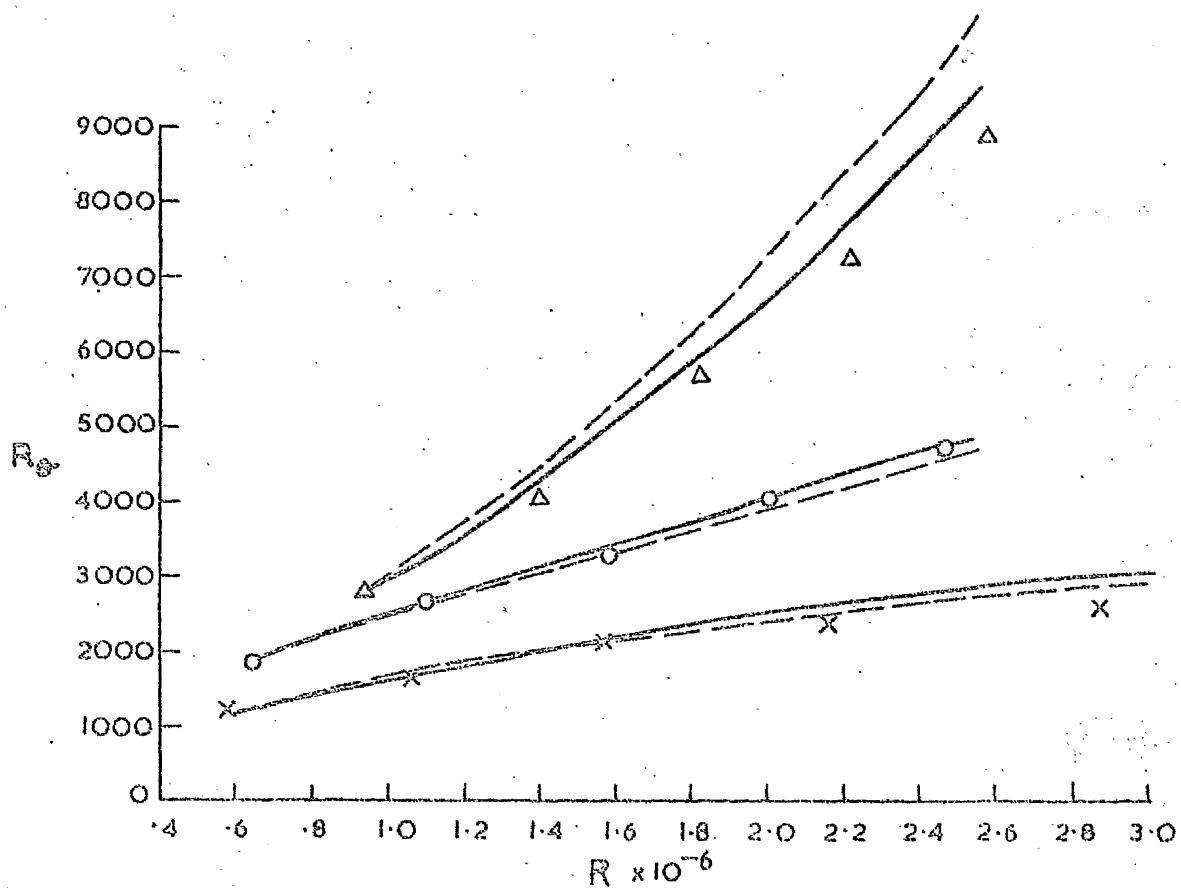
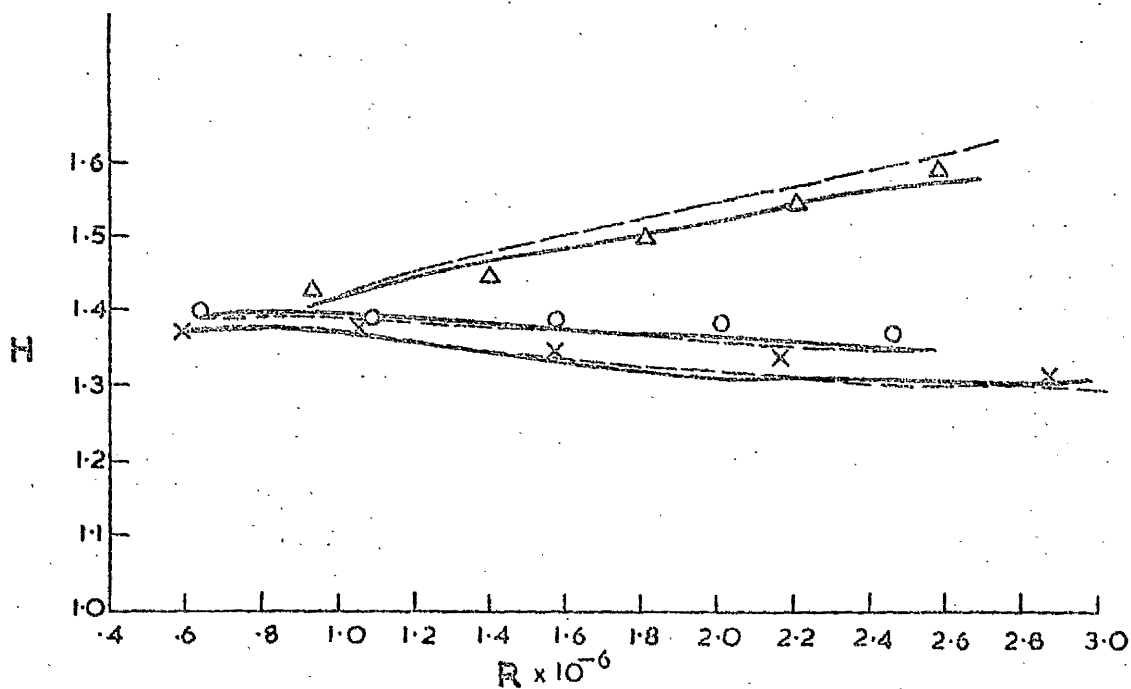
x — FAVOURABLE PRESSURE GRADIENT —
 o — ZERO " "
 Δ — ADVERSE " "

— MIXING LENGTH PREDICTION

— T.K.E. METHOD PREDICTION

| $\frac{2V}{U_s^2} \frac{dU_s}{dx}$ |
|------------------------------------|
| $+40 \times 10^{-8}$ |
| 0 |
| -40×10^{-8} |

FIG 3 PREDICTIONS OF FRICTION FACTOR AND STANTON NUMBER FOR CONSTANT PRESSURE GRADIENT PARAMETERS



TEST

- A2 x FAVOURABLE PRESSURE GRADIENT
 A1 o ZERO " "
 A3 Δ ADVERSE " "

- MIXING LENGTH PREDICTION
 — T.K.E. METHOD PREDICTION

FOR CONSTANT
 PRESSURE GRADIENT
 PARAMETERS.

FIG 4 PREDICTIONS OF SHAPE FACTOR AND Re

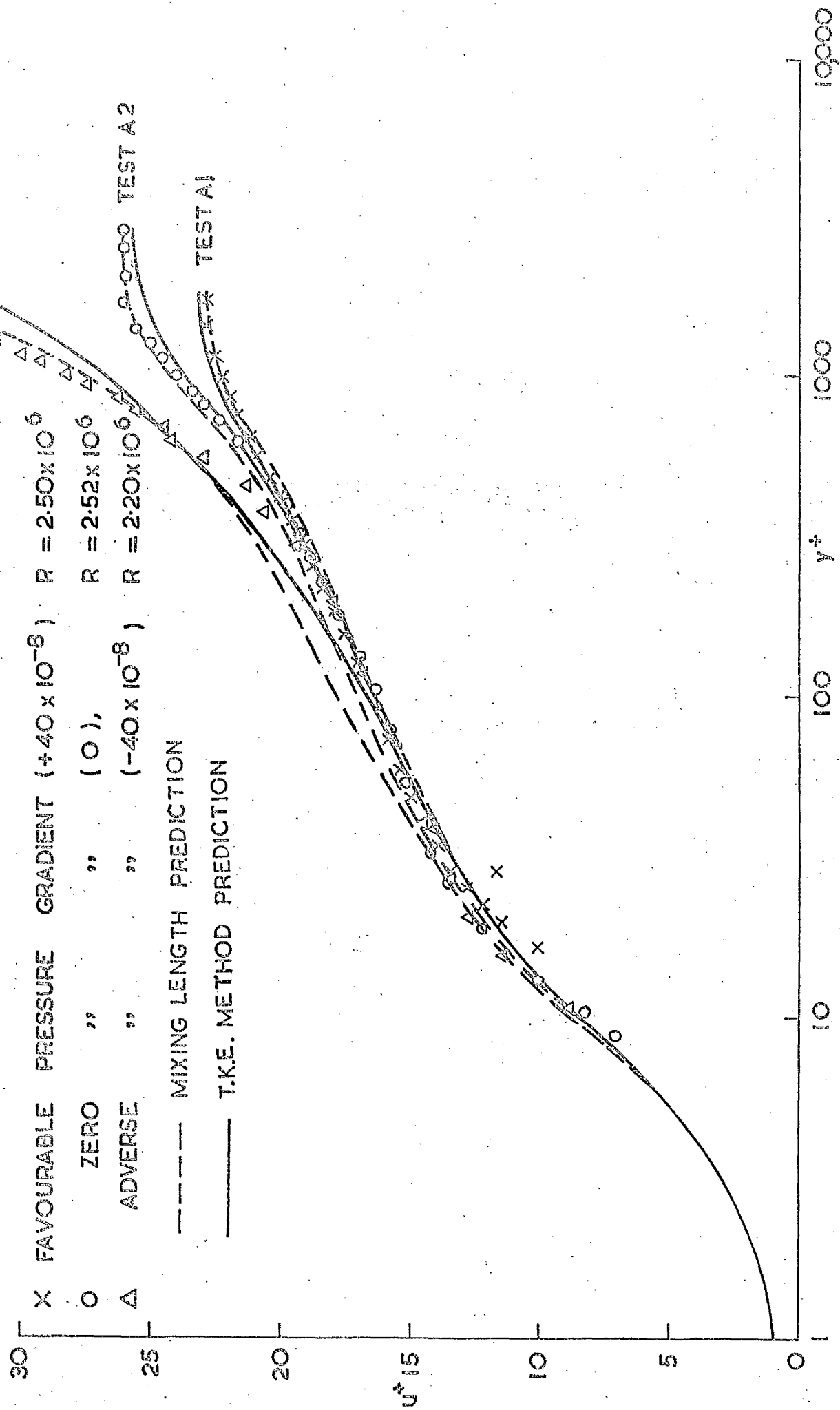


FIG 5 PREDICTIONS AND MEASUREMENTS OF DIMENSIONLESS VELOCITY PROFILES
 — CONSTANT PRESSURE GRADIENT PARAMETERS

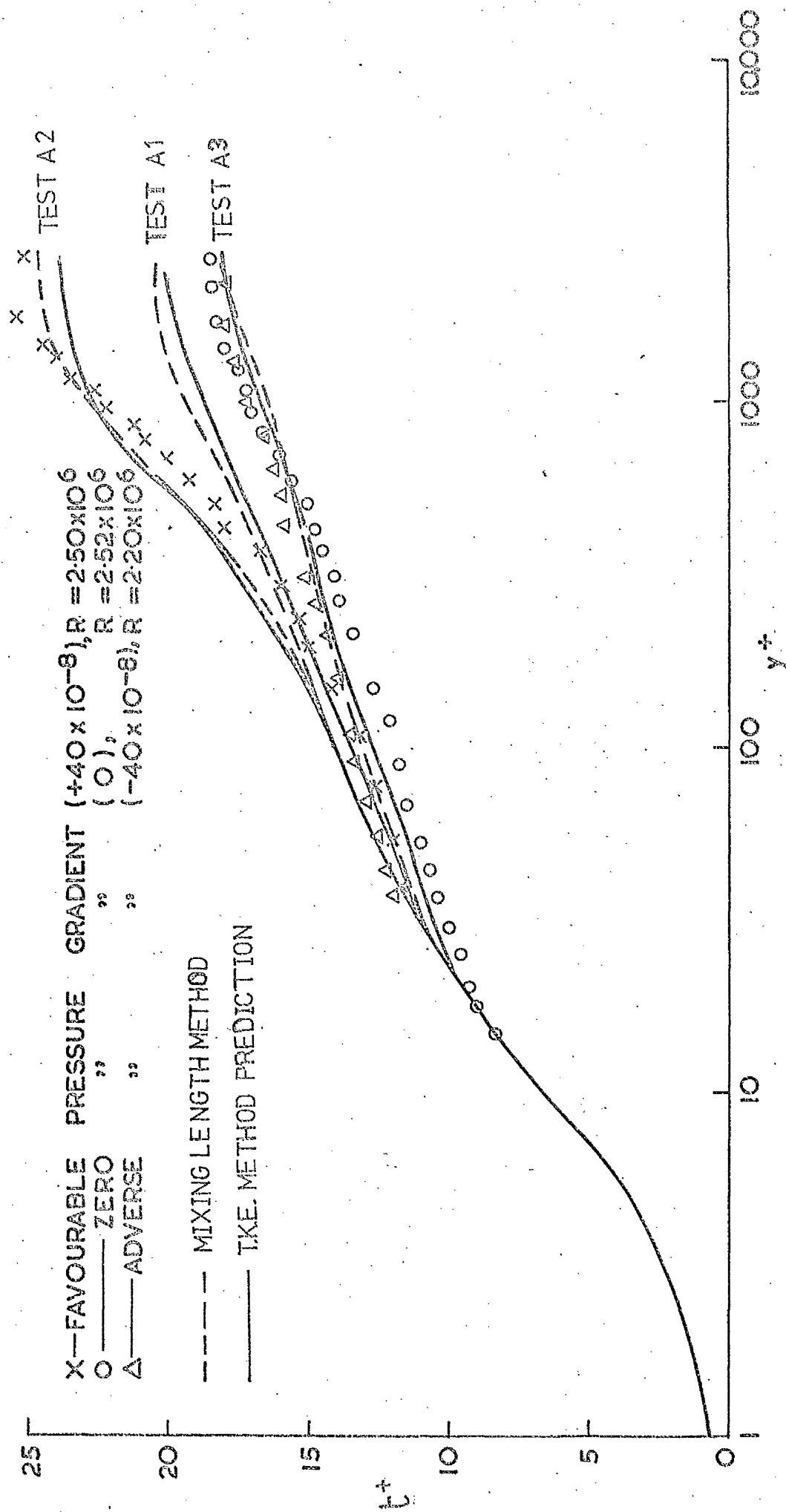


FIG 6 PREDICTIONS AND MEASUREMENTS OF DIMENSIONLESS TEMPERATURE
 PROFILES—CONSTANT PRESSURE GRADIENT PARAMETERS.

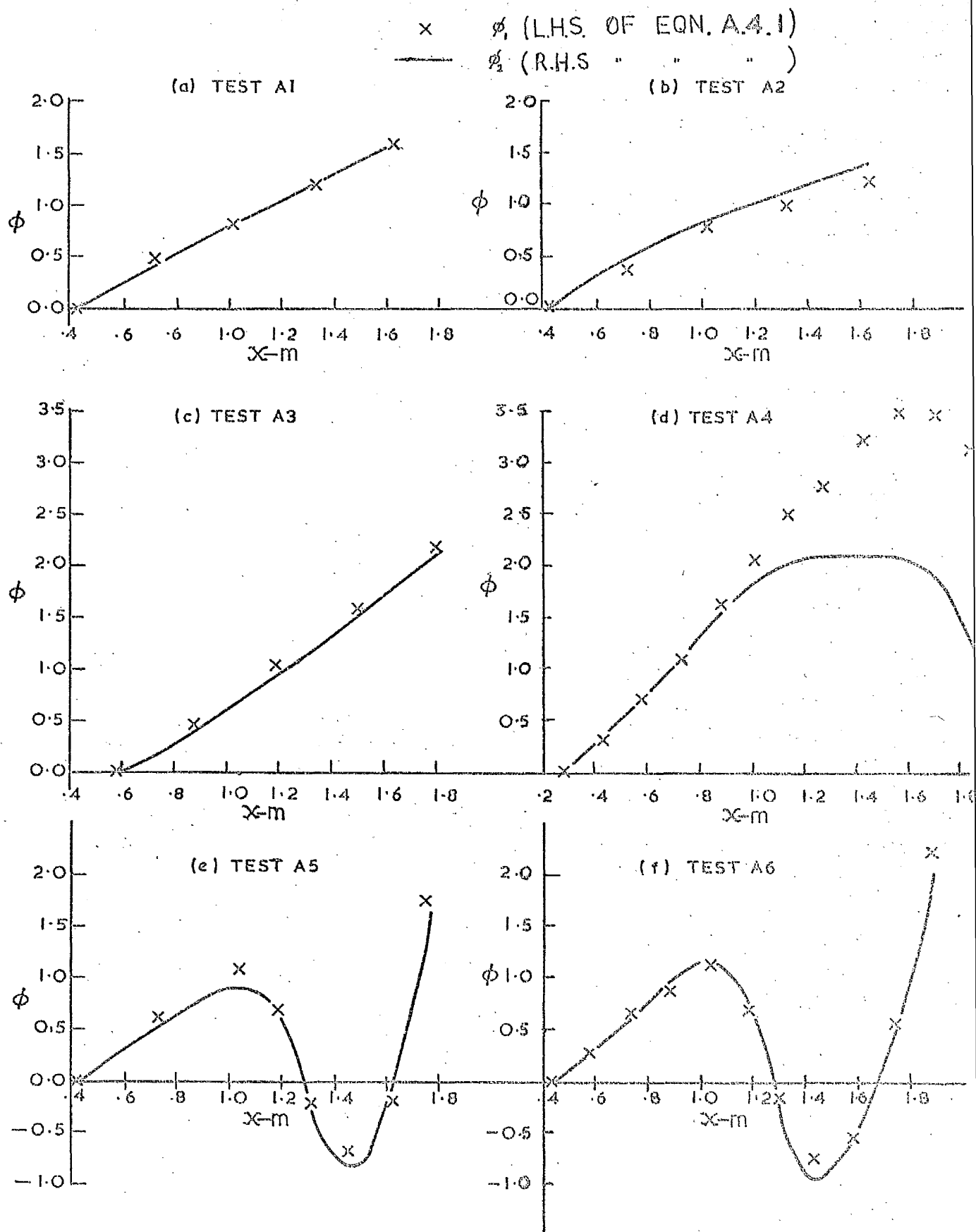


FIG 7 TWO-DIMENSIONALITY CHECKS ON VELOCITY
BOUNDARY LAYERS

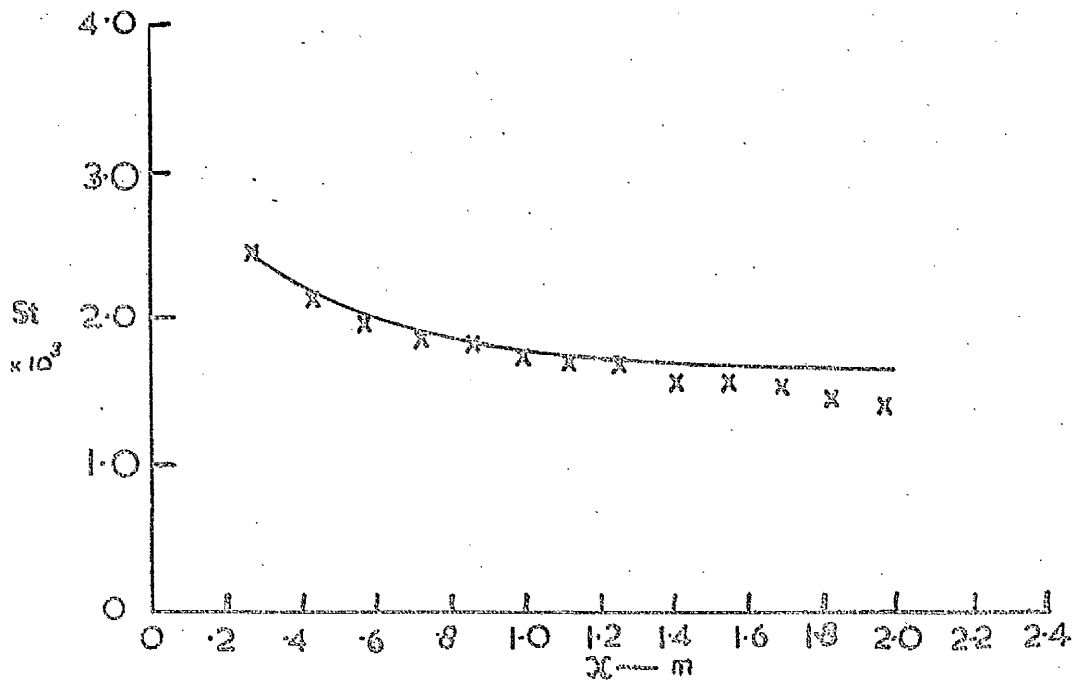
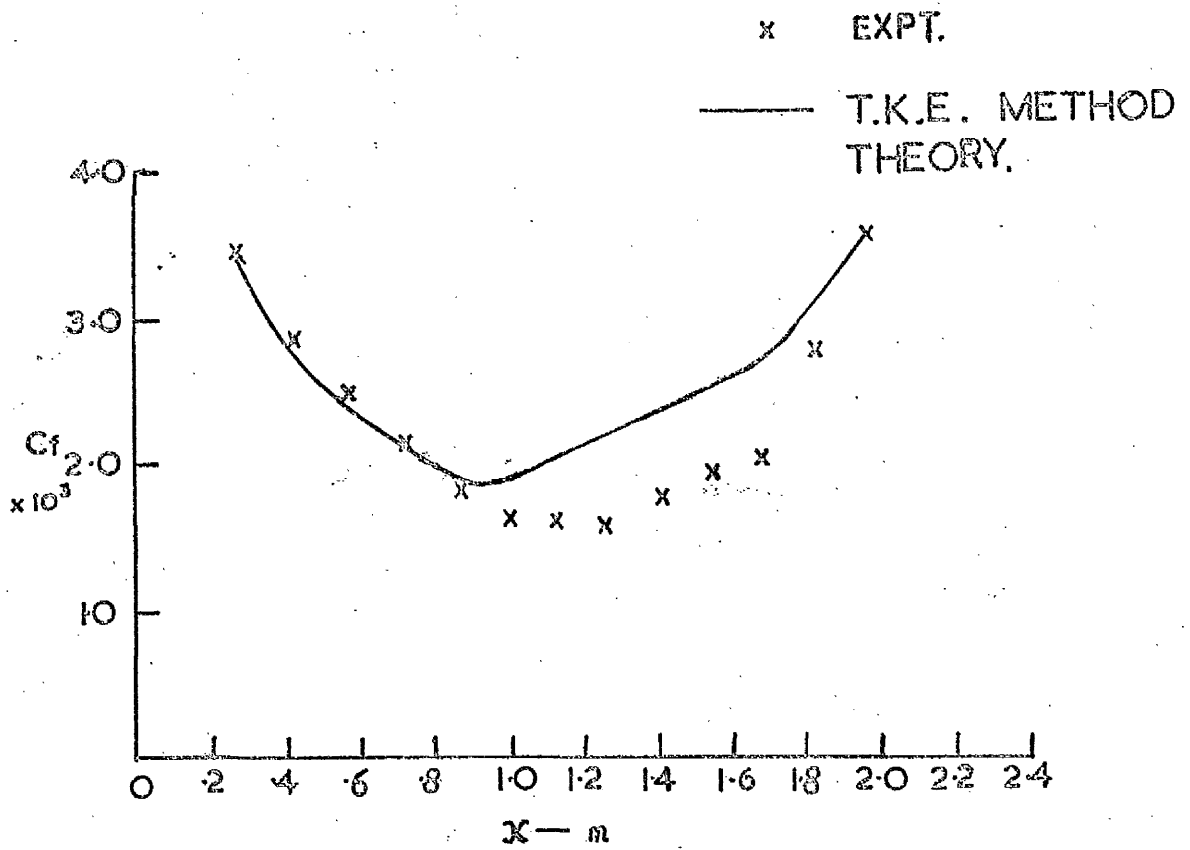


FIG. 8 PREDICTIONS AND MEASUREMENTS OF FRICTION
FACTOR AND STANTON NUMBER DISTRIBUTIONS
— TEST A4.

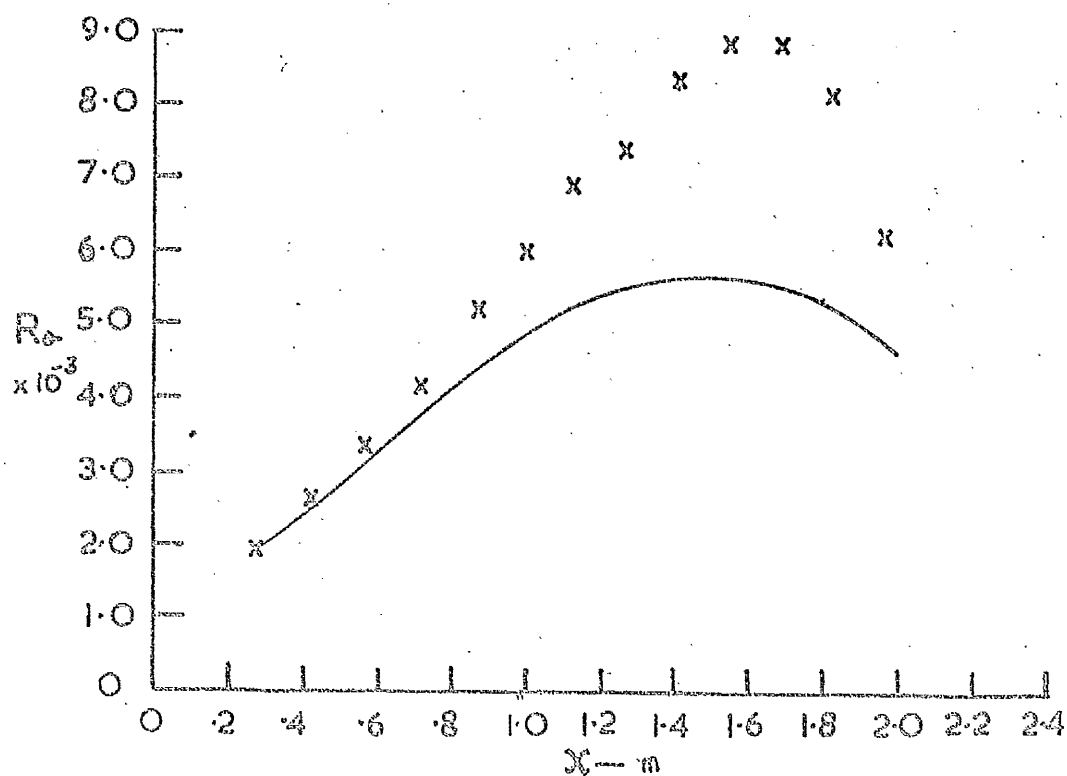
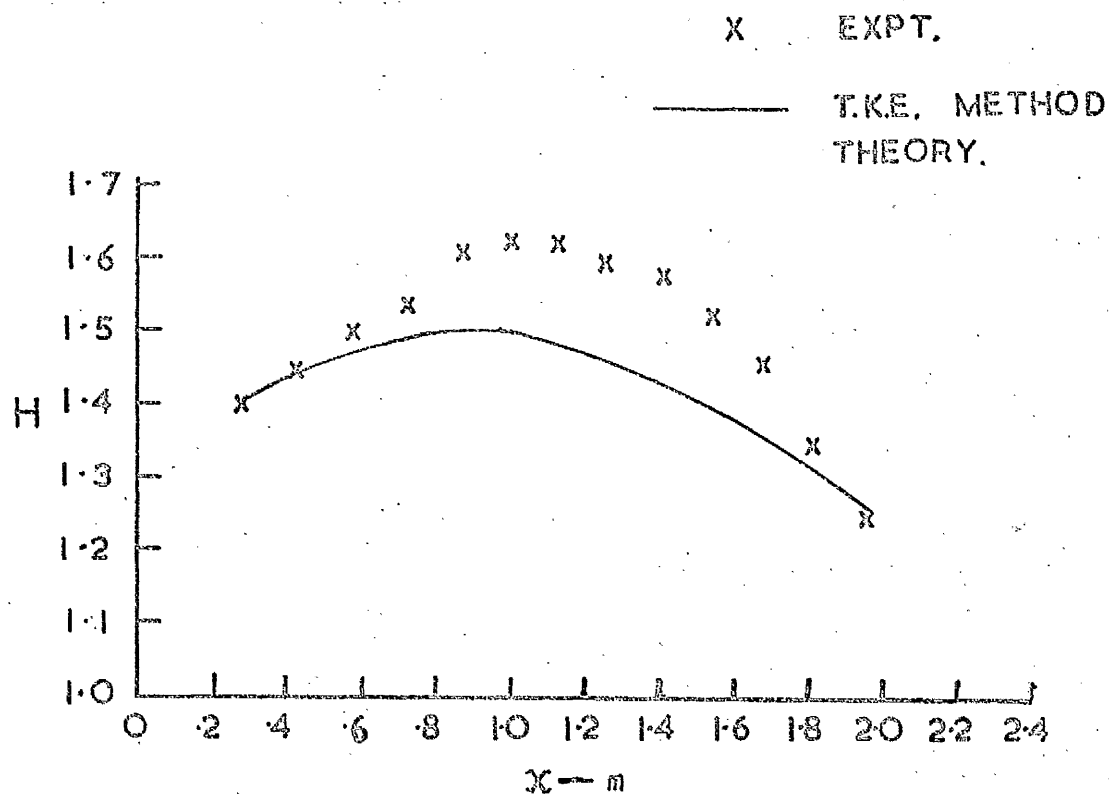


FIG 9 PREDICTIONS AND MEASUREMENTS OF
SHAPE FACTOR AND R_0 DISTRIBUTIONS
— TEST A4

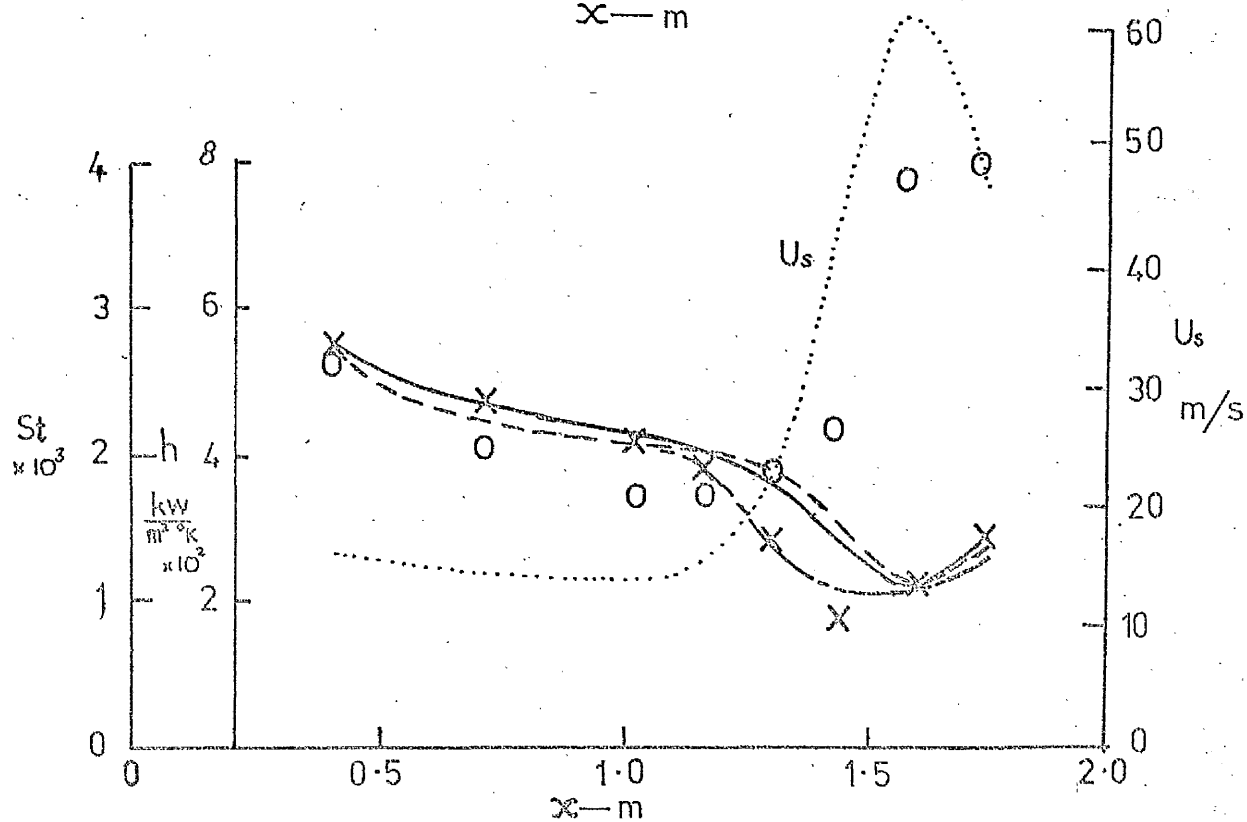
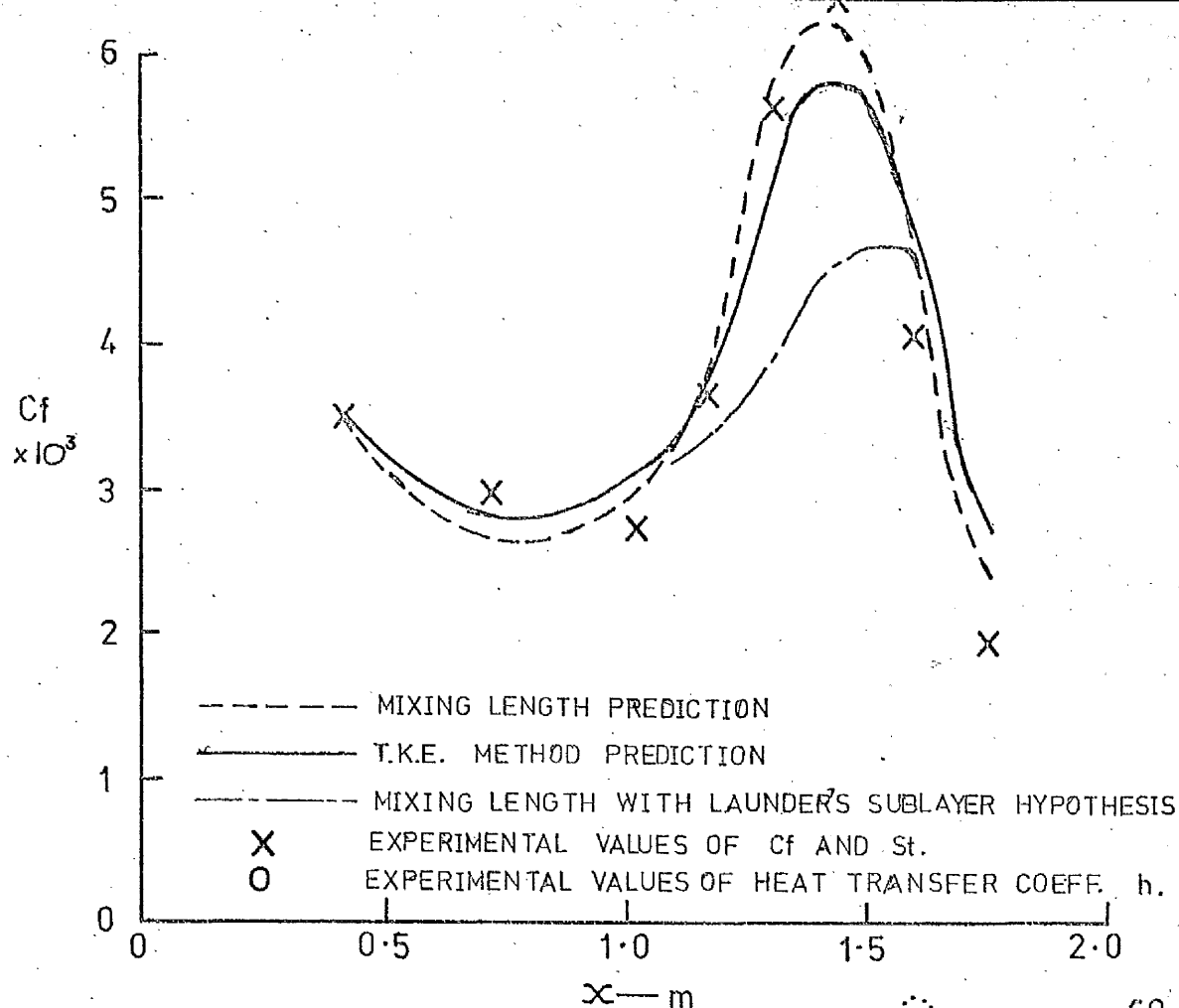


FIG 10 FRICTION FACTOR AND STANTON
NUMBER IN THE LAMINARIZATION
REGION—TEST A 5

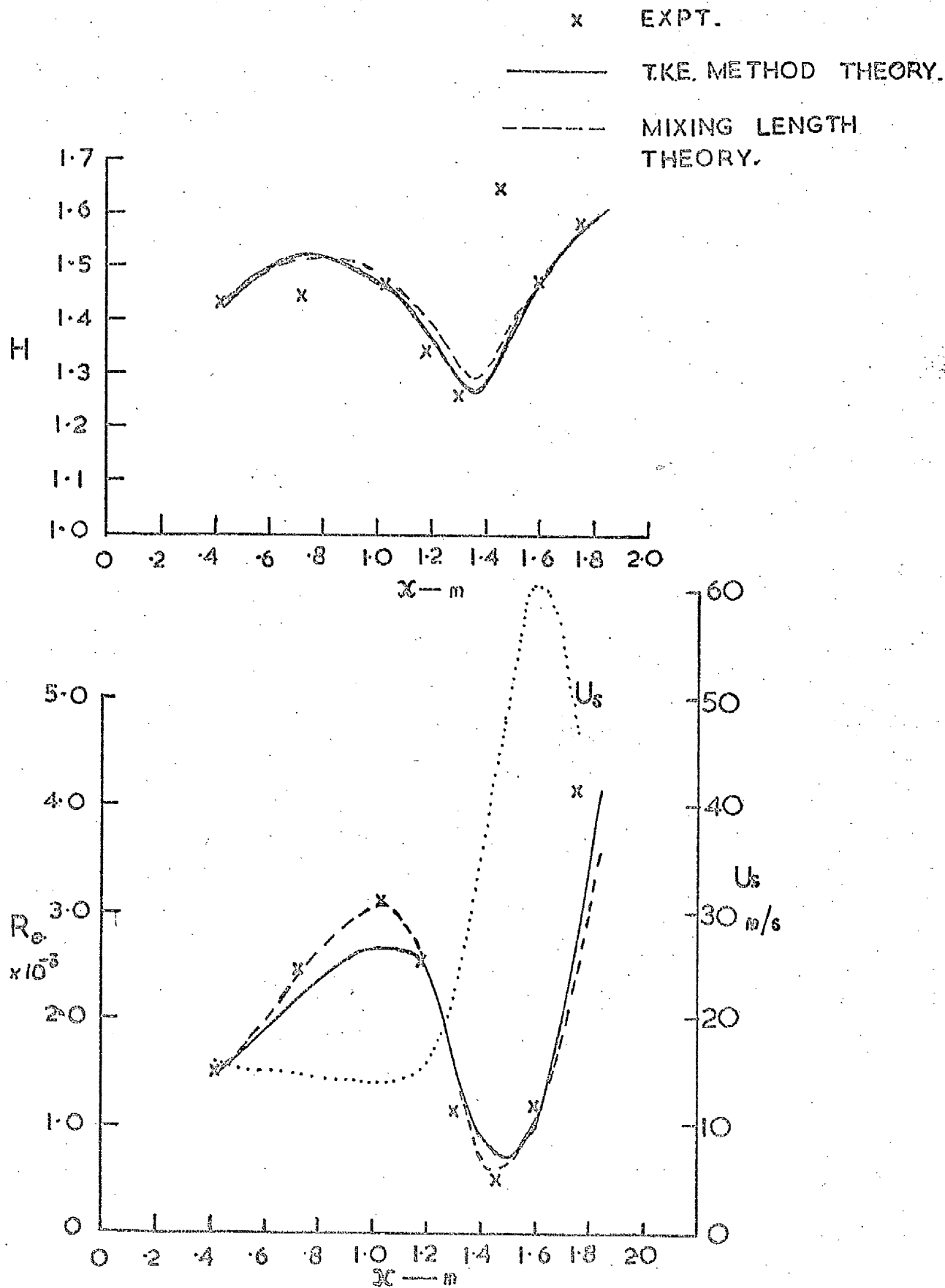


FIG II PREDICTION AND MEASUREMENTS OF H AND Re DISTRIBUTIONS IN THE LAMINARIZATION REGION — TEST A 5

| SYMBOL | STATION NO. | DISTANCE FROM LEADING EDGE | PRES. GRAD. PARAMETER $\frac{2\nu}{U_s^2} \frac{dU_s}{dx}$ |
|----------|-------------|----------------------------|--|
| o | 3 | 1.029m | $+0.104 \times 10^{-6}$ |
| x | 6 | 1.450m | $+2.990 \times 10^{-6}$ |
| Δ | 7 | 1.600m | $+0.363 \times 10^{-6}$ |

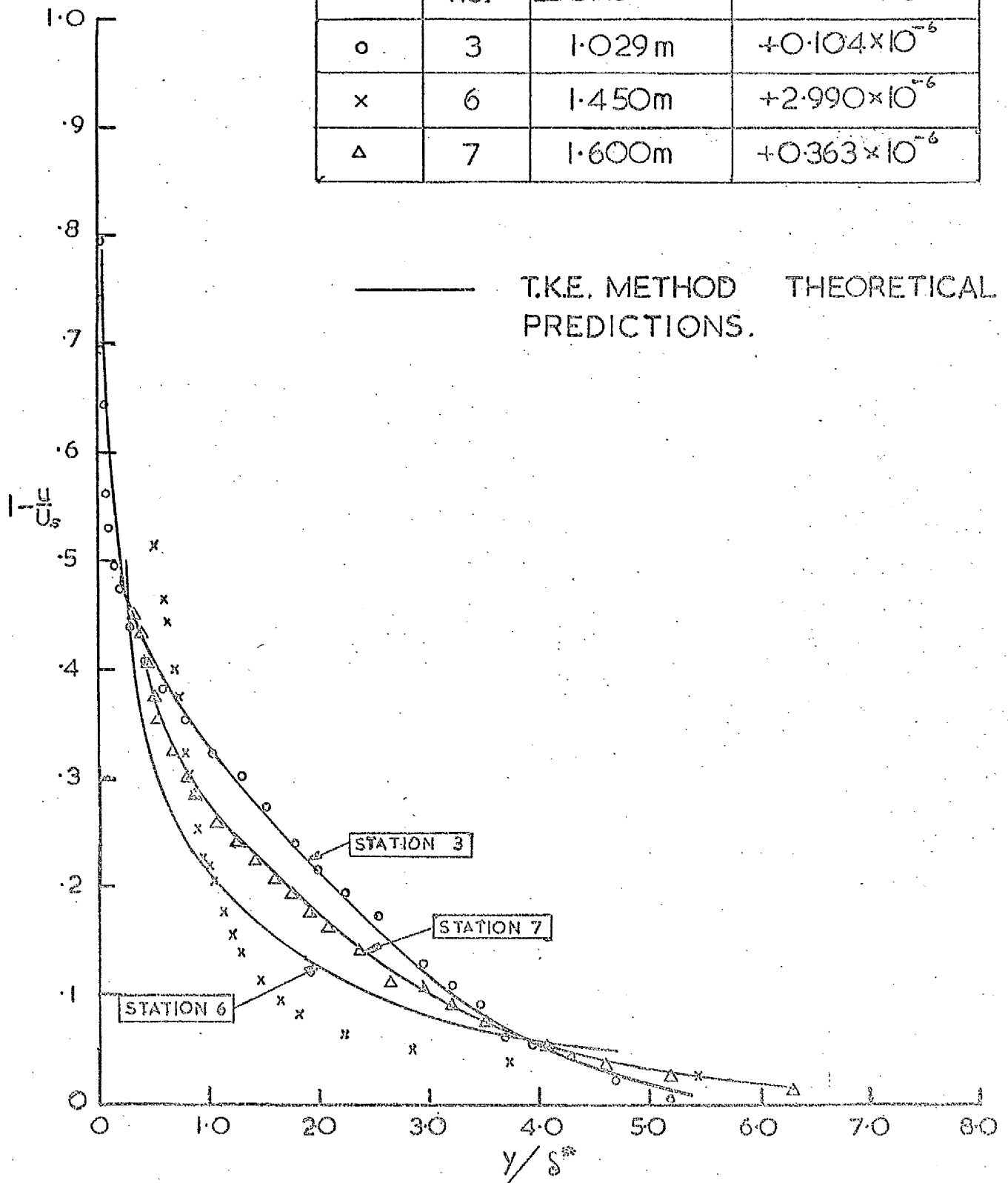


FIG 12 PREDICTIONS AND MEASUREMENTS OF DIMENSIONLESS VELOCITY PROFILES

| SYMBOL | STATION NO. | DISTANCE FROM LEADING EDGE | PRES. GRAD. PARAMETER |
|----------|-------------|----------------------------|-------------------------|
| o | 3 | 1.029 m | $+0.104 \times 10^{-6}$ |
| x | 6 | 1.450 m | $+2.990 \times 10^{-6}$ |
| Δ | 7 | 1.600 m | $+0.363 \times 10^{-6}$ |

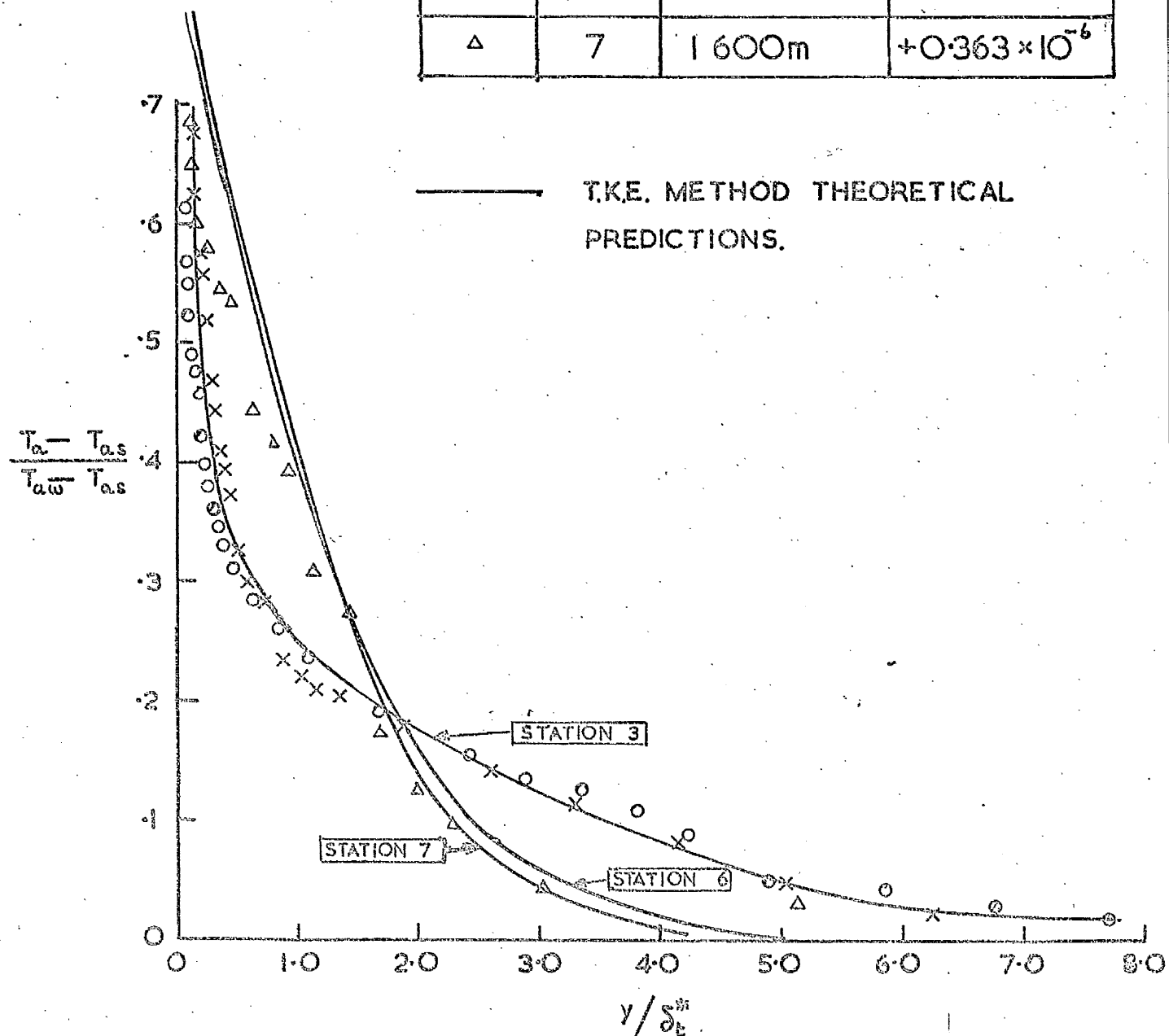
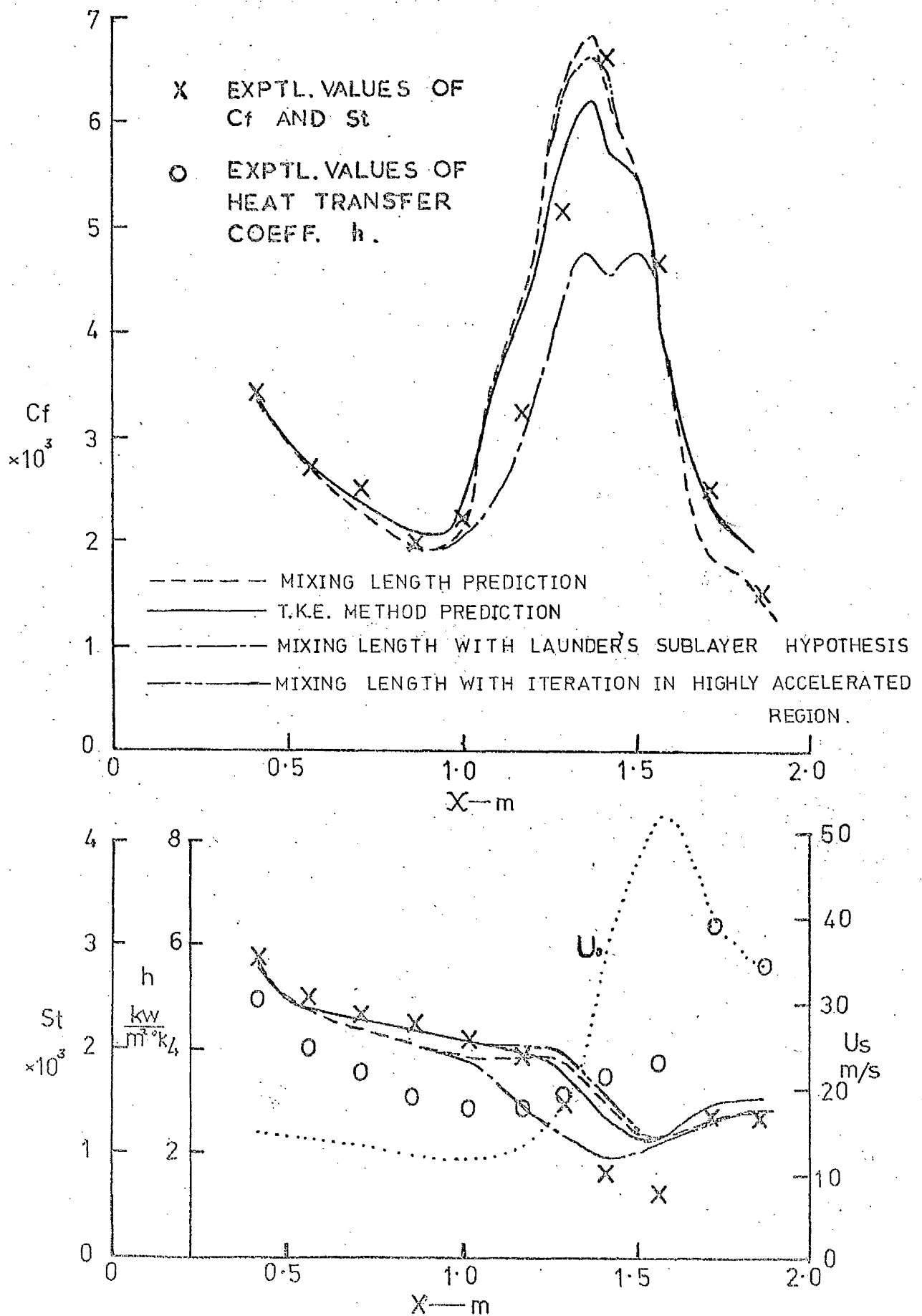


FIG. 13 PREDICTIONS AND MEASUREMENTS OF DIMENSIONLESS TEMPERATURE PROFILES



**FIG 14 FRICTION FACTOR AND STANTON
NUMBER IN THE LAMINARIZATION
REGION—TEST A6**

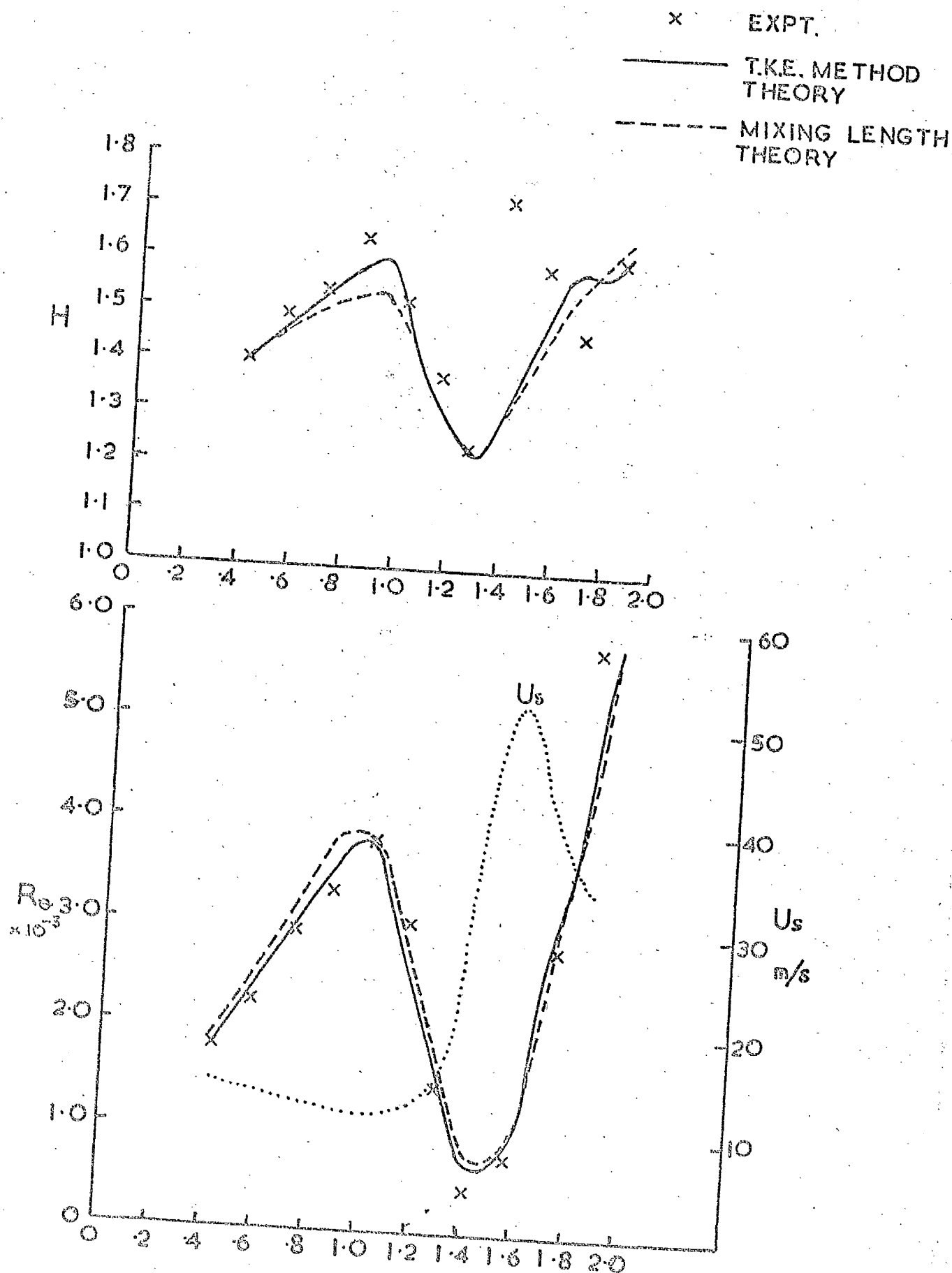


FIG 15 PREDICTION AND MEASUREMENT OF H
 AND Re DISTRIBUTIONS IN THE
 LAMINARIZATION REGION — TEST A6

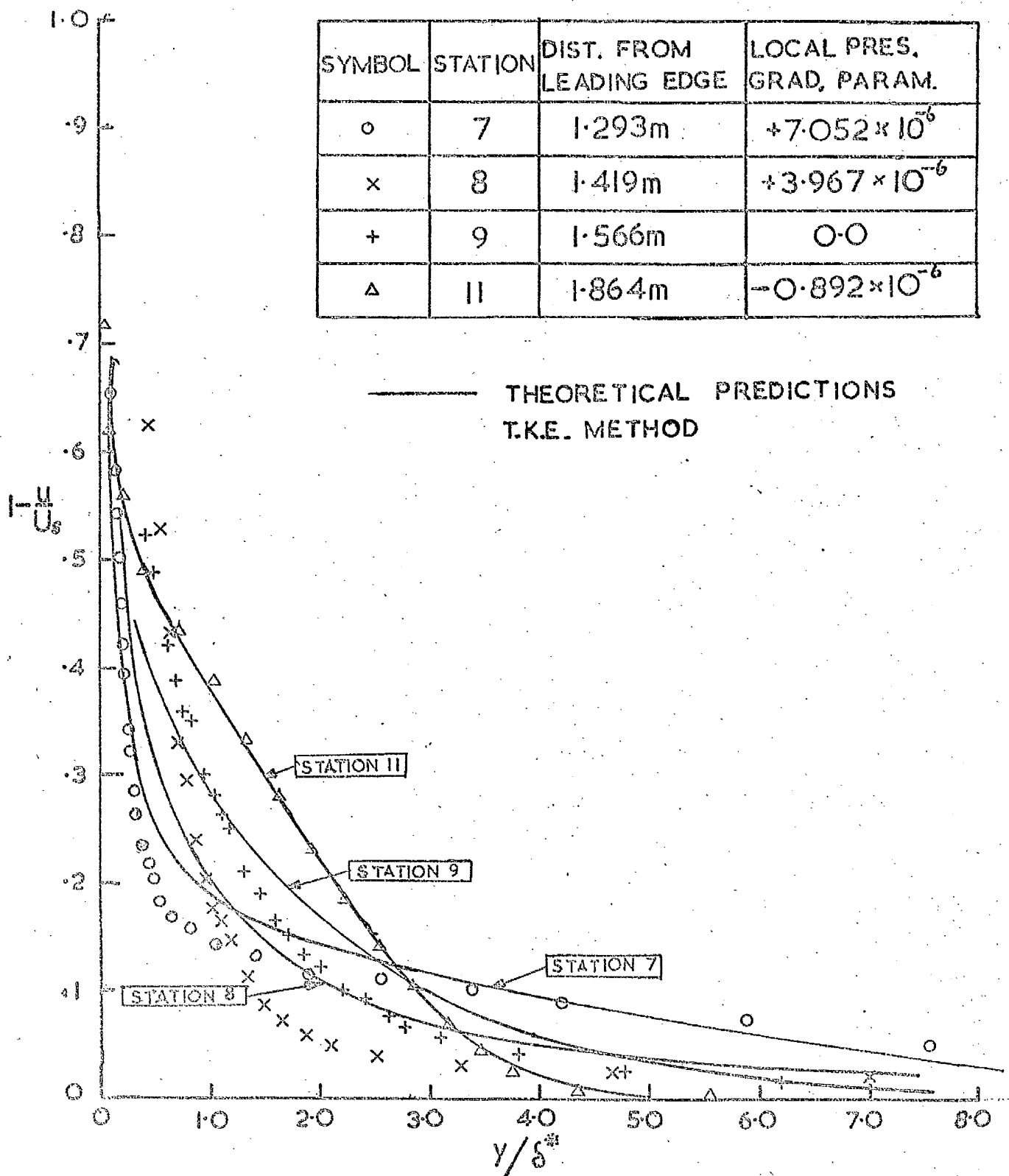


FIG 16 PREDICTIONS AND MEASUREMENTS OF
DIMENSIONLESS VELOCITY PROFILES

| SYMBOL | STATION | DIST. FROM LEADING EDGE | LOCAL PRES. GRAD. PARAM. |
|----------|---------|-------------------------|--------------------------|
| o | 7 | 1.293m | $+7.052 \times 10^{-6}$ |
| x | 8 | 1.419m | $+3.967 \times 10^{-6}$ |
| + | 9 | 1.566m | 0.0 |
| Δ | 11 | 1.864m | -0.892×10^{-6} |

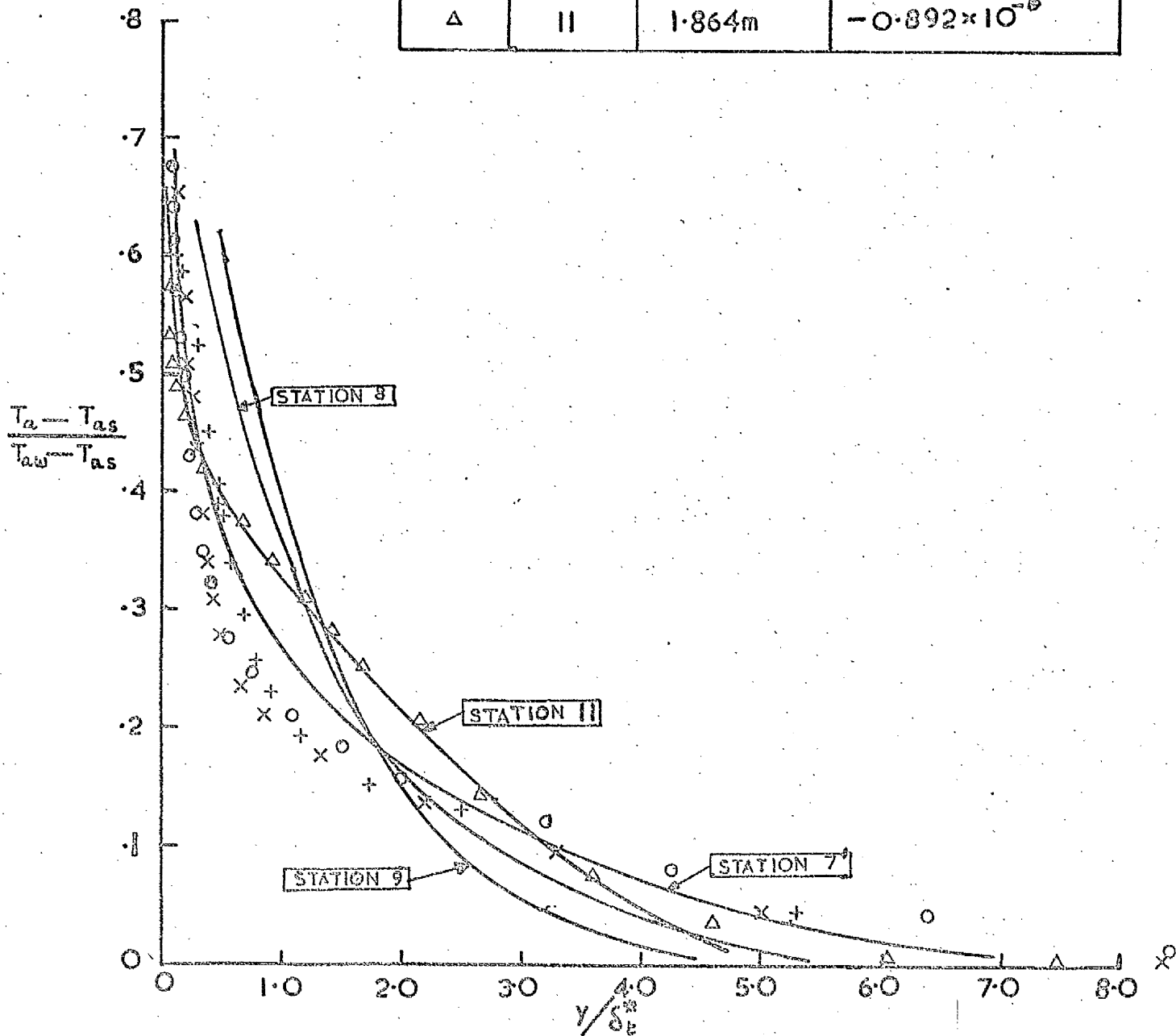
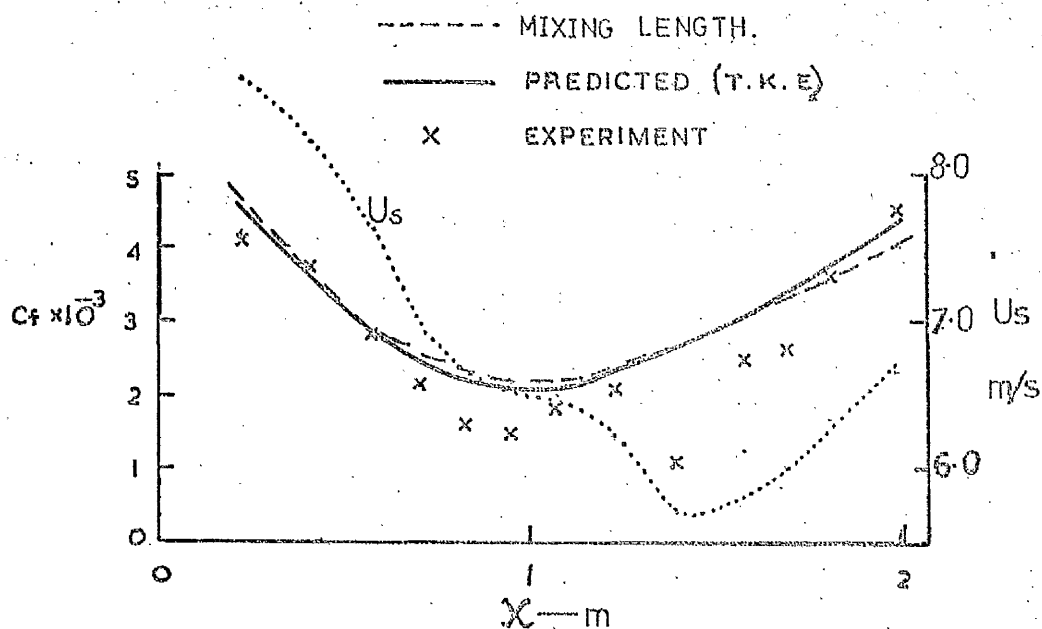
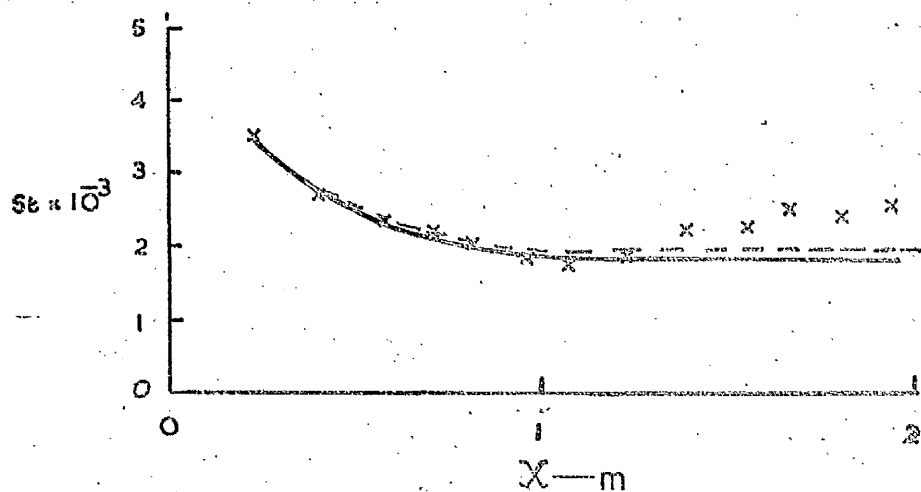


FIG 17 PREDICTION AND MEASUREMENTS OF
DIMENSIONLESS TEMPERATURE PROFILES

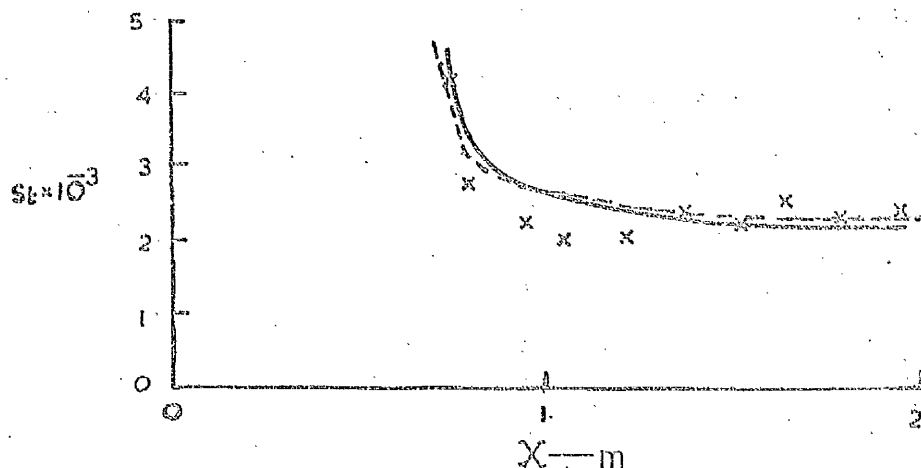
— TEST A6



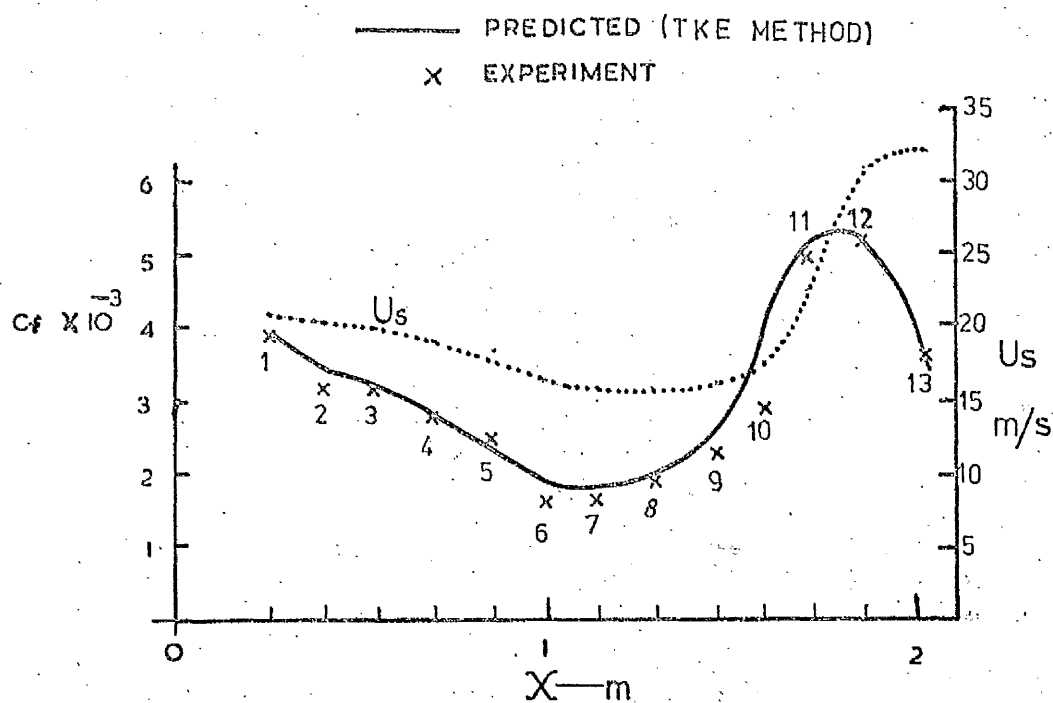
PREDICTION & EXPERIMENTAL VALUES OF ($C_f \sim X$) TEST A7



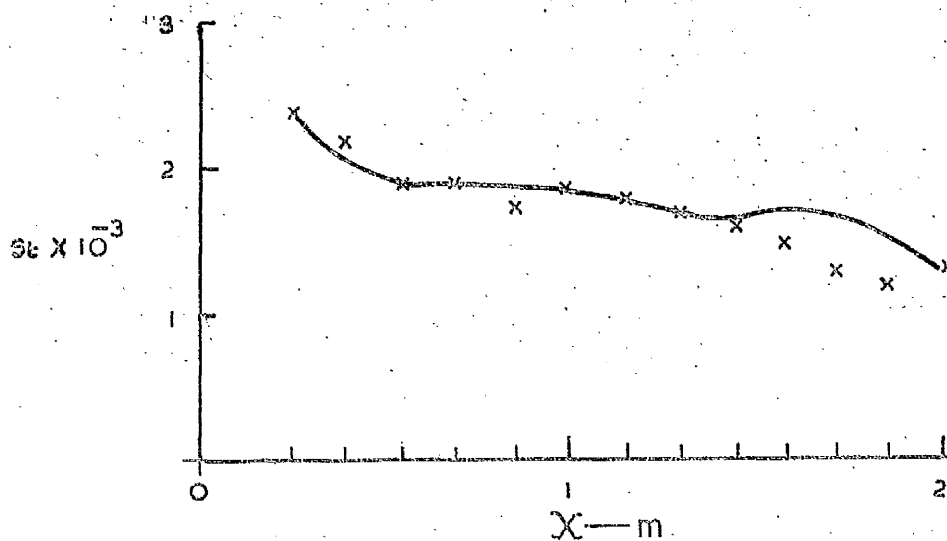
PREDICTION & EXPERIMENTAL VALUES OF ($St \sim X$) TEST A7
HEAT APPLIED FROM THE LEADING EDGE



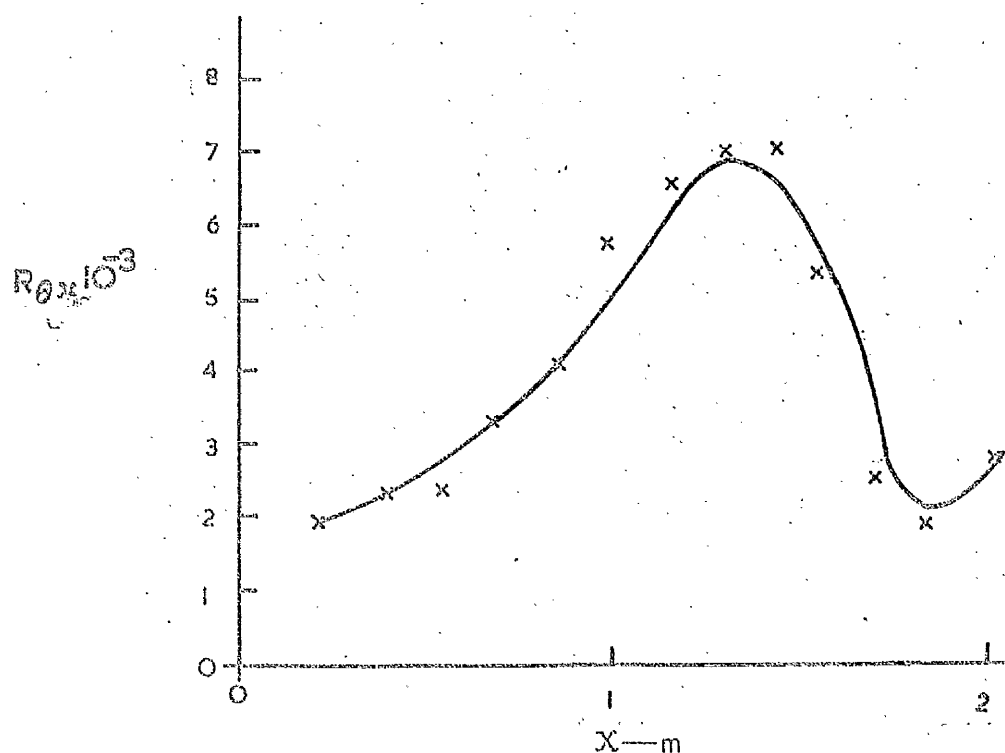
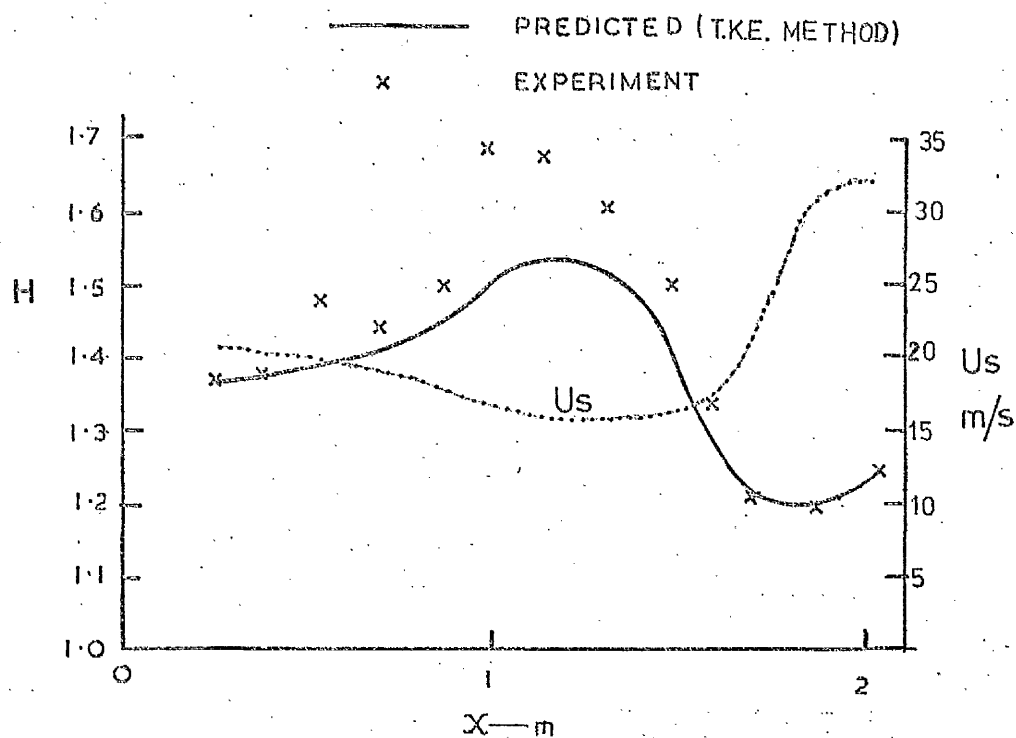
PREDICTION & EXPERIMENTAL VALUES OF ($St \sim X$) TEST A7
HEAT APPLIED AT A DISTANCE OF 0.686 M FROM
THE LEADING EDGE



PREDICTION & EXPERIMENTAL VALUES OF (C_f-x) TEST A 8



PREDICTION & EXPERIMENTAL VALUES OF $(St-x)$ TEST A 8

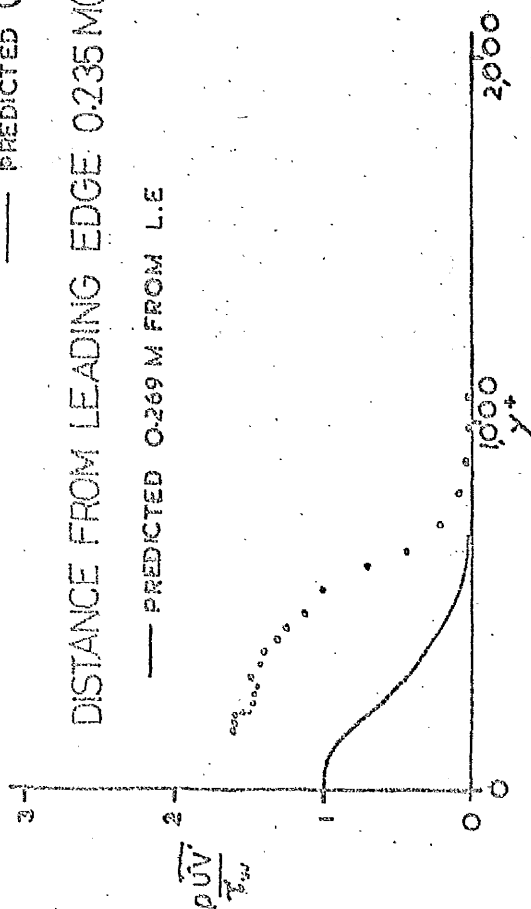


EXPERIMENTAL AND PREDICTED VALUES OF SHAPE

FACTOR H AND REYNOLDS NUMBER R_θ TEST A 8

FIG 20

° EXPERIMENTAL POINTS
— PREDICTED (T.K.E. METHOD)



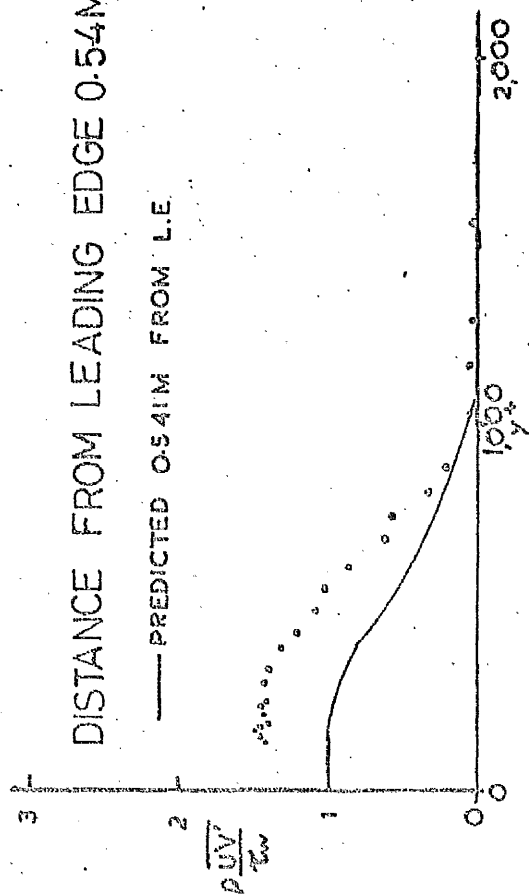
DISTANCE FROM LEADING EDGE 0.235 M (1)

— PREDICTED 0.385 M FROM L.E.

1000 2000

y^+

DISTANCE FROM LEADING EDGE 0.391 M (2)



DISTANCE FROM LEADING EDGE 0.541 M (3)

— PREDICTED 0.677 M FROM L.E.

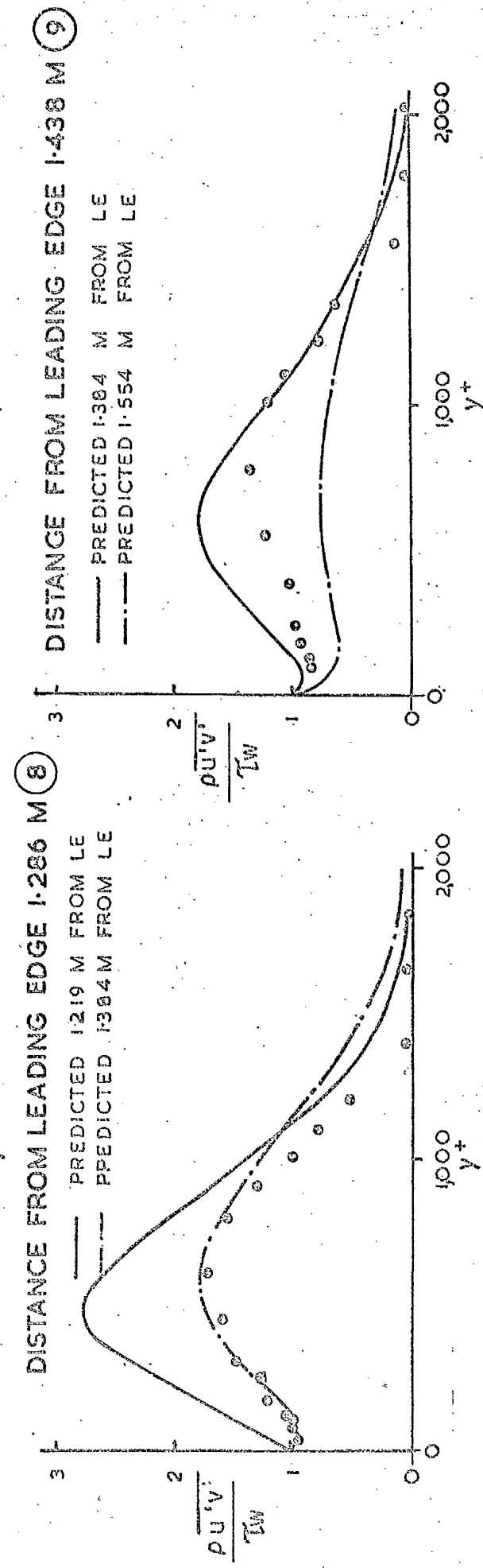
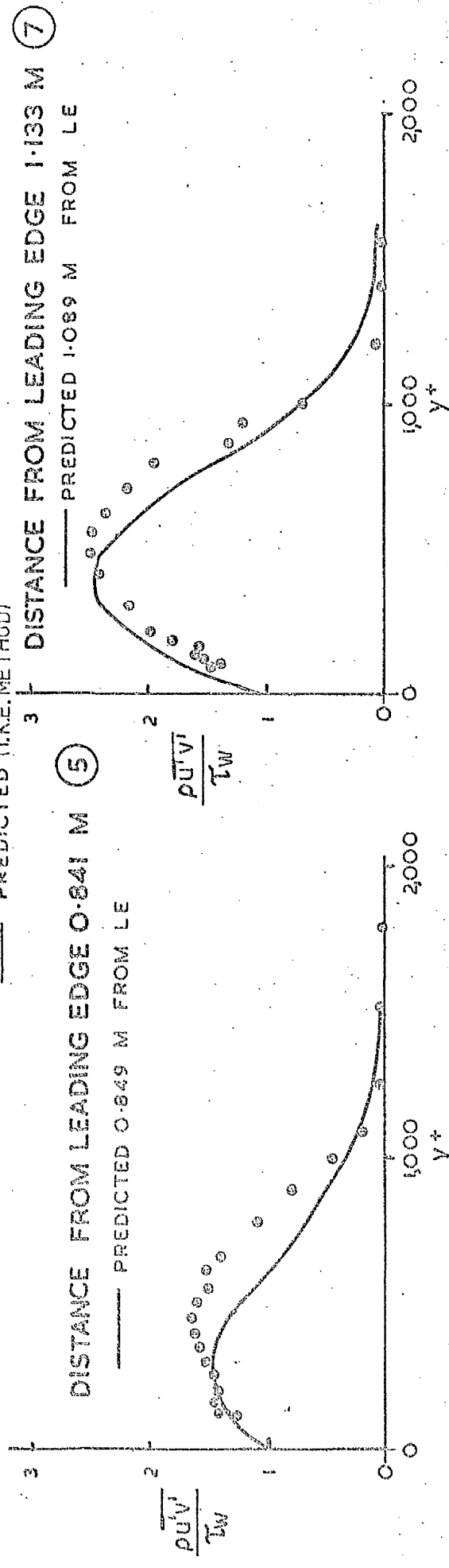
1000 2000

y^+

DISTANCE FROM LEADING EDGE 0.689 M (4)

EXPERIMENTAL & PREDICTED TURBULENT SHEAR STRESS PROFILES—TEST A8

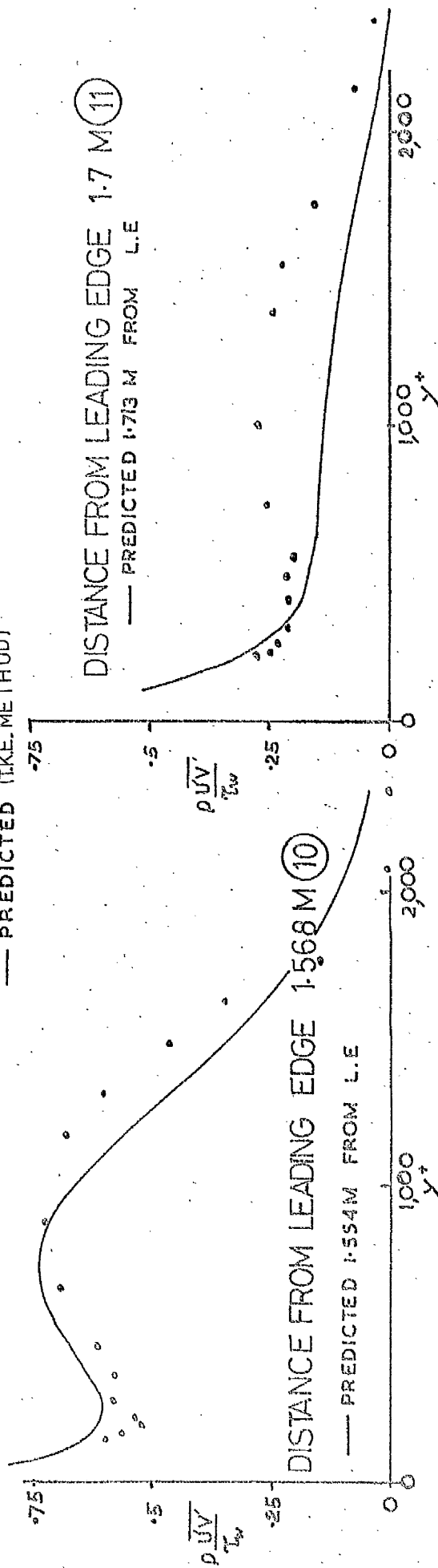
FIG 21



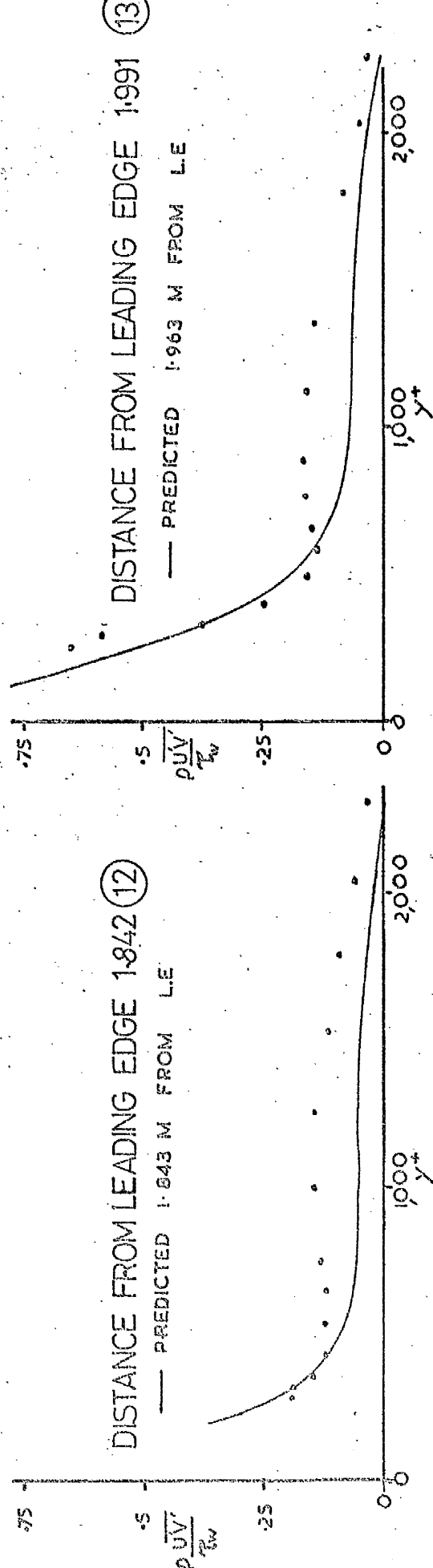
EXPERIMENTAL & PREDICTED TURBULENT SHEAR STRESS PROFILES—TEST A 8

FIG 22

• EXPERIMENTAL POINTS
— PREDICTED (TKE METHOD)



DISTANCE FROM LEADING EDGE 1.7 M (11)
— PREDICTED 1.713 M FROM L.E



DISTANCE FROM LEADING EDGE 1.991 (13)
— PREDICTED 1.963 M FROM L.E

EXPERIMENTAL & PREDICTED TURBULENT SHEAR STRESS PROFILES—TEST A 8

• EXPERIMENT
 — PREDICTED (I.K.E. THEORY)

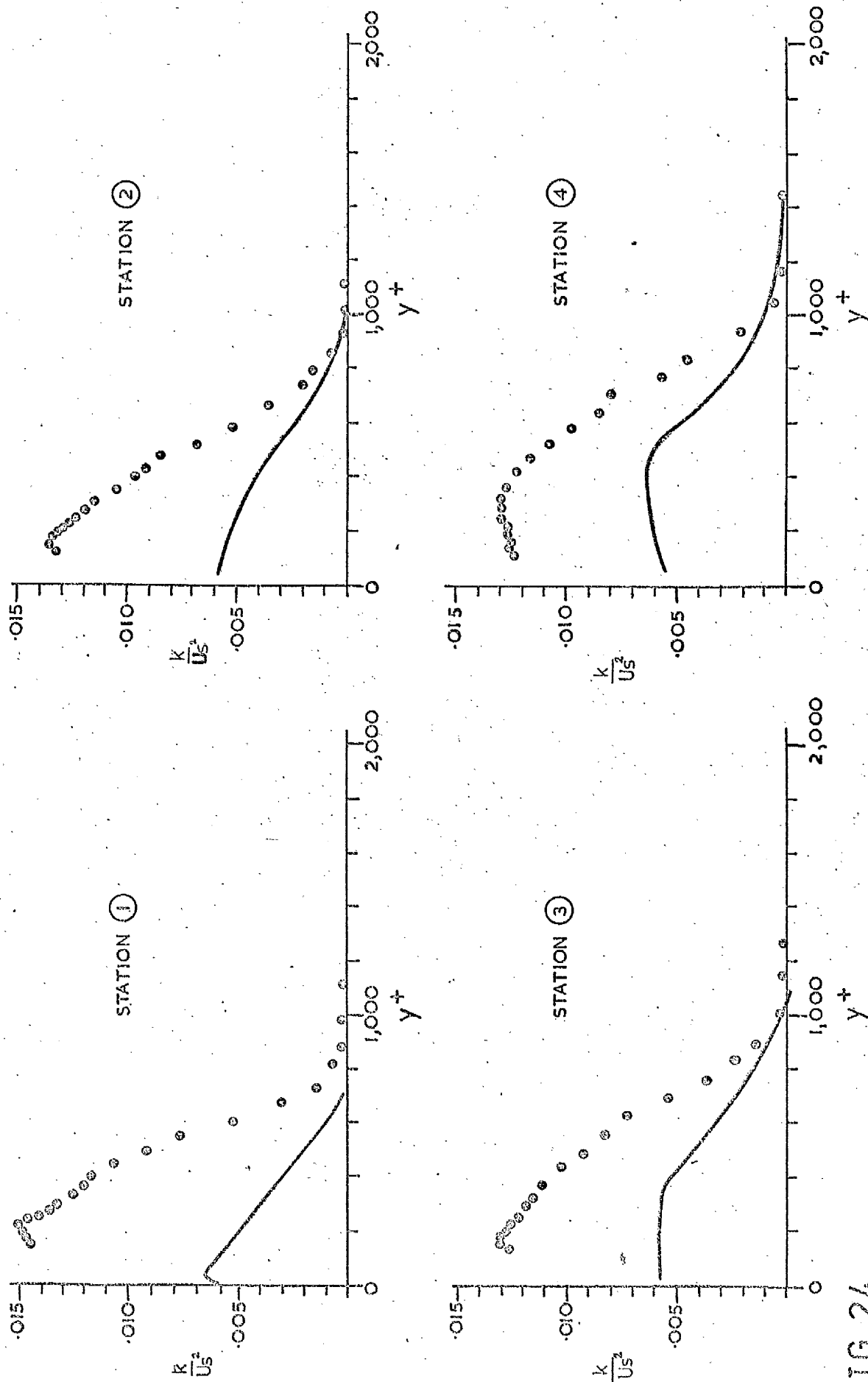
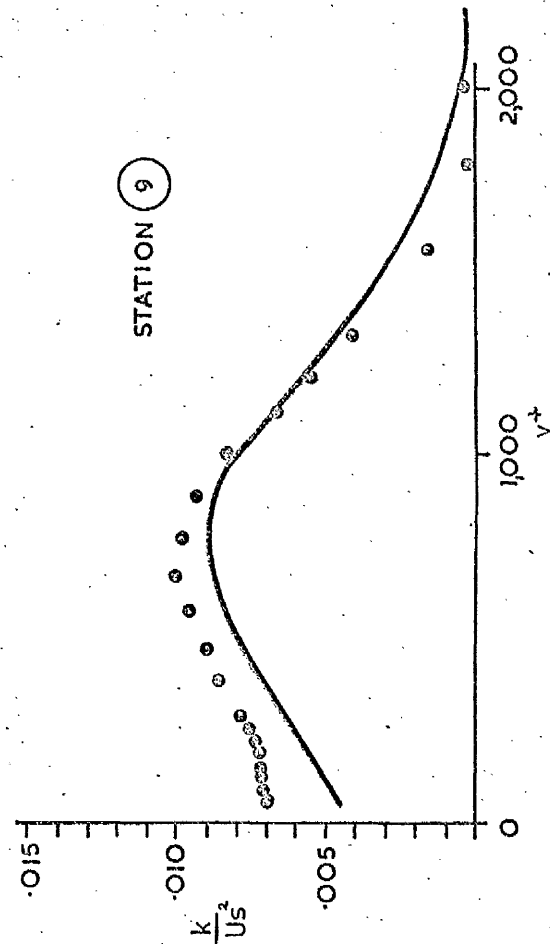
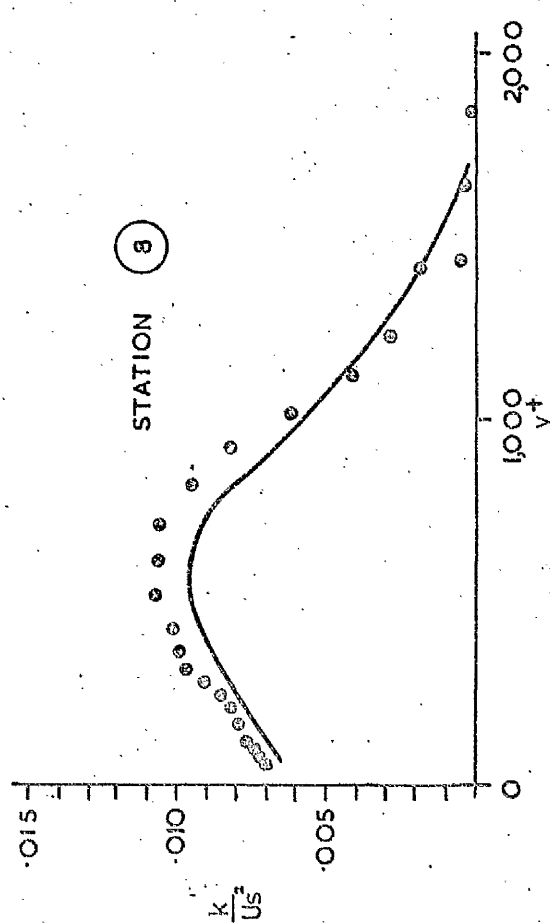
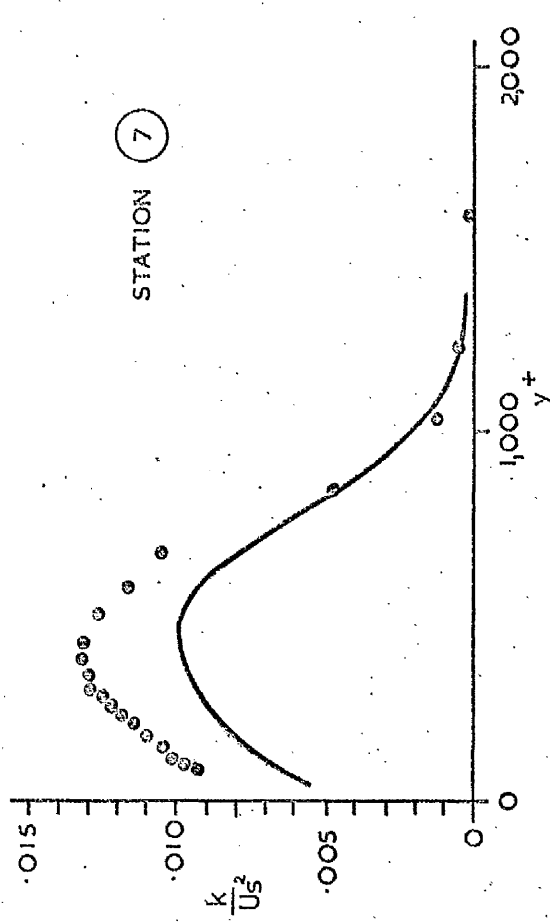
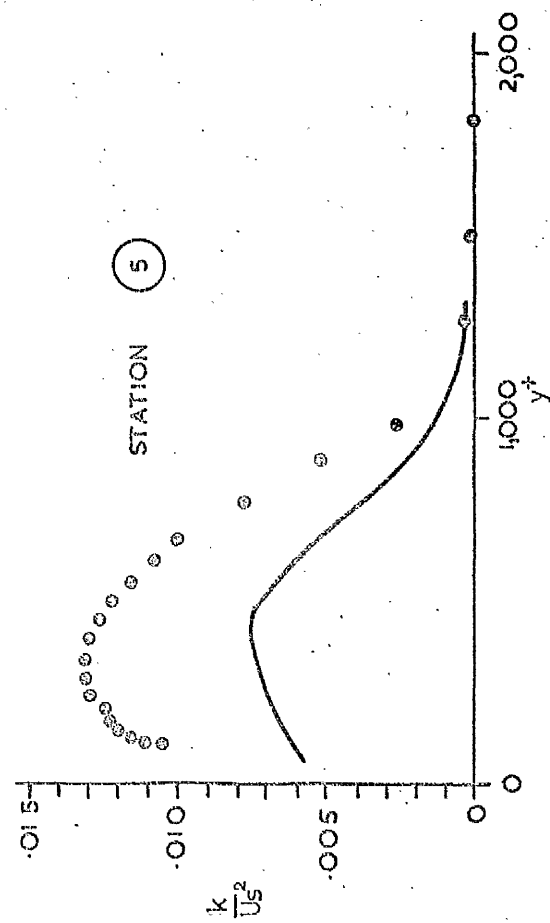
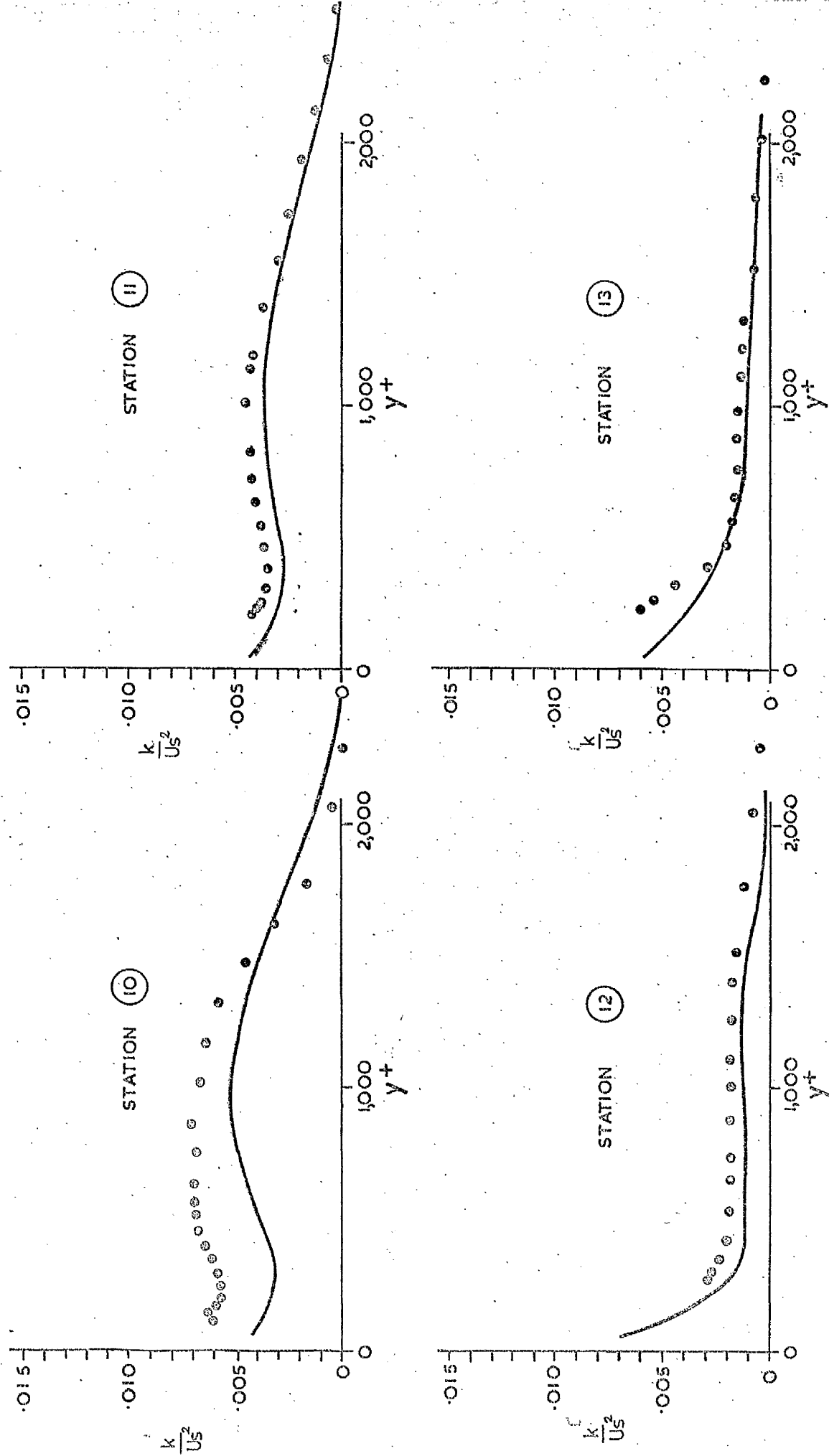


FIG 24



THEORETICAL AND EXPERIMENTAL PROFILES OF TURBULENT KINETIC ENERGY — TEST A 8

FIG 25



THEORETICAL AND EXPERIMENTAL PROFILES OF TURBULENT KINETIC ENERGY—TEST A8

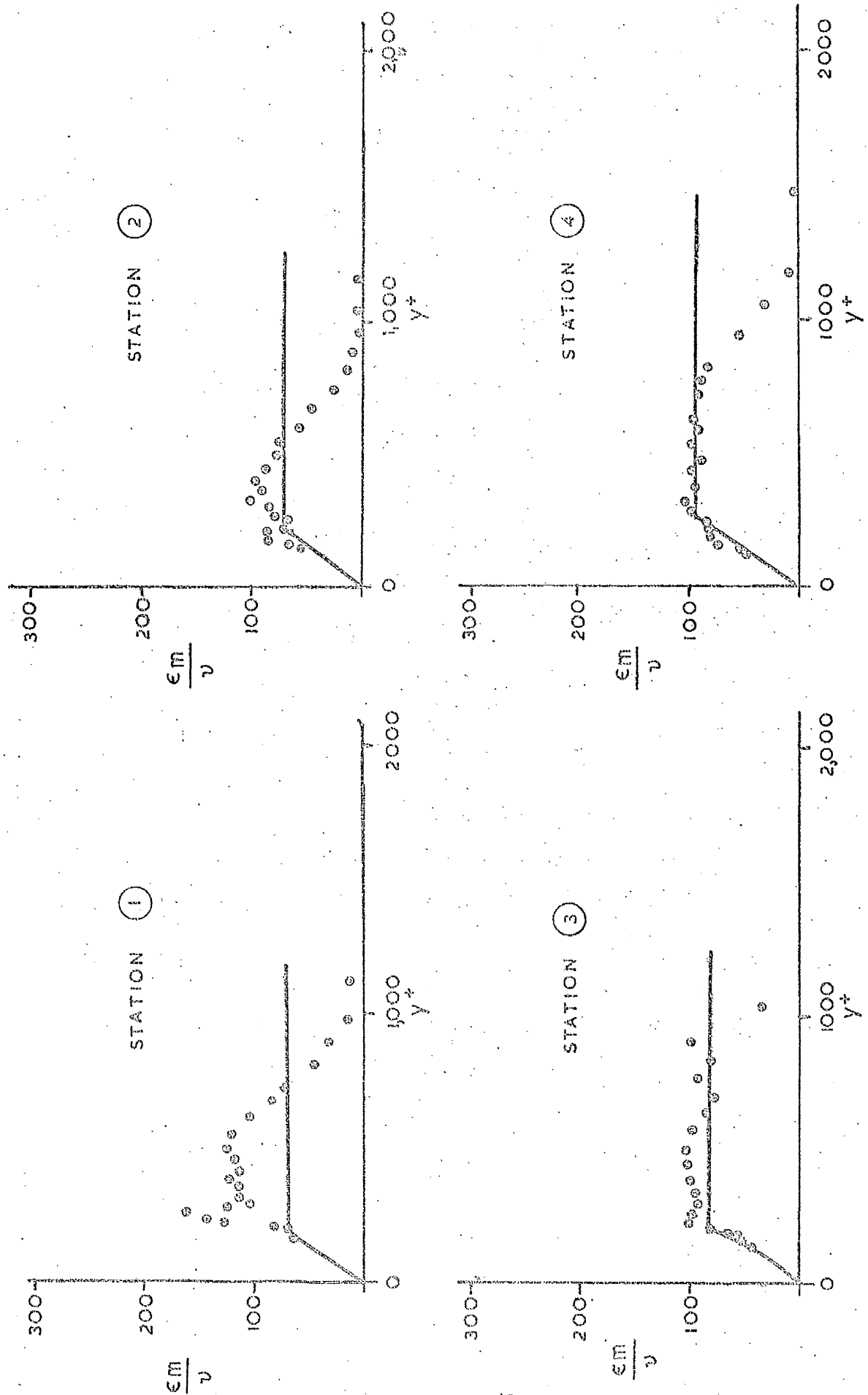


FIG 27

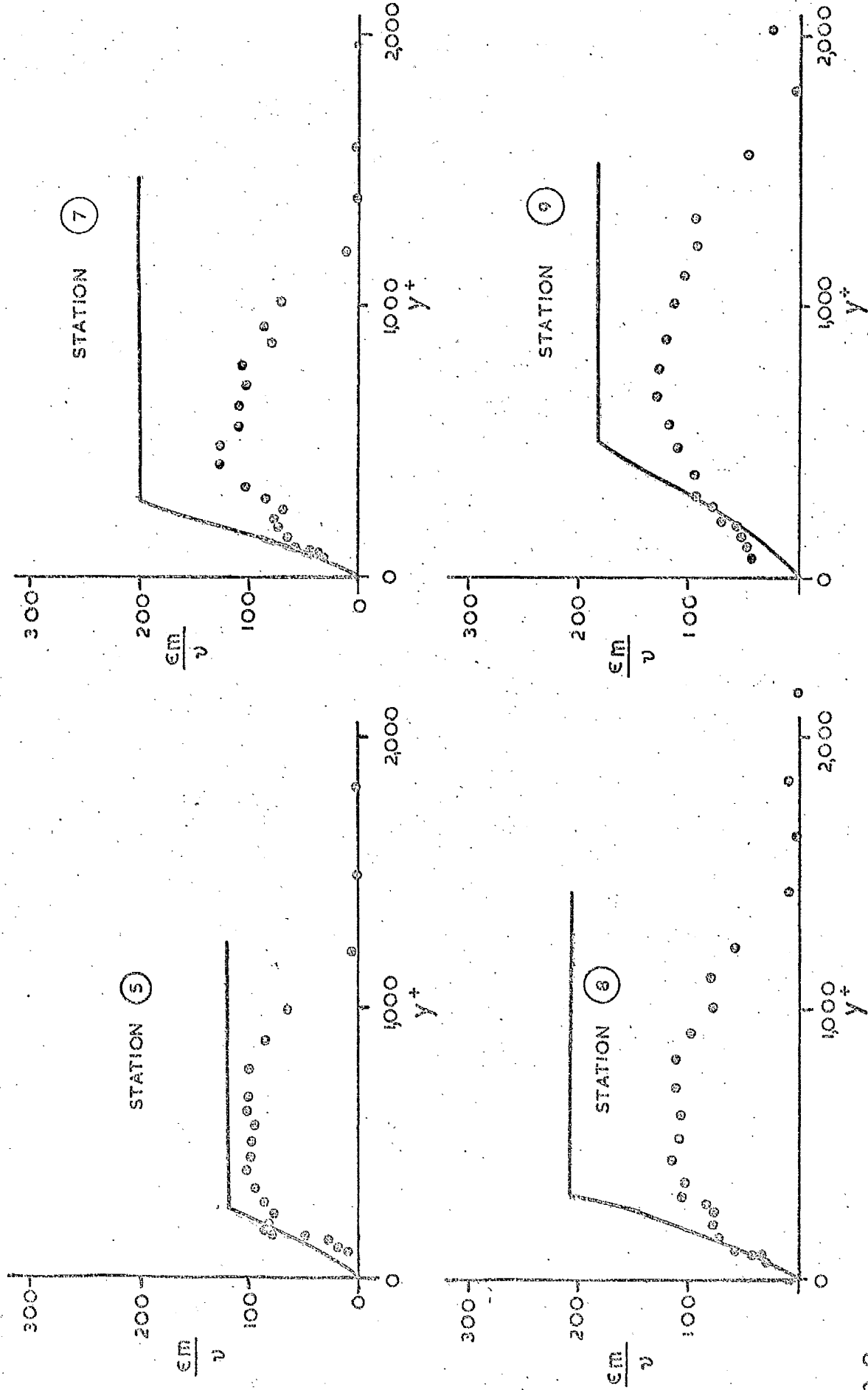


FIG 28

THEORETICAL AND EXPERIMENTAL PROFILES OF EDDY DIFFUSIVITY OF MOMENTUM

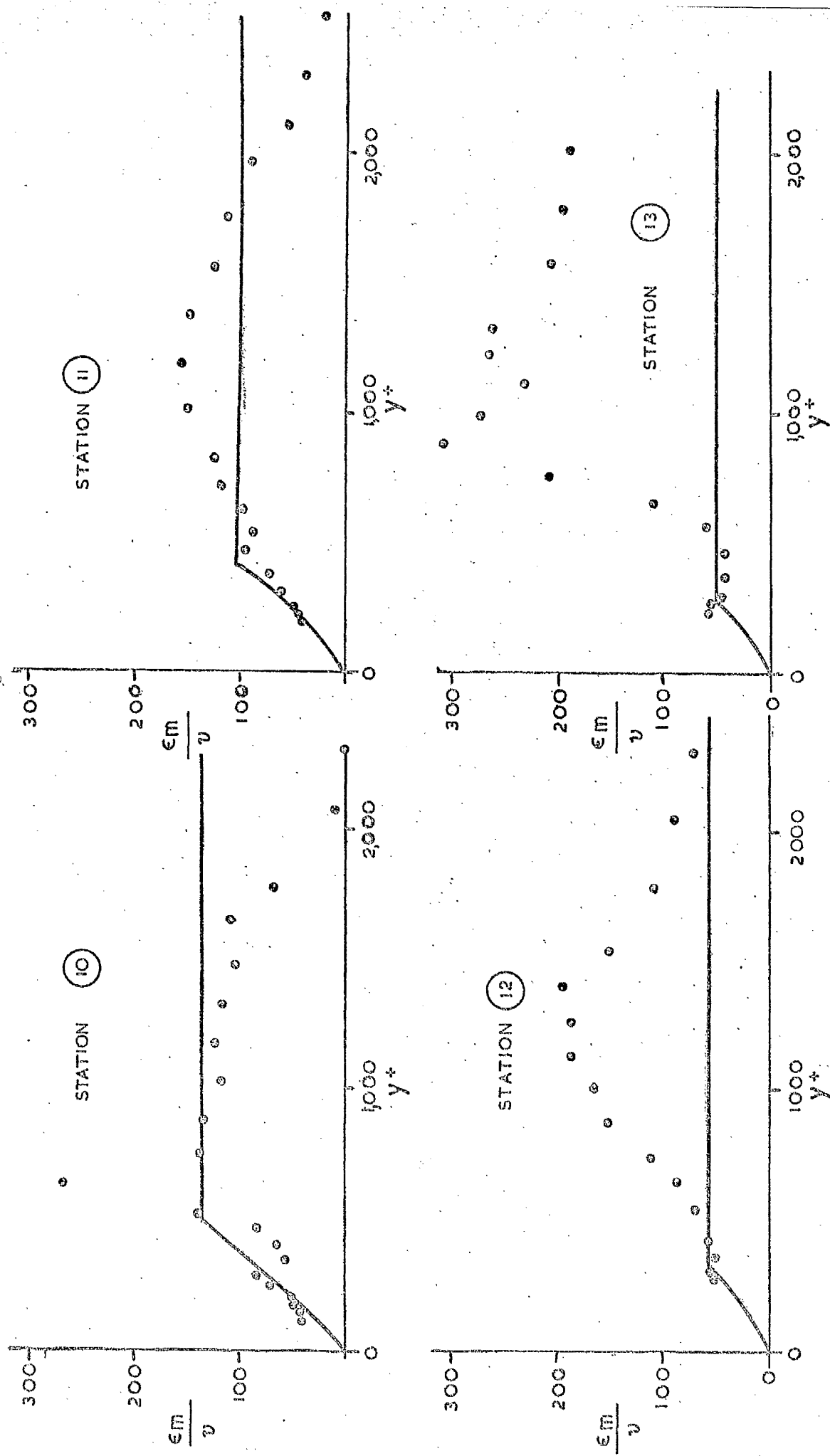


FIG 29

THEORETICAL AND EXPERIMENTAL PROFILES OF EDDY DIFFUSIVITY OF

MOMENTUM—TEST A8

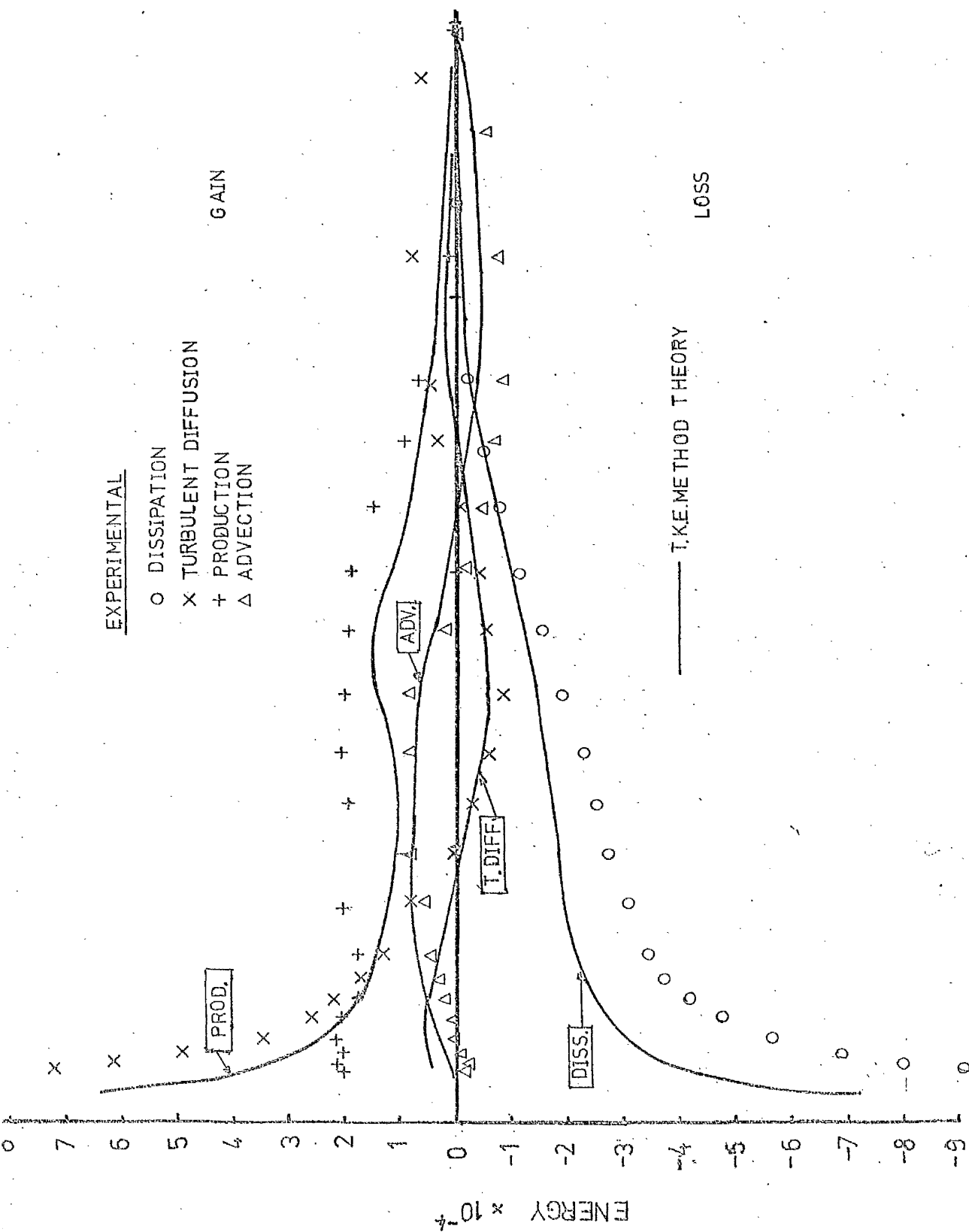


FIG 30 PREDICTED AND EXPERIMENTAL TURBULENT KINETIC
 ENERGY BALANCE—TEST A8—STATION 9

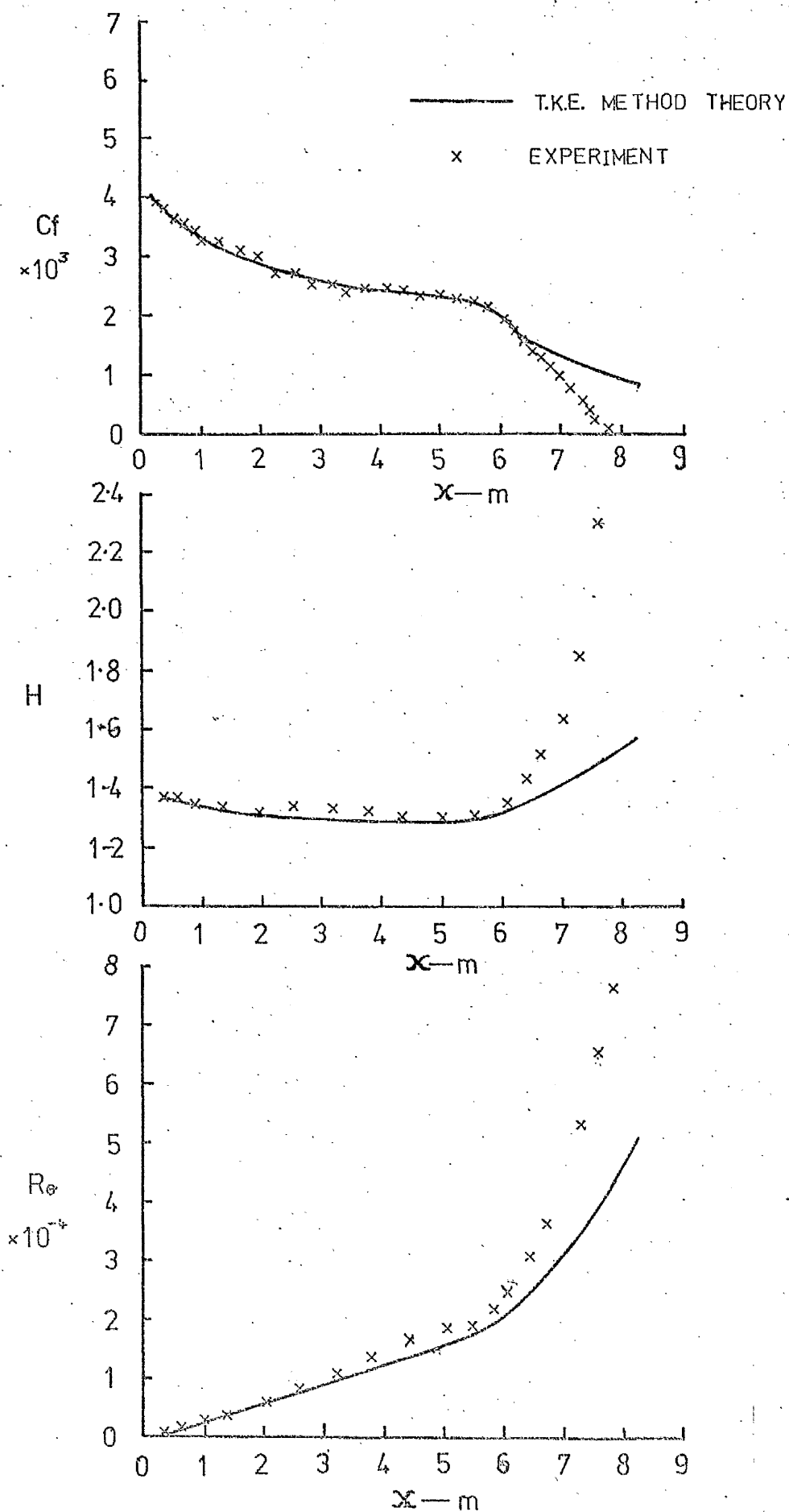
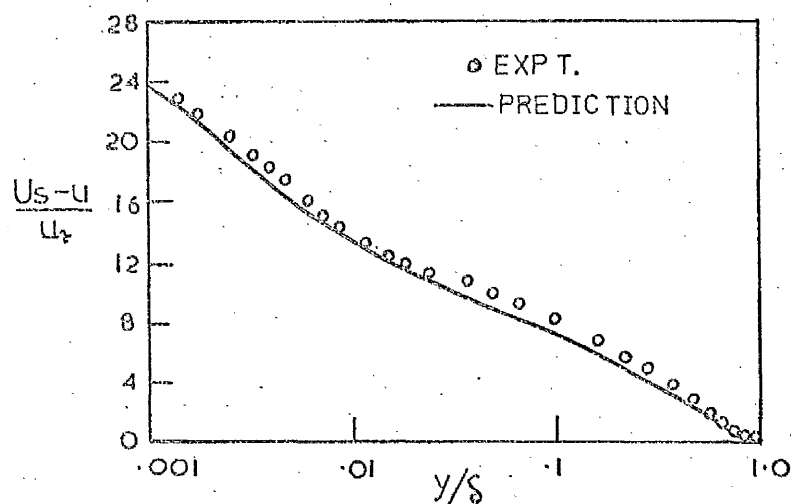
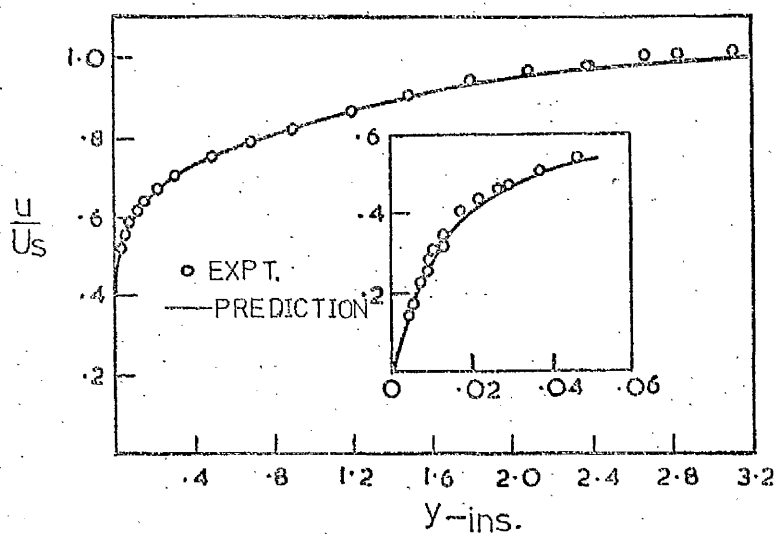


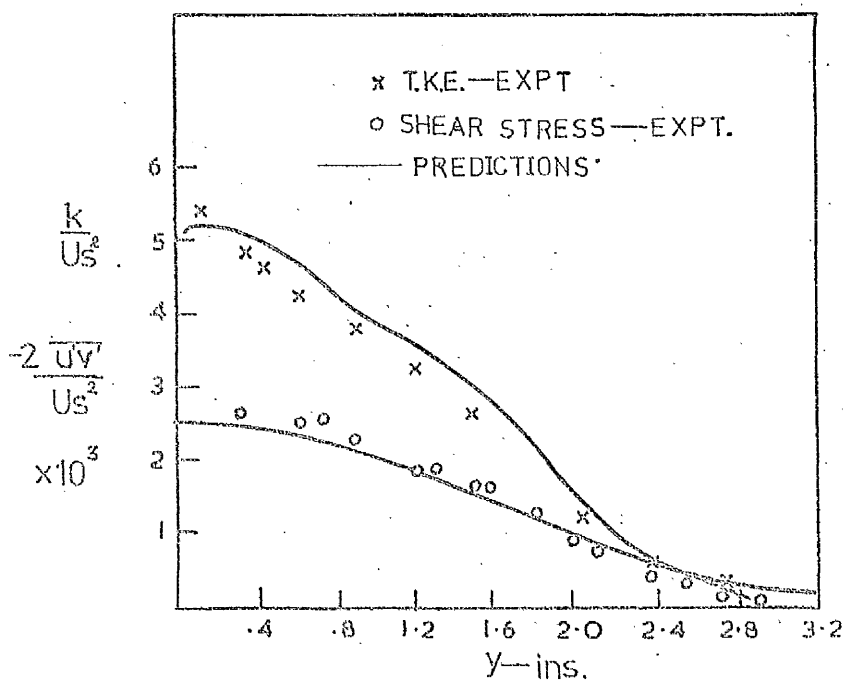
FIG 31 COMPARISON OF THEORY WITH RESULTS OF SCHUBAUER AND KLEBANOFF [21]



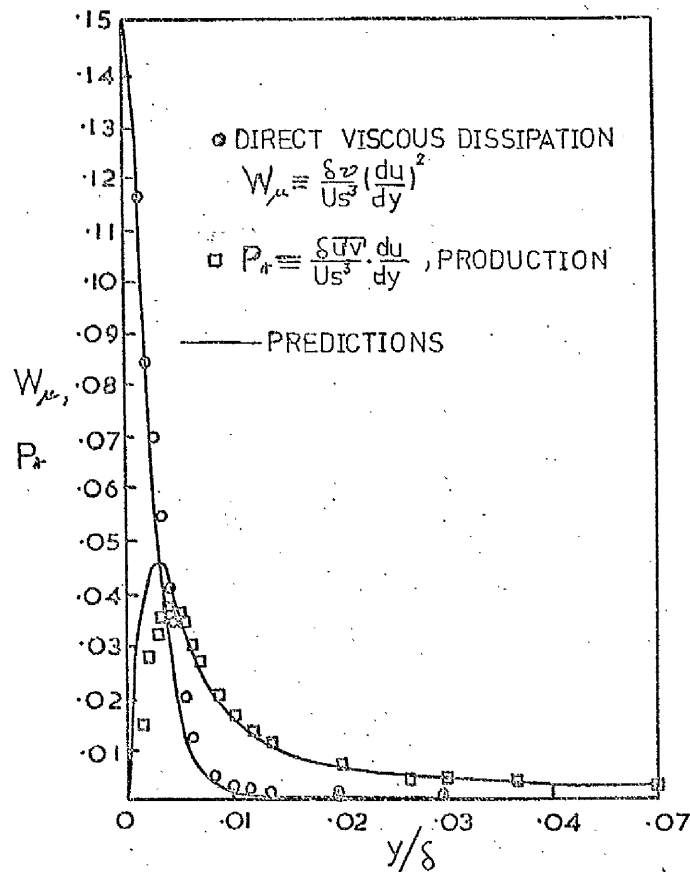
(a) DEFECT VELOCITY PROFILE



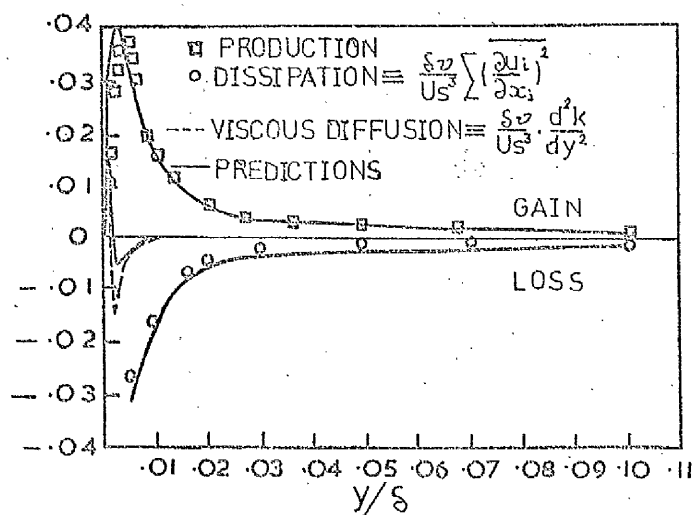
(b) MEAN VELOCITY PROFILE



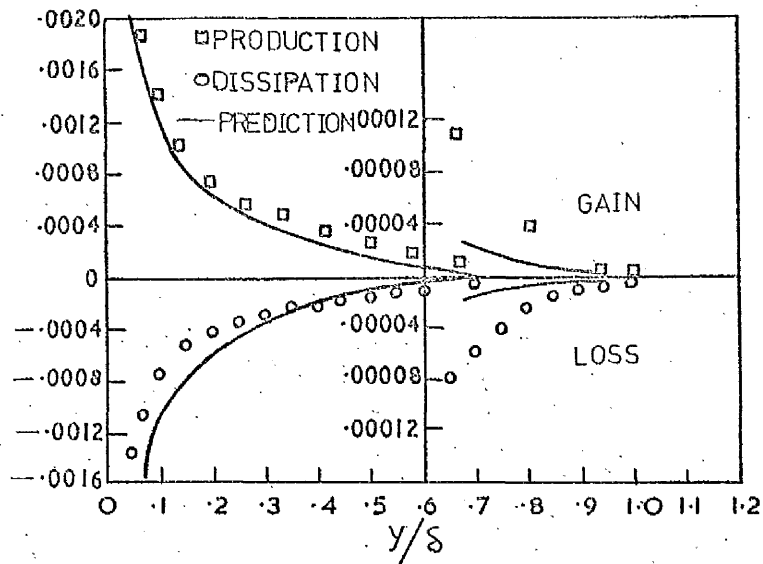
(c) TURBULENT KINETIC ENERGY AND SHEAR STRESS PROFILES



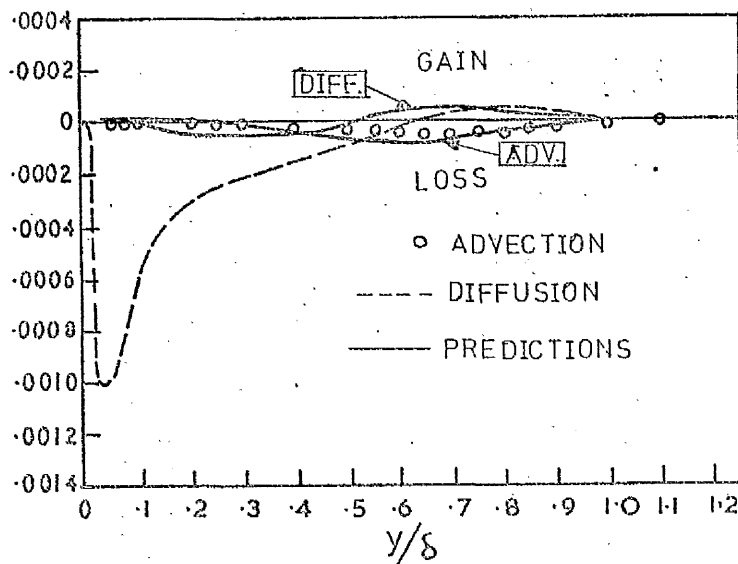
(a) DIRECT VISCOUS DISSIPATION AND PRODUCTION OF TURBULENT ENERGY NEAR WALL.



(b) PRODUCTION AND DISSIPATION IN REGION NEAR WALL



(a) PRODUCTION AND DISSIPATION IN REGION AWAY FROM WALL



(b) DIFFUSION AND ADVECTION

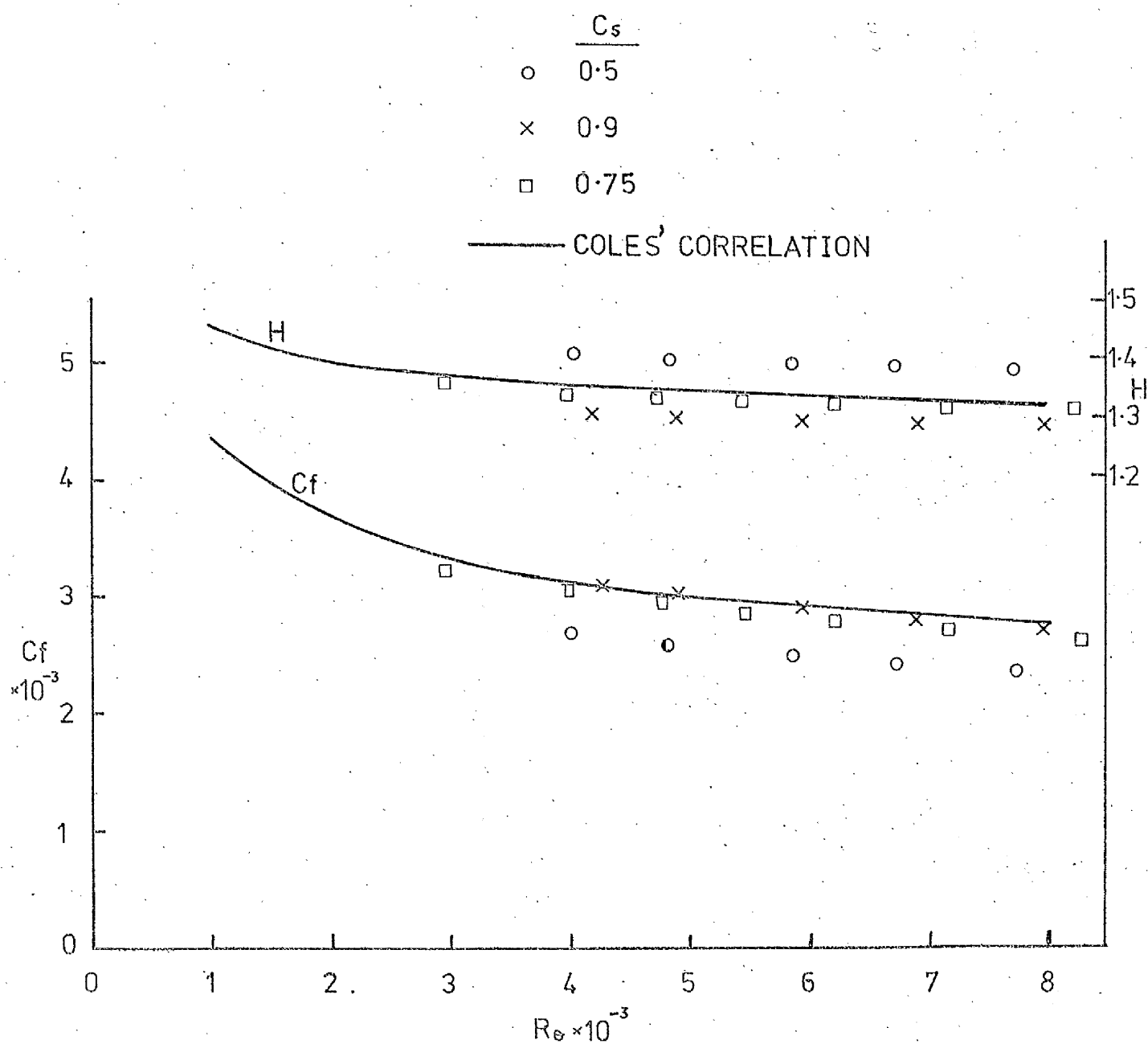


FIG 35 EFFECT OF OUTER LAYER CONSTANT
VARIATION ON ZERO PRESSURE
GRADIENT BOUNDARY LAYERS.

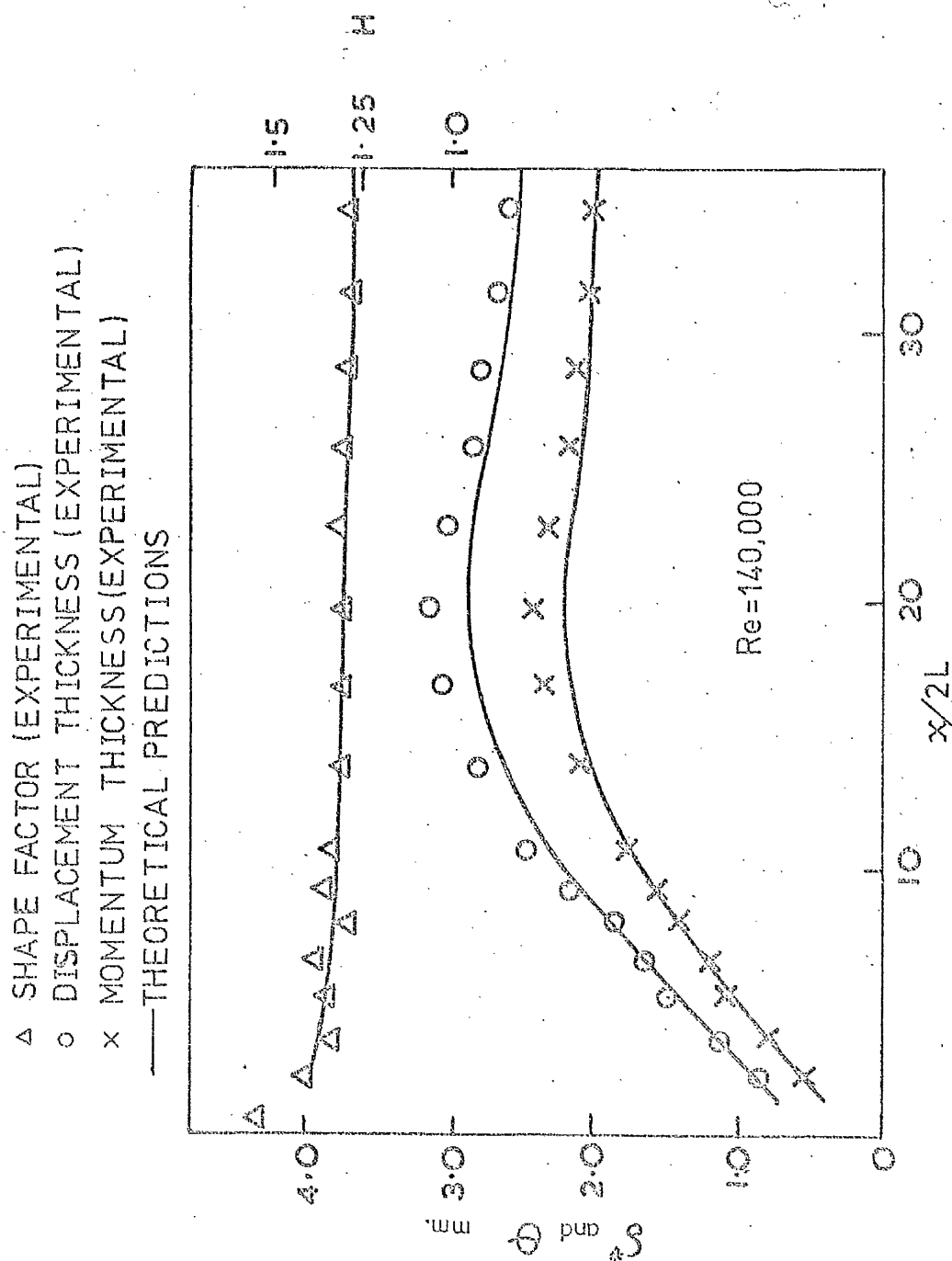


FIG 36 DISPLACEMENT AND MOMENTUM THICKNESS AND SHAPE FACTOR VARIATIONS ALONG THE PARALLEL WALL DUCT

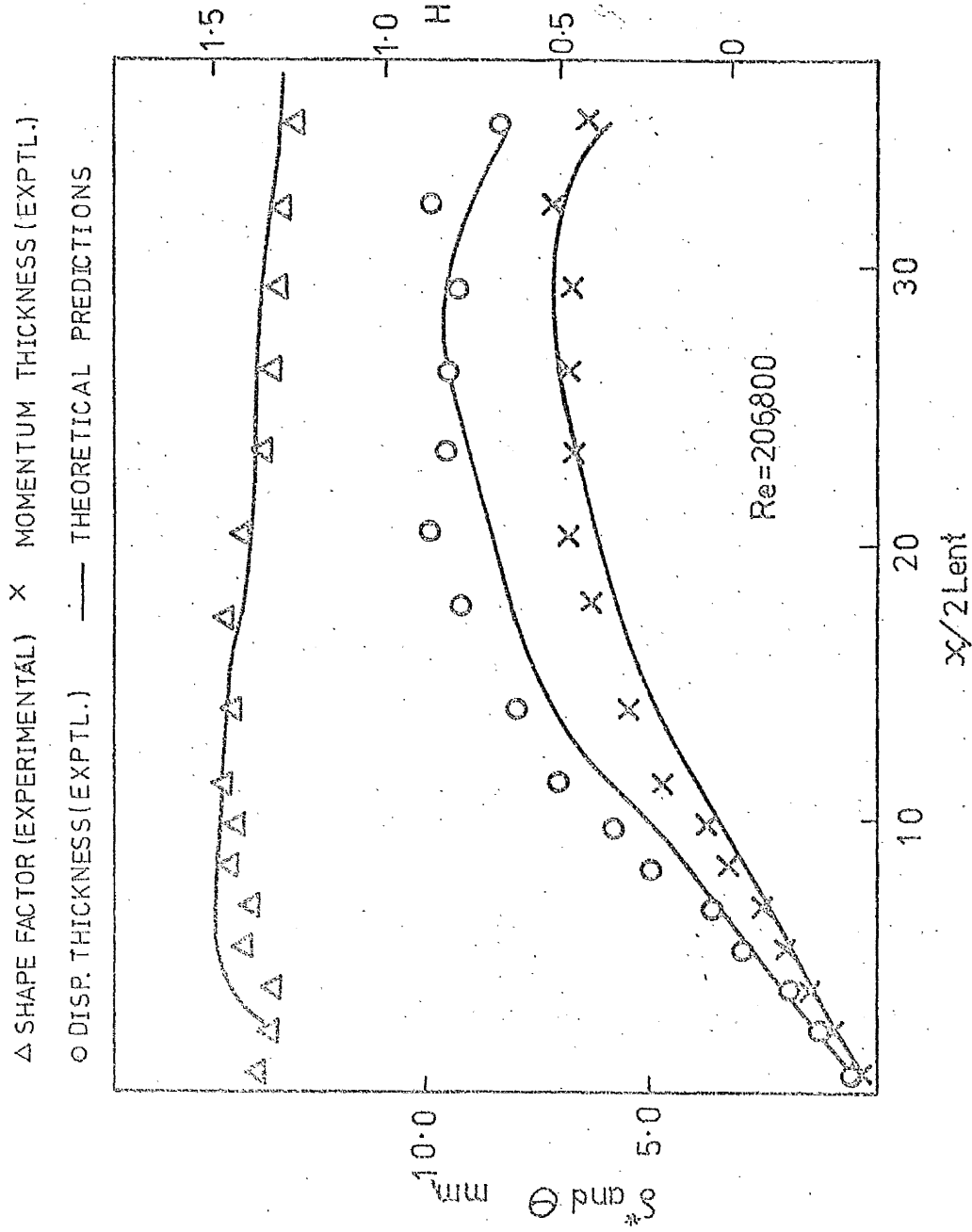


FIG 37 DISPLACEMENT AND MOMENTUM THICKNESS AND SHAPE FACTOR VARIATIONS ALONG THE DIVERGING DUCT

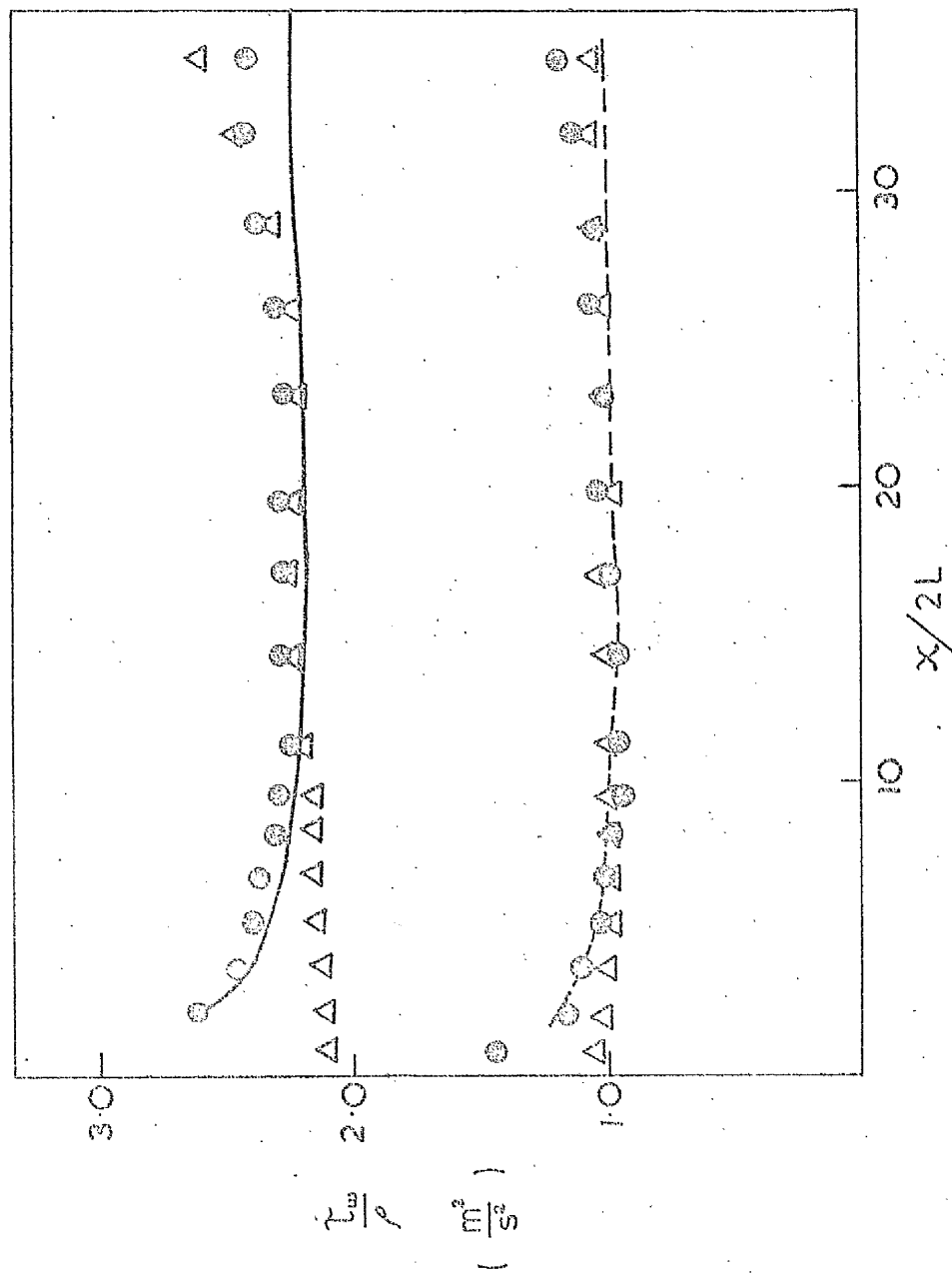


FIG 38 WALL SHEAR STRESS VARIATION ALONG THE PARALLEL

WALL DUCT

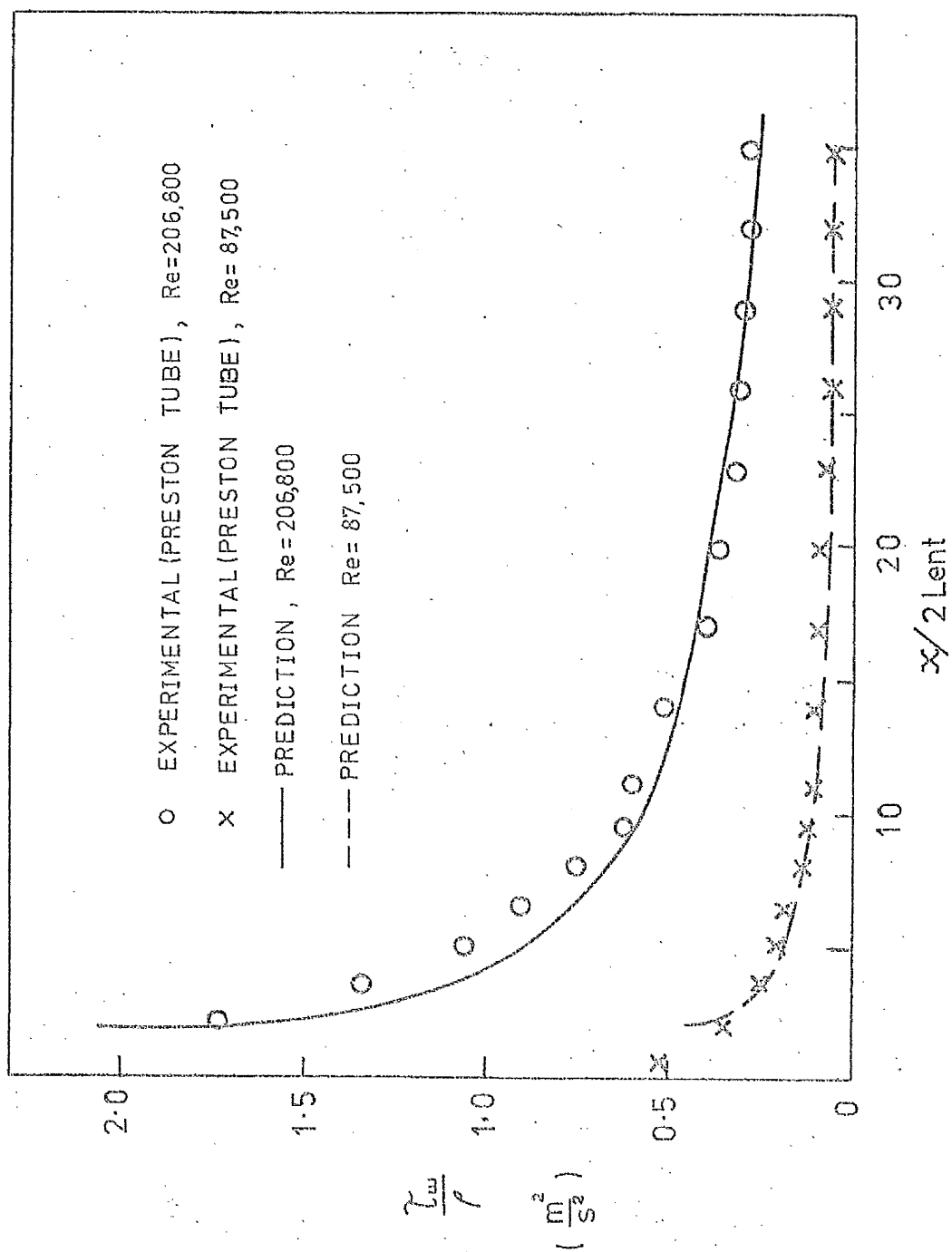


FIG 39 WALL SHEAR STRESS VARIATION ALONG THE DIVERGING DUCT.

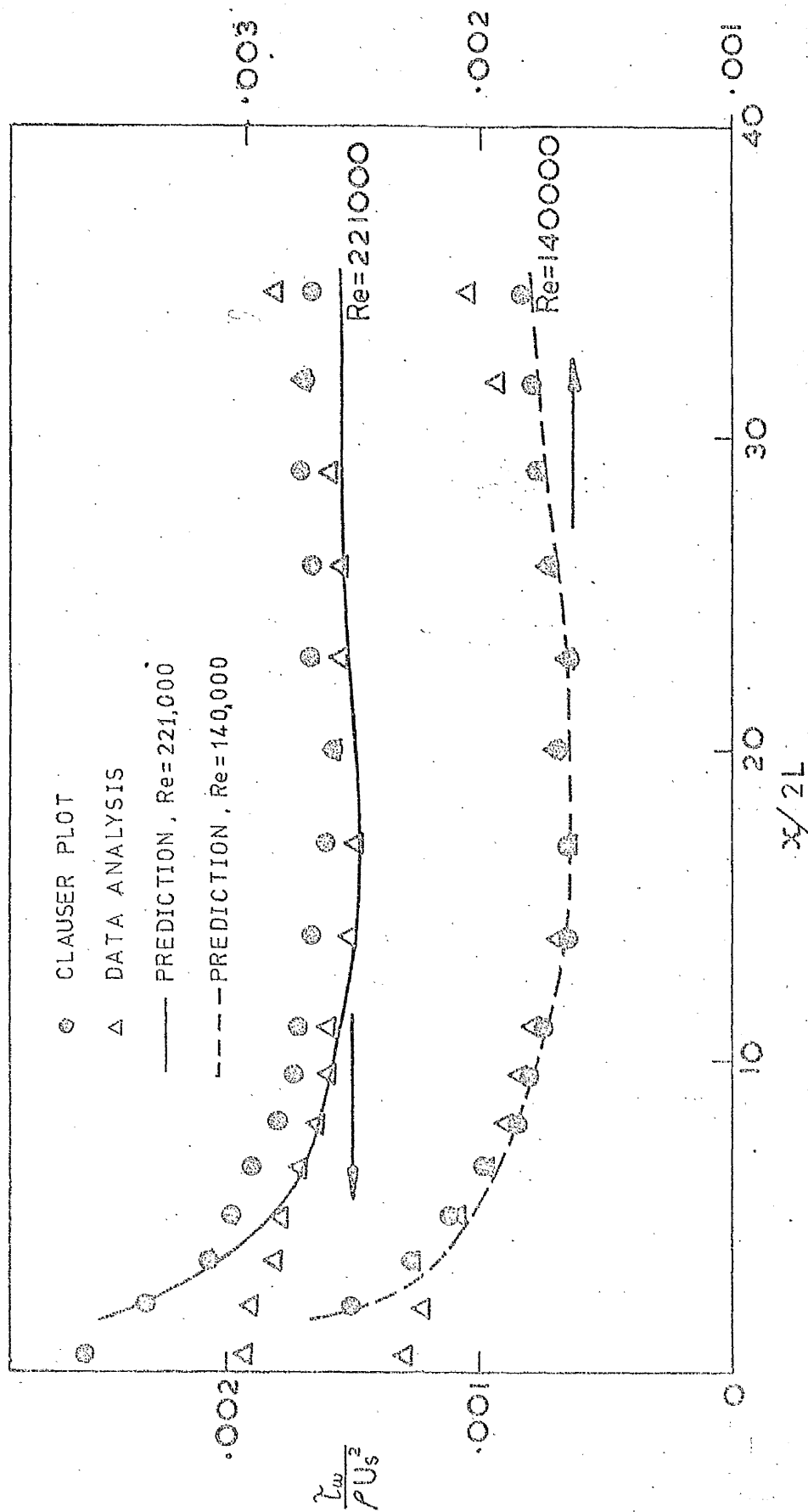


FIG 40 FRICTION FACTOR VARIATION ALONG PARALLEL WALL DUCT

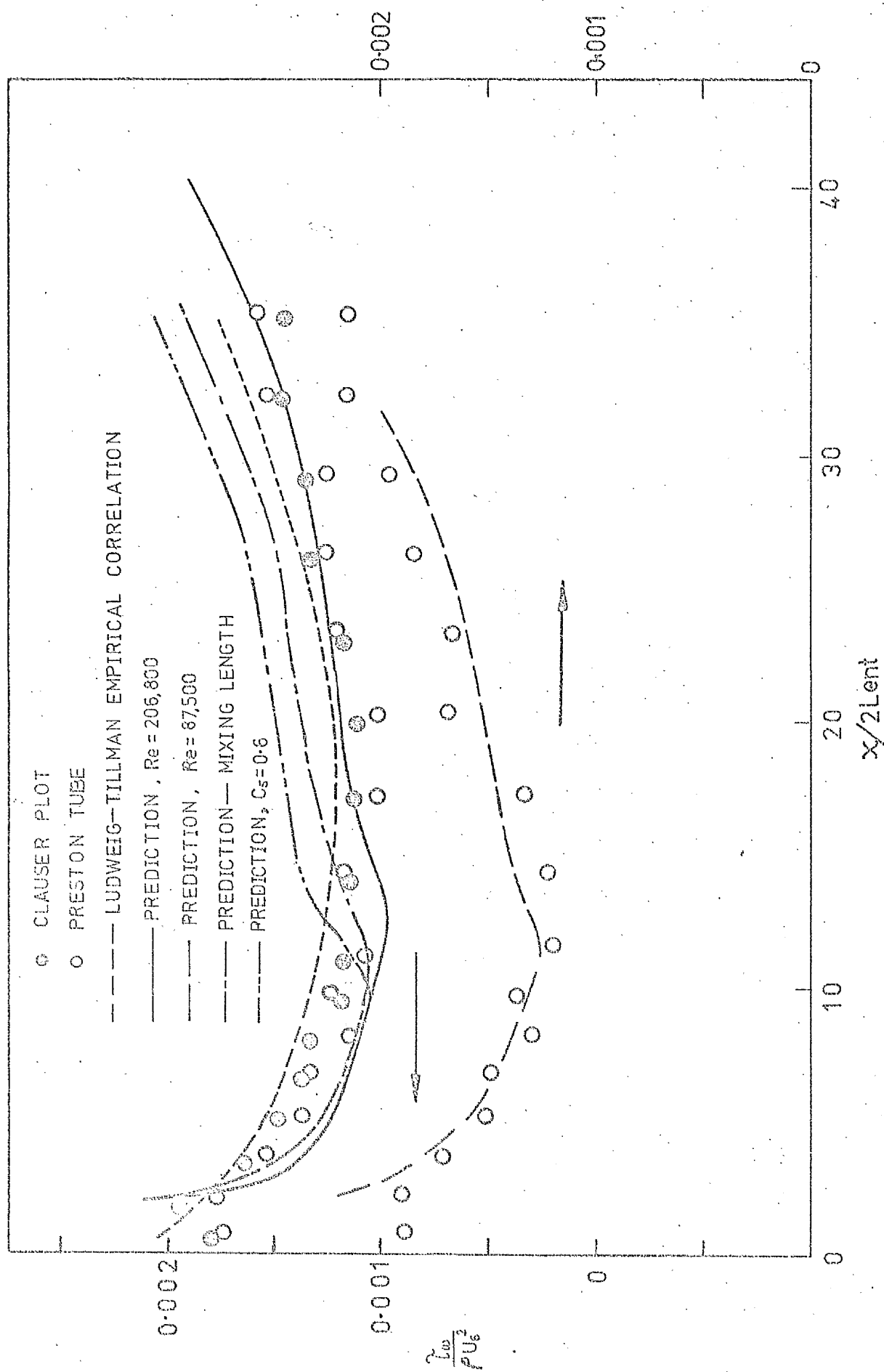
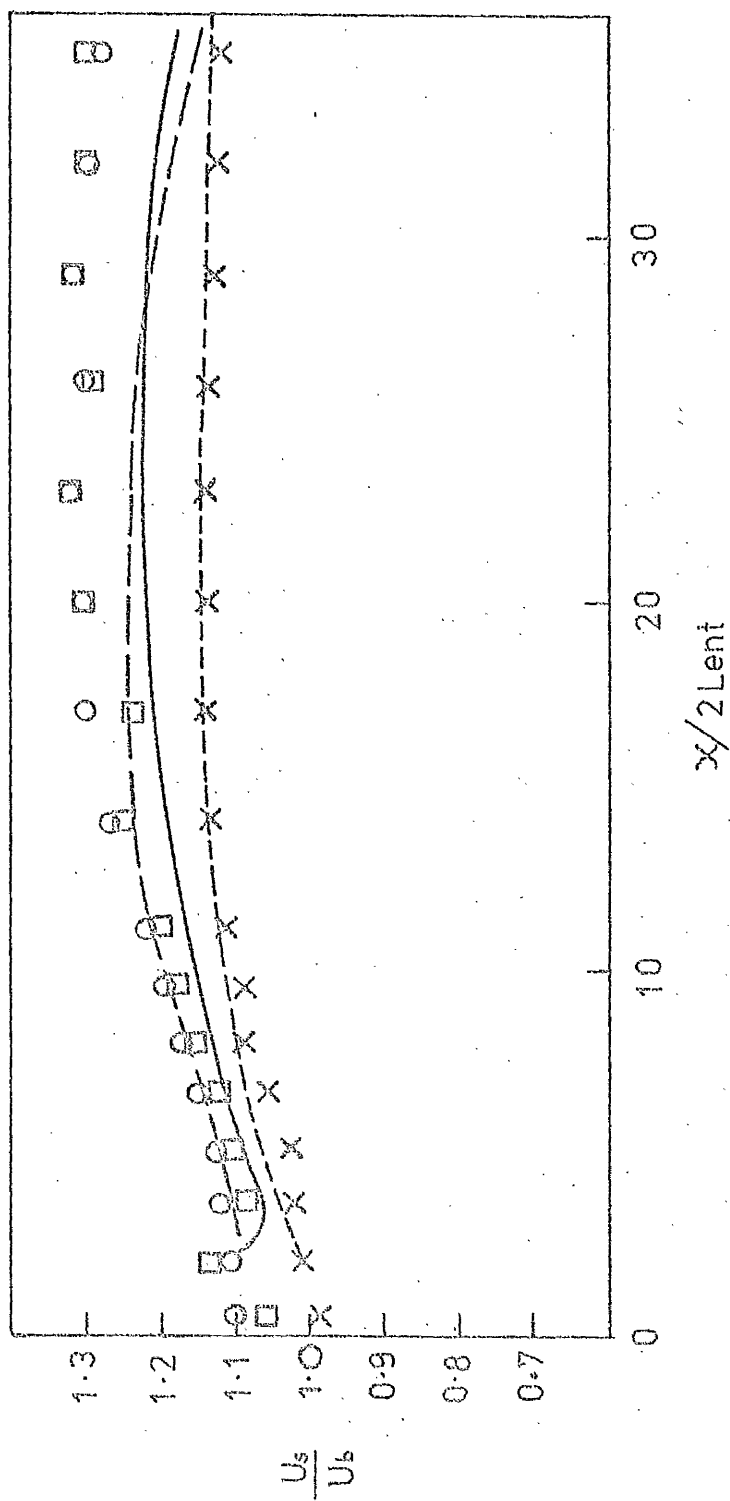


FIG 41 FRICTION FACTOR VARIATION ALONG DIVERGING DUCT.



| EXPERIMENTAL | THEORETICAL PREDICTIONS | DUCT GEOMETRY |
|--------------|-------------------------|---------------|
| ○ | — | DIVERGING |
| □ | - - - | DIVERGING |
| × | - · - · - | PARALLEL WALL |

$Re = 206,800$

$Re = 87,500$

$Re = 140,000$

FIG 4.2 VARIATION OF U_s/U_b ALONG PARALLEL AND DIVERGING DUCTS.

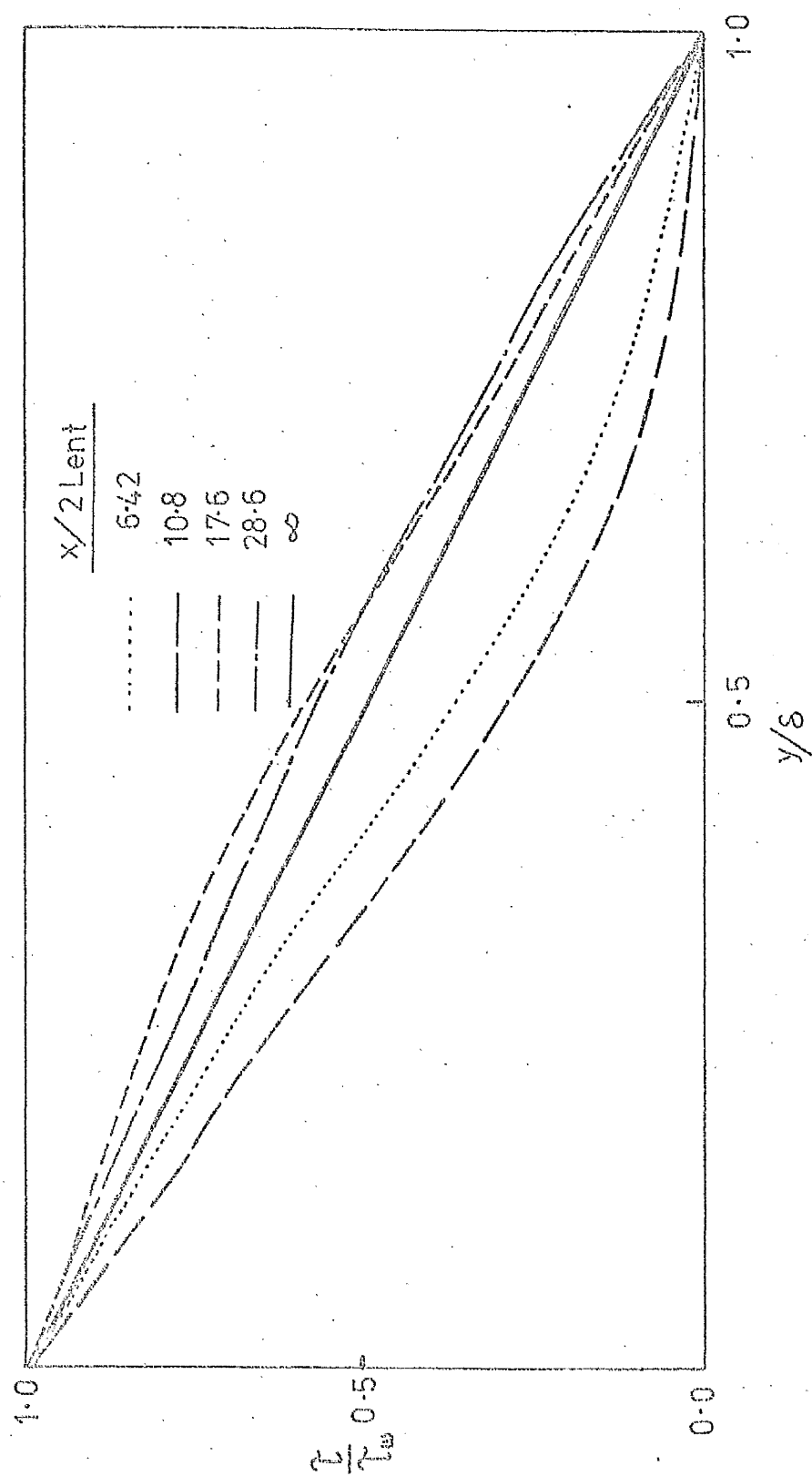


FIG 43 PREDICTED SHEAR-STRESS DISTRIBUTION IN THE BOUNDARY LAYER AT VARIOUS POSITIONS ALONG THE PARALLEL WALL DUCT.

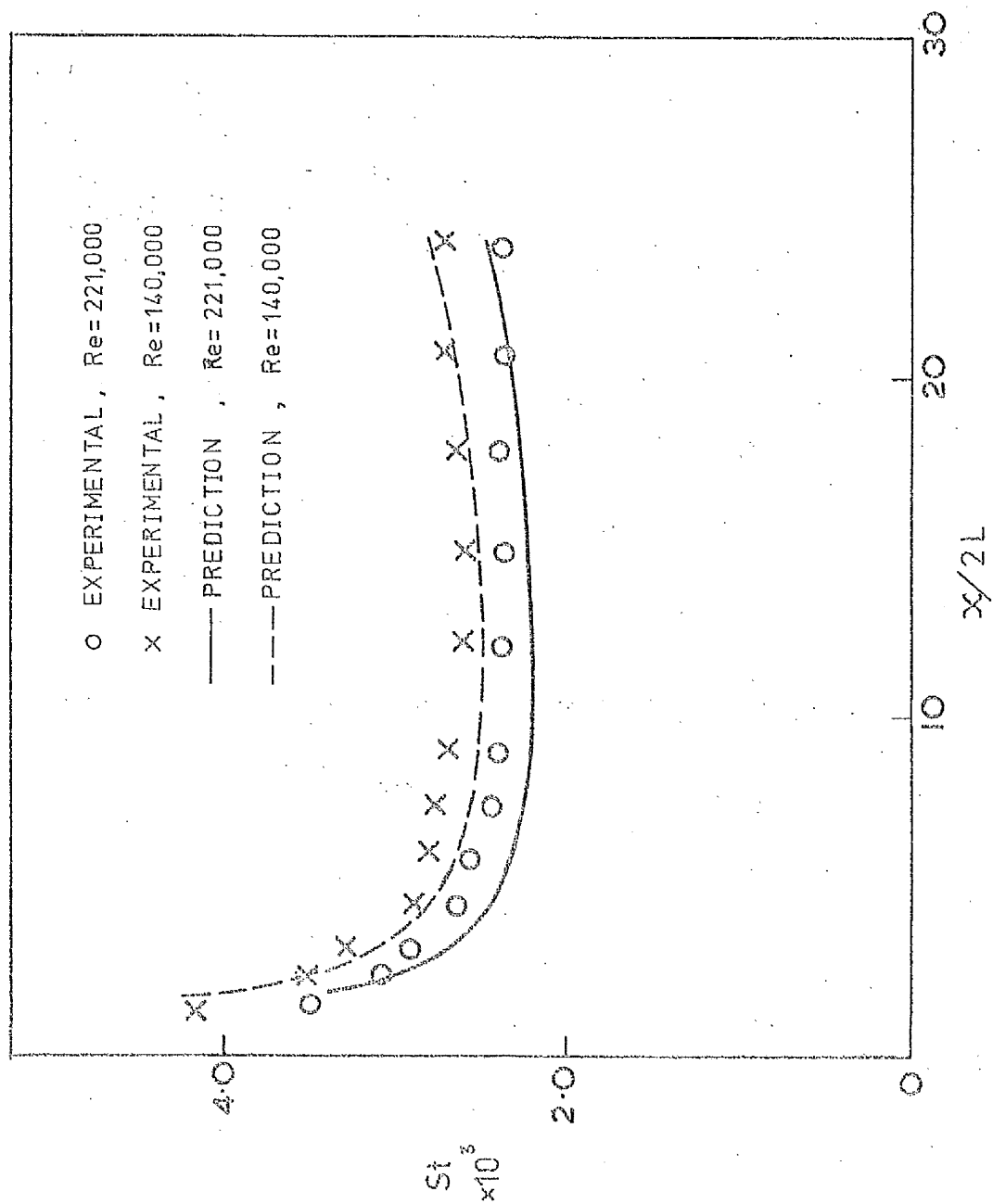


FIG 44 BULK STANTON NUMBER VARIATION ALONG PARALLEL WALL DUCT

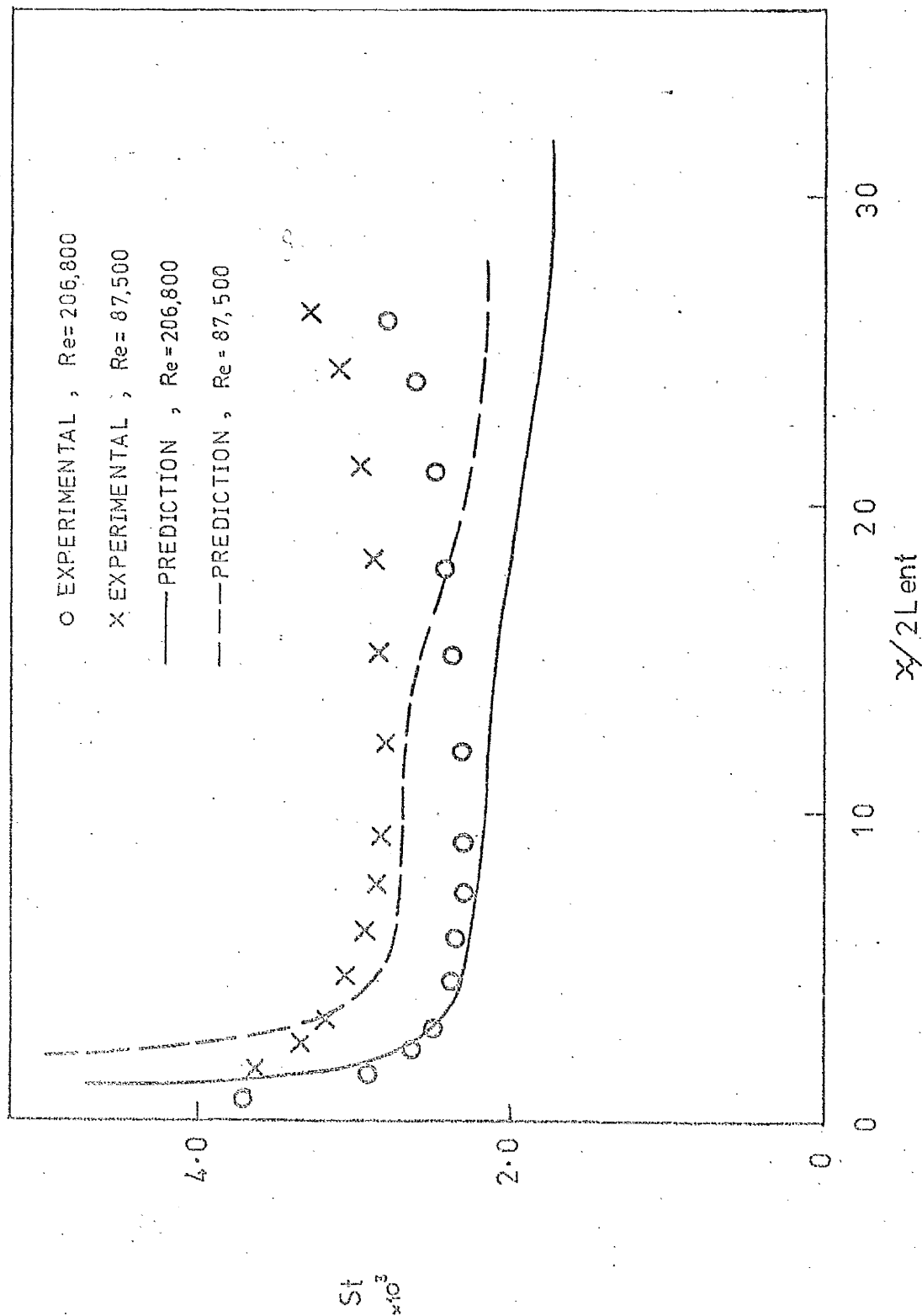


FIG 45 BULK STANTON NUMBER VARIATION ALONG DIVERGING DUCT.

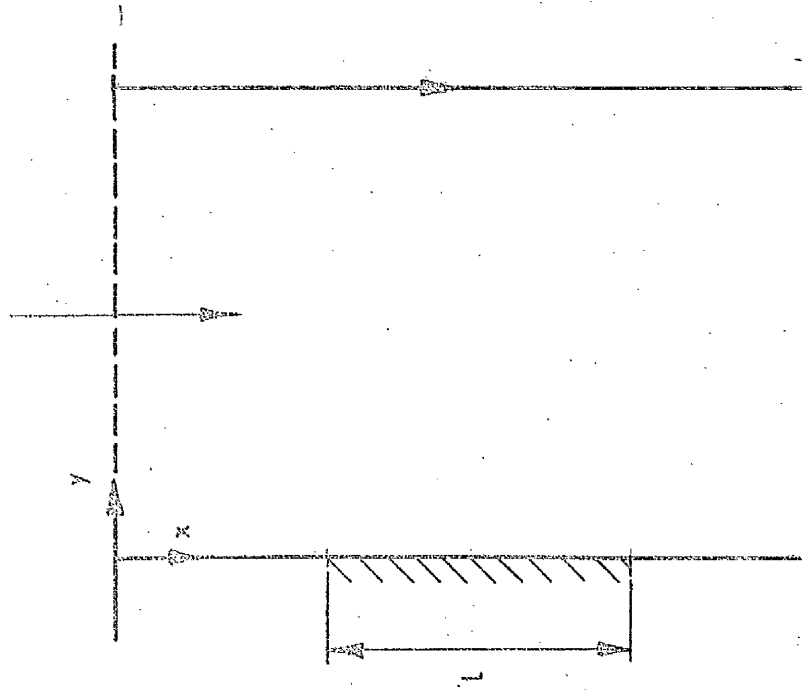
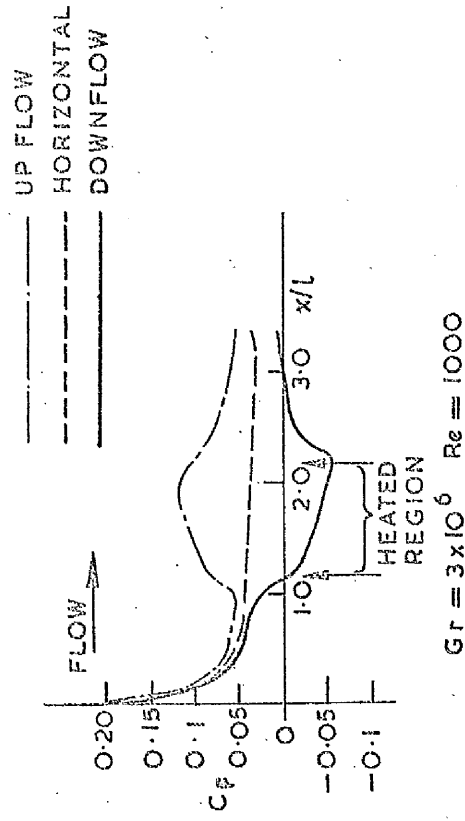
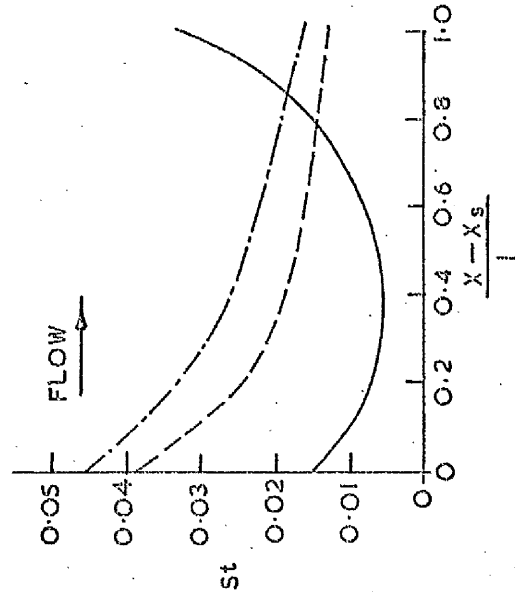


FIG 46 COORDINATE SYSTEM



$$Gr = 3 \times 10^6 \quad Re = 1000$$

FIG 47 FRICTION FACTOR DISTRIBUTION ALONG WALL



$$Gr = 3 \times 10^6 \quad Re = 1000$$

FIG 48 STANTON NUMBER DISTRIBUTION ALONG HEATED PATCH

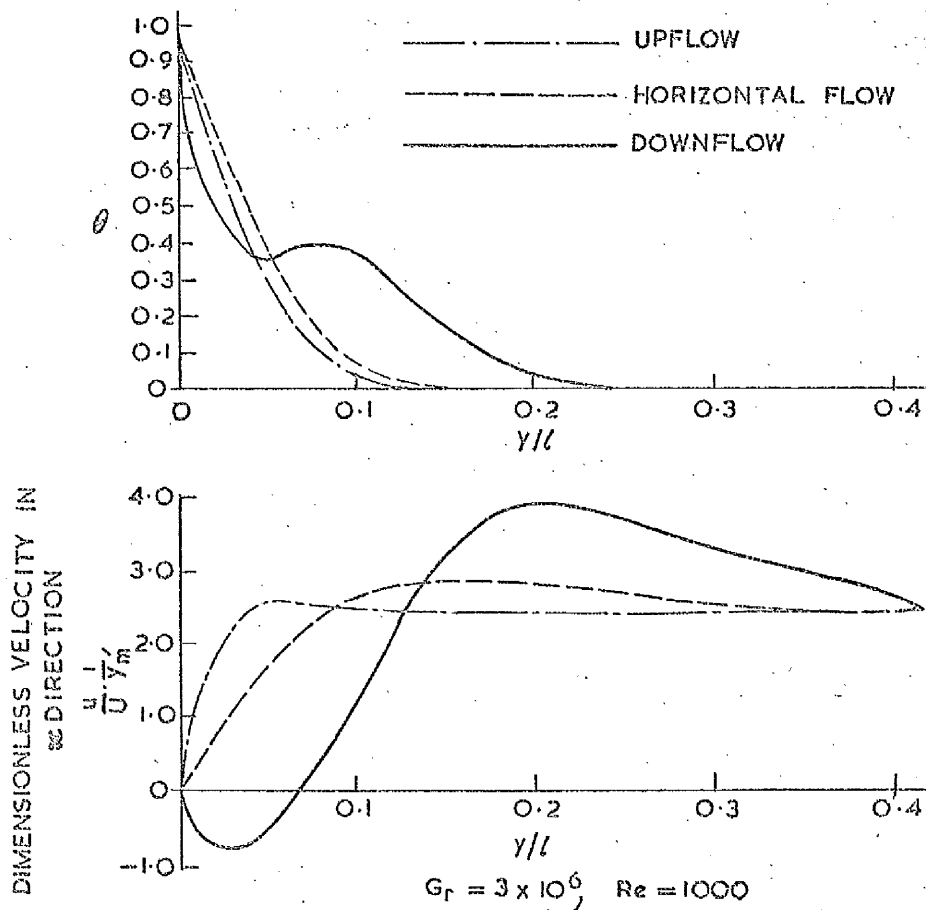


FIG 49 DIMENSIONLESS TEMPERATURE AND VELOCITY PROFILES AT EXIT FROM HEATED PATCH

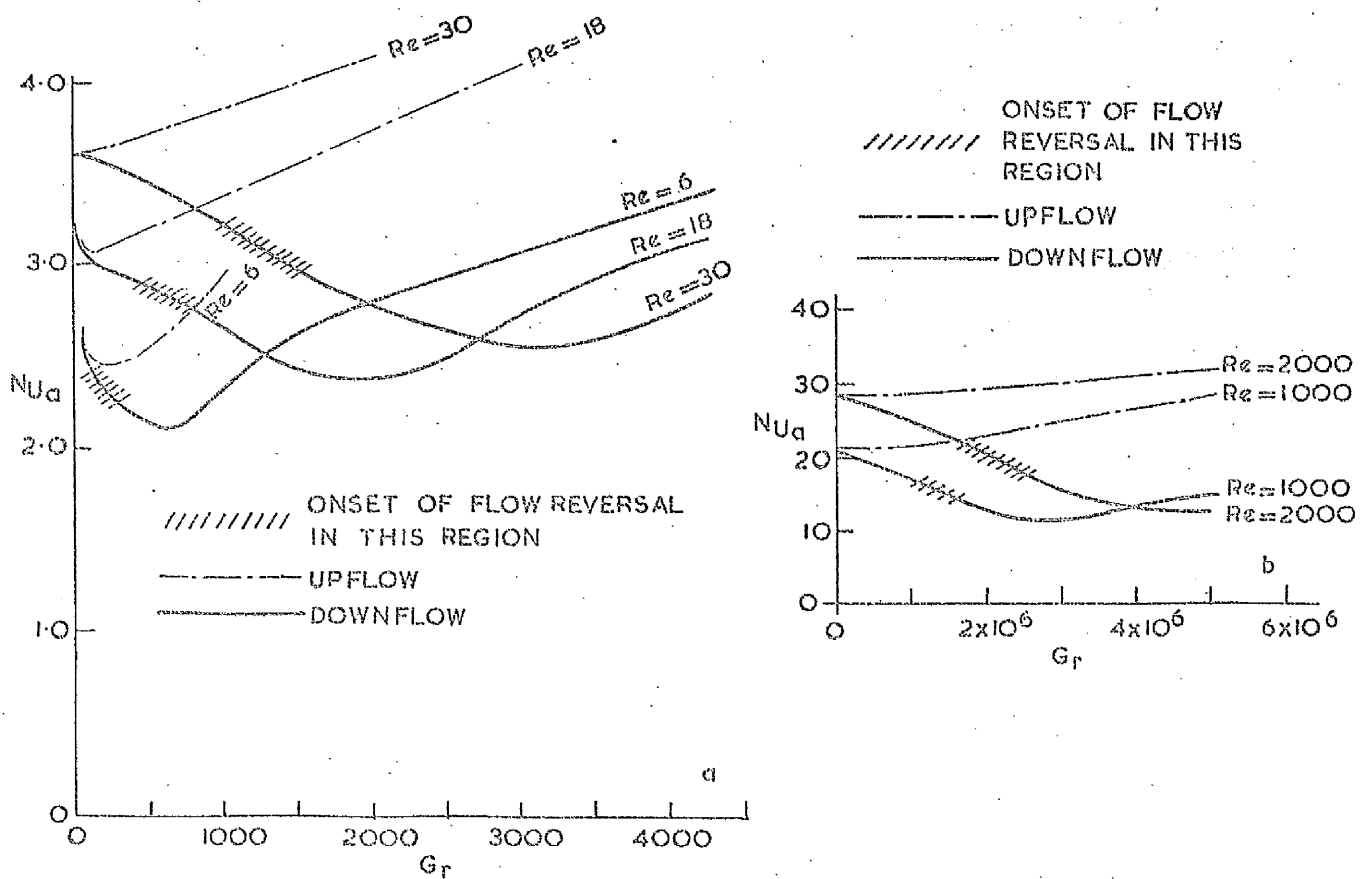


FIG 50 MEAN NUSSULT NUMBER VERSUS GRASHOF NUMBER FOR DIFFERENT REYNOLDS NUMBERS.

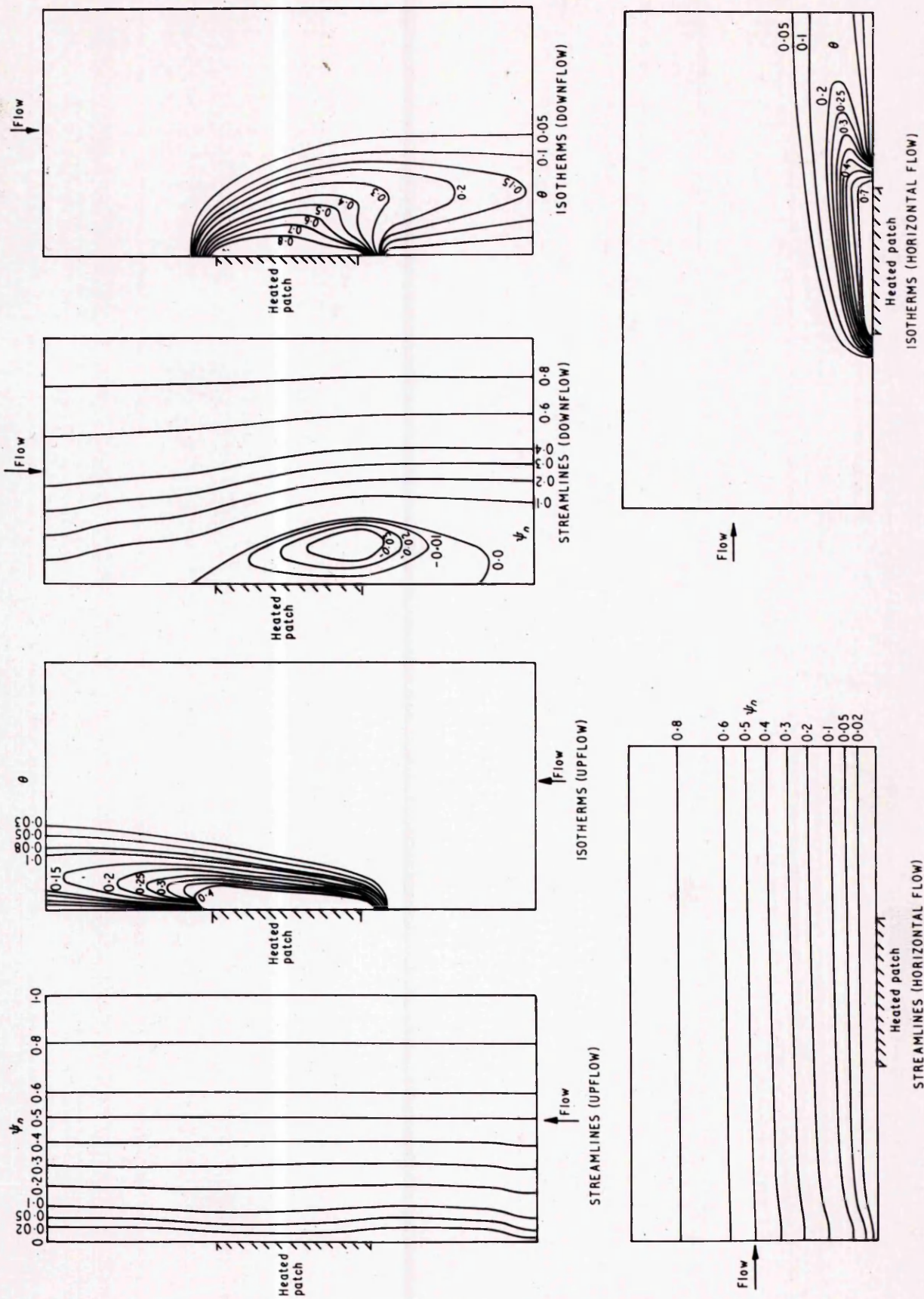


Fig 51 Streamlines and isotherms for the three flow directions

$Gr = 3 \times 10^6$, $Re = 1000$.

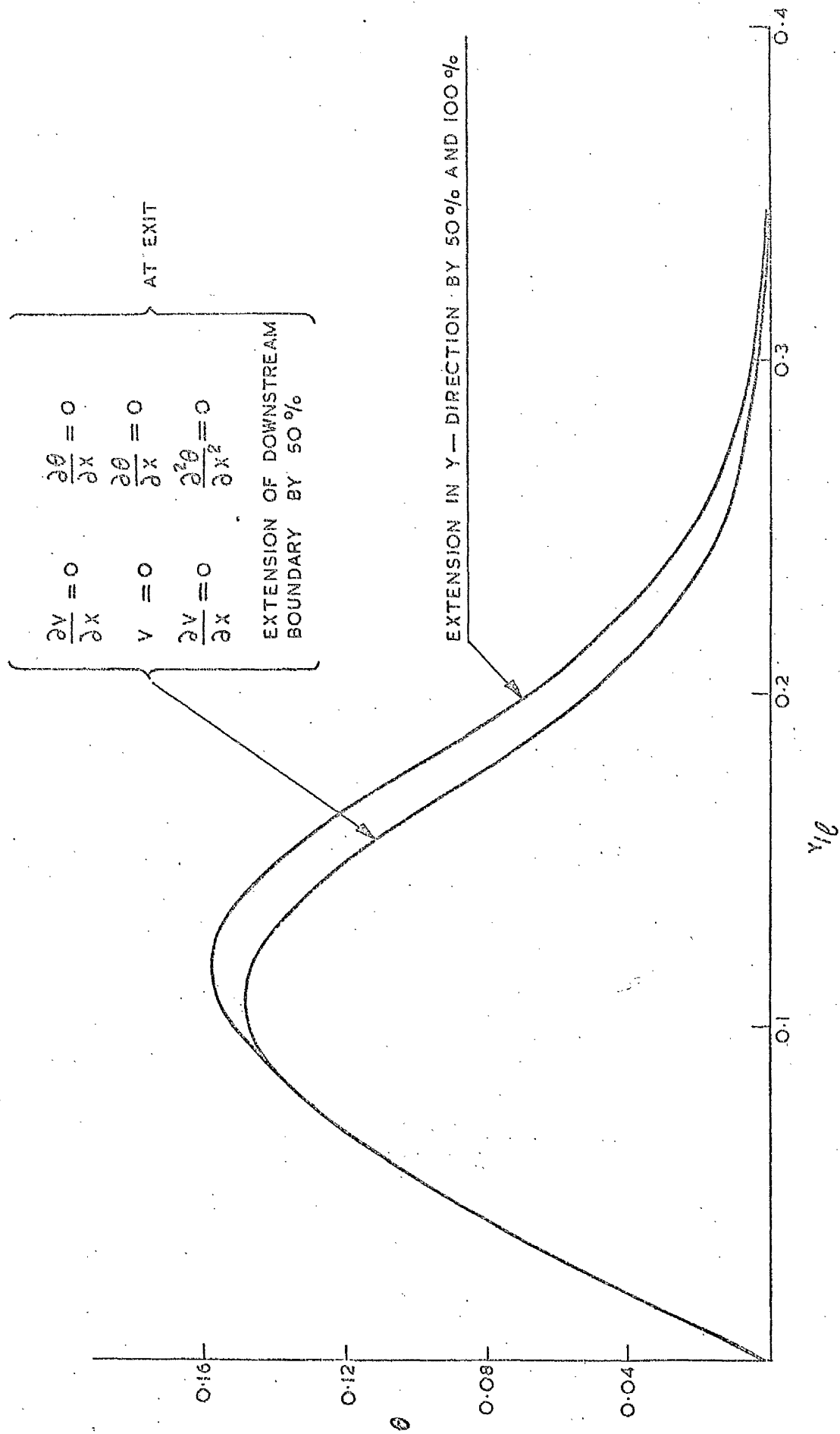


FIG 52

INFLUENCE OF CHOICE OF EXIT BOUNDARY CONDITION TEMPERATURE
PROFILES AT EXIT OF FIELD IN DOWNFLOW

$Re = 1000$

$Gr = 3 \times 10^6$

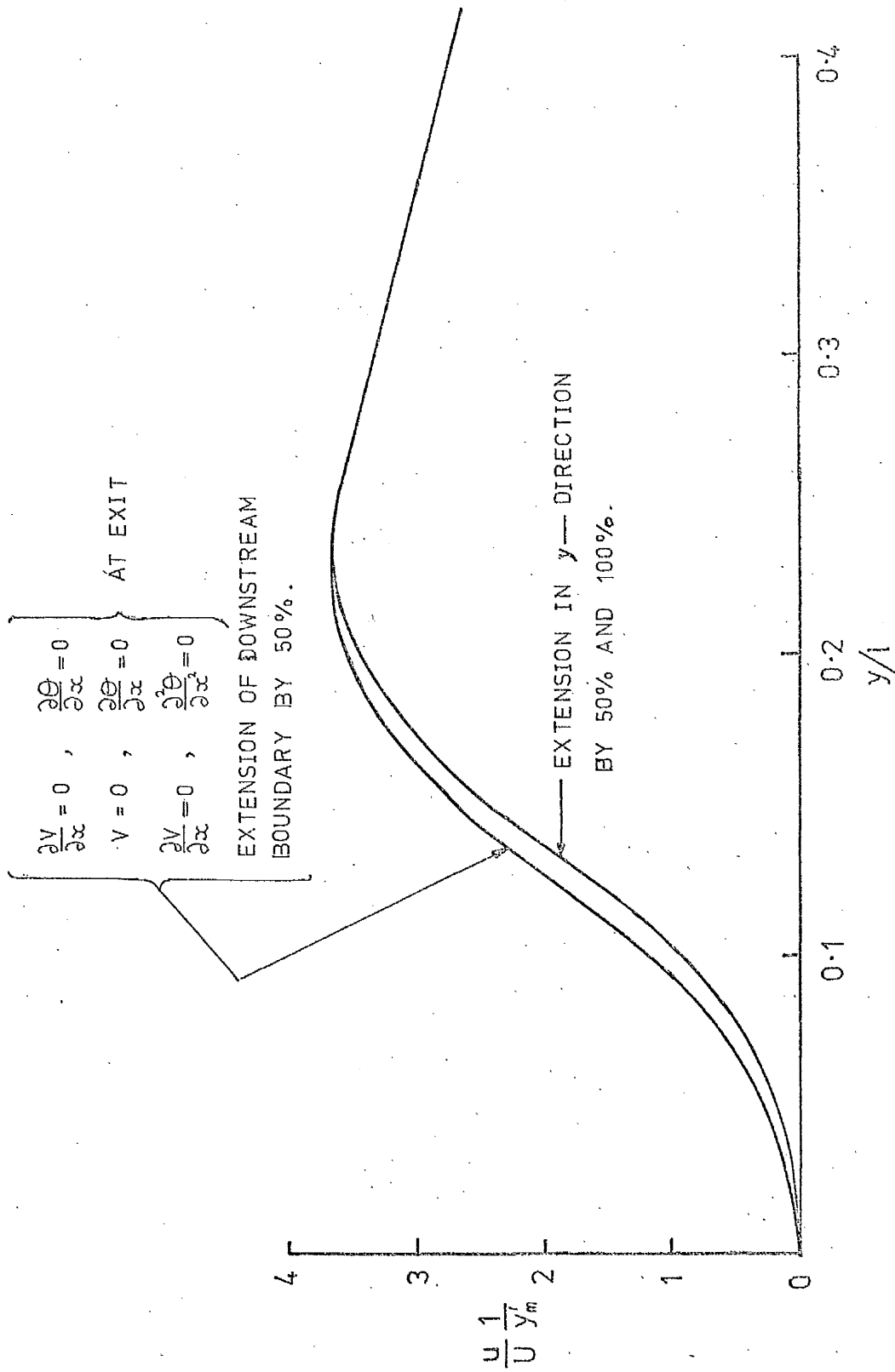


FIG 53 INFLUENCE OF CHOICE OF EXIT BOUNDARY CONDITIONS—

VELOCITY PROFILES AT EXIT OF FIELD IN DOWNFLOW

$Re=1000$
 $Gr=3 \times 10^6$

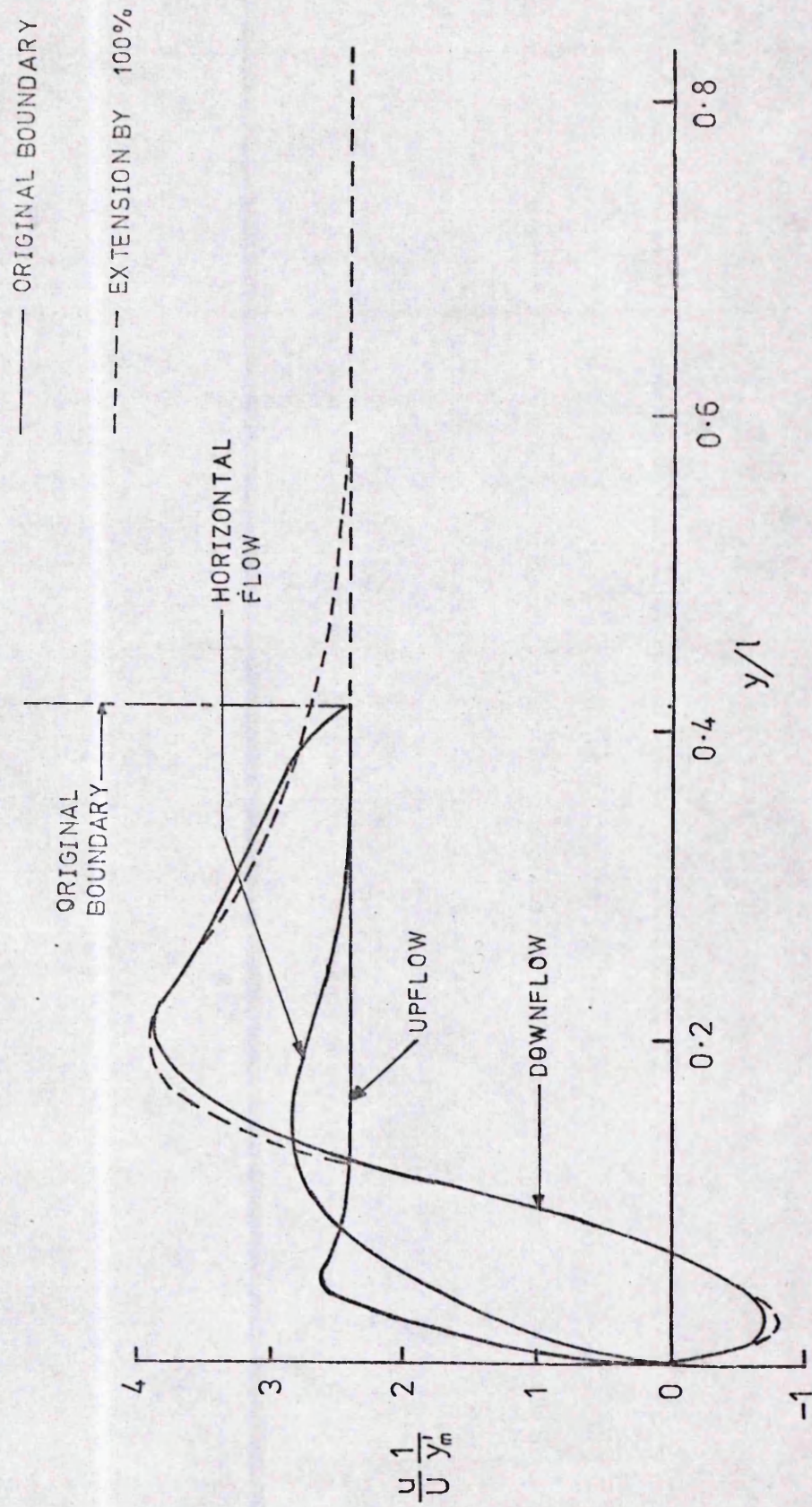


FIG 54 INFLUENCE OF EXTENSION OF BOUNDARY IN y -DIRECTION ON
 VELOCITY PROFILES AT THE EXIT FROM HEATED PATCH. $Re=1000$
 $Gr=3 \times 10^6$

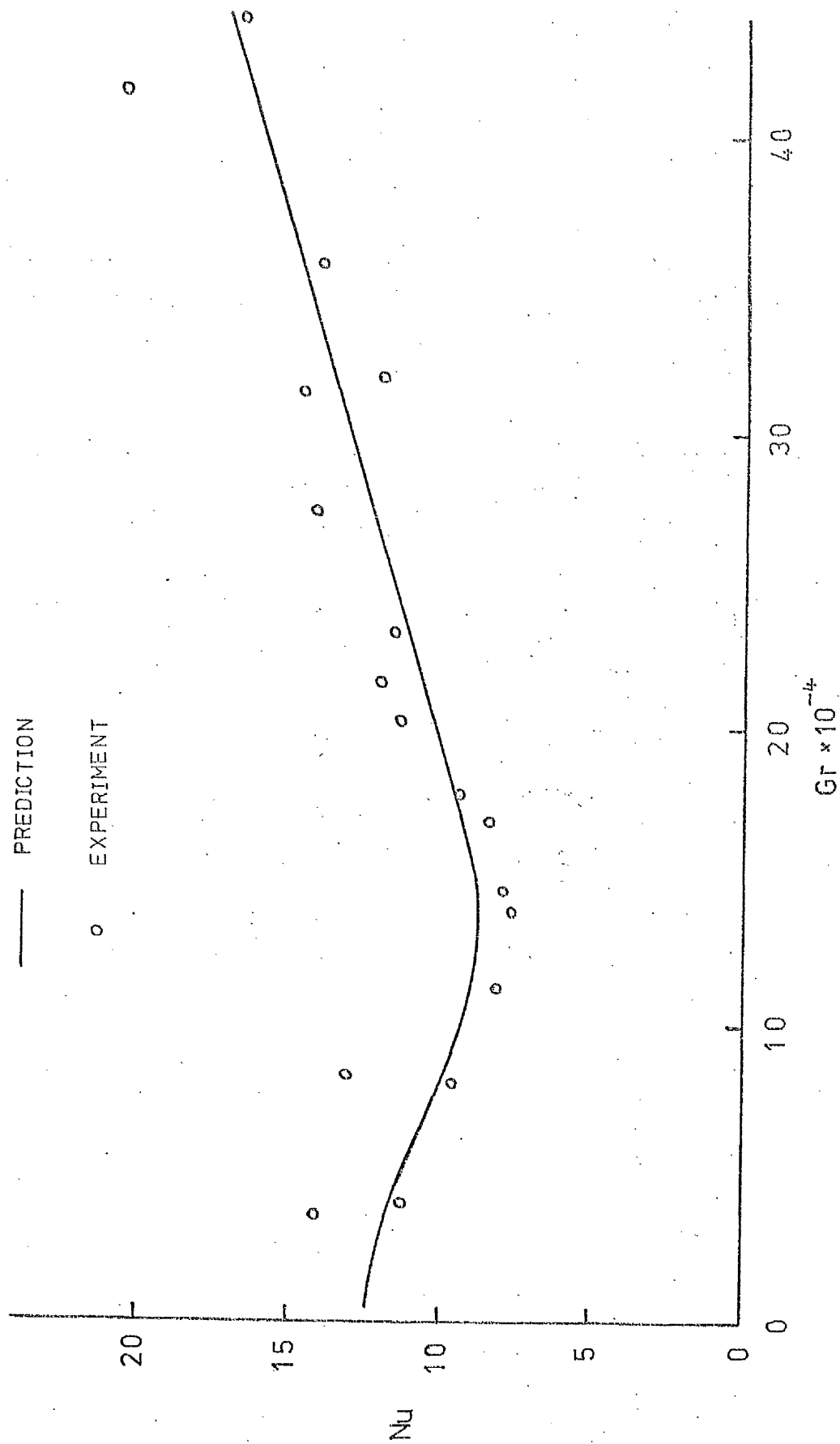


FIG 55 VARIATION OF MEAN NUSSELT NUMBER WITH GRASHOF

NUMBER — $Re=120$

$Re = 120$

HEATED PATCH

HEATED PATCH

HEATED PATCH

$Gr = 6.2 \times 10^4$

$Gr = 7.4 \times 10^4$

$Gr = 7.6 \times 10^4$



HEATED PATCH

$G = 2 \times 10^4$

HEATED PATCH

HEATED PATCH

FIG 57

FLOW VISUALIZATION

$Re = 350$

HEATED PATCH

HEATED PATCH

HEATED PATCH

$Gr = 21.5 \times 10^4$

$Gr = 23.0 \times 10^4$

$Gr = 26.0 \times 10^4$

HEATED PATCH



Gr-210-10

HEATED PATCH



Gr-210-10

HEATED PATCH



Gr-210-10

HEATED PATCH

Gr=42.2*10⁴



HEATED PATCH

Gr=27.5×10⁴

HEATED PATCH

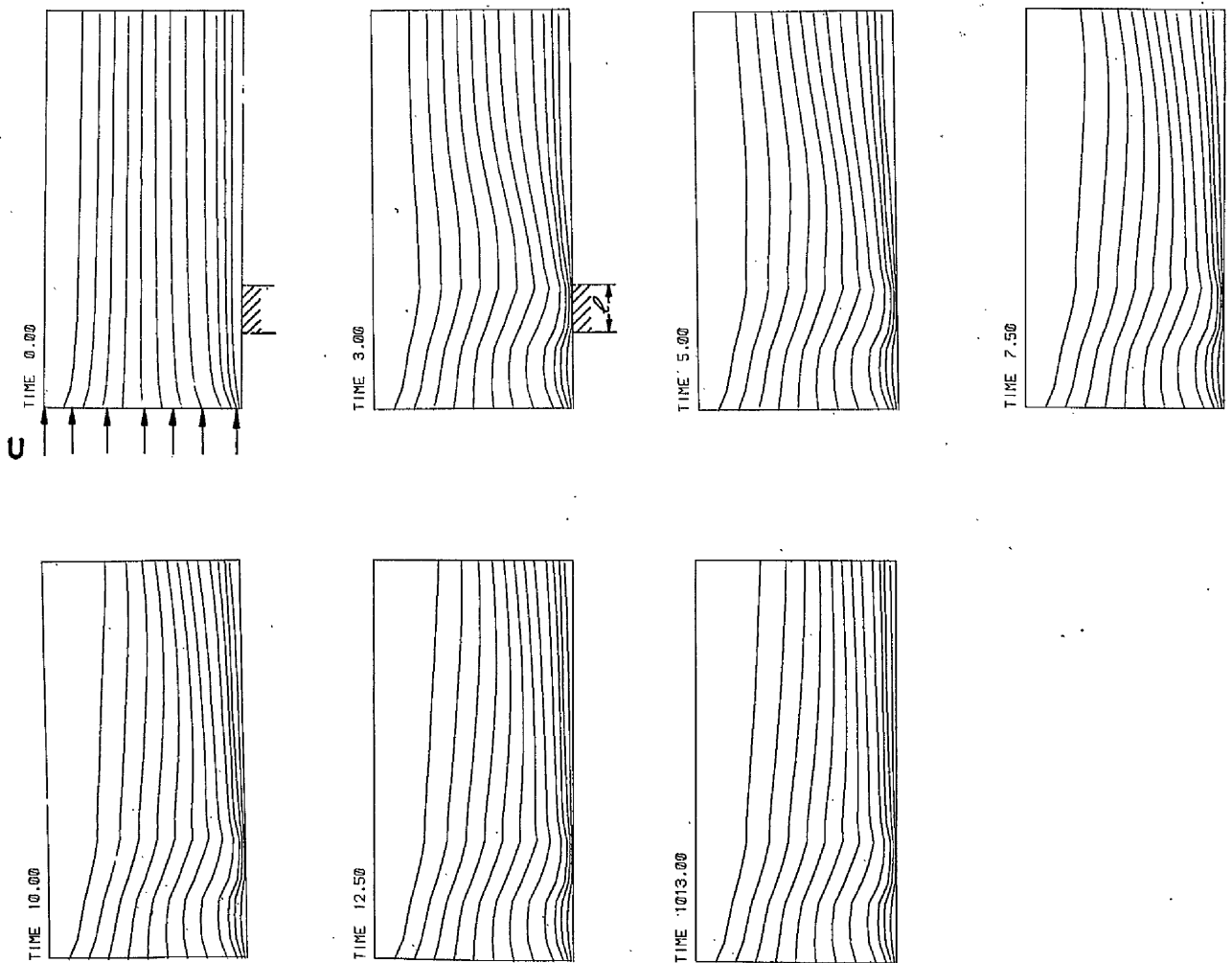
Gr=37.2×10⁴

HEATED PATCH

Gr=42.2×10⁴

FIG 59 (a)

TRANSIENT COMBINED FORCED AND NATURAL CONVECTION IN A PARALLEL CHANNEL
CONDITIONS AS BEFORE BUT WITH UPFLOW



TRANSIENT COMBINED FORCED AND NATURAL CONVECTION IN A PARALLEL CHANNEL

AT TIME ZERO A PATCH ON ONE WALL IS SUDDENLY INCREASED IN TEMPERATURE TO T_1 . THE CONTOUR PLOTS SHOW THE SUBSEQUENT STREAMLINE DEVELOPMENT.

NOTE. LATERAL SCALE IS EXPANDED: $Re = \frac{U_0 \ell}{\nu} = 2 \times 10^3$; $Pr = 1.0$; $Gr = \frac{g \ell^3 (T_1 - T_0)}{\nu^2} = 3 \times 10^7$; DIMENSIONLESS TIME $-\frac{U_0}{\nu}$; θ - TIME: CHANNEL DIMENSIONS 24/1.

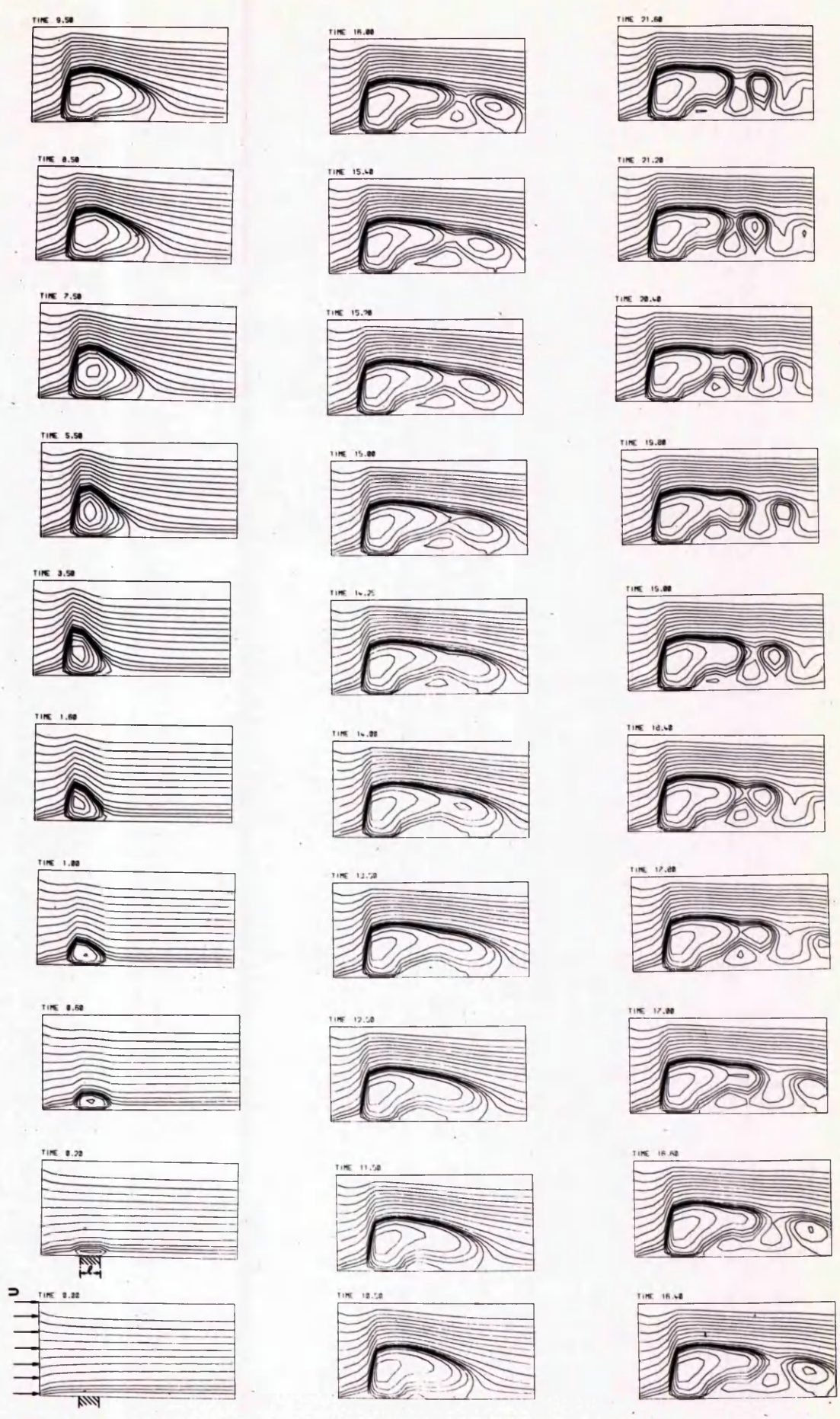
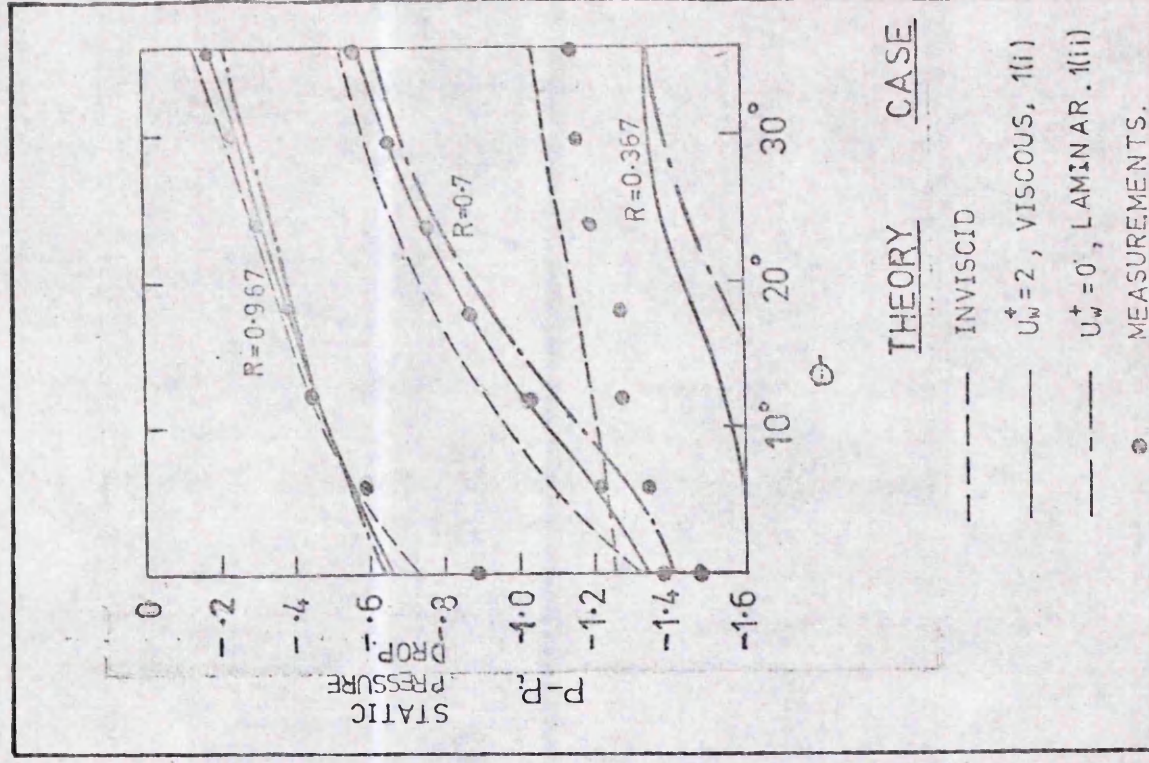
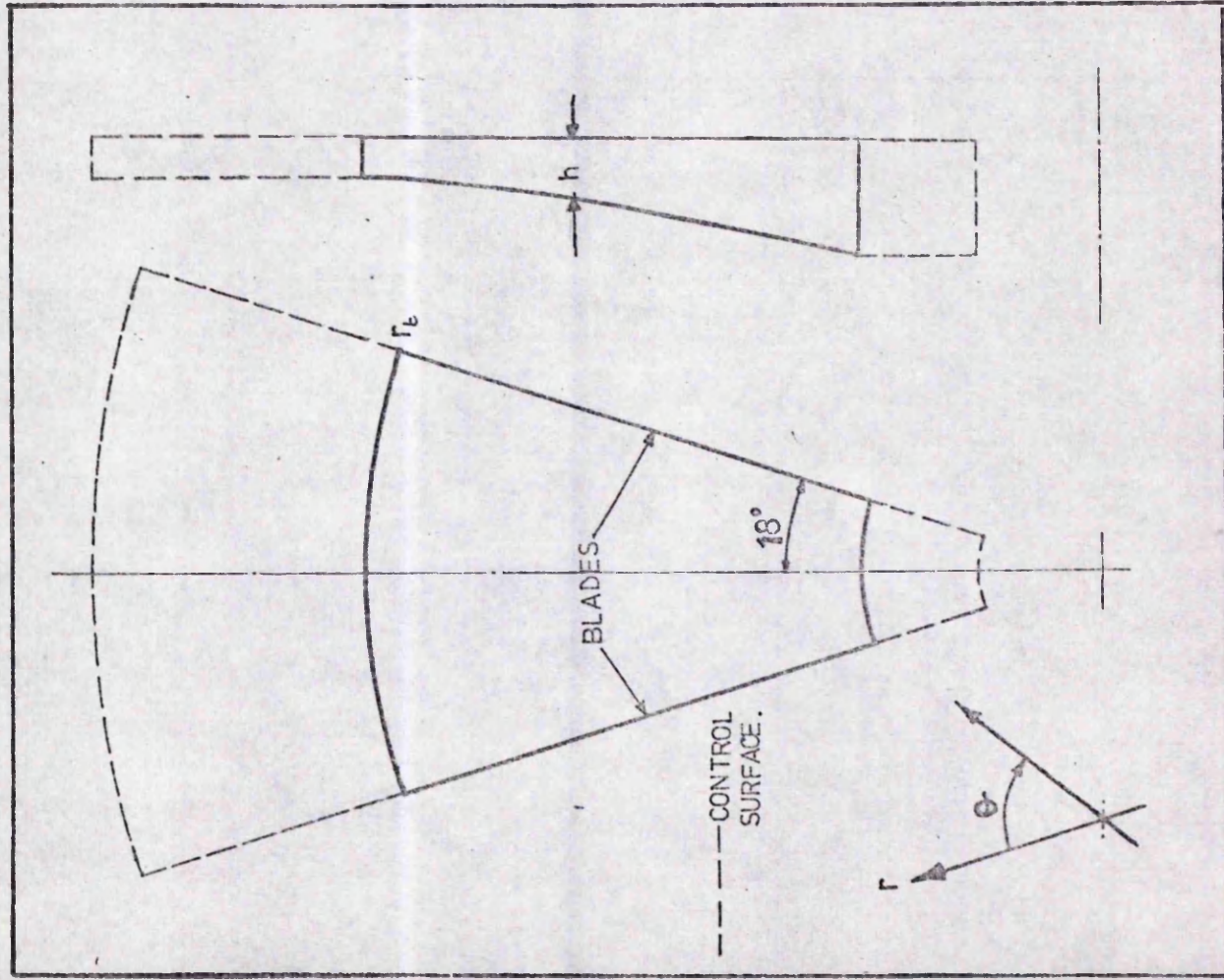


FIG 59 (b)



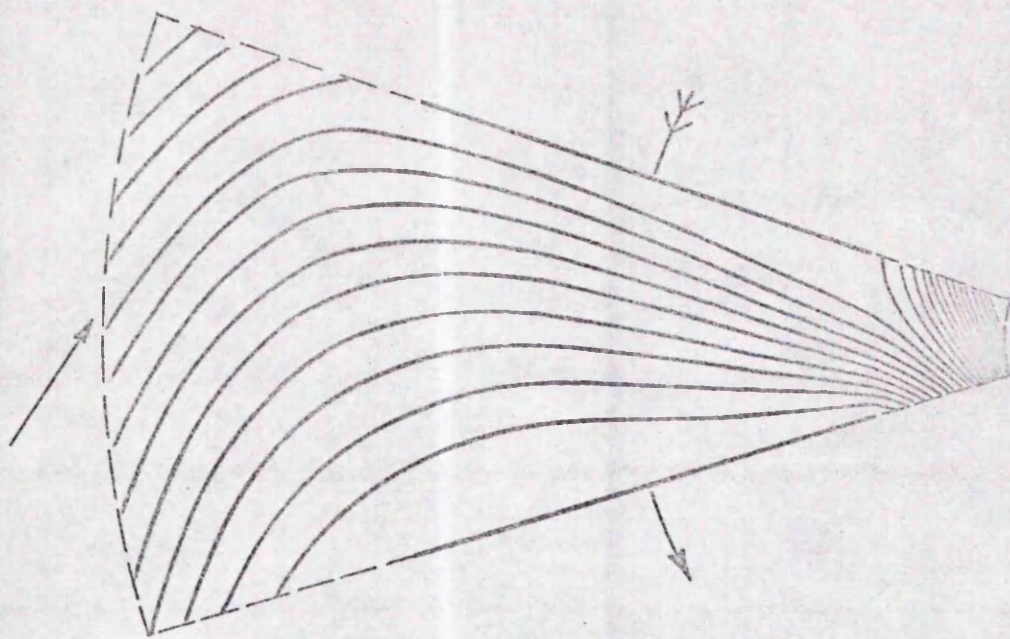
NOTE: SEE TABLE (i) FOR KEY TO CASE NUMBERS,
ie. appendix 3.

FIG 60(a) COORDINATE AND CONTROL SYSTEMS

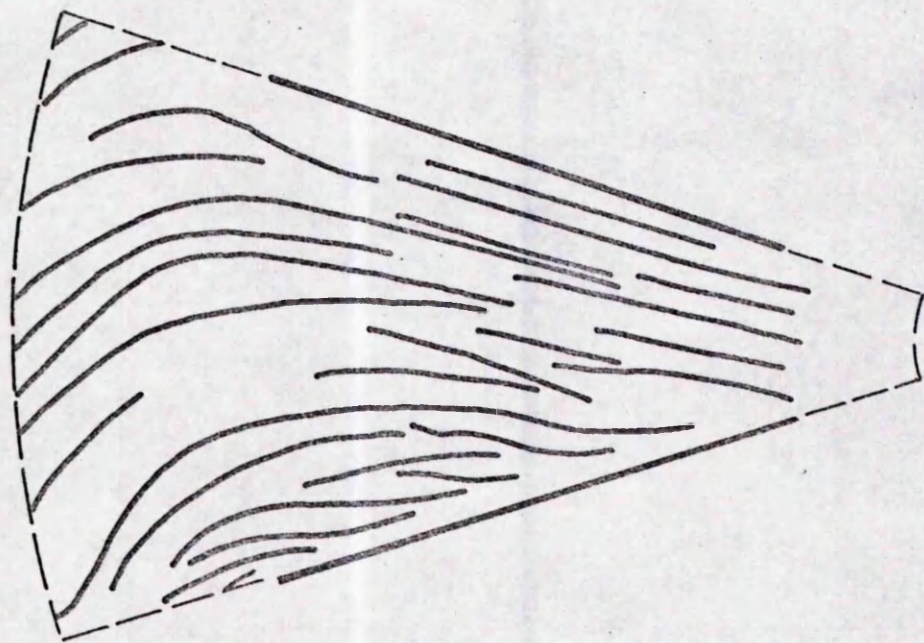
FIG 60(b) PREDICTED AND MEASURED STATIC PRESSURE DROP THROUGH ROTOR—CASE 1

Comparison of predicted streamlines with observed
streakline obtained by the method of ref. [47]

Note: In all cases the experimental values of R_e and R_o
based on the laminar viscosity are $\times 100$ the values in
Appendix 3, table (i). In other words the predictions
are based on an assumed turbulent viscosity of 100 times
the laminar value.



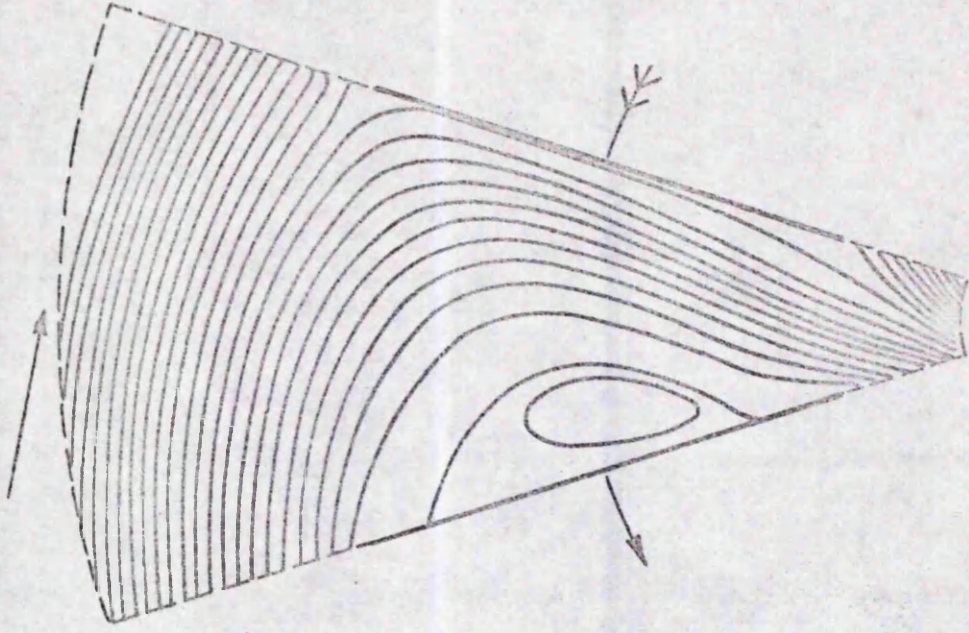
THEORY



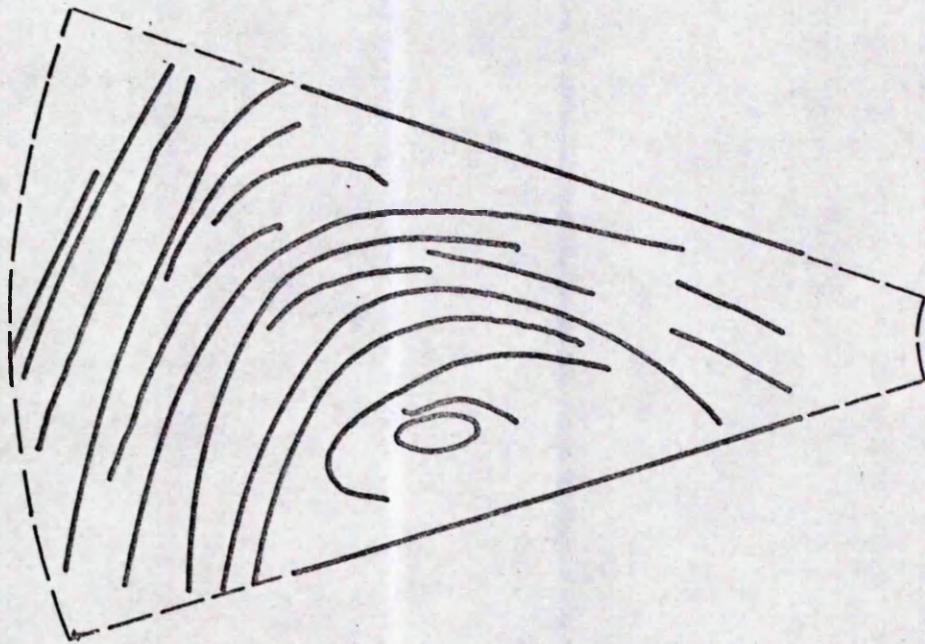
EXPERIMENT

+

FIG 61 EXPERIMENTAL STREAKLINES AND PREDICTED STREAMLINE
DISTRIBUTION—CASE 1



THEORY

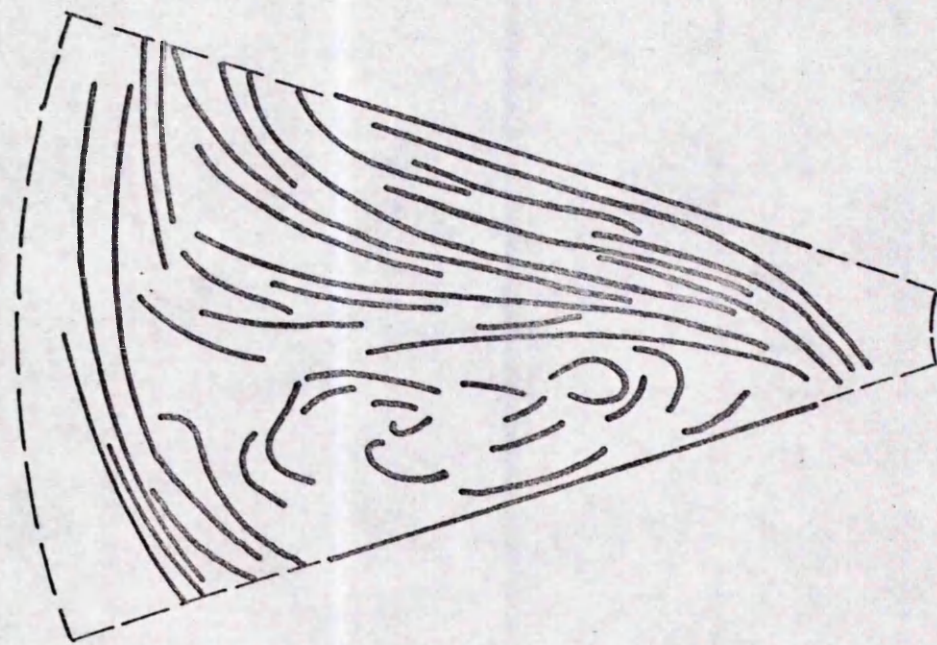


+

EXPERIMENT

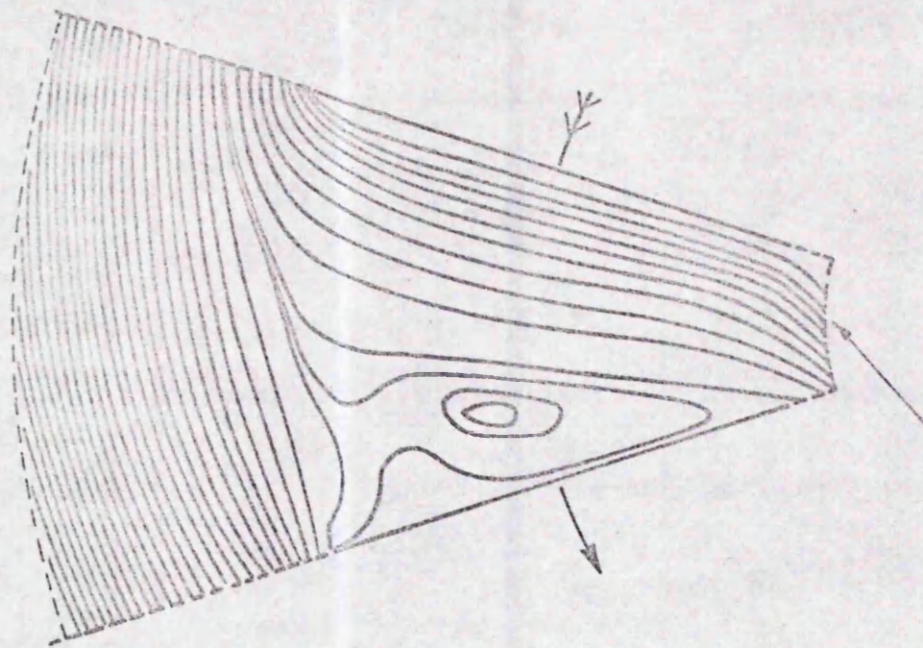
FIG 62 EXPERIMENTAL STREAKLINES AND PREDICTED STREAMLINE

DISTRIBUTION—CASE 2



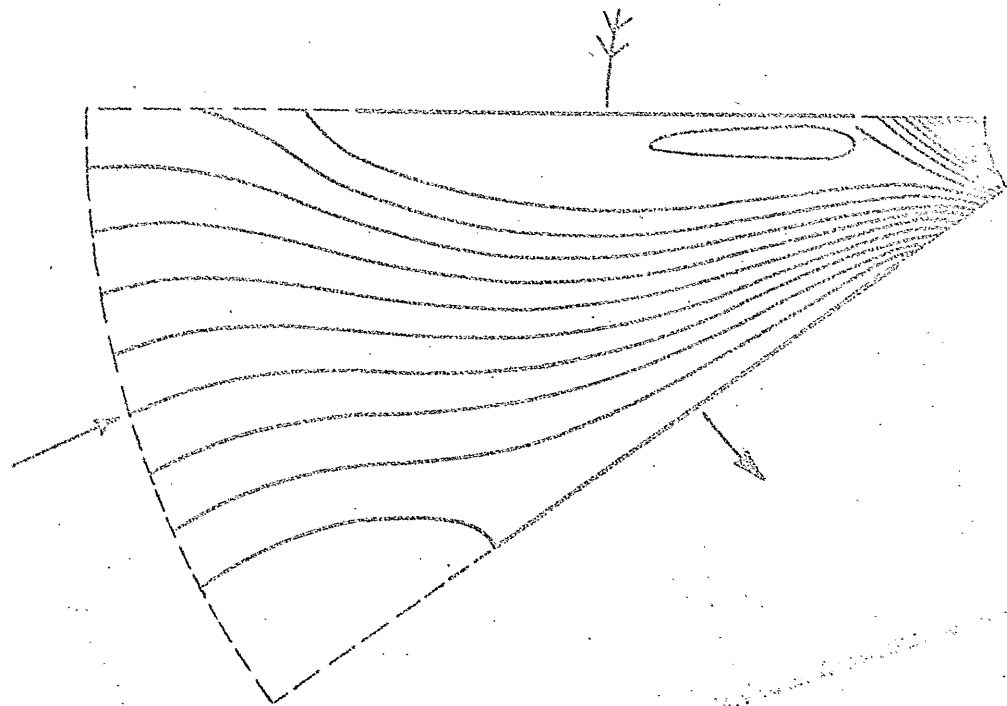
+

EXPERIMENT



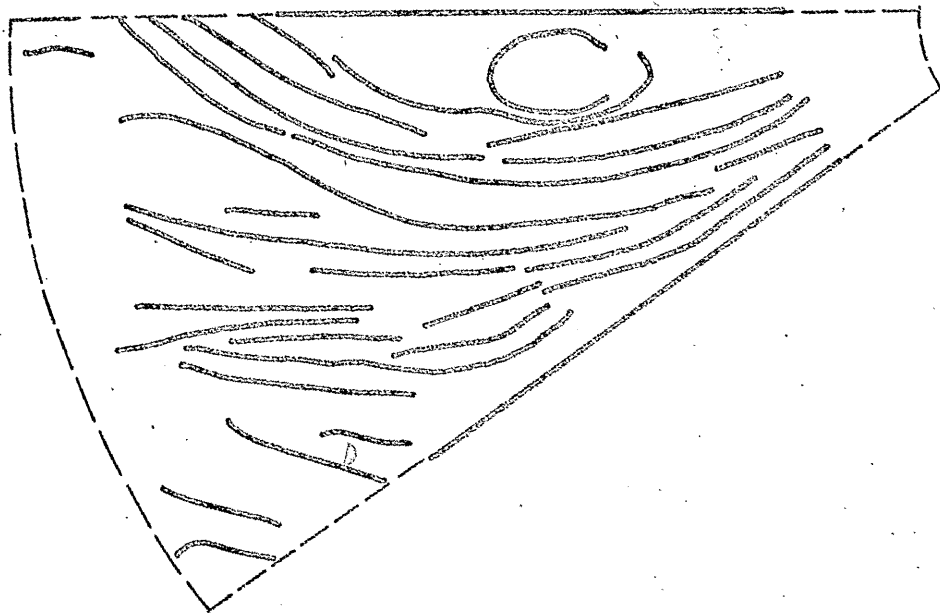
THEORY

FIG 63 EXPERIMENTAL STREAKLINES AND PREDICTED STREAMLINE



THEORY

STREAMLINE — CASE 4



EXPERIMENTAL

EXPERIMENTAL STREAKLINES

FIG 64

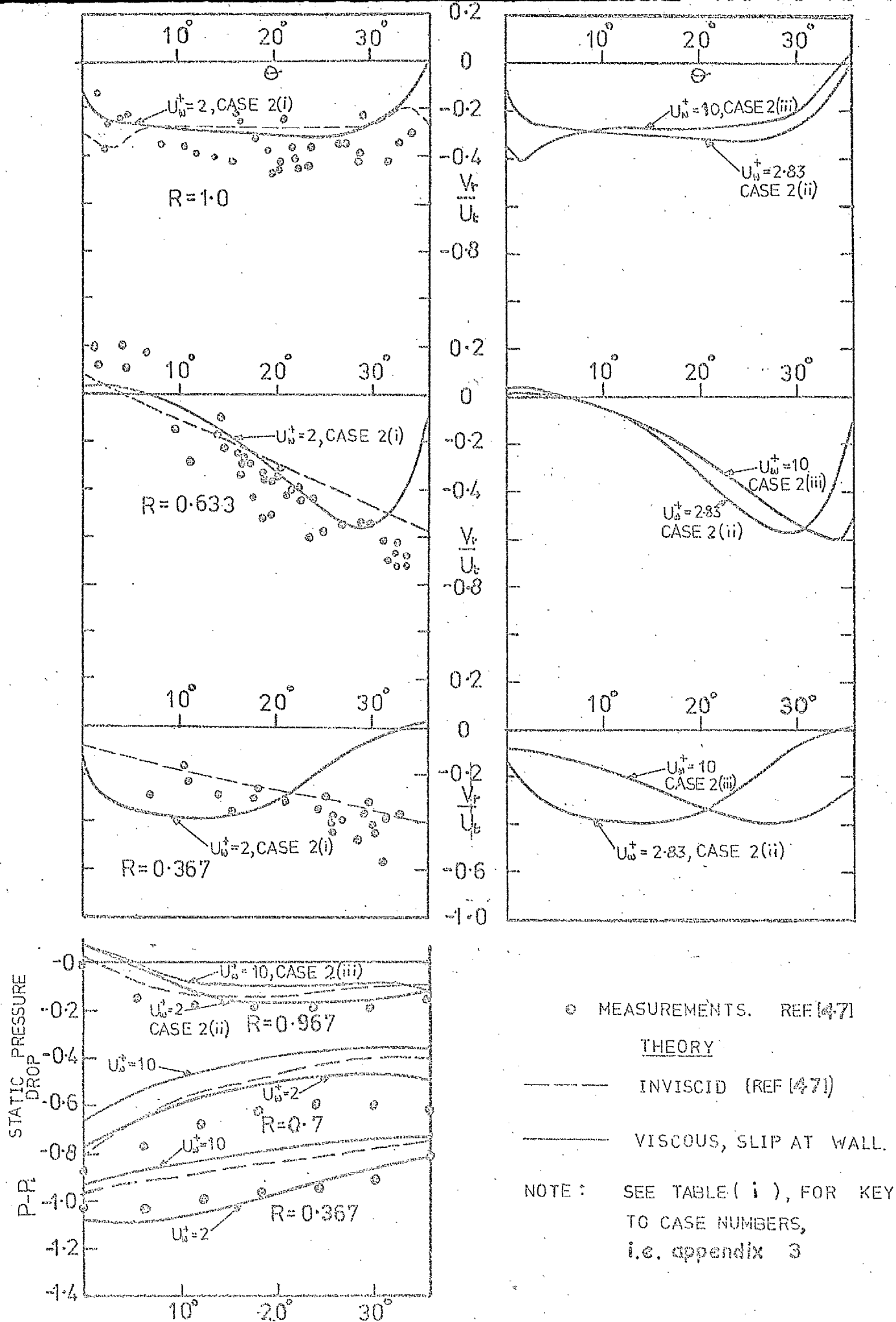


FIG. 66. PREDICTED AND MEASURED RADIAL VELOCITY AND PRESSURE DROP DISTRIBUTIONS—CASE 2

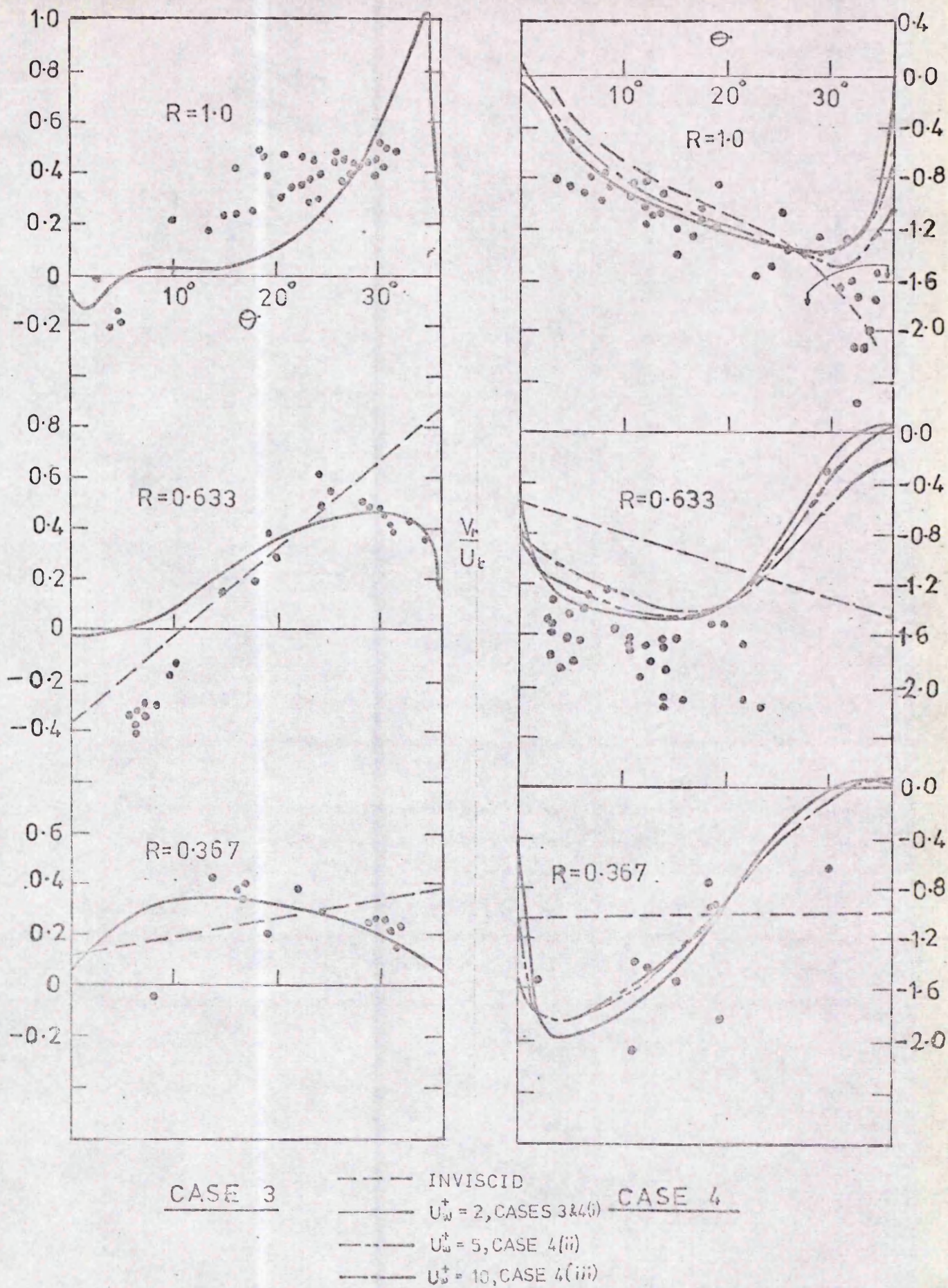


FIG 67 PREDICTED AND MEASURED RADIAL VELOCITY DISTRIBUTIONS—CASES 3 AND 4

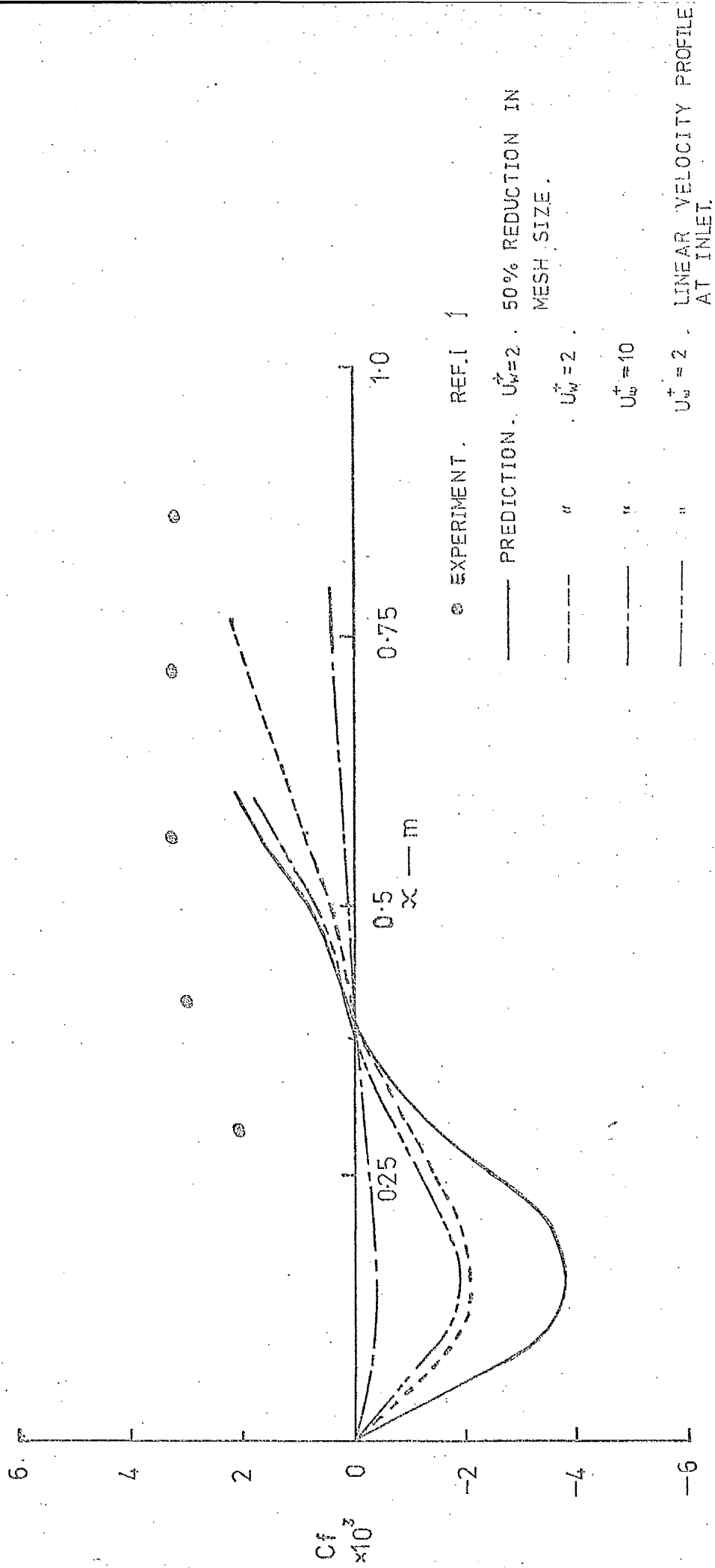


FIG 68 FRICTION FACTOR DISTRIBUTION DOWNSTREAM OF STEP

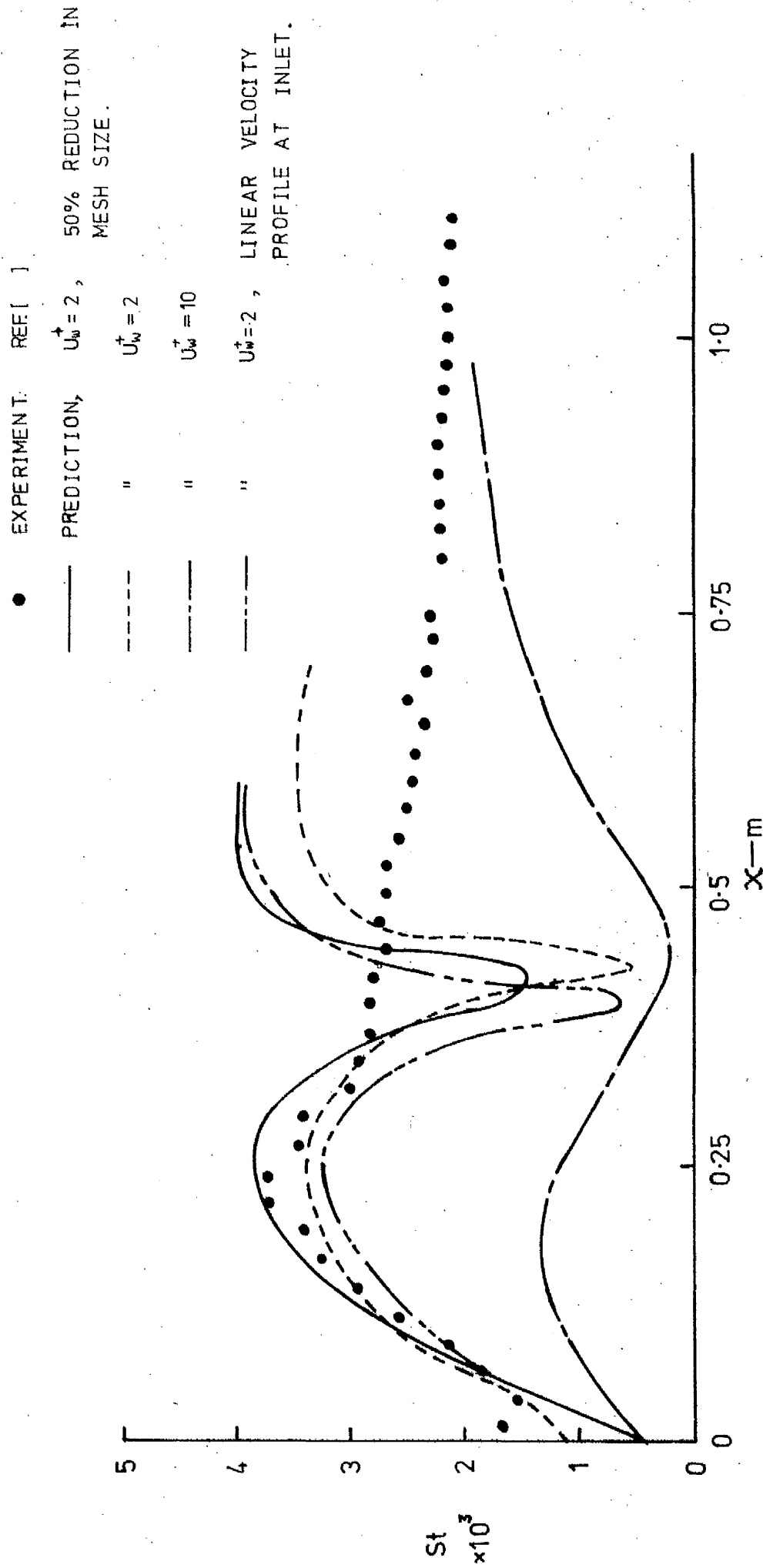


FIG 69 STANTON NUMBER DISTRIBUTION DOWNSTREAM OF STEP